Jochen Heitger

Numerical Simulations of Gauge-Higgs Models on the Lattice

1997

Theoretische Physik

Numerical Simulations of Gauge-Higgs Models on the Lattice

Inaugural-Dissertation
zur Erlangung des Doktorgrades
der Naturwissenschaften im Fachbereich Physik
der Mathematisch-Naturwissenschaftlichen Fakultät
der Westfälischen Wilhelms-Universität Münster

vorgelegt von
Jochen Heitger
aus Hamm
1997

Dekan:	Prof. Dr. F.-K. Holtmeier
Erster Gutachter:	Prof. Dr. G. Münster
Zweiter Gutachter:	Prof. Dr. M. Stingl
Tag der mündlichen Prüfungen:	
Tag der Promotion:	

Diese Version der Arbeit unterscheidet sich von der im Dekanat zur Begutachtung eingereichten durch geringfügige orthographische, stilistische und inhaltliche Korrekturen.

Für Margret, mit Tizian und Thalia

Contents

Introduction **1**

The Two-Dimensional U(1)–Higgs Model 10

The Four-Dimensional SU(2)–Higgs Model 14

Part I: The $2D$ U(1)–Higgs Model **25**

1 The model **26**

1.1 Continuum and lattice model 26

1.2 Basic observables 30

1.2.1 Wilson and Polyakov loops 31

1.2.2 Topological charge 33

1.2.3 Correlation functions 36

1.3 Limiting cases 39

2 Numerical simulation **44**

2.1 Instanton hits 44

2.1.1 Implementation 45

2.1.2 Optimization and checks 48

2.1.3 A remark on dislocations 50

2.2 Updating scheme 51

2.2.1 Scalar field overrelaxation 51

2.2.2 Optimization 53

3 Continuum limit and topological susceptibility **55**

3.1 Lines of constant physics 55

3.2 Scaling behaviour of χ_{top} 62

3.3 Criterion for asymptotic scaling of χ_{top} 67

3.3.1 Idea and derivation 68

3.3.2 Numerical analysis and discussion . . . 72
3.4 Confinement by instantons . . . 77
3.4.1 Derivation in the continuum . . . 78
3.4.2 Numerical analysis on the lattice . . . 82

4 Some phase structure investigations 87
4.1 Comparison with the $D = 4$ model . . . 87
4.1.1 Observables . . . 89
4.1.2 Numerical analysis . . . 91
4.2 Generalization of the fixed length case . . . 94
4.2.1 Phase structure of both models . . . 94
4.2.2 Classical versus quantum continuum limit . . . 98

Summary 100

Part II: The $4D$ SU(2)–Higgs Model 101

5 The model and electroweak phase transition 102
5.1 Continuum and lattice model . . . 102
5.1.1 Basic observables . . . 106
5.1.2 Finite temperature and phase diagram . . . 108
5.2 Fixing the parameters . . . 112
5.3 Numerical simulation . . . 114

6 Thermodynamic quantities 117
6.1 Critical temperature . . . 118
6.1.1 Effective potential . . . 118
6.1.2 Order parameters . . . 120
6.1.3 Hysteresis . . . 121
6.1.4 Two-coupling method . . . 122
6.1.5 Constrained-simulation method . . . 123
6.2 Interface tension . . . 125
6.2.1 Perturbation theory . . . 127
6.2.2 Histogram method . . . 128
6.2.3 Two-coupling method . . . 129
6.2.4 Vacuum tunneling in finite volumes . . . 134

7 Simulations on isotropic lattices **136**
7.1 Critical κ and interface tension for $m_H \simeq 16$ GeV . . . 136
7.1.1 Numerical results . . . 137
7.1.2 Conclusion . . . 141
7.2 Critical κ and interface tension for $m_H \simeq 35$ GeV . . . 142
7.2.1 Numerical results . . . 142
7.2.2 Conclusion . . . 146
7.3 Continuum limit of T_c/m_H for $m_H \simeq 35$ GeV . . . 147
7.3.1 Critical hopping parameter at $L_t = 3$ . . . 149
7.3.2 Continuum extrapolation and discussion . . . 154

8 Quantum corrections to the coupling anisotropies **158**
8.1 Perturbative analysis . . . 158
8.2 Non-perturbative analysis . . . 161
8.2.1 Simulation and its parameters . . . 162
8.2.2 Correlation functions and masses . . . 164
8.2.3 Wilson loops and static potentials . . . 167
8.2.4 Numerical results and discussion . . . 172
8.3 Conclusion . . . 173

9 Simulations on anisotropic lattices **174**
9.1 Some tests and qualitative observations . . . 174
9.2 Critical κ and interface tension for $m_H \simeq 80$ GeV . . . 179
9.3 Discussion and outlook . . . 187

Summary **190**

Appendices **190**

A Basics of simulating field theories **191**
A.1 Lattice notations and conventions . . . 191
A.2 Monte Carlo methods . . . 193
A.2.1 Standard algorithms . . . 193
A.2.2 Gauge and scalar field updates in the SU(2)–Higgs model . . . 194
A.3 Expectation values and autocorrelations . . . 197

B Tools of data analysis **200**

B.1 Methods of error determination 200
B.1.1 Jackknife analysis 200
B.1.2 Bootstrap analysis 201
B.2 Least-squares fits 203
B.3 Ferrenberg-Swendsen reweighting 205

References **206**

Introduction

Today it is widely believed and formidably established by experiments that the **minimal standard model** (MSM), which constitutes one of the major breakthroughs in our theoretical understanding of elementary particle physics, provides a good candidate for an appropriate and self-consistent description of nearly all processes and phenomena involving particle energies at least up to the grand unification scale of $M_{\mathrm{GUT}} \simeq 10^{15} - 10^{16}$ GeV well below the scale of the Planck mass $M_{\mathrm{Pl}} \simeq 10^{19}$ GeV [2, 12]. It covers three of the four fundamental forces, namley the electromagnetic, weak, and strong interactions in the mathematical framework of modern **quantum field theory** [1, 4, 5]. Apart from the still missing verification of the existence of the elusive Higgs particle, whose coupling to the elementary fermions and the gauge vector bosons is postulated to generate their masses, and some other quite artificial pieces including the redundancy related to the many free and independent mass and coupling parameters in the model, the experimental progress and confirmation of the theoretical predictions of the MSM in the so far accessible energy range is of impressive success. So up to now we are left with no significant evidence for any departures from the MSM.

However, in spite of these experimental discoveries and theoretical developments, it has also become an increasingly accepted view in the last few years that, as energies above M_{GUT} towards the distant energy horizon M_{Pl} are reached, where the influence of quantum gravity effects is expected to be substantial and thus can no longer be neglected, the MSM has to be extended to some more general theory, presumably incorporating new physics with novel phenomena [12]. There is theoretical evidence, as well as still a great portion of speculation, that the **minimal supersymmetric standard model** (MSSM), which arranges fermions and boson in common multiplets, could be an important step in the direction of such a **grand unified theory** (GUT) of electroweak, strong, and gravitational interactions. Another plausible argument in favour of the GUT scenario is the so-called hierarchy problem. It emerges from the fact that the running couplings of the MSM approximately coincide at the GUT-scale M_{GUT}, whereas at the same time it is necessary to have a natural mechanism, which stabilizes the symmetry breaking scales of an all unifying gauge group, say SU(5) or SO(10), against the scale of the electroweak gauge group $\mathrm{SU}(2) \otimes \mathrm{U}(1) \otimes \mathrm{SU}(3)$. Otherwise one could not explain, why light particles with masses in the range of a few MeV or GeV exist

in a theory, whose typical energy scale is settled up to 15 orders of magnitude higher. Under these aspects the MSM can preliminarily be looked upon as a symmetry broken effective theory of an — perhaps supersymmetrically — extended model, since nature obviously does not obey a manifest supersymmetry. Experimental indications for the latter are yet to be awaited and hopefully may be found with the aid of the next generation of elementary particle accelerators.

One of the most restrictive guiding principles for the design of the MSM has been the requirement of its **renormalizability**. In the language of quantum field theory it offers an solution to the fundamental difficulty that after the canonical quantization of an interacting classical field theory one rapidly runs into divergent expressions signalling the mathematical inconsistency of the procedure. This deficit then shows up as divergences in a set of Feynman diagrams, which determine the perturbation theory, i.e. the mostly at best asymptotic expansion of expectation values of functions containing the basic field variables of the model in powers of the interaction strengths. Summarizing the main idea to one sentence, in renormalizable quantum field theories the infinities in the expansions of perturbation theory can be absorbed into a redefinition of the bare coupling constants and masses, while keeping the physical couplings and masses fixed [1, 4]. Nevertheless, it turns out that especially for quantum field theories with strong couplings a mathematically solid definition beyond perturbation theory is urgently needed.

Pioneered by K. G. Wilson in its seminal paper about quark confinement in low energy quantum chromodynamics (QCD) more than twenty years ago [14], the research area of **Euclidean quantum field theory formulated on a space-time lattice**, in order to introduce a natural gauge invariant cutoff into the theory, has become an important pillar of theoretical and computational particle physics. After the exact analogy to a classical statistical mechanical system with its defining partition function had already payed off by analytical studies in many ways, it was recognized soon that this discretized and genuinely non-perturbative approach to the theory of quantum fields is optimally suited for numerical simulations, which are based on statistical Monte Carlo (MC) methods. Consequently, it is not astonishing that since the early eighties, when the encouraging era of modern high performance computers began, lattice field theory fastly developed to a kind of numerical 'industry' for calculating elementary particle properties and their interactions by 'measuring' some of the key quantities on the lattice without compromising approximations. Here the computer may be considered merely as a device, which serves to randomly generate appropriate field configurations and to estimate expectation values of gauge invariant functions of the gauge, scalar, and/or fermion fields in their representation as lattice-regularized Euclidean functional (or path) integrals from them. These integrals should then in principle be evaluated for different volumes of the system and different lattice spacings a, and an extrapolation of the results to infinite volume and $a = 0$ must be taken

at the end. In this sense lattice field theory became an important branch of theoretical physics, which provides an essential supplementation of all the experimental methods in high energy physics, where much progress and satisfactory numerical precision have been achieved in the past, including such conceptual questions of quark confinement and how the hadrons arise as bound states of quarks and gluons. Its primary limitation is set by the momentary hardware restrictions in computing power, but the current prospect that there is no end in sight for a dramatic evolution of the most advanced computer systems brings a unique flavour to the area of lattice field theory.

For a presentation of the theoretical background and the foundations of quantum field theory on a lattice with an exhaustive review of its various analytical as well as numerical applications, the reader is invited to consult one of the standard references [16, 17, 18, 19]. Furthermore, an almost complete collection of recent results can be found in the proceedings of the annually held lattice conferences [15].

In the concept of lattice regularization the origin of renormalization in quantum field theory may now be viewed as to be reflected in those relations, which describe the change in the bare coupling constants under a change of the ultraviolet momentum cutoff proportional to the inverse lattice constant $1/a$, whereas the physical content of the theory is required to be maintained. Conventionally, this process is expressed in terms of the correlation length $\xi^{(\mathrm{phys})}$. It gives the physical length scale of all typical (quantum) fluctuations in the system and is equal to the inverse of the physical mass gap $m^{(\mathrm{phys})}$ in the theory:

$$\frac{1}{m^{(\mathrm{phys})}} \equiv \xi^{(\mathrm{phys})} = a\xi \quad \Leftrightarrow \quad \xi = \frac{1}{am^{(\mathrm{phys})}}\,. \tag{1}$$

Sending now the lattice cutoff to infinity, which amounts to perform the **continuum limit** $a \to 0$, corresponds to a vanishing mass in lattice units, $am^{(\mathrm{phys})} \to 0$, and to a diverging correlation length $\xi \to \infty$, whereby the critical behaviour of a second order phase transition as known from systems in statistical mechanics is encountered. At the same time the physical quantities $\xi^{(\mathrm{phys})}$ or $m^{(\mathrm{phys})}$ must be kept fixed during this procedure, and one recovers (non-perturbative rather than perturbative) renormalizability to be equivalent to the existence of a quantum continuum limit for the lattice-regularized theory.

The subject of this work are coupled gauge-Higgs systems on the lattice — namely, the U(1)–Higgs model in two and the SU(2)–Higgs model in four dimensions — in the framework of numerical simulations by means of MC methods.

A convincing motivation for the general interest in understanding the physical impact of these theories should start from the well known fact that the two-dimensional abelian Higgs model with U(1)–gauge symmetry and the SU(2)–Higgs sector of the MSM share some prominent features, which are related to baryon number violation and sphaleron transition rates at finite temperature T. These parallels basically originate from the **non-trivial topological structure of continuum gauge theories** in both systems arising from an

approximately periodic shape of the underlying potentials. Mathematically, it may be abstracted to the statement that the periodic functions on $\mathbb{R}$ and $\mathbb{R}^3$, which take their values in the gauge groups U(1) and SU(2), respectively, fall into different homotopy classes of the same homotopy group [7, 8]:

$$\begin{aligned} \mathrm{U}(1) \cong S^1 \quad &\Rightarrow \quad \Pi_1\left(\mathrm{U}(1)\right) = \Pi_1\left(S^1\right) = \mathbb{Z} \\ \mathrm{SU}(2) \cong S^3 \quad &\Rightarrow \quad \Pi_3\left(\mathrm{SU}(2)\right) = \Pi_3\left(S^3\right) = \mathbb{Z}\,. \end{aligned} \tag{2}$$

More precisely, the differentiable group manifolds of $G = \mathrm{U}(1)$ and $G = \mathrm{SU}(2)$ are assumed to be compactified to the spheres S^1 and S^3, respectively, and each possible local gauge transformation $U = U(x)$ is classified according to the equivalence classes of maps from G onto itself, which form the homotopy groups of G in (2) to be identified with the group $\mathbb{Z}$. This corresponds to an infinite number of classical gauge vacua labelled by an integer, the so-called Chern-Simons number N_{CS}. It reads

$$N_{\mathrm{CS}} \equiv \frac{1}{24\pi^2} \int \mathrm{d}^3x\, \epsilon^{ijk} \mathrm{Tr}\left(U\partial_i U^{-1} \cdot U\partial_j U^{-1} \cdot U\partial_k U^{-1}\right) \in \mathbb{Z} \tag{3}$$

and, as a homotopy invariant, remains constant under continuous deformations of the periodic mappings U. The integer variation of N_{CS} under large gauge gauge transformations of the kind in eq. (7) gives the topological charge of the gauge field[1]. Here only written for the SU(2)–case with the dual field strength tensor defined as $*F_{\mu\nu} \equiv \frac{1}{2}\,\epsilon^{\mu\nu\rho\sigma} F_{\rho\sigma}$ and summation over the indices $r = 1, 2, 3$ of the group generators understood,

$$Q_{\mathrm{top}} \equiv -\frac{1}{16\pi^2} \int \mathrm{d}^4x\, \mathrm{Tr}\left\{ *F_{\mu\nu}(x) F_{\mu\nu}(x) \right\} = \frac{g^2}{32\pi^2} \int \mathrm{d}^4x\, *F^r_{\mu\nu}(x) F^r_{\mu\nu}(x) \in \mathbb{Z}\,, \tag{4}$$

it equals the change in the Chern-Simons number between two topologically distinct vacua: $Q_{\mathrm{top}} = \Delta N_{\mathrm{CS}}$. In ordinary jargon this quantity tells, how often the gauge field wraps around the compact sphere S^3 to visit a fixed element of the gauge group G.

For fermionic theories with fields ψ, the topological charge Q_{top} is intimately connected to the famous Atiyah-Singer index theorem of differential geometry [7]. There it is found that the topological charge of the coupled gauge field configurations has to be identified with the difference in the number of zero modes of the Dirac operator with positive (or right-handed: n_{R}) and negative (or left-handed: n_{L}) chirality,

$$\Delta Q_5 = Q_5(t = \infty) - Q_5(t = -\infty) = \int \mathrm{d}^4x\, \partial_\mu j^\mu_5(x) = 2N_f\left(n_{\mathrm{R}} - n_{\mathrm{L}}\right) = 2N_f \Delta N_{\mathrm{CS}}\,, \tag{5}$$

[1] In the mathematical literature this quantity is also called winding number or Pontryagin index. Thus referring to theories defined on a finite space-time lattice with periodic boundary conditions in all directions, which in the continuum limit can be regarded to live on a space-time manifold isometrically isomorphic to a four-dimensional torus $\mathbb{T}^4$, one would say that the principal bundle over $\mathbb{T}^4$, where the gauge potential is a connection in, are characterized — up to gauge transformations — by a single integer, the topological charge Q_{top} [8, 41].

where N_f denotes the number of fermion (quark) flavours. This non-conservation of the axial charge $Q_5(t) = \int \mathrm{d}^3x\, j_5^0(x)$ is an immediate consequence of the generically non-perturbative triangle anomaly $\partial_\mu j_5^\mu = 2N_f \frac{g^2}{16\pi^2} \left(*F^r_{\mu\nu} F^r_{\mu\nu}\right)$ for the axial (chiral) current $j_5^\mu \equiv \overline{\psi}\gamma^\mu\gamma_5\psi$ [23], which can be deduced from the non-classical behaviour of the functional integral measure under the chiral transformations of the fermion fields on the quantum level [25].

For instance, these considerations may be directly applied to topologically induced **baryon number violating processes** within the electroweak sector of the MSM. Since only the left-handed fermions participate in weak interactions, the SU(2)–gauge fields do exclusively couple to their currents, and the weak interaction also possesses fermionic zero modes, whose presence leads to anomalies. On those physical grounds one expects that, with $q_{c,f}$ representing the quark fields and c their color index, both the flavour-singlet axial vector currents $j_5^\mu = \overline{q}_{c,f}\gamma^\mu\gamma_5 q_{c,f}$ and thereby the vector current $j_B^\mu \equiv \frac{1}{3}\sum_{c,f} \overline{q}_{c,f}\gamma^\mu q_{c,f}$ are anomalous and thus not conserved. This means that baryon number violation in the MSM is caused by the non-trivial winding of the SU(2)–gauge field, which changes $B(t) = \int \mathrm{d}^3x\, j_B^0(x)$ between two times t_1 and t_2 by an amount

$$\Delta B = \frac{N_f}{16\pi^2} \int_{t_1}^{t_2} \mathrm{d}t \int \mathrm{d}^3x\, \partial_\mu j_B^\mu(x) = 2N_f \Delta N_{\mathrm{CS}}\,. \tag{6}$$

However, the probability for the related tunneling events, provided by transitions via instanton-like field configurations introduced below, is tiny. At zero temperature it is proportional to the square of the exponentially suppressed, semiclassical tunneling amplitude $\mathrm{e}^{-8\pi^2/g^2} \simeq 10^{-85}$ with g being the SU(2)–gauge coupling, i.e. many orders of magnitude smaller than any known radioactive decay.

If, on the other hand, fermions are coupled through e_0 to the gauge field in the two-dimensional case, there is as well an anomalous current j_5^μ satisfying $\partial_\mu j_5^\mu = 2N_f \frac{e_0}{4\pi} (\epsilon^{\mu\nu} F_{\mu\nu})$, whose charge Q_5 moves with the Chern-Simons number N_{CS} according to $Q_5(t) = 2N_f \Delta N_{\mathrm{CS}}$.

A characteristic implication of the vacuum structure of gauge theories is that it forbids to go from one vacuum to another by performing small gauge transformations, continuously deformable from the identity. Nevertheless, it is possible to construct explicitly the tunneling path connecting different homotopically non-equivalent vacuum states, the **instantons**. As finite-energy solutions of the classical equations of motion with $Q_{\mathrm{top}} = 1$ for theories in Euclidean space-time, they are of pure gauge type $U\partial_\mu U^{-1}$ on the boundary of G and genuinely interpolate in time between gauge field configurations differing by a large gauge transformation

$$A_\mu \longrightarrow A'_\mu = U A_\mu U^{-1} - \frac{i}{g} U \partial_\mu U^{-1}\,. \tag{7}$$

Assuming the temporal (axial) gauge $A_0 \equiv 0$, their significance is to mediate tunneling transitions through the potential barriers separating these vacua, resulting in change of $Q_{\mathrm{top}} = \Delta N_{\mathrm{CS}}$ according to the formulas in eqs. (3) and (4).

In the two-dimensional U(1)–Higgs model this instanton solution is known as the Nielsen-Olesen vortex [28], which comes from a translation invariant, quantized magnetic flux tube configuration within the three-dimensional phenomenological Landau-Ginzburg theory of superconductivity. Its four-dimensional counterpart in pure SU(2)–gauge theory is the BPS-instanton [26]. The theory of instantons and its various applications in quantum field theory, among which I only want to mention the existence of the θ–vacuum [27], the explanation of the so-called $\mathrm{U(1)_A}$–puzzle (i.e. the absence of a ninth Goldstone boson in QCD, see the next paragraph), and possible mechanisms for quark confinement, are extensively documented in the literature [1, 7]. For a recent review of this broad research area, especially emphasizing the rôle of instantons in QCD and related models, one might consult ref. [10].

The importance of topologically non-trivial field configurations in elementary particle physics can also be quantified by the **Witten-Veneziano formula** [34],

$$\chi_{\mathrm{top}}^{(\mathrm{quenched})} = \frac{f_\pi^2}{4N_f}\left(m_\eta^2 + m_{\eta'}^2 - 2m_K^2\right), \tag{8}$$

which relates the topological susceptibility

$$\chi_{\mathrm{top}} \equiv \int \mathrm{d}^4x \, \langle q_{\mathrm{top}}(x) q_{\mathrm{top}}(0)\rangle = \lim_{V\to\infty} \frac{1}{V} \left\langle Q_{\mathrm{top}}^2 \right\rangle , \tag{9}$$

measuring the fluctuations of the topological charge in the QCD vacuum, to the decay constant f_π of the π–meson and the masses of the mesons η, η', and K. It yields a resolution of the $\mathrm{U(1)_A}$–problem, namely, how in the spontaneous breaking of the true continuum chiral symmetry $\mathrm{U(1)_V} \otimes \mathrm{SU(3)_V} \otimes \mathrm{SU(3)_A}$ to $\mathrm{U(1)_V} \otimes \mathrm{SU(3)_V}$ the ninth Goldstone boson, the pseudoscalar meson η', which in nature stays massive even in the chiral limit of vanishing quark masses, acquires its mass. However, there are some subtleties in connection with eq. (8), since within full QCD in the presence of massless quark flavours the topological charge is screened, and $\chi_{\mathrm{top}} = 0$. Hence, the left hand side is meant to be valid only in the quenched approximation without dynamical fermions ($N_f = 0$, that is pure gauge theory, which is much easier to compute), while the η'–correlation function is pathological in this case, and the η' mass on the right hand side has to be determined in full QCD. By the way, the obvious contradiction that the quantities entering the Witten-Veneziano identity are actually defined in different theories gets not yet really solved by the fact that, strictly speaking, it is derived in the limit of QCD with infinitely many colors $N_c \to \infty$. Nevertheless, this relation implies a reasonable estimate of the quenched topological susceptibility $\chi_{\mathrm{top}}^{(\mathrm{quenched})} \simeq (180 \text{ MeV})^4$ and a good description of the pseudoscalar meson spectrum [10].

The **lattice approach to the inherent topology** in quantum field theory touched

up to now has been a challenging task from the very beginning, since the rich topological structure emenating from the gauge sector of the model under consideration might get lost by the finiteness of the discretized space-time volume in the straightforward transcription into the lattice language [35, 41]. For this reason numerical investigations of topological properties of lattice gauge theories are known to be difficult and time consuming, if one attempts to preserve the important quantization effects of topological objects also on the lattice.

Most of the prescriptions to define the topological charge on the lattice are based on its field-theoretic continuum representation in eq. (4). The naive discretization of the integral over the field strengths $*FF \propto \epsilon^{\mu\nu\rho\sigma}\mathrm{Tr}\,(U_{\mu\nu}U_{\rho\sigma})$ leads to an appropriate sum over the elementary plaquettes $U_{\mu\nu}$ in the $\mu\nu$–plane of the lattice, which is simple to implement and has the right classical continuum limit [36], but with the obvious disadvantage that this expression is in general not even necessarily integer-valued and thus does not possess any topological meaning at all. Additionally, the naive topological charge suffers from large renormalization effects and mixes with other lattice operators (e.g. the unit operator and the gluon condensate).

A far more sensible and sophisticated lattice evaluation of Q_{top} is provided by the geometrical definition [37, 39, 40], which ensures that Q_{top} has nearly the same topological significance as in the continuum. It may be looked upon as the viablest example of a fibre bundle construction in non-abelian lattice gauge theories [8, 41]. Keeping away from a singular set of exceptional configurations, which form a lower dimensional submanifold in the space of all periodic lattice gauge fields and which are expected to be unimportant for sufficiently smooth ones (but might perhaps spoil the continuum limit of χ_{top} though), it has all the wanted properties of a reasonable and well-defined topological charge on the lattice, which are: Correct classical continuum limit, gauge invariance, independence of continuous deformations of the field, and restriction to integer values. Although its implementation is technically quite complicated and computationally very demanding in general, this proposal has become state of the art, for both the gauge group SU(3) [42] and for SU(2) too [42, 43]. Later I will apply the geometrical lattice definition of the topological charge to the two-dimensional U(1)–model as well, where it straightforwardly simplifies to a sum over the real-valued phases of the plaquettes variables.

Fermionic methods for calculating the topological charge rely on the connection between instantons and fermionic zero modes entering the divergence of the chiral current in the continuum index theorem (5). Exceptionally small eigenvalues of the Dirac operator on the lattice have been identified and could be counted directly. Furthermore it was demonstrated that the corresponding eigenvectors have the (at least approximately) correct chirality and are spatially correlated with instantons [44]. The definition of Q_{top} through a fermionic expectation value is not sensitive to dislocations, but it is plagued with the well known problems arising from the difficulty of defining chiral fermions on the lattice [19]. Moreover,

in fermionic methods one has to handle contributions from renormalization effects too, and as a consequence they have never been pursued very vigorously. A rare exception is — to my knowledge — ref. [45], where the fermionic methods were successfully applied to two-dimensional QED with staggered and Wilson fermions in order to analyze the spectrum of the lattice Dirac operator and to calculate the topological susceptibility from it.

Since most of the difficulties with the field-theoretical and geometrical algorithms are related to fluctuations on very short scales, it is natural to combine them with some sort of smoothing procedure in order to pick out the classical instanton configurations. The most popular method of this type is the cooling algorithm [46], in which one locally minimizes the action in a MC simulation. This operation quickly eliminates short-range quantum fluctuations and eventually leads to smooth configurations, corresponding to the classical content of the original field and dominated by instantons indeed. Unfortunately, as a still severe problem, which appears to be difficult to cure for the non-abelian gauge theories SU(2) and SU(3), the cooling method is not stable against the scale invariance of the instanton solution in the continuum. As a consequence of the non-locality introduced by the related relaxation steps, dislocation-like objects loose their energy density under cooling faster than the physical objects of the size of the correlation length so that the instanton action on the lattice may considerably underestimate the continuum action. This reflects the unpleasant feature that cooled instanton configurations, whose extension gets comparable or even smaller than the lattice spacing, can not be resolved reliably and result in systematic uncertainties for $Q_{\rm top}$ and $\chi_{\rm top}$.

Today, as a recent and very promising development in this field, where already large effort has been invested, the different topological charge definitions are also used in conjunction with various concepts of improvement, like cooling with improved lattice actions [47], blocking, renormalization group transformations, and improved or perfect lattice actions and operators as e.g. considered in refs. [48, 49].

In addition to the barrier penetration between topologically distinct vacua via quantum tunneling at zero temperature discussed above, there is also a finite-temperature mechanism for $Q_{\rm top}$–changing processes, induced by the **sphaleron** [30, 32], which is supposed to contribute to the rate of baryon number violating processes and hence to be essential ingredient for the scenario of electroweak baryogenesis within the MSM. It is a (non-stable) saddlepoint solution of the Euclidean equations of motion in the static field approximation justified at high temperatures T, has $Q_{\rm top} = 1/2$, and lies midways between two neighbouring vacua so that transition across the barrier tops can occur classically through thermally activated field fluctuations.

The relevance of these kinds of transitions and estimates for the magnitude of its rate have been addressed in numerous investigations of two- and four-dimensional gauge-Higgs models at finite temperature in the continuum and on the lattice [33, 62, 93, 154]: The latter

in most cases within real-time MC simulations, combined with solving the respective classical equations of motion by integrating them numerically as initial conditions for the evolution of $Q_{\rm top}$ in time, but also in the imaginary time formalism of Euclidean lattice field theory [65].

Another intriguing property, which the two models have in common, is the phenomenon of **spontaneous breakdown of the gauge symmetry**, which would give rise to a first or second order phase transition at some critical temperature $T = T_c$ between a strongly coupled symmetric ('confinement', $T > T_c$) phase and a weakly coupled phase of broken symmetry ('Higgs', $T < T_c$). Both phases are characterized by a completely massive spectrum, created through gauge invariant local operators acting on proper eigenstates of the underlying Hamiltonian, which can consist of vector bound states of scalar constituent quarks and scalar bound states in the former, and of fundamental massive gauge vector bosons and the Higgs particle in the latter. In the usual folklore this — sometimes continuous — evolution with T is associated with the dynamical **Higgs mechanism**, in which the initially massless gauge vector bosons ('Goldstone modes') of the theory acquire non-zero masses by their interactions with the scalar Higgs field ϕ, whose vacuum expectation value develops a non-zero value, thus rendering the vector bosons massive and the forces they mediate short-ranged ('screening').

But owing to a general theorem [21], local gauge invariance can not be broken spontaneously, since the gauge symmetry transformations to be employed act only on a finite number of field variables restricted to a compact space-time volume, which means that all physical observables are gauge invariant by construction. Moreover, there exists no true gauge invariant local order parameter for such a phase transition, which can distinguish between the low-temperature Higgs phase and the high-temperature symmetric phase [22][2]. The low lying resonances of the bound states corresponding to the composite field operators in the symmetry restored phase are complementary to the elementary excitations in the Higgs phase corresponding to the Higgs particle and the vector bosons. Therefore, in a strict sense, there is no gauge symmetry restoration across T_c at high-temperatures and the local gauge symmetry remains always intact, although, of course, there still can be phase transitions. If an local order parameter with a value non-identically vanishing in both phases is desired though, the gauge has to be fixed. A popular choice in this case is the vacuum expectation value of the scalar field in unitary gauge, which typically is large in the symmetry-broken Higgs phase and small — albeit definitely non-zero — in the symmetric phase. The gauge invariant substitute of it is the scalar condensate, i.e. the global expectation value of the composite operator $\phi^+\phi$.

[2] In ref. [22] it is also proven that in lattice non-abelian gauge-Higgs systems with matter in the fundamental representation of the gauge group and fixed length of the scalar field, the Higgs and symmetric phases are continuously connected, i.e. Higgs and confinement regimes belong to the same phases of the theory.

My thesis is divided into two parts, which both are organized in the same way, and I give only a short outline of its central topics here. A more detailed survey of the individual subjects and some further motivations will follow in the subsequent sections. I always begin with a short introduction to the models in the continuum and on the lattice from the viewpoint of quantum field theory. Then, after reporting about some aspects of the numerical realization in the MC simulations, I will focus on the results obtained and their physical interpretation. Some of the material, which is covered by this thesis, has already been published in refs. [64, 136, 139, 140, 141].

Within the **two-dimensional U(1)–Higgs model** the continuum limit of the lattice theory with variable length of the scalar field is studied. In addition, the numerical simulations concentrate on the scaling behaviour of the topological susceptibility at zero temperature and its rich interplay with the phase structure of this model. My MC investigations of the **four-dimensional SU(2)–Higgs model** participate in a project [134, 135, 137], which is aimed to clarify the nature and the strength of the finite-temperature electroweak phase transition (EWPT) by large-scale lattice simulations from first principles. A characteristic thermodynamic quantity in this context is the interface tension, which is determined for different physical situations, essentially in dependence on given values for the mass of the Higgs boson.

Finally, to make the whole presentation more self-contained, a few remarks on the MC approach to simulating field theories on the lattice, supplied by some frequently used notations, conventions, and numerical tools, are postponed to the appendices.

Part I: The Two-Dimensional U(1)–Higgs Model

I have already sketched in the general introduction, that the two-dimensional U(1)–Higgs model can serve as a toy model for the SU(2)–Higgs sector of the electroweak theory in four dimensions. It is a superrenormalizable field theory by definition, i.e. there is only one primitive first order divergence in the 2–point function, and it has a similar non-trivial topological structure, which is, however, much more transparent and easier to catch in practice due to the lower dimensionality of space-time.

Whereas detailed studies of the model with various methods are available [22, 54, 55, 56, 57, 58, 59, 60, 62, 63], it is not well understood within the Euclidean lattice approach, above all for variable length of the scalar field, where extensive investigations are still missing. Hence, I examine non-perturbatively the continuum limit in this case, whose formal existence in addition to the feature of a permanently confined fractional charge have been proven rigorously in mathematical terms many years ago [53], and I will answer the question, whether it is qualitatively different from the model with fixed length of the scalar field. In particular, I investigate by different methods the scaling behaviour of the topological sus-

ceptibility at zero temperature along the lines of constant physics, whose position in bare lattice parameter space can be uniquely determined and which specify this continuum limit. Both items will be discussed in chapter 3. As an imaginable application for future work, it should then in principle become possible to compare the topological susceptibility from the lattice with the instanton transition rate $\Gamma_{\rm inst}$ via

$$\chi_{\rm top} = \frac{1}{V} \left\langle Q_{\rm top}^2 \right\rangle = \frac{1}{V} \left\langle \left[N_{\rm CS}(t) - N_{\rm CS}(0) \right]^2 \right\rangle \stackrel{t\to\infty}{\longrightarrow} \frac{\Gamma_{\rm inst}}{V_s} , \tag{10}$$

where $V = V_s t$ denotes the space-time volume, and which is calculable in the continuum with semiclassical methods within the dilute gas approximation by means of fluctuation determinants [61, 79].

The existing theoretical and numerical interest in this model is also feeded by the possibility that the variable scalar field length could presumably modify the relatively simple phase structure of analytically connected Higgs and confinement regimes in the lattice model with fixed length, similar to analogous systems in four dimensions [19, 83, 86, 112]. To appreciate this issue, an instanton-induced confinement mechanism of fractional test charges in the dilute gas approximation is numerically confirmed in chapter 3 as well, and I elucidate some further characteristics of the abelian Higgs model in different regions of bare parameter space by considering suitable observables (i.e. global order parameters) for phase transitions in lattice systems, where the gauge degrees of freedom are coupled to scalar matter fields. The latter will be addressed in chapter 4.

The continuum limit of the abelian Higgs model with fixed scalar field length is the XY–model, which in traditional statistical mechanics is better known as the O(2)–sigma or the two-dimensional, planar Heisenberg model. It describes a system of two-dimensional spin vectors with unit modulus and nearest-neighbour interaction, and it has a number of physical applications (e.g. two-dimensional magnets and crystals or superconducting films in liquid helium). Owing to a general theorem [20], two-dimensional models with a continuous symmetry can not have an ordered phase at non-zero temperature and, therefore, ordinarily do not have a phase transition at finite temperature. The XY–model is special, because it undergoes a phase transition at a critical temperature $T_c > 0$, although, in agreement with the Mermin-Wagner theorem cited above, the transition is not characterized by a local order parameter. Both the low- and the high-temperature phase are disordered, but the spin-spin correlation function changes from exhibiting a power-law decay in the region $T < T_c$, to an exponential decay at $T > T_c$ as usual, signalling a phase transition. The mechanism of this transition was clarified in ref. [67], see also refs. [4, 68, 70] for related investigations. For $T < T_c$, the system is dominated by spin waves, their fluctuations are small, and the periodic character of the angle variable parametrizing the Hamiltonian of the model can be ignored. For temperatures $T > T_c$, topological objects classified by an integer winding number $Q_{\rm top}$ become crucial for the dynamics of the phase transition, most prominently those with $Q_{\rm top} = \pm 1$ called vortices (instantons) and antivortices (antiinstantons), respec-

tively. Namely, at $T \lesssim T_c$ the system consists of a somewhat more ordered phase, which is populated by tightly bound vortex-antivortex pairs in coexistence with the spin wave excitations, and their correlators are power-behaved. This attractive, binding force between vortices and antivortices is a consequence of the long-ranged logarithmic Coulomb potential they feel at low T. Hence, the pairs vortices and antivortices form an infinitely dilute gas of vortex molecules there, whose influence on the physics of the model is strongly suppressed[3]. When the temperature is raised above T_c, the molecules begin to dissociate, and a dense plasma of nearly free vortices (and antivortices) develops, which governs the long distance behaviour of the system. In fact, since the entropy of an isolated vortex is essentially the logarithm of all possible vortex positions, the entropy dominates over their free energy, and the vortices get important at $T \gtrsim T_c$. Their presence then implies that the system is even more disordered than below T_c with spin-spin correlators falling off exponentially. Furthermore, one can also show that the XY–model is equivalent to a two-dimensional Coulomb gas. Now the Kosterlitz-Thouless phase transition describes the transition from a system of dipoles to an ionized plasma, whose correlation length ξ is nothing but the Debye screening length, which has for $T \to T_c$ an essential singularity at the transition point of the type $\xi \sim \exp\left\{c\,|T - T_c|^{-1/2}\right\}$ rather than the power-law divergence observed in ordinary phase transitions [68].

In view of this interesting topological content, the lattice U(1)–Higgs model has received much attention in earlier investigations. Most of its properties were studied in that case, where the modulus of the scalar field is frozen to unity. For instance, there is a collection of articles, which treat the model in the so-called Villain approximation [54, 55]. Here one performs an appropriate duality transformation from statistical mechanics to obtain an effective Lagrangian, which explicitly contains the topological excitations as an ensemble of vortices of finite size interacting through a short-ranged potential. As established in different approaches, e.g. by strong coupling expansion, renormalization group studies, and in the Hamiltonian formulation of the theory, the authors do not find an indication for a phase transition inside the phase diagram of the lattice abelian Higgs model. At any value of the inverse gauge coupling $\beta = 1/a^2 e_0^2$, both in the strong and weak coupling regimes as well as at intermediate β, the theory confines and there is no phase boundary separating a Higgs from a confinement region. Nevertheless, there are qualitative differences in dependence on the sign of the scalar mass term representing the temperature variable T in the model. As a consequence of the compact nature of the gauge symmetry U(1), the plasma of vortices tends to disorder the system and destroys the ordinary Higgs mechanism for non-integer external charges, which would be expected to be at work when T decreases. In the references just mentioned it was verified indeed that the vortices cause Wilson loops of fractional charges to

[3] A qualitatively similar situation is found in QCD, whose phases resemble those of the XY–model, but with the only difference that the rôles of high- and low-temperature phase are interchanged: In the XY–model instantons are excited at high T, while in QCD they are suppressed [10].

obey the area law, i.e. they are confined, whereas integer external charges stay still screened by the scalar field. Here the Wilson loop decays like its perimeter and fails as a signature of confinement [22]. Then the continuum limit $a \to 0$ ($\beta \to \infty$), arriving at the two-dimensional XY–model, ends in phase transition at some $T = T_c$ between a broken symmetry phase displaying the Higgs phenomenon ($T < T_c$), in which the confinement property gets lost and where one meets the theory of a free massive vector meson, and a symmetric confinement phase ($T > T_c$) corresponding to free massless electrodynamics, where the Coulomb potential rises linearly with the distance.

In some references it has also been pointed out the lattice abelian Higgs model with fixed length can be mapped to a theory for type-II superconductors, if coupled to an external electromagnetic field [59], or to massive Schwinger, Thirring, and sine-Gordon models [54]. A renormalization group analysis in combination with a fractionally charged Wilson loop in the latter [56] underlines the preceding picture of an analytic crossover in this model for finite values of β, which occurs from a low-temperature phase of paired instantons and antiinstantons with very low effective instanton density at long distances, thus justifying the valid approximation of a dilute gas of instantons, to a high-temperature phase, where the interactions of instantons and antiinstantons due to the attractive force between them become negligible and no significant cancellation mechanism takes place.

A lattice study of the U(1)–Higgs model with variable length has been performed in ref. [58]. Here a modified cooling algorithm was applied to identify localized lattice vortices, and it was observed that the topological susceptibility χ_{top} is often overestimated and deviates from scaling. On the one hand, the authors tried to explain it by the presence of dislocation-like field configurations as short-ranged lattice excitations still carrying topological charge $Q_{\text{top}} \neq 0$, because an background Q_{top}–operator proposed in ref. [38] to be improved in this respect seemed to render χ_{top} less affected by such scaling violations. However, the MC simulations of the article have been restricted to a choice for the lattice parameters, which orientated itself by the classical continuum limit of the model. In the same context the authors state that the continuum limit of the quantized theory has not been investigated so far, i.e. one actually does not know, how to tune the bare couplings of the model with the lattice constant in its course $a \to 0$ on a renormalization group trajectory. So on the other hand, they also suppose this missing information to be at least partly responsible for the scaling violations of χ_{top} and suggest that this issue should be clarified in future.

Therefore, the present non-perturbative investigation of the lattice abelian Higgs model in two dimensions constitutes an important supplementation to this series of publications. It is intended to fill the gap in the literature of a more thorough study of that version, in which the scalar field length is a variable degree of freedom, with special emphasis on the continuum limit of the full quantum theory and its topology on the lattice.

Part II: The Four-Dimensional SU(2)–Higgs Model

One of the fundamental goals of elementary particle physics is to understand the origin of the observed baryon asymmetry, which has developed from an initial charge-symmetric state in the hot and dense universe, as it was realized directly after the Big Bang at temperatures of the order of the Planck scale $T \simeq M_{\rm Pl}$. This phenomenon can be quantified as a net dimensionless baryon to photon number ratio of $n_{\rm B}/s \simeq 10^{-9} - 10^{-10}$, where $s \propto n_\gamma$ is the entropy density, and it expresses a fact, which is well established for a long time: Our whole galaxy cluster consists almost exclusively of matter. Since no mechanism to separate matter and antimatter on such large scales is known so far [11], the baryon asymmetry of the universe is one of the most challenging cosmological problems to be resolved by the theory of elementary particle physics. The prerequisites for a successful generation of baryon number, which are commonly known as the three Sakharov conditions [98], can be enumerated as

- baryon number non-conservation,
- C– and CP–violation,
- and departure from thermal equilibrium.

Obviously, the MSM fulfills these three conditions: Baryon number is violated by anomalous fermion number non-conservation as outlined above, C– and CP–symmetry violation are encountered by the chiral character of the electroweak interaction and explicit phases in the Cabibbo-Kobayashi-Maskawa (CKM) quark-mixing matrix, respectively, and non-equilibrium processes occur at the finite-temperature first order electroweak phase transition (EWPT). As in principle the attractive possibility of MSM baryogenesis is opened, the main interest in the electroweak phase transition in the early universe emerges from the question, whether it alone can provide a mechanism for the observed matter-antimatter asymmetry within the framework of the MSM [100].

In contrast to pure Yang-Mills theory, there are no exact minima of the Euclidean action in the topological sectors with $Q_{\rm top} \neq 0$ for such theories, where the Higgs mechanism is operative. However, it was found in ref. [24] that for instanton sizes $\rho_{\rm inst}$ with $\rho_{\rm inst} \lesssim v^{-1}$ and v denoting the vacuum expectation value of the Higgs field, approximate instanton solutions to the field equations do exist. Consequently, although fermion number is preserved in the MSM at the classical level, neither baryon (B) nor lepton (L) numbers are conserved in electroweak theory at the quantum level. While the $(B-L)$–symmetry remains unbroken owing to anomaly cancellation, $B+L$ is violated. Unfortunately, the electroweak coupling constant $\alpha_W = g^2/4\pi$, with g being the SU(2)–gauge coupling, is small, and this means that under ordinary $T \simeq 0$ conditions the tunneling events provided by these (approximate) instanton solutions are too rare to be of any physical importance. More precisely, the instanton transition rate at zero temperature, proportional to the semiclassical tunneling

probability as noted in the general introduction, is still $\Gamma \simeq \mathrm{e}^{-4\pi/\alpha_W} \simeq 10^{-170} \simeq 0$ and therefore unobservably small. But a more viable constellation for electroweak baryogenesis arises as one leaves the usual weak coupling regime of the theory, e.g. by increasing the collision energy of the interacting particles or by raising the temperature towards the EWPT, which has become an issue of renewed attention in the past.

According to the ideas of cosmology and elementary particle physics, the electroweak phase transition has taken place during the cooling epoch of the early universe at a temperature of the order $T \simeq \mathcal{O}(100)$ GeV $\simeq \mathcal{O}(10^{16})$ K, roughly $t \simeq 10^{-11} - 10^{-12}$ s after the Big Bang[4]. With decreasing temperature this transition distinguishes between a high-temperature phase, usually referred as symmetric phase, and the low-temperature Higgs phase with spontaneously broken symmetry [89, 99]. An order parameter of this transition is the vacuum expectation value of the scalar field $v = v(T)$, which has a small value at high temperature, where the electroweak symmetry is restored ($T > T_c$), and a larger one in the Higgs phase ($T < T_c$). This symmetry breaking quantity represents the stable non-trivial minimum of the low energy effective potential $V_{\mathrm{eff}} = V_{\mathrm{eff}}(\phi, T)$ for the scalar Higgs field ϕ at finite temperature, i.e. the value of the free energy of the system in a uniform and static background of field variables, which is at the critical temperature $T = T_c$ degenerate with the trivial minimum corresponding to the symmetric phase separated by the energy barrier:

$$\left.\frac{\mathrm{d}V_{\mathrm{eff}}(\phi, T_c)}{\mathrm{d}\phi}\right|_{\phi=v} = 0\,, \quad V_{\mathrm{eff}}(v, T_c) = V_{\mathrm{eff}}(0, T_c)\,. \tag{11}$$

The effective potential is in general a gauge dependent quantity, but the values of V_{eff} at its minima are gauge invariant. Due to the presence of a term cubic in ϕ with negative sign, the EWPT is known from the perturbative effective potential to be of first order and weakening when the self-coupling of ϕ increases, which in the macroscopic description of equilibrium thermodynamics [3] says by definition that a first derivative of the respective thermodynamic potential, for instance the latent heat, has a finite discontinuity at $T = T_c$. Systems undergoing a first order phase transition are accompanied by characteristic signals in the vicinity of T_c, namely metastability, coexistence of the two phases, jumps of globally averaged quantities like order parameters, and hysteresis effects. Its dynamics are governed by the — possibly quite violent — non-equilibrium process of nucleation, expansion, and percolation of bubbles of the new phase inside the old one. Nevertheless, one can guess the equilibrium approximation to the EWPT to be guaranteed before the phase transition and soon after it is completed, in regions far enough from the moving bubble walls, which tend to disturb the electroweak plasma [91, 93]. This remark suggests that equilibrium statistical mechanics can be applied to evaluate the static properties of the phase transition, such as

[4]For comparison, the QCD phase transition between a phase of a weakly interacting, deconfined quark-gluon plasma, where the short-distance behaviour of matter is dominated by the asymptotic freedom of QCD, and a confinement phase with spontaneous chiral symmetry breaking and the bound quark systems of hadronic matter met today, has occured at lower temperatures around $T \simeq \mathcal{O}(100)$ MeV.

critical temperature, jump of the order parameter, latent heat, or interface tension.

As the universe cools down, the anomalous baryon number violating processes, which are rapid in the MSM at high T, will tend to erase any baryon asymmetry, which may perhaps be created by some other mechanism — except eventually originating from $(B-L)$–violating new physics — at higher energies between the electroweak and the grand unification scale M_{GUT}. So if the baryon asymmetry is completely washed out at temperatures T far above the weak scale, the observed baryon number must proceed from physical processes close to the critical temperature T_c, at which the EWPT takes place. A necessary condition for this scenario of electroweak baryogenesis is a transition of strong enough first order type, whereas for a weak transition every asymmetry generated at the phase transition would be washed out in the Higgs phase again, because at temperatures T larger than the vector (W– or gauge) boson mass m_W, the anomalous baryon and lepton number violation in the MSM is enhanced. The strength of the EWPT does crucially depends on the value of the Higgs boson mass m_H, and within the MSM it has already been accepted that the requirement of preserving the baryon number generated at the weak scale imposes too strong bounds on the Higgs mass as to stay consistent with the present experimental limits. This is shortly sketched in the next paragraph.

At $T > T_c$ in the symmetric phase the exponential suppression of the baryon number non-conserving transitions is absent. Its rate per unit volume is given by the power-counting estimate

$$\Gamma \simeq c\,(\alpha_W T)^4 \ , \tag{12}$$

where $c \simeq \mathcal{O}(1)$ is a constant [31]. In order to quantitatively estimate the generated baryon number in the symmetry broken Higgs phase at $T < T_c$ after the EWPT, one should take into account the baryon number violation in the context of topology changing processes by sphaleron transitions. Once a sphaleron is thermally created, the system can jump up to the top (saddle point) of the potential barriers and roll down into the neighbouring vacuum to overcome them classically. Such transitions are also at work in the Higgs phase, and there they are still exponentially damped but now only by a Boltzmann factor in the rate

$$\Gamma \simeq T^4 \exp\left\{-\frac{E_{\mathrm{sph}}(T)}{T}\right\} \ , \tag{13}$$

where the sphaleron energy E_{sph}, which is equal to the height of the potential barrier separating two topologically inequivalent vacua, is given by

$$E_{\mathrm{sph}}(T) \simeq C\,\frac{2m_W(T)}{\alpha_W(T)} \tag{14}$$

with $C = C(\frac{m_H}{m_W}) \simeq \mathcal{O}(2)$ being a slowly varying function of the scalar quartic self-coupling λ, the gauge boson mass m_W, and $\alpha_W = g^2/4\pi$ the gauge coupling of the weak interaction as before [100]. This energy is of the magnitude $E_{\mathrm{sph}} \simeq \mathcal{O}(10)$ TeV. Recoursing to the finite-temperature effective potential, a leading order perturbative computation in the broken

phase [92] shows that

$$\frac{m_W(T)}{g^2T} \sim \frac{v(T)}{gT} \sim \frac{g^2}{\lambda} \sim \frac{m_W^2(0)}{m_H^2(0)}\,, \quad T \lesssim T_c\,, \tag{15}$$

i.e. the baryon violation rate (13) is sensitive to the zero-temperature ratio of Higgs and W–boson masses, which simultaneously controls the reliability of perturbation theory in the Higgs phase near T_c (typically up to the range $m_H \simeq 35$ GeV $-$ 40 GeV at least). The rates (12) and (13) are now to be compared to the expansion rate of the universe in inflationary cosmology [11, 93]:

$$\Gamma_{\rm U} = \frac{1}{t_{\rm U}} \simeq c\left(\frac{T}{M_{\rm Pl}}\right)T\,, \quad c \simeq \mathcal{O}(10^{-1})\,. \tag{16}$$

While at $T > T_c$ one has $\Gamma \gg \Gamma_{\rm U}$ for a wide range of temperatures $T_c < T < 10^{-1}M_{\rm Pl}\alpha_W^4 \simeq 10^{12}$ GeV, in which the anomalous B–violating processes are fast, the situation is more subtle at $T < T_c$: If the phase transition were weakly first order ($m_W(T_c)$ is small), second order, or of the crossover type, one has $\Gamma \gtrsim \Gamma_{\rm U}$ so that the B–violating processes would be approximately in equilibrium, any net primordial $(B+L)$–number would be subsequently erased by unsuppressed sphaleron processes in the broken phase, and no effective baryon number will survive at $T < T_c$ after the phase transition has completed. On the other hand, if the phase transition were strongly first order ($m_W(T_c)$ is large enough), one has $\Gamma \ll \Gamma_{\rm U}$, the B–violating processes get very slow, and a primordial matter-antimatter asymmetry could in principle be preserved until today. The obtained condition, under which the previously generated baryon excess will not be washed out after the EWPT, implies a bound on the sphaleron energy of $E_{\rm sph}(T_c)/T_c \gtrsim 45$ or equivalently, translates in the MSM into the condition[5]

$$\frac{v(T_c)}{T_c} \gtrsim 1 \tag{17}$$

on the vacuum expectation value of the Higgs field $v = v(T)$. In this case electroweak baryon number non-conservation switches off immediately after the phase transition and continues to operate further in the opposite case. Since $v(T_c)/T_c$ is inversely proportional to the scalar quartic coupling λ in eq. (15), the requirement of preserving the once generated baryon asymmetry puts an upper bound on the value of the Higgs boson mass m_H, which actually depends on the particle content of the theory at energies of the order of the electroweak scale. In view of the present rather stringent experimental constraints on the Higgs mass by the current lower limit of

$$m_H > 65 \text{ GeV} \tag{18}$$

from LEP at CERN [13] in the MSM with a top quark of mass $m_{\rm t} \simeq 175$ GeV, the forelast inequality can hardly be fulfilled, which means that the B–violating reactions are also fast after the phase transition and not negligible as necessary for successful MSM baryogenesis.

[5]Strictly speaking, this condition must be fulfilled at the temperature $T = T_c^{(<)}$ after the phase transition has finished. It can be considerably lower than the critical temperature T_c defined before [103].

Hence, one can not evade to anticipate the following generic conclusion: The lower m_H–limit (18) renders the EWPT so weakly first order that within the MSM an explanation of the observed asymmetry between matter and antimatter in the universe must be ruled out.

Although more recent analyses seem to discourage baryogenesis within the MSM as well due to the still far too small CP–violation, simple non-minimal models with genuinely additional sources of CP–violation beyond the CKM-mechanism or an extended Higgs sector may produce a sufficient asymmetry and are therefore promising alternatives, see e.g. the detailed but partly somewhat dated review articles [90, 91, 92, 93]. In any case it is clear, however, that the present baryon asymmetry of the universe has been finally determined at the EWPT, because B–violating processes fall out of thermal equilibrium at the corresponding critical temperature [100]. For this reason a quantitative understanding of the EWPT in the framework of the MSM is still a basic requirement for the discussion of every model of baryogenesis at the weak scale, including reliable knowledge of its order and — provided that it is of first order — its strength in dependence of the Higgs boson mass.

The common analytical tool for the examination of the EWPT is (finite T) resummed perturbation theory [102, 103, 104, 105, 107], which amounts to execute a high-temperature expansion of self-energy diagrams, whose leading term is added as a thermal mass to the tree-level mass in the propagator. This technique works well for low and intermediate Higgs masses ($m_H \lesssim 50$ GeV), where it predicts a first order phase transition of decreasing strength. In fact, the quantitative agreement of two-loop resummed perturbation theory with the numerical lattice data is quite good for most observables so that non-perturbative effects are small and the perturbative expansion can be taken seriously in this mass range. If m_H increases towards higher values around 70 GeV and above, where according to eq. (15) the convergence of the perturbative series is bad and the strength of the EWPT is expected to decrease rapidly, its validity is not ensured any longer and no definite statement can be made. These uncertainties can be traced back to irreparable infrared divergences of the bosonic sector in the symmetric phase, related to the zero-frequency Matsubara modes of finite-temperature field theory [101]. Here perturbation theory fails, because the massless gauge bosons (e.g. $m_W = 0$ in perturbation theory) does not yield the intrinsic infrared cutoff, which is needed to have finite momentum integrals at temperatures $T > T_c$, and to prevent the loop expansion parameter $\lambda/g^2 \sim g^2 T/m_W$ to become arbitrarily large. Consequently, as the leading contribution always comes from the symmetry broken Higgs phase at $T < T_c$, where $m_W > 0$ provides a natural infrared cutoff and thus perturbation theory is well defined for $\lambda/g^2 \sim g^2 T/m_W \ll 1$, it is only feasible for strong transitions and low Higgs masses. If, despite these infrared incapabilities of the symmetric phase, perturbation theory without any explicit infrared cutoff would be taken seriously even at $m_H \gtrsim 70$ GeV, the phase transition is suggested to remain weakly first order there [105, 107].

The breakdown of perturbation theory for larger Higgs masses, above all in the symmetric phase, calls for a systematic and fully controllable non-perturbative treatment of the

regularized theory formulated on a space-time lattice [19, 118, 120, 121, 134, 135, 137, 122]. Starting point of this approach is the electroweak sector of the MSM, which is built up from a $\mathrm{SU(2)_L} \otimes \mathrm{U(1)}_Y$–symmetric chiral gauge theory, where Y denotes hypercharge and L the coupling of the gauge fields to the left-handed chiral components of the fermion doublets. As it gets settled during the finite-temperature EWPT, the chiral symmetry is broken through the non-vanishing vacuum expectation value of the $SU(2)_{\mathrm{L}}$–doublet complex scalar Higgs field with $Y = 1$. Its physical meaning is that the vector bosons (W and Z) as well as the quarks and charged leptons acquire masses via their couplings to the Higgs field. Since the Weinberg angle θ_W, entering the ratio $g'/g = \tan\theta_W$ of the U(1)– and SU(2)–gauge couplings $\frac{1}{2}g'$ and g, is relatively small and the Yukawa couplings of the quark and lepton families to the scalar field are weak in most cases, it is legitimate to neglect them in a first approximation, which essentially corresponds to setting θ_W and the Yukawa coupling of the heavier top quark to zero[6]. Both contributions can in principle be taken into account perturbatively and do not change the qualitative features of the phase diagram of the theory, but it has also been conjectured that in the vicinity of the phase transition point the inclusion of the $U(1)$–factor and the top quark mass could lead to non-perturbative effects of numerical importance [147, 149]. Now one is left with the purely bosonic fundamental SU(2)–Higgs model as a prototype theory for the electroweak sector of the MSM, containing all characteristic ingredients — and especially incorporating the fatal infrared problems, which cause perturbation theory to become more and more questionable with increasing m_H — for a thorough study of the phenomena described above. Beyond that, if some presently unknown matter particles were heavy relative to the scale of the scalar vacuum expectation value, the Higgs quartic self-coupling λ might be strong in the relevant parameter region, and non-perturbative analyses by means of numerical MC methods are recommended.

The second part of my thesis is a completion of large scale numerical simulations of the four-dimensional SU(2)–Higgs model on the lattice, which have been initiated in refs. [134, 135, 137]. They were originally intended to explore the phenomenological viability of the generation of the baryon asymmetry in the universe at the EWPT by investigating its nature and its thermodynamic properties from first principles. Since they focused on Higgs boson masses below 50 GeV and this mass range is already ruled out by the actual experimental bound of $m_H \gtrsim 66$ GeV in eq. (18), their primary scope is to establish suitable methods for extracting physical quantities from the lattice simulations, and to compare with available data from resummed perturbation theory or dimensional reduction — also in the realm of weak first order phase transitions — in order to hint at systematic errors in these approaches. My investigations are centred around the determination of the interface tension between the competing phases. As an characteristic element in the theory of a high-temperature equilibrium ensemble of elementary particles, this macroscopic observable deserves a precise

[6] The neglection of the fermionic content of the theory does also circumvent the known difficulties to put chiral fermions consistently on the lattice.

estimation, because it is a quantitative measure for the strength of the phase transition. In chapter 7 I will exemplarily demonstrate that for $m_H \lesssim 35$ GeV the phase transition in the SU(2)–Higgs model is quite strongly of first order and relatively easy to study on the lattice, although the interface tension decreases with increasing pole Higgs boson mass m_H by many orders of magnitude, hence signalling a substantial decrease in the strength of the EWPT. This intimates the fact that as a consequence of the weak gauge coupling $g^2 \simeq 0.5$, the observed first order phase transition gets very weak with growing m_H already near $m_H \simeq m_W \simeq 80$ GeV, is a potential complication to deal with in the numerical simulations of the thermodynamics of the electroweak plasma within the lattice discretization. Namely, the hierarchy of scales

$$a \ll \frac{1}{2\pi T} \ll \frac{1}{m_W(T)} \lesssim \frac{1}{m_H(T)} \ll La\,, \tag{19}$$

with a the lattice spacing and L the spatial lattice extent, in which the screening lengths (i.e. correlation lengths or inverse masses) at $T \simeq T_c$ near the phase transition become much larger than the inverse temperature, necessitates large spatial lattice sizes to achieve the physical volumes, which are required so that metastability holds, two-peak structures of order parameters can develop, and at the same time, that the lattice is fine enough to resolve the interface between the phases. For instance, at $m_H \gtrsim 80$ GeV the lowest excitations have masses already so small compared to the temperature ($m_{H,W} \ll T$) that one expects a typical finite-temperature simulation on an isotropic lattice to need several hundred lattice points in the spatial directions even for a temporal extension of $L_t = 2$. Such kinds of inhibiting lattice sizes exceed any presently accessible computer resources. Having these difficulties in mind, I will follow the strategy of an anisotropic lattice regularization to handle the foregoing two-scale problem. This appealing remedy, which exploits the simple idea that finite-temperature field theory can be conveniently implemented on anisotropic lattices with different spacings in temporal and spatial directions, solves the problem with the distinct mass scales in a natural way [19, 130, 133]. Another advantage is, well known and often used in QCD, that this formulation allows for an independent variation of temperature and physical volume. Moreover, it is optimally designed to reach more realistic and experimentally still approved values of $m_H \simeq 80$ GeV, where the three-dimensional effective gauge-Higgs models — to be briefly discussed below — claim a termination of the first order EWPT line and the begin of a smooth crossover behaviour with two continuously connected phases [149, 145, 152]. Of course, in the glance of this prediction and as a first interesting application of the anisotropic lattice approach, I have also undertaken numerical simulations to determine the interface tension in a Higgs mass region nearly identical with these publications. The results, which will be reported in chapter 9, are not yet compatible with zero and thus suggest that, at least on $L_t = 2$ lattices, the extremely weak character of the first order phase transition is still visible for a Higgs boson mass value of $m_H \simeq 80$ GeV. Some of the MC simulations on lattices with anisotropic lattice spacings were furthermore devoted to

the non-perturbative verification of the perturbative calculation of the quantum corrections to the coupling anisotropy parameters, which has been carried out in ref. [138]. I will proof in chapter 8 that, within the high precision of the MC data, the perturbative one-loop coupling anisotropies remain unchanged for the practically reasonable lattice parameters of the four-dimensional SU(2)–Higgs model.

In the last years big effort has been invested in several other methods to investigate the EWPT. Important results to be notified were obtained by usage of the ε–expansion [108], average action [109, 111], (exact) renormalization group [110], and the dimensionally reduced effective theory in three dimensions [143, 144, 146, 147, 150], see e.g. refs. [97, 96] for concise and more general status reports of the whole subject.

The latter approach, advocated by the authors of refs. [146, 147], is based on dimensional reduction, which is another powerful tool to study phase transitions in weakly coupled gauge-Higgs theories. Its idea deduces from the known concept that equilibrium finite-temperature field theory is equivalent to Euclidean zero-temperature field theory defined via its generating functional integral

$$Z = \int \mathcal{D}[A,B,\phi,\psi]\, \mathrm{e}^{-S[A,B,\phi,\psi]}\,, \quad S[A,B,\phi,\psi] = \int_0^{1/T} \mathrm{d}t \int \mathrm{d}^3x\, \mathcal{L}_{A,B,\phi,\psi}(x) \tag{20}$$

on a finite 'time' interval $1/T$, supplied with periodic boundary conditions for bosons (ϕ) and antiperiodic ones for fermions (ψ) [6, 94]. Here the notation is A, B for the gauge fields and $S[\cdots], \mathcal{L}(x)$ for the Euclidean action and Lagrange density, respectively. Motivated by the approximate factorization of weakly-interacting high-momentum modes from strongly-coupled infrared ones in the formal substitution $\int \mathrm{d}^4k \to T\sum_\omega \int \mathrm{d}^3k$ for the Feynman rules of perturbation theory at finite T, the recipe of dimensional reduction is to integrate out perturbatively all the 'superheavy' non-static modes (valid up to momenta $k \ll T$) in the Fourier decomposition of the fields with non-zero Matsubara frequencies $\omega = \omega_n^{(\mathrm{b})} \equiv 2\pi nT$ for bosons and $\omega = \omega_n^{(\mathrm{f})} \equiv (2n+1)\pi T$ for fermions, $n = \pm1, \pm2, \ldots$, and successively the 'heavy' scale corresponding to adjoint (triplet) Higgs fields as the remainder of the timelike components of the four-dimensional gauge fields as well (valid up to momenta $k \lesssim gT^2 \ll gT$):

$$\mathrm{e}^{-S_{\mathrm{eff}}^{(D=3)}} = \int \mathcal{D}[A,B,\phi,\psi]_{n\neq 0}\, \mathrm{e}^{-S[A,B,\phi,\psi]}\,, \quad Z = \int \mathcal{D}[A,B,\phi]^{(D=3)}\, \mathrm{e}^{-S_{\mathrm{eff}}^{(D=3)}}\,. \tag{21}$$

Then one derives relations between the (mass and coupling) parameters of the dimensionally reduced model and the parameters of the underlying four-dimensional theory and the temperature by a perturbative matching condition, which requires that the 2–, 3–, and 4–point one-particle irreducible Green functions in three dimensions computed with an effective Lagrangian coincide with the initial static Green functions evaluated in the full theory in four dimensions up to some accuracy, that is up to some power of the coupling constant. While the perturbative calculations in the continuum entering the whole reduction procedure are

free of any infrared divergences, and its ultraviolet divergences can be removed by the usual counterterms of the zero-temperature perturbations theory, this construction ends up with a superrenormalizable, purely bosonic finite-temperature effective theory of the static ($n = 0$) modes in three dimensions, which inherently retains all the infrared problems of the original one and contains its fermionic content in the perturbative dependencies of its variables on the full theory. Finally, the resulting model, a three-dimensional $\mathrm{SU}(2) \otimes \mathrm{U}(1)$ gauge-Higgs system defined through eq. (21), with its essentially remaining non-perturbative dynamics of the phase transition, is put on the lattice and examined by numerical MC methods as in the case of four dimensions. As a consequence of its superrenormalizability, the bare lattice variables of the regularized $3D$–theory can be linked with the physical, renormalized parameters of the continuum $3D$–theory in a — actually two-loop — perturbative calculation near the continuum limit. This enables to find a dimensional mapping in terms of the running mass and coupling parameters of the $4D$–theory at scale μ and temperature T between the lattice renormalization scheme and the renormalization scheme in the continuum chosen to be $\overline{\mathrm{MS}}$, which gets exact in the continuum limit $a \to 0$ [93, 147, 149].

The $3D$ effective $\mathrm{SU}(2) \otimes \mathrm{U}(1)$–Higgs model plays the role of an universal theory, which describes a number of extensions of the MSM like the (extended) MSSM or an electroweak theory with two scalar Higgs doublets. What solely changes when going from one theory to another are the explicit relations between the initial $4D$–parameters and those of the effective model. As the complexity of the lattice discretization caused by the different scales of eq. (19) is in part avoided by having integrated over the smallest length scale proportional to $(2\pi T)^{-1}$ before — thus making the numerical simulations technically less demanding — the method of dimensional reduction is assumed to be justified for $30\ \mathrm{GeV} \lesssim m_H \lesssim 240\ \mathrm{GeV}$ [96].

An obvious disadvantage of dimensional reduction is, however, that in order to obtain the simplest possible, local effective theory, one neglects higher-dimensional radiatively generated operators with smaller coefficients and non-local operators ensued at high-loop orders too. From this feature one can infer the danger that in taking only this simple three-dimensional form of the action instead of the more general multi-parameter action, there may arise discrepancies in its reliability to represent the 'true' theory in the perturbative region deeply inside the Higgs phase, where it has been optimized, and at the same time near the phase transition or in the symmetric phase. At least two further open questions in this integration procedure, which give rise to occasion for some criticism, should be stressed: Firstly, the gauge coupling g is not that small, i.e. the infinitely many heavy modes, which have been integrated out, are still close to the excitations left in the theory, and secondly, since in the three-dimensional effective theory all modes to be integrated over are more massive than the temperature scale $\mathcal{O}(T)$, it should rather be treated as a cutoff theory with non-local terms instead of merely studying the continuum limit and neglecting the latter. On the contrary, recall that by construction the anisotropic lattice approach to the original theory in four

dimensions does not suffer from these problems. Hence, although the dimensional reduction technique can be used successfully to test classes of EWPT models, neither its correctness nor its efficiency can be stated doubtlessly, and the quality of the approximations involved, which in practice are difficult to estimate quantitatively, have to be controlled. So the hope is that the combined outcome of resummed perturbation theory and of reduced and, in particular, four-dimensional unreduced numerical simulations will yield a complete understanding of the thermodynamics of the EWPT.

Recently, as referred to before, one has also addressed the question, whether the EWPT line separating the symmetric phase from the broken phase ends at some critical Higgs mass $m_H^{(\mathrm{crit})}$, and what could replace it at slightly larger m_H. The groups employing the approach of dimensional reduction in combination with MC simulations of the $3D$–theory have meanwhile given strong support that the first order EWPT ceases to exist at $m_H^{(\mathrm{crit})} \lesssim 80$ GeV, i.e. it becomes a transition of the second kind at $m_H = m_H^{(\mathrm{crit})}$, and turns into a sharp but already smooth crossover at larger m_H–values. In this part of parameter space the system would behave very regularly, without any long-range order and strong deviations from thermal equilibrium. Their arguments are based on different attempts to determine the value of the upper critical Higgs mass numerically, either by investigating the volume dependence of the susceptibility of the scalar (Higgs) condensate [149], by plainly inquiring for a vanishing of the discontinuity of the scalar condensate itself (which is proportional to the latent heat [152]), or by an analysis of the Lee-Yang zeroes of the partition function, whose breakdown of finite-size scaling at $m_H \simeq m_H^{(\mathrm{crit})}$ is able to indicate the change of a first order transition into an analytic crossover [145, 152]. However, the exact position of this endpoint is still some matter of debate and prolonged research activity.

The present results from all the intensive studies within the various frameworks mentioned above, which disfavour every scenario of electroweak baryogenesis relying on a strong first order EWPT within the MSM, can be summarized to the statement that the constraint (17) does not hold for any physically realistic Higgs mass in the MSM, also if the influence of the mass of the top quark $m_{\mathrm{t}} \simeq 175$ GeV and/or the U(1)–gauge group factor are included into the calculations[7] [147, 149, 152]. Therefore, it is extremely improbable that there are any observational cosmological remnants coming from the electroweak epoch in the history of the early universe. However, it appears still possible to satisfy this constraint in a specific portion of parameter space in the low-energy MSSM, where the critical Higgs mass $m_H^{(\mathrm{crit})}$, beyond which the first order phase transition changes into an analytic crossover, can be significantly larger than in the MSM. In addition, the MSSM contains some extra sources of CP–violating phases arising from the soft-supersymmetry breaking parameters associated with the stop mixing angle. Here the baryogenesis window is bordered by the restrictions of

[7] For instance, it was shown in ref [147] within the $3D$–model that the influence of the fermions leads to a significant shift in the critical temperature T_c, whereas the the ratio $v(T_c)/T_c$ stays roughly unaffected (below 3 %).

the lightest stop mass being smaller than the top mass, the lightest Higgs boson mass lying below 80 GeV, the pseudoscalar Higgs boson being heavier than 130 GeV, and the ratio of scalar vacuum expectation values fulfilling $\tan\beta \lesssim 3$ [155].

Nevertheless, I have to emphasize that the four-dimensional SU(2)–Higgs model and the synthesis of analytical and numerical methods applied to it retain their importance as a theoretical laboratory for the electroweak sector of the MSM. Endowed with the qualitative as well as quantitative insights from this model, it may than be placed into a broader context of multi-Higgs or supersymmetric extensions of the MSM in the near future, where further progress has to be expected in forthcoming explorations. Finally, if thereupon the emerging picture will be indeed such that the observed baryon asymmetry of the universe can naturally be explained within extended versions of the MSM, this prospect would be particularly fascinating as the involved physics at the electroweak scale will be probed experimentally in LEP2 and the LHC at CERN relatively soon.

Part I:
The $2D$ U(1)–Higgs Model

Chapter 1

The model

In this chapter I describe the model under study in its continuum and lattice formulations. Then the basic observables, which have been used in the numerical investigations presented later, are introduced, and I conclude with some short remarks on the limiting cases of the model. These allow for useful cross-checks of its numerical implementation as discussed in the next chapter.

1.1 Continuum and lattice model

After Wick rotation from Minkowski to Euclidean space the two-dimensional U(1)–Higgs model is given by the continuum action

$$S[A,\phi_0] = \int \mathrm{d}^2x\, \mathcal{L}(x)\,, \quad \mathcal{L}(x) = \mathcal{L}_\mathrm{g}(x) + \mathcal{L}_\phi(x) \tag{1.1}$$

with local Lagrange densities

$$\mathcal{L}_\mathrm{g}(x) = \frac{1}{4}\, F_{\mu\nu}(x) F_{\mu\nu}(x) \tag{1.2}$$

$$\mathcal{L}_\phi(x) = \frac{1}{2}\, |D_\mu \phi_0(x)|^2 + \frac{1}{2}\, m_0^2 |\phi_0(x)|^2 + \frac{\lambda_0}{4!}\, |\phi_0(x)|^4 + \frac{3}{2}\, \frac{m_0^4}{\lambda_0} \tag{1.3}$$

in terms of the charged scalar Higgs field $\phi_0(x) \in \mathbb{C}$ and the gauge field $A_\mu(x) \in \mathbb{R}$, which are coupled via the covariant derivative $D_\mu = \partial_\mu - ie_0 A_\mu(x)$ with bare gauge coupling e_0, ensuring the invariance of the model under local U(1)–gauge transformations

$$\phi_0(x) \to \phi_0'(x) = \mathrm{e}^{-i\alpha(x)}\, \phi_0(x)\,, \quad A_\mu(x) \to A_\mu'(x) = A_\mu(x) - \frac{1}{e_0}\, \partial_\mu \alpha(x) \tag{1.4}$$

with $\alpha(x) \in \mathbb{R}$. The field strength $F_{\mu\nu}(x) = \partial_\mu A_\nu(x) - \partial_\nu A_\mu(x)$, $\mu,\nu \in \{1,2\}$, is gauge invariant, and the constant in (1.3) has been added to combine the quadratic and the quartic self-interaction terms to

$$\mathcal{L}_\phi = \frac{1}{2}\, |D_\mu \phi_0|^2 + \frac{\lambda_0}{4!} \left(|\phi_0(x)|^2 - v_0^2 \right)^2, \tag{1.5}$$

where $v_0 = |\langle\phi_0\rangle|$ is interpreted as the classical vacuum expectation value of the Higgs field,

$$v_0^2 = \frac{3\,\overline{m}_0^2}{\lambda_0}\,, \quad m_0^2 \equiv -\frac{1}{2}\,\overline{m}_0^2\,, \tag{1.6}$$

which marks the minima of the classical potential, i.e. the second term in eq. (1.5). Its general shape is a two-dimensional, rotational symmetric double-well in the field space spanned by $\mathrm{Re}\,\phi_0$ and $\mathrm{Im}\,\phi_0$, whose minima lie on a circle with radius v_0. Thus the particle content of the theory can be read off from this potential by distinction between its two phases in dependence of the sign of the bare mass squared[1]. More precisely, there is a symmetric phase for $m_0^2 > 0$ with a massive scalar particle (charged meson) of bare mass m_0^2 and its antiparticle, and a broken symmetry phase for $m_0^2 < 0$, where the Higgs phenomenon takes place and Higgs and vector bosons (neutral scalar and vector mesons) of bare masses

$$m_{H,0}^2 = \overline{m}_0^2 = \frac{\lambda_0 v_0^2}{3}\,, \quad m_{W,0}^2 = e_0^2 v_0^2 \tag{1.7}$$

are present. The Higgs field vacuum expectation value drops out in the dimensionless mass ratio

$$R_{HW,0}^2 \equiv \frac{m_{H,0}^2}{m_{W,0}^2} = \frac{\lambda_0}{3e_0^2}\,, \tag{1.8}$$

whose non-perturbatively renormalized generalization will prove to be an important quantity for the continuum limit of the lattice model. The bare masses in (1.7) are most easily derived in the unitary gauge. This amounts to decompose $\phi_0(x) = \rho(x)\,\mathrm{e}^{\,i\omega(x)}$ and fix $\alpha(x) \equiv \omega(x)$ so that $\phi_0'(x) = \rho(x) \in \mathbb{R}^{\geq 0}$ and $A_\mu'(x) = A_\mu(x) - \frac{1}{e_0}\,\partial_\mu\omega(x) \equiv B_\mu(x)$ from eq. (1.4). In the symmetric phase the field $B_\mu(x)$ would naively resemble a massless photon, which is, however, no physical degree of freedom in two dimensions because of the lack of any transverse direction.

One could wonder, why no higher even powers of ϕ_0 enter the scalar part (1.3) of the action. Due to the dimensionlessness of the scalar field in two dimensions, see below, such terms are in principle not ruled out a priori as e.g. in four dimensions, where they are irrelevant on dimensional grounds in the classification of renormalization group theory. But the two-dimensional model is superrenormalizable and as a consequence, operators of higher order play no rôle from the start, since the renormalization process does not generate any new, i.e. field dependent operators as counterterms in Lagrangian [1, 4].

The lattice regularization of the model proceeds in the standard fashion [19]. Referring to the notational conventions in appendix A.1, eqs. (1.1) – (1.3) are discretized according to

$$\int \mathrm{d}^D x \;\longrightarrow\; a^D \sum_{x\in\Lambda}\,, \quad D\text{: space-time dimension}\,, \tag{1.9}$$

[1]This is closely analogous to the field theoretic approach to investigations of critical phenomena and second order phase transitions within the Landau-Ginzburg model of statistical mechanics [3, 4].

with the additional requirement that the desired lattice action (as well as the initial continuum action with a scalar field $\phi_0(x)$ of canonical, 'engineering' mass or rather inverse length dimension $(D-2)/2$ for arbitrary D) has to be dimensionless. If one substitutes the lattice version of the covariant derivative (A.6) and redefines the continuum variables by their lattice counterparts,

$$\phi_0(x) = \sqrt{2\kappa}\,\varphi_x\,, \quad a^2\lambda_0 = \frac{6\lambda}{\kappa^2}\,, \quad a^2 m_0^2 = \frac{1-2\lambda}{\kappa} - 4\,, \tag{1.10}$$

the scalar field part of the lattice action becomes

$$S_\phi[U,\varphi] = \sum_{x\in\Lambda}\left\{-2\kappa\sum_{\mu=1}^{2}\mathrm{Re}\left(\varphi^*_{x+\hat{\mu}}U_{x,\mu}\varphi_x\right) + |\varphi_x|^2 + \lambda\Big(|\varphi_x|^2-1\Big)^2\right\} \tag{1.11}$$

modulo a constant contribution of $(1-2\lambda-4\kappa)^2/4\lambda - \lambda$ for each lattice point $x\in\Lambda$. The scalar field $\varphi_x\in\mathbb{C}$ lives on the lattice sites, and $U_{x,\mu}\in\mathrm{U}(1)$ in the compact formulation, representing the gauge degrees of freedom, denotes a directed link from x to $x+\hat{\mu}$ in lattice direction $\mu\in\{1,2\}$, see figure 1.1. The discretization of the pure gauge field part (1.2) yields the commonly known Wilson action

$$S_{\mathrm{g}}[U] = \beta\sum_{x\in\Lambda}\Big(1-\mathrm{Re}\,U_{\mathrm{p},x}\Big) \tag{1.12}$$

with the identification

$$\beta = \frac{1}{a^2 e_0^2}\,, \tag{1.13}$$

which reproduces the continuum expression (1.2) up to errors of order $\mathcal{O}(a^2)$. The sum in eq. (1.12) goes over all oriented plaquettes $U_{x;\mu\nu}$, $1\le\mu<\nu\le D$, attached to the lattice sites $x\in\Lambda$. For $D=2$ these are the ordered link products

$$U_{\mathrm{p},x} = U_{x;12} \equiv U_{x,1}U_{x+\hat{1},2}U^*_{x+\hat{2},1}U^*_{x,2} \tag{1.14}$$

as also depicted in figure 1.1. The relation of the link variables to the continuum gauge fields $A_\mu(x)$ is supplied by the phases $A_{x,\mu}$ in

$$U_{x,\mu} = \mathrm{e}^{\,iA_{x,\mu}}\,, \tag{1.15}$$

and the choice $A_{x,\mu}\in[-\pi,\pi)$ would guarantee

$$A_{x,\mu} = e_0 a A_\mu(x)\,, \quad \tilde{F}_{x;\mu\nu} \equiv A_{x+\hat{\mu},\nu} - A_{x,\nu} - A_{x+\hat{\nu},\mu} + A_{x,\mu}\,, \tag{1.16}$$

in the formal continuum limit $a\to 0$. However, on physical grounds it is more natural to restrict the phases of gauge invariant link combinations to the standard interval $[-\pi,\pi)$. Hence, I introduce the lattice field strength F_x through

$$U_{\mathrm{p},x} = \mathrm{e}^{\,iF_x}\,, \quad F_x \equiv \tilde{F}_{x;12} - 2\pi\,\mathcal{NI}\left(\frac{\tilde{F}_{x;12}}{2\pi}\right)\in[-\pi,\pi)\,, \quad \mathcal{NI}\,(\cdot)\text{: next integer} \tag{1.17}$$

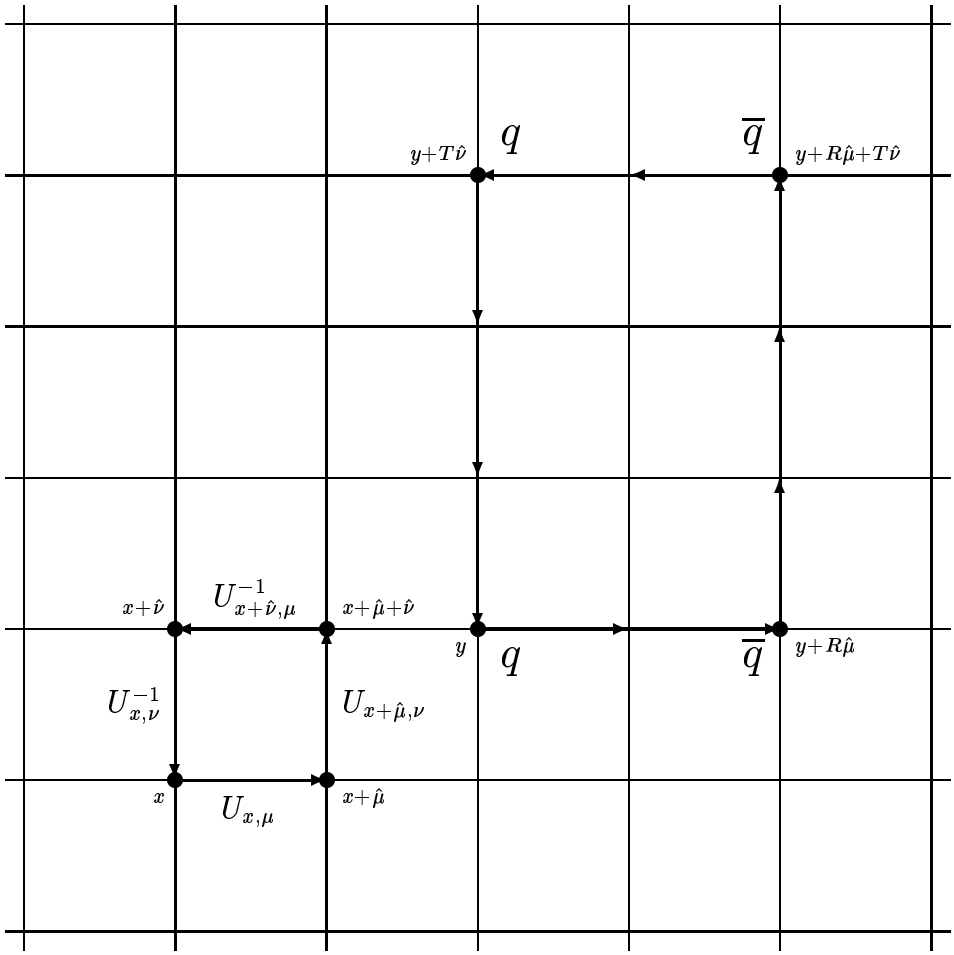

Figure 1.1: *Part of a lattice plane with* ***1.) left object:*** *four directed link variables building an elementary lattice plaquette* $U_{x;\mu\nu}$ *with* $U^{-1}_{x,\mu} = U_{x+\hat{\mu},-\mu}$ *and* $U^{-1}_{x,\mu} = U^{*}_{x,\mu}$, *and* ***2.) right object:*** $R \times T$ *Wilson loop* $U_{\mathcal{C}_{R,T}}$ *of a* $q\overline{q}$*–pair around a lattice path* $\mathcal{C}_{R,T}$ *as introduced in section 1.2. Here is* $R = 2$ *and* $T = 3$, *and in two dimensions* $\mu = 1$ *and* $\nu = 2$.

so that the continuum field strength $F_{\mu\nu}(x)$ in $D = 2$ is recovered to be

$$a \to 0 : \quad F_x = e_0 a^2 F_{12}(x) \tag{1.18}$$

with the coupling e_0 absorbed. The phases $A_{x,\mu}$ are then determined in arbitrary gauge by the demand to strictly obey the lattice version of Stokes' theorem $F = \mathrm{d}A$ [52, 73]. An avoidance of any $\mathrm{mod}\, 2\pi$–ambiguities in the lattice field strength F_x by the prescription (1.17) is necessary for unique definitions of the topological charge and fractionally charged Wilson loops in the following section. When the scalar field is further decomposed into length and phase,

$$\varphi_x = \rho_x \, \mathrm{e}^{\, i\omega_x} \,, \quad \rho_x \in \mathbb{R}^{\geq 0} \,, \quad \omega_x \in \mathbb{R} \,, \tag{1.19}$$

the lattice action of the U(1)–Higgs model ultimately reads

$$S[U,\varphi] \;\; = \;\; S_{\mathrm{g}}[U] + S_{\phi}[U,\varphi] \tag{1.20}$$

$$S_{\rm g}[U] = \beta \sum_{x\in\Lambda} \left\{ 1 - \cos\left(A_{x,1} + A_{x+\hat{1},2} - A_{x+\hat{2},1} - A_{x,2} \right) \right\} \tag{1.21}$$

$$S_{\phi}[U,\varphi] = \sum_{x\in\Lambda} \left\{ -2\kappa \sum_{\mu=1}^{2} \rho_x \rho_{x+\hat{\mu}} \cos B_{x,\mu} + \rho_x^2 + \lambda \left(\rho_x^2 - 1\right)^2 \right\} \tag{1.22}$$

and is well suited for numerical simulations. Here the gauge invariant φ–link phases $B_{x,\mu}$ in the scalar part,

$$B_{x,\mu} \equiv -\omega_{x+\hat{\mu}} + A_{x,\mu} + \omega_x \,, \tag{1.23}$$

equal the gauge fields $A_{x,\mu}$ in the unitary gauge, which has $\omega_x \equiv 0$ and $\varphi_x \equiv \rho_x$. The functional integral over field space of the continuum theory now becomes a generically infinite product of ordinary integrations over all lattice sites and every field degree of freedom allocated to them[2].

The lattice parameters of the model are β for the gauge field dynamics, the scalar hopping parameter κ in front of the kinetic in eq. (1.22), and the coupling λ, which is responsible for the fluctuations of the Higgs field length (radial) mode ρ_x. Together with (1.10) and (1.13) the equations (1.6) – (1.8) directly translate into

$$a^2 m_{H,0}^2 = \frac{2\lambda}{\kappa^2}\, v_0^2 \,, \quad a^2 m_{W,0}^2 = \frac{1}{\beta}\, v_0^2 \,, \quad R_{HW,0}^2 = \frac{2\beta\lambda}{\kappa^2} \tag{1.24}$$

$$v_0^2 = 2\kappa \left(1 + \frac{2\kappa - \frac{1}{2}}{\lambda} \right) \,. \tag{1.25}$$

The bare vector mass $am_{W,0}$ can also be obtained from the leading non-constant contribution in the expansion of the $\cos B_{x,\mu}$–term in the scalar part (1.22) of the action. If the physical, i.e. renormalized masses or the Higgs field vacuum expectation value would approximately fulfill these tree-level relations in a region of parameter space, one could speak of the lattice theory — as the full quantum theory, which implicitly contains all perturbative and non-perturbative corrections by definition — behaving classically. Apart from finite renormalizations, this is merely to be expected for the Higgs to vector mass ratio R_{HW}, since the cancelling v_0^2 embodies the only primitive divergence of the theory in two dimensions.

1.2 Basic observables

I mainly consider gauge invariant, local primary quantities, which already appear in the lattice action per point S_x. Arranging eqs. (1.20) – (1.22) as $S[U,\varphi] = \sum_{x\in\Lambda} S_x$ with

$$S_x = \beta P_{{\rm pl},x} - 4\kappa L_{\varphi,x}^{+} + R_x + \lambda Q_x \,, \tag{1.26}$$

[2]The transformation of the integral measure belonging to (1.19) gives rise to an $\ln \rho_x$–term, which has to be incorporated in (1.22) for all updating algorithms of the Higgs field length ρ_x alone.

I introduce the length variables of the Higgs field,

$$R_x \equiv |\varphi_x|^2 = \varphi_x^* \varphi_x = \rho_x^2 \,, \quad Q_x \equiv (\rho_x^2 - 1)^2 \,, \tag{1.27}$$

the plaquette observable

$$P_{\mathrm{pl},x} \equiv 1 - \mathrm{Re}\, U_{\mathrm{p},x} = 1 - \cos F_x \,, \tag{1.28}$$

and the φ–links

$$L^{\pm}_{\varphi,x} = \frac{1}{2} \sum_{\mu=1}^{2} L^{\pm}_{\varphi;x\mu} \,, \quad L^{\pm}_{\varphi;x\mu} \equiv \left\{ \begin{array}{l} \mathrm{Re}\left(\varphi^*_{x+\hat{\mu}} U_{x,\mu} \varphi_x\right) = \rho_x \rho_{x+\hat{\mu}} \cos B_{x,\mu} \\ \mathrm{Im}\left(\varphi^*_{x+\hat{\mu}} U_{x,\mu} \varphi_x\right) = \rho_x \rho_{x+\hat{\mu}} \sin B_{x,\mu} \end{array} \right. . \tag{1.29}$$

Their expectation values and statistical errors are computed numerically by averaging over the number of lattice points and configurations (measurements) as sketched in section A.3 of appendix A. The non-perturbatively renormalized vacuum expectation value of the Higgs field[3] can be defined with help of the scalar length $\rho_x = |\varphi_x|$ as

$$v_R \equiv \sqrt{2\kappa}\, \langle \rho \rangle \,, \quad \langle \rho \rangle = \langle \varphi \rangle \Big|_{\text{unitary gauge}} . \tag{1.30}$$

1.2.1 Wilson and Polyakov loops

Beyond the former observables, I measured Wilson loops of space-time extensions R and T,

$$W(R,T) \equiv \left\langle \mathrm{Re}\, U_{\mathcal{C}_{R,T}} \right\rangle \,, \tag{1.31}$$

where $U_{\mathcal{C}_{R,T}}$ stands for the ordered link product around a rectangular closed path $\mathcal{C}_{R,T} \in \Lambda$ of extensions $R \times T$, and each lattice loop with this geometry is meant to be included in the expectation value. They are gauge invariant by construction and, as illustrated in figure 1.1 of section 1.1 for the two-dimensional case with $x = (x_1, x_2) = (\mathrm{x}, t) \in \Lambda$, have an interpretation as the probability for generation of an external, static quark-antiquark $(q\overline{q})$ pair at Euclidean time $t = 0$, its propagation in space from x = 0 to x = R, and later annihilation at time $t = T$.

The Wilson loops are known to offer a criterion for static quark confinement. To see this, let $\mathcal{H}_{q\overline{q}}$ be the Hilbert space of the quark-antiquark sector in the Hamiltonian formalism for lattice gauge fields [17, 19], whose states $\Psi^{(n)}$ form a complete set of eigenvectors of the Hamiltonian operator $H_{q\overline{q}}$, i.e.

$$H_{q\overline{q}}\, \Psi^{(n)} = E_n \Psi^{(n)} \,. \tag{1.32}$$

If the spacelike locations $\boldsymbol{x}$ and $\boldsymbol{y}$ of the static quark charges lie on a common lattice axis at distance R, the static quark potential $V(R) \equiv E_0$ is defined as the energy E_0 of the ground

[3] A renormalization factor, which is supposed to tend to unity in the continuum limit, is ignored in this definition.

state $\Psi^{(0)}$ in $\mathcal{H}_{q\bar{q}}$. When inserting a complete set of eigenvectors, one has for an arbitrary $\Psi \in \mathcal{H}_{q\bar{q}}$ and non-vanishing overlap between Ψ and $\Psi^{(0)}$:

$$\langle\Psi|\mathrm{e}^{-TH_{q\bar{q}}}|\Psi\rangle = \sum_n |\langle\Psi^{(n)}|\Psi\rangle|^2\,\mathrm{e}^{-aTE_n} \overset{T\to\infty}{\sim} |\langle\Psi^{(0)}|\Psi\rangle|^2\,\mathrm{e}^{-aTV(R)}\,. \tag{1.33}$$

The gauge invariant left hand side of this equation can in temporal (axial) gauge just be identified with $W(R,T)$ so that the important relation

$$aV(R) = -\lim_{T\to\infty}\frac{1}{T}\ln W(R,T) \tag{1.34}$$

follows. Two characteristic asymptotic behaviours of large Wilson loops are then to be distinguished. Namely, there is static quark confinement for loops obeying the area law

$$W(R,T) \overset{R,T\to\infty}{\sim} C\,\mathrm{e}^{-\alpha RT}\,, \tag{1.35}$$

which gives a linearly rising potential

$$aV(R) \overset{R\to\infty}{\sim} \alpha R\,, \quad \alpha \equiv -\lim_{R\to\infty}\frac{1}{R}aV(R) \tag{1.36}$$

with α called the string tension, or a perimeter law behaviour

$$W(R,T) \overset{R,T\to\infty}{\sim} c\,\mathrm{e}^{-\mu(R+T)}\,, \tag{1.37}$$

which is typical for Higgs and Coulomb phases in lattice gauge theories without matter fields.

Returning to two dimensions, the pure gauge theory, presently equivalent to pure (1+1)–dimensional quantum electrodynamics (QED) and one of the limiting cases in the next section, can provide a nice check for numerical Wilson loop calculations in this context. There the infinite-volume formula

$$W(R,T) = \left[\frac{I_1(\beta)}{I_0(\beta)}\right]^A \tag{1.38}$$

holds [17, 19, 45], $A = RT$ the area enclosed by the Wilson loop in lattice units and $I_k(\beta)$, $k \in \mathbb{Z}$, the modified Bessel functions of order k, and the static potential is

$$V(R) = -\ln\left[\frac{I_1(\beta)}{I_0(\beta)}\right]\cdot R \overset{\beta\to\infty}{\sim} \frac{R}{2\beta} = \frac{a^2e_0^2R}{2}\,, \tag{1.39}$$

which reproduces the linear continuum Coulomb potential in one space dimension after expansion of the modified Bessel functions for large arguments [17, 189]. It can be shown by a strong (gauge) coupling calculation that eq. (1.38) is also a good approximation on finite lattices for small enough β, and in fact it was possible to confirm its right hand side by numerical simulations with a proper choice of the lattice parameters, e.g. for the plaquette $\langle\cos F\rangle = W(1,1)$ on a 16×16 lattice with $\beta = 10.0$ and scalar hopping parameter $\kappa = 0$ the agreement was still better than 1 %.

For an external test source q of fractional charge, q being non-integer, I use the identity for the Wilson loop integral in the continuum

$$\begin{aligned} W_q[\mathcal{A}] &\equiv \left\langle \mathrm{Re}\,\exp\left\{ iq \oint_{\partial\mathcal{A}} \mathrm{d}x_\mu A_\mu(x) \right\} \right\rangle \\ &= \left\langle \mathrm{Re}\,\exp\left\{ iq \int_{\mathcal{A}} \mathrm{d}^2x\, F_{12}(x) \right\} \right\rangle , \quad \mathcal{A}\text{: two-dimensional area} \end{aligned} \tag{1.40}$$

to obtain a unique lattice prescription for the corresponding Wilson loop in the compact formulation,

$$W_q(R,T) = \left\langle \mathrm{e}^{\,iq\sum_{x\in\mathcal{A}_{R,T}} F_x} \right\rangle , \tag{1.41}$$

with $\mathcal{A}_{R,T} \subset \Lambda$ as area of the path $\mathcal{C}_{R,T} = \partial\mathcal{A}_{R,T}$. The restriction of the lattice field strength to $F_x \in [-\pi,\pi)$ realized in eq. (1.17), together with the lattice analogue of Stokes' theorem $F = \mathrm{d}A$ to establish the gauge link phases $A_{x,\mu}$, leaves no $\mathrm{mod}\,2\pi$–ambiguities, which would arise for the standard form in terms of $A_{x,\mu}$–sums as inferred from the definition (1.31). Moreover, this makes sense opposed to $A_{x,\mu} \in [-\pi,\pi)$, because F_x is gauge invariant, and $\beta \to \infty$ ($a \to 0$) forces $F_x \propto a^2$ to vanish faster than $A_{x,\mu} \propto a$, whereas the latter may stay non-zero on single links, e.g. in vortices.

A special case are the Polyakov loops as world lines of a static quark in a Wilson loop, i.e. for $D = 2$ with $x = (x_1, x_2) \in \Lambda$,

$$L_{\mathrm{P}} \equiv \left\langle \frac{1}{L_1} \sum_{x_1=1}^{L_1} \mathrm{Re} \prod_{x_2=1}^{L_2} U_{x,2} \right\rangle \tag{1.42}$$

or, respectively, the Polyakov loop correlations

$$P(R) \equiv \left\langle \frac{1}{L_1} \sum_{x_1=1}^{L_1} \left(\mathrm{Re} \prod_{x_2=1}^{L_2} U^*_{x,2} \right) \left(\mathrm{Re} \prod_{x_2=1}^{L_2} U_{x+R\hat{\imath},2} \right) \right\rangle = W(R,T)\Big|_{T=L_2} , \tag{1.43}$$

whose extension to fractional charges is

$$P_q(R) \equiv W_q(R,T)\Big|_{T=L_2} \tag{1.44}$$

with the Wilson loops to be computed according to eq. (1.41). The affiliated static potential is now defined in view of eq. (1.34) through these Polyakov loop correlations as

$$V_q(R) \equiv -\frac{1}{q^2 L_2} \ln P_q(R) \tag{1.45}$$

and will enter the scenery in sections 3.4 and 4.1 of the later chapters.

1.2.2 Topological charge

Let M be the two-dimensional manifold of compactified Euclidean space-time with boundary ∂M supposed to be a one-sphere S^1. Throughout the perimeter of M, which as a circle can be

parametrized by an angle θ, the field variables of the theory must approach a pure gauge form, i.e. their boundary conditions on S^1 are $\phi_0(x)\,|_{S^1} = C\,\mathrm{e}^{\,i\alpha(\theta)}$ and $A_\mu(x)\,|_{S^1} = \frac{i}{e_0}\,\mathrm{e}^{\,i\alpha(\theta)}\partial_\mu \mathrm{e}^{\,-i\alpha(\theta)}$ with some constant C and function $\alpha(\theta) \in \mathbb{R}$. Then the topological charge in the continuum reads

$$Q_{\mathrm{top}} \equiv \frac{e_0}{4\pi}\int_M \mathrm{d}^2x\,\epsilon_{\mu\nu}F_{\mu\nu}(x) = \frac{e_0}{2\pi}\int_M \mathrm{d}^2x\,F_{12}(x)\,. \tag{1.46}$$

With $U^*_{x;12} = U_{x;21}$ from (1.14) its naive lattice discretization involving the field strength F_x in (1.17) of section 1.1 is

$$Q_{\mathrm{top}}^{(\mathrm{naive})} = \frac{1}{4\pi i}\sum_{x\in\Lambda}\epsilon_{\mu\nu}U_{x;\mu\nu} = \frac{1}{4\pi i}\sum_{x\in\Lambda}\left(U_{x;12} - U^*_{x;12}\right) = \frac{1}{2\pi}\sum_{x\in\Lambda}\sin F_x\,. \tag{1.47}$$

This charge converges with a rate $Q_{\mathrm{top}}^{(\mathrm{naive})} = \frac{e_0}{2\pi}\sum_{x\in\Lambda}a^2F_{12}(x) + \mathcal{O}(a^3)$ to the continuum expression (1.46) and is not necessarily integer-valued.

I adopt the geometrical lattice definition of the topological charge instead [37, 40], which relies upon the existence of a piecewise continuous and differentiable interpolation of the lattice gauge field. More precisely, the procedure consists of gauge fixing and using a sensible interpolation to reconstruct a smooth gauge field from the discrete lattice data. For a finite lattice with the topology of a — in the general case four-dimensional — torus, the topological information contained in the actual continuum gauge configuration resides in the so-called transition functions, which connect the gauge fields on the boundaries of the elementary lattice cells. In the two-dimensional theory this construction simplifies to the sum of the uniquely projected plaquette angles

$$Q_{\mathrm{top}} = \frac{1}{2\pi}\sum_{x\in\Lambda}F_x\,, \quad F_x \in [-\pi,\pi)\,. \tag{1.48}$$

Proof:
In fact, it is possible to duplicate the explicit construction quite lucidly in the case of two dimensions. Following refs. [38, 43], I introduce the cells

$$c(x) \equiv \{\mathfrak{x}\in\mathbb{R}^2 \,|\, \forall\mu : 0 \le (\mathfrak{x}_\mu - x_\mu) \le 1\}\,, \quad x\in\Lambda\subset\mathbb{Z}^2\,,$$

covering the torodial lattice $\Lambda = \mathbb{T}^2$, which is thought to be embedded in $\mathbb{R}^2$. They intersect along the faces $f(x,\mu) \equiv c(x)\cap c(x-\hat{\mu})$. According to the fibre bundle construction in the continuum [7, 8], the whole information about the topology of the gauge field configuration is carried by the transition functions defined on the boundaries of regions, in which a non-singular gauge potential can be defined in a global way. They take values in the gauge group and, denoted as $v_{x,\mu}(\mathfrak{x})$ when transcribed into the setup on the lattice, relate the gauge potentials $A_{x,\nu}$ and $A_{x-\hat{\mu},\nu}$ of the neighbouring cells $c(x)$ and $c(x-\hat{\mu})$ on the faces $f(x,\mu)$ by a transformation of the type $A_{x-\hat{\mu},\nu} = A_{x,\nu} + i\,v^{-1}_{x,\mu}(\mathfrak{x})\,\partial_\nu\,v_{x,\mu}(\mathfrak{x})$. At the corner of four overlapping cells the transition functions must satisfy the cocycle condition $v_{x-\hat{\mu},\nu}(\mathfrak{x})v_{x,\mu}(\mathfrak{x}) = v_{x-\hat{\nu},\mu}(\mathfrak{x})v_{x,\nu}(\mathfrak{x})$, and at the corners of the faces they equal $v_{x,\mu}(\mathfrak{x}) = w_{x-\hat{\mu}}(\mathfrak{x})w^{-1}_x(\mathfrak{x})$, where

the parallel transporter $w_x(\mathfrak{x})$ is used to gauge fix the links to the complete axial gauge in each cell. By interpolation this formula is extended to the whole face, and the interpolating fields in the interior of the cells [37] appear in two dimensions with $y = x$ or $y = x - \hat{\mu}$, $\mu \neq \nu \in \{1, 2\}$, and $0 \leq \mathfrak{x} \leq 1$ to be explicitly

$$v_{x,\mu}(\mathfrak{x}) = \left[\, s^{x-\hat{\mu}}_{x,\mu}(\mathfrak{x}) \,\right]^{-1} v_{x,\mu}(x) \left[\, s^{x}_{x,\mu}(\mathfrak{x}) \,\right], \quad s^{y}_{x,\mu}(\mathfrak{x}) = \Big[w_y(x) U_{x,\nu} w_y^{-1}(x + \hat{\nu}) \Big]^{\mathfrak{x}}.$$

In passing from continuum to the lattice, the original definition (1.46) can now be written in terms of these lattice quantities, which absorb the gauge coupling e_0, as

$$\begin{aligned} Q_{\text{top}} \;=\; \frac{e_0}{4\pi} \int_M \mathrm{d}^2x\, \epsilon_{\mu\nu} F_{\mu\nu}(x) \;&=\; \frac{1}{2\pi} \sum_{x\in\Lambda} \sum_{\nu=1}^{2} \int_{\partial c(x)} \mathrm{d}\mathfrak{x}_\nu \, A_{x,\nu} \\ &=\; \frac{i}{2\pi} \sum_{x\in\Lambda} \sum_{\mu,\nu=1}^{2} \epsilon_{\mu\nu} \int_{f(x,\mu)} \mathrm{d}\mathfrak{x}\, v^{-1}_{x,\mu}(\mathfrak{x})\, \partial_\nu\, v_{x,\mu}(\mathfrak{x}) \\ &=\; \sum_{x\in\Lambda} q(x) \;=\; \sum_{x\in\Lambda} \sum_{\mu=1}^{2} (-1)^\mu \left(k_{x,\mu} - k_{x+\hat{\mu},\mu} \right) \end{aligned}$$

with surface integrals over the faces of the lattice cells, whose integrands are total divergences:

$$(-1)^\mu k_{y,\mu} = -\frac{\epsilon_{\mu\nu}}{2\pi i} \int_{f(x,\mu)} \mathrm{d}\mathfrak{x} \, \left[\, s^{x}_{y,\mu}(\mathfrak{x}) \,\right]^{-1} \partial_\nu \left[\, s^{x}_{y,\mu}(\mathfrak{x}) \,\right] = -\frac{\epsilon_{\mu\nu}}{2\pi i} \int_{f(x,\mu)} \mathrm{d}\mathfrak{x}\, \partial_\nu \ln \left[\, s^{x}_{y,\mu}(\mathfrak{x}) \,\right].$$

After putting in $s^x_{y,\mu}(\mathfrak{x})$, $y = x, x - \hat{\mu} \in \Lambda$, from above and evaluating the integrals together with eq. (1.14) and the U(1)–valued link variables $U_{x,\mu}$ fulfilling $U^{-1}_{x,\mu} = U^*_{x,\mu}$, some little algebra gives

$$\begin{aligned} q(x) \;&=\; \frac{1}{2\pi i} \Big\{ \ln \Big[w_x(x + \hat{1}) U_{x+\hat{1},2} w_x^{-1}(x + \hat{1} + \hat{2}) \Big] - \ln \Big[w_x(x + \hat{2}) U_{x+\hat{2},1} w_x^{-1}(x + \hat{2} + \hat{1}) \Big] \\ &\quad - \ln \Big[w_x(x) U_{x,2} w_x^{-1}(x + \hat{2}) \Big] + \ln \Big[w_x(x) U_{x,1} w_x^{-1}(x + \hat{1}) \Big] \Big\} \\ &=\; \frac{1}{2\pi i} \ln \Big[U_{x,1} U_{x+\hat{1},2} U^{-1}_{x+\hat{2},1} U^{-1}_{x,2} \Big] \;=\; \frac{1}{2\pi i} \ln U_{\mathrm{p},x} \end{aligned}$$

for the lattice topological charge density $q(x)$ to be summed over all sites $x \in \Lambda$. Restricting the logarithm to its main branch $\ln U_{\mathrm{p},x} \in [-\pi, \pi)$, one recovers the lattice field strength in the plaquettes $U_{\mathrm{p},x} = U_{x;12} = \mathrm{e}^{\,iF_x}$, $F_x \in [-\pi, \pi)$, from eq. (1.17) and finally arrives at expression (1.48) for Q_{top}, which unambiguously defines the topological charge on a two-dimensional lattice, q.e.d.

The geometrical method provides a well defined topological charge for almost all gauge configurations, apart from the ambiguous assignment of Q_{top} to configurations with $F_x = \pi$ for at least one $x \in \Lambda$. Such finite-action configurations, which separate the different topological sectors on the lattice[4], are called exceptional; the set of these fields has zero

[4] In the continuum these gauge configurations have infinite action.

measure in the functional integral and can be ignored. Moreover, $Q_{\rm top}$ is gauge invariant and takes only integer values. This can be seen from the vanishing of $\sum_{x\in\Lambda}\tilde{F}_{x;12}=0$ on a periodic lattice so that $F_x-\tilde{F}_{x;12}=2\pi n_x$ with a vortex $n_x\in\mathbb{Z}$ and therefore

$$Q_{\rm top}=\sum_{x\in\Lambda} n_x\in\mathbb{Z}\,. \tag{1.49}$$

The naive and geometrical lattice definitions of $Q_{\rm top}$ do only differ by terms of order $\mathcal{O}(F_x^3)$.

The topological susceptibility $\chi_{\rm top}$ is given by the expectation value

$$\chi_{\rm top}\equiv\frac{1}{V}\left\langle Q_{\rm top}^2\right\rangle \tag{1.50}$$

with $V=a^2\Omega=a^2L_1L_2$ being the physical space-time volume in lattice units. In contrast to four dimensions, the topological structure of two-dimensional pure gauge theory is relatively simple, and the leading β–dependence of $\chi_{\rm top}$ is analytically known here. Under the assumption that the local — approximately Gaussian — fluctuations decouple from those of $\chi_{\rm top}$, justified in the limit $\beta\to\infty$, i.e. $a\to 0$ from eq. (1.13) and $\Omega\to\infty$, one splits the gauge field into a topologically trivial fluctuating field with $Q_{\rm top}=0$ and a background field configuration with constant field strength in the minima of the non-trivial topological sectors. Neglecting the former contributions, the topological susceptibility is written as an infinite sum over all these sectors $k\in\mathbb{Z}$,

$$a^2\chi_{\rm top}=\frac{1}{\Omega}\left\langle k^2\right\rangle\simeq\frac{1}{\Omega}\,\frac{\sum_{k\in\mathbb{Z}}k^2\,\mathrm{e}^{\,-S_k}}{\sum_{k\in\mathbb{Z}}\mathrm{e}^{\,-S_k}}\,, \tag{1.51}$$

with S_k and $F_{k,x}$ as pure gauge action (1.12) and field strength of the sector with $Q_{\rm top}=k$, respectively:

$$S_k=\beta\sum_{x\in\Lambda}\frac{1}{2}\,F_{k,x}^2=\frac{2\pi^2\beta}{\Omega}\,k^2\,,\quad F_{k,x}=\frac{2\pi k}{\Omega}\,. \tag{1.52}$$

After replacing the sums by integrals in the $\beta\to\infty$ and infinite-volume limits, one can perform the Gaussian integrations to get the behaviour

$$\beta\to\infty\,,\,\Omega\to\infty:\quad a^2\chi_{\rm top}\longrightarrow\frac{1}{4\pi^2\beta}\,. \tag{1.53}$$

Higher corrections in $1/\beta$ are available in an advanced derivation [45] by strong coupling expansion techniques in terms of Bessel functions similar to eqs. (1.38) and (1.39), but their knowledge is not necessary for the sequel.

1.2.3 Correlation functions

The particle masses of the theory in lattice units are basically extracted from correlation functions of gauge invariant, local operators at zero momentum [19]. To this end the relevant

operators O_x are averaged within the timeslices at $1 \leq t \leq L_t$ of volume $\Omega_s = L_1 L_2 L_3$ by summing over the spacelike coordinates $\boldsymbol{x}$ in $x = (\boldsymbol{x}, t) \in \Lambda$,

$$O(t;\boldsymbol{p}) = \frac{1}{\sqrt{\Omega_s}} \sum_{\boldsymbol{x}} \mathrm{e}^{\,i\boldsymbol{p}\cdot\boldsymbol{x}} O_x \,, \tag{1.54}$$

because this projects onto intermediate states with spatial components $\boldsymbol{p}$ of the lattice momentum $p = (\boldsymbol{p}, p_4)$. Inserting a complete set of eigenstates $\Psi^{(n)}$ of the Hamiltonian H, only the lightest state $\Psi^{(0)}$ of lowest energy lying above the vacuum it acts on, which has the quantum numbers of O_x and likewise a non-vanishing overlap with it, dominates the correlation function for large t:

$$\begin{aligned} \langle O(t;\boldsymbol{p}) O(0;\boldsymbol{p}) \rangle &= \langle 0 | O(0;\boldsymbol{p})\, \mathrm{e}^{-Ht} O(0;\boldsymbol{p}) | 0 \rangle \\ &= \sum_n \left| \langle \Psi^{(n)} | O(0;\boldsymbol{p}) | 0 \rangle \right|^2 \mathrm{e}^{-aE_n t} \\ &\overset{t\to\infty}{\sim} \left| \langle \Psi^{(0)} | O(0;\boldsymbol{p}) | 0 \rangle \right|^2 \mathrm{e}^{-aE_0 t} \,. \end{aligned} \tag{1.55}$$

If there is a single-particle state in a given channel, the lowest energy in the spectrum of H, isolated by projecting out the zero-momentum ($\boldsymbol{p} = 0$) part of O_x to avoid any nearly degenerate states carrying small spatial momenta, is assigned to the physical mass of this particle. Then the connected correlation functions

$$\langle O(t;\boldsymbol{p}) O(0;\boldsymbol{p}) \rangle_{\mathrm{c}} \equiv \langle O(t;\boldsymbol{p}) O(0;\boldsymbol{p}) \rangle - \langle O(t;\boldsymbol{p}) \rangle \, \langle O(0;\boldsymbol{p}) \rangle \tag{1.56}$$

are shown to be the spatial Fourier transforms of the connected Green functions, and their asymptotic exponential decays at vanishing spatial momenta are governed by the physical masses, which are determined through the complex singularities closest to the origin of the corresponding propagators in momentum space (pole or on-shell masses).

Applied to two dimensions with $x = (x_1, x_2) \in \Lambda$ and $p = (p_1, p_2)$, it follows from the lattice O(2)–symmetry and temporal translation invariance that a product of two timeslice averages (1.54) at distance t is

$$\begin{aligned} O(t;p_1) O(0;p_1) &= \frac{1}{2} \sum_{z_1=1}^{L_1} \cos(p_1 z_1)\, O_0 O_z \,, \quad z \in \Lambda \,,\, 0 \equiv (0,0) \,,\, z_1 = x_1 + y_1 \\ &= \left(\sum_{x_1=1}^{L_1} \cos(p_1 x_1)\, O_x \right) \left(\sum_{y_1=1}^{L_1} \cos(p_1 y_1)\, O_y \right) \,. \end{aligned} \tag{1.57}$$

Hence, the connected timeslice correlation functions (1.56) can actually be calculated as disconnected expectation values

$$\Gamma_O(t;p_1) \equiv \left\langle \frac{1}{\Omega} \sum_{x_2=1}^{L_2} \left(\sum_{x_1=1}^{L_1} \cos(p_1 x_1)\, O_x \right) \left(\sum_{y_1=1}^{L_1} \cos(p_1 y_1)\, O_y \right) \right\rangle \tag{1.58}$$

with $x, y \in \Lambda$, $t = y_2 - x_2 = 0, 1, \ldots, L_2 - 1$, and the shifts of each fixed t–distance in the direction of propagation via the sum over x_2 to enlarge the statistics. Their exponential fall offs on a periodic lattice are expected to have the cosh–like shapes symmetric with respect to the central time distance $t = L_2/2$,

$$\begin{aligned} \Gamma_O(t; p_1) &= A \left[\mathrm{e}^{-Mt} + \mathrm{e}^{-M(L_2 - t)} \right] + C \\ &= 2A\mathrm{e}^{-M\frac{L_2}{2}} \cosh \left[M \left(\frac{L_2}{2} - t \right) \right] + C \,, \end{aligned} \tag{1.59}$$

and for $p_1 = 0$ the decay energy is the physical mass of a particle in the channel under study. The ansatz (1.59) presumes that this lowest state is well separated from all possible excitations of higher energies, whose faster decaying subdominant contributions to the correlation function should be negligibly suppressed already after a few t–distances. The lattice version of the energy-momentum dispersion relation in two dimensions,

$$a^2 m^2 + 2 \left[1 - \cos(a p_1) \right] = 2 \left[\cosh(aE) - 1 \right], \quad p_1 = \frac{2\pi}{a L_1} n_1 \tag{1.60}$$

with $n_1 = 0, 1, \ldots, L_1 - 1$, reducing to the continuum expression when expanding

$$a^2 m^2 + a^2 p_1^2 = a^2 E^2 + \mathcal{O}(a^4 p_1^4, a^4 E^4) \,, \tag{1.61}$$

connects the particle masses with the decay energies $M = aE$ of the correlation functions $\Gamma_O(t; p_1)$ with non-vanishing spatial momenta $p_1 > 0$ and can serve as a consistency check for the reliability of the mass values computed in this way. First estimates of the decay constants in the correlation functions — also useful, for instance, as initial input values of the starting parameters for the χ^2–minimizing routine in the fitting procedure — are obtainable by considering effective masses

$$M_{\mathrm{eff}}(t; L_2) \equiv \operatorname{arcosh} \left\{ \frac{\Gamma_O(t+1; p_1) + \Gamma_O(t-1; p_1)}{2\Gamma_O(t; p_1)} \right\} , \tag{1.62}$$

at time separations $t = 1, \ldots, L_2/2 - 1$, and looking for plateaus in the extrapolation $t \to \infty$, which is limited in practice by the finiteness of the extension L_2. More details and numerical results are given in appendix B.2 and section 3.1.

In general, suitable lattice operators O_x for the mass channels of interest are constructed via their transformations under the discrete lattice symmetries. These are the transformations of the cubic group, to which the rotation group in the continuum characterizing the spin J of a physical state in Hilbert space is broken down on a cubic lattice, the parity P as the space reflection, and charge conjugation parity C being complex conjugation. As elaborated in refs. [50, 19], the eigenstates of the Hamiltonian can now be classified according to the unitary irreducible representations labelled by J^{PC} of the total symmetry group on the lattice, composed from the product of the three kinds of discrete symmetries enumerated before. Usually, the lattice regularization may split the representation, according to which

some state with the desired quantum numbers in the continuum transforms, into a direct sum of irreducible lattice representations. Therefore one must require that the lowest state in the superposition of eigenstates created by O_x from the vacuum, whose mass will dominate the corresponding correlation function, belongs to the component of the lattice decomposition with the correct quantum numbers J^{PC} of the discretized continuum representation.

Due to the fact that there is only one spacelike direction on a two-dimensional lattice, appropriate operators in the Higgs and vector channel are alone distinguished by their parities $P = +1$ and $P = -1$, respectively. This leads to the scalar operators

$$O_x \in \{\rho_x^2, L^+_{\varphi;x1}\} \tag{1.63}$$

for am_H in the Higgs mass channel and to the vector-like operators

$$O_x \in \{L^-_{\varphi;x1}, F_x, \sin F_x\} \tag{1.64}$$

for am_W in the vector mass channel. Viewing at eq. (1.56), a constant contribution to the correlation function $\Gamma_O(t;p_1)$ in (1.58) has to be expected, if $\langle O(t;p_1)\rangle \neq 0$. Since this is the case for scalar operators at zero momentum, whilst vector operators and thus also those of higher momenta have $\langle O(t;p_1)\rangle = 0$, the full three-parametric form of eq. (1.59) is merely employed in the Higgs channel with $p_1 = 0$. In the fits of all other correlation functions the constant C can be safely ignored from the beginning[5].

1.3 Limiting cases

Let me go for an excursion to the limiting cases of the two-dimensional U(1)–Higgs model. In the space of the parameters β, κ, and λ entering the lattice actions presented in section 1.1 they are:

- $\beta = 0$ **or** $\kappa = \infty$ **or** $\lambda = 0$
  These are trivial limits without any physical meaning, because in the first case one gets an ultralocal theory after performing the $U_{x,\mu}$–integrations in the functional integral, and in the second one the theory is frozen due to $U_{x,\mu} \equiv \mathbf{1}$ in the unitary gauge. Both models have no phase transitions in lattice parameter space. Setting $\lambda = 0$ gives a gauged scalar model without interaction (free field theory).

- $\kappa = 0$
  In this limit one arrives at pure gauge theory, since the scalar field action $S_\phi = S_\phi[\varphi]$ has no kinetic term and is ultralocal, leading to a decoupling of gauge and scalar sectors. There is no phase transition with β in two dimensions, and the Wilson loops

[5]Recall that the states created by a product of two vector operators always transform like scalars, i.e. $\Gamma_O(t;p_1)$ does, of course, not vanish for vector-like operators.

obey the area law, signalling the theory to be always confined. The last point is directly deduced from the fact, that in two dimensions, i.e. with only one space dimension, the Coulomb potential is linear in the distance as in eq. (1.39).

- $\beta = \infty$ **and** $\lambda = \infty$
  For $\beta = \infty$, i.e. $ae_0 = 0$, one has a pure scalar model, because $U_{\mathrm{p},x} \equiv \mathbf{1}$, and each $U_{x,\mu}$ becomes a gauge transform of $\mathbf{1}$. Taking also $\lambda = \infty$ gives the fixed length case with $|\varphi_x| \equiv 1$ ('Ising limit'). This is the two-dimensional XY-model with its Kosterlitz-Thouless phase transition [67] at $\kappa = \kappa_c \simeq 0.56$ [70] between a massive vortex phase characterized by excitations of liberated vortex-antivortex pairs ($\kappa < \kappa_c$) and a massless spin wave phase ($\kappa > \kappa_c$). At finite $\beta < \infty$ this transition is expected to become a continuous crossover [54, 22, 56] between analytically connected confinement ($\kappa < \kappa_c$) and Higgs regimes ($\kappa > \kappa_c$). I will come back to this scenario in chapter 4.

- $\beta = \infty$ **and** $\lambda < \infty$
  Again the model is purely scalar, but with variable scalar field lengths $|\varphi_x| = \rho_x \in \mathbb{R}^{\geq 0}$. Now one is brought to the two-dimensional case of two–component ϕ^4–theory ($\phi^4_{n=2}$), which is extensively investigated in the literature with different methods [19, 74, 75, 76, 166, 167].

I want to finish this section with two further tests of the Monte Carlo (MC) program used, which are provided by the limiting cases just mentioned. I begin with the pure gauge theory ($\kappa = 0$), where simple expectation values involving the scalar field length ρ_x can be calculated exactly. Owing to the special, non-interacting form of the scalar field action (1.22) in this case,

$$S_\phi[\varphi] = \sum_{x\in\Lambda} \left\{ \rho_x^2 + \lambda \left(\rho_x^2 - 1\right)^2 \right\} , \tag{1.65}$$

the generating functional for the scalar sector alone reads

$$\begin{aligned} Z_\lambda &= \int \mathcal{D}[\varphi]\, \mathrm{e}^{-S_\phi[\varphi]} = \int \prod_{x\in\Lambda} \mathrm{d}\rho_x\, \rho_x\, \mathrm{e}^{-\sum_{x\in\Lambda}\left\{\rho_x^2 + \lambda(\rho_x^2-1)^2\right\}} \\ &= \Omega \int_0^\infty \mathrm{d}\rho\, \rho\, \mathrm{e}^{-[\,\rho^2+\lambda(\rho^2-1)^2\,]} \equiv \Omega I_\lambda , \end{aligned} \tag{1.66}$$

and the expectation value of an observable $O = O(\{\rho\})$ has the path integral representation, see also eq. (A.10) in appendix A.2,

$$\langle O \rangle_{Z_\lambda} = \frac{1}{Z_\lambda} \int \mathcal{D}[\varphi]\, \mathrm{e}^{-S_\phi[\varphi]}\, O(\{\rho\}) = \frac{1}{I_\lambda} \int_0^\infty \mathrm{d}\rho\, \rho\, O(\{\rho\})\, \mathrm{e}^{-[\,\rho^2+\lambda(\rho^2-1)^2\,]} . \tag{1.67}$$

For the factorization of the partition function Z_λ in the third equality of eq. (1.66), the decoupling of all lattice points $x \in \Lambda$ and their field variables has been used. For instance,

a straightforward calculation with some changes in the integration variable yields thereupon the closed analytic expressions

$$\langle\rho^2\rangle_{Z_\lambda} = \frac{1}{\sqrt{\pi\lambda}}\,\frac{\mathrm{e}^{-\lambda c^2}}{1-\mathrm{erf}\left(c\sqrt{\lambda}\right)} - c \tag{1.68}$$

$$\langle\rho^4\rangle_{Z_\lambda} = -\frac{c}{\sqrt{\pi\lambda}}\,\frac{\mathrm{e}^{-\lambda c^2}}{1-\mathrm{erf}\left(c\sqrt{\lambda}\right)} + \frac{1}{2\lambda} + c^2\,, \quad c = \frac{1-2\lambda}{2\lambda} \tag{1.69}$$

with the error function [189]

$$\mathrm{erf}\, z = \frac{2}{\sqrt{\pi}}\int_0^z \mathrm{d}t\,\mathrm{e}^{-t^2}\,, \quad z \in \mathbb{R}, \tag{1.70}$$

which can be extended to general powers $\gamma_{2k} \equiv \langle\rho^{2k}\rangle_{Z_\lambda}$, $k \in \mathbb{Z}^{\geq 0}$, and for the odd ones $\gamma_{2k+1} = 0$ because of the symmetric integration interval. In numerical simulations at $\kappa = 0$ these formulas were perfectly confirmed up to the last significant digit outside the error bars.

The second test applies to the case $\beta = \infty$, where the gauge fields are fixed to $U_{x,\mu} \equiv \mathbf{1}$. Then the scalar field action (1.11) is

$$\begin{aligned} S_\phi[\varphi] &= -2\kappa\sum_{x\in\Lambda}\sum_{\mu=1}^{2}\mathrm{Re}\left(\varphi^*_{x+\hat{\mu}}\varphi_x\right) + \sum_{x\in\Lambda}\left\{\rho_x^2 + \lambda\left(\rho_x^2-1\right)^2\right\} \\ &= -2\kappa\Omega L_\varphi + \sum_{x\in\Lambda}\left\{\rho_x^2 + \lambda\left(\rho_x^2-1\right)^2\right\} \end{aligned} \tag{1.71}$$

with the hopping term written as volume average of $L^+_{\varphi,x}$ in eq. (1.29),

$$\begin{aligned} L_\varphi &\equiv \frac{1}{\Omega}\sum_{x\in\Lambda}\sum_{\mu=1}^{2}\mathrm{Re}\left(\varphi^*_{x+\hat{\mu}}\varphi_x\right) \\ &= \frac{1}{2\Omega}\sum_{x\in\Lambda}\sum_{\mu=1}^{2}\left(\varphi^*_{x+\hat{\mu}}\varphi_x + \varphi^*_x\varphi_{x+\hat{\mu}}\right) = \frac{1}{2\Omega}\sum_{<xy>}\varphi^*_y\varphi_x\,, \end{aligned} \tag{1.72}$$

and the sum over $< xy >$ means all directed pairings of nearest neighbours $x, y \in \Lambda$ in both lattice directions due to the U(1)–symmetry. Its relation to the scalar energy density ϵ_φ for arbitrary space-time dimension D is

$$\frac{1}{2\kappa}\,\langle\epsilon_\varphi\rangle_{Z_{\kappa,\lambda}} = \langle L_\varphi\rangle_{Z_{\kappa,\lambda}} = D\left\langle\mathrm{Re}\left(\varphi^*_y\varphi_x\right)\right\rangle_{Z_{\kappa,\lambda}}\,. \tag{1.73}$$

Now the generating functional

$$Z_{\kappa,\lambda} = \int\mathcal{D}[\varphi]\,\mathrm{e}^{-S_\phi[\varphi]} = \int\mathcal{D}[\varphi]\,\mathrm{e}^{2\kappa\Omega L_\varphi}\,\mathrm{e}^{-\sum_{x\in\Lambda}\left\{\rho_x^2+\lambda(\rho_x^2-1)^2\right\}} \tag{1.74}$$

implies

$$\langle L_\varphi\rangle_{Z_{\kappa,\lambda}} = \frac{1}{2\Omega}\,\frac{\mathrm{d}}{\mathrm{d}\kappa}\,\ln Z_{\kappa,\lambda} = \frac{1}{2\Omega}\,\frac{\mathrm{d}}{\mathrm{d}\kappa}\ln\left(\frac{Z_{\kappa,\lambda}}{Z_\lambda}\right)\,, \tag{1.75}$$

but at the same time the identity

$$\frac{Z_{\kappa,\lambda}}{Z_\lambda} = \left\langle \mathrm{e}^{\,2\kappa\Omega L_\varphi} \right\rangle_{Z_\lambda} , \quad Z_\lambda = \int \prod_{x\in\Lambda} \mathrm{d}\rho_x \, \rho_x \, \mathrm{e}^{\,-\sum_{x\in\Lambda}\left\{\rho_x^2+\lambda(\rho_x^2-1)^2\right\}} \tag{1.76}$$

holds true, if the subscript λ refers to the situation with $\kappa = 0$ as in eqs. (1.66) and (1.67). This amounts to perform a hopping parameter expansion around $\kappa = 0$ by expanding the exponential

$$\begin{aligned} \mathrm{e}^{\,2\kappa\Omega L_\varphi} \;&=\; \mathrm{e}^{\,\kappa\sum_{<xy>}\varphi_y^*\varphi_x} \;=\; \sum_{k=0}^{\infty} \frac{\kappa^k}{k!} \sum_{<xy>_1\cdots<xy>_k} \varphi_{y_1}^*\varphi_{x_1}\cdots\varphi_{y_k}^*\varphi_{x_k} \\ &=\; 1 + \sum_{n=1}^{\infty} \frac{\kappa^{2n}}{(2n)!} \sum_{i\in\mathcal{G}} l_{n,i}\, p_{n,i}\, w_{n,i} \,, \end{aligned} \tag{1.77}$$

so that $\left\langle \mathrm{e}^{\,2\kappa\Omega L_\varphi} \right\rangle_{Z_\lambda}$ becomes via the weight factors $w_{n,i}$, containing products of the scalar fields, a sum in proper products of the expectation values already met before,

$$\left\langle \varphi_{y_1}^*\varphi_{x_1}\cdots\varphi_{y_k}^*\varphi_{x_k} \right\rangle_{Z_\lambda} = \langle \rho^{2k} \rangle_{Z_\lambda} = \gamma_{2k} \,, \quad k \le n \,, \tag{1.78}$$

since the field variables on different lattice sites decouple in the partition function Z_λ with $\kappa = 0$ as above. The prescription (1.77) says to sum at each order n over the set $\mathcal{G}$ of all graphs, which consist of n pairings of directed bonds (i.e. arrows) in both directions with the property that their initial and final endpoints have to be exactly associated with each other, multiplied with the number of the possible positions $l_{n,i}$ within the lattice and with the number of permutations $p_{n,i}$ of the bonds itself. In this way one finds for the ratio of partition functions in (1.76) up to three orders in κ^2 the expansion[6]

$$\begin{aligned} \frac{Z_{\kappa,\lambda}}{Z_\lambda} \;=\;& 1 + \Omega D\gamma_2^2\kappa^2 + \Omega D\left\{\frac{1}{2}(\Omega D - 2D - 1)\gamma_2^4 + (2D-1)\gamma_2^2\gamma_4 + \frac{1}{4}\gamma_4^2\right\}\kappa^4 \\ &+\Omega D\left\{\left[\frac{1}{6}\Omega^2 D^2 - (2D-1)^2 - \frac{1}{6}(3\Omega D - 16D + 8)(4D-1)\right.\right. \\ &\left.+(D-1)(\Omega D - 4D - 2) + \frac{1}{3}\right]\gamma_2^6 + \left[(2D-1)^2 + \frac{1}{4}\Omega D + D - \frac{7}{4}\right]\gamma_2^2\gamma_4^2 \\ &+(2D-1)(\Omega D - 6D + 2)\gamma_2^4\gamma_4 + \frac{2}{3}(2D-1)(D-1)\gamma_2^3\gamma_6 + 8(D-1)^2\gamma_2^2\gamma_4 \\ &\left.+\frac{1}{2}(2D-1)\gamma_2\gamma_4\gamma_6 + \frac{1}{36}\gamma_6^2\right\}\kappa^6 + \mathcal{O}(\kappa^8) \,, \end{aligned} \tag{1.79}$$

and after inserting it into eq. (1.75), the expectation value $\langle L_\varphi \rangle_{Z_{\kappa,\lambda}}$ can be calculated in this approximation either by hand or with the aid of a computer algebra program. Note that the volume dependence of $Z_{\kappa,\lambda}/Z_\lambda$ cancels when taking the logarithm in (1.75) as it should be, because the resulting free energy has to be an extensive quantity. Finally, after numerical

[6] For control, one can verify that the first two orders in κ^2 of the same expansion for the one-component scalar model with Z_2–symmetry reproduces the results given in [19, 75].

$\langle L_\varphi \rangle_{Z_{\kappa,\lambda}}$	simulation	$\mathcal{O}(\kappa)$	$\mathcal{O}(\kappa^3)$	$\mathcal{O}(\kappa^5)$
$(\lambda, \kappa) = (0.1, 0.1)$	0.1691(2)	0.1590	0.1684	0.1692
$(\lambda, \kappa) = (\infty, 0.2)$	0.4242(3)	0.4	0.424	0.4242

Table 1.1: *Comparison between numerical simulation results and a hopping parameter expansion in κ at $\beta = \infty$ and two representative λ–values. The observable considered is the scalar energy density $L_\varphi = \epsilon_\varphi / 2\kappa$, and the expansion of the partition function went up to three orders in κ^2. The MC data are from measurements over 200000 configurations on a 16×16 lattice.*

evaluation of the integrals γ_2, γ_4, see eqs. (1.68) and (1.69), and γ_6, I obtained for $D = 2$ the expansions

$$\langle L_\varphi \rangle_{Z_{\kappa,\lambda}} = 1.589876\,\kappa + 9.411771\,\kappa^3 + 75.785093\,\kappa^5 + \mathcal{O}(\kappa^7) \tag{1.80}$$

$$\langle L_\varphi \rangle_{Z_{\kappa,\infty}} = 2\,\kappa + 3\,\kappa^3 + 0.\overline{6}\,\kappa^5 + \mathcal{O}(\kappa^7)\,, \tag{1.81}$$

which are confronted with estimates for $\langle L_\varphi \rangle_{Z_{\kappa,\lambda}}$ defined by (1.73) from numerical simulations in table 1.1. The second row corresponds to the two-dimensional XY–model ($\lambda = \infty$), and it is evident that the κ^5–term of the hopping parameter expansion is yet necessary to get a satisfactory agreement with the quite precise MC data.

As a by-product in the case of the XY–model, I also reproduced some results of ref. [69] for the scalar energy density ϵ_φ and the susceptibility $\chi = \langle M^2 \rangle / \Omega$, $M^2 \equiv \left(\sum_{x\in\Lambda} \mathrm{Re}\,\varphi_x\right)^2 + \left(\sum_{x\in\Lambda} \mathrm{Im}\,\varphi_x\right)^2$ the squared magnetization, here evaluated in the Lorentz gauge $\triangle_\mu A_{x,\mu} = \frac{1}{a}\sum_{\mu=1}^{2}(A_{x+\hat{\mu},\mu} - A_{x,\mu}) = 0$.

Chapter 2

Numerical simulation

This chapter deals with some aspects of the numerical simulation of the lattice U(1)–Higgs model. A short introduction to the subject of Monte Carlo (MC) simulations is found in appendix A, so I mainly concentrate on the features necessary for the numerical computation of the topological quantities of interest and only discuss the final updating scheme. The simulations (with a program written in FORTRAN77) were performed on UNIX and VMS workstations of WWU in Münster, Germany, and to a small extent on the SP2 of HLRZ in Jülich, Germany.

2.1 Instanton hits

As announced in the introduction, the central question I want to address later is, how the topological susceptibility (1.50),

$$\chi_{\mathrm{top}} \equiv \frac{1}{V} \left\langle Q_{\mathrm{top}}^2 \right\rangle ,$$

does behave in the continuum limit. But in ordinary MC simulations with only local updating steps the tunneling time between two distinct topological sectors, each of them corresponding to configurations with a certain fixed difference in the number of instantons and antiinstantons, is exponentially suppressed with $1/a^2 e_0^2 = \beta$ so that such indispensable transitions might actually never occur. In the case of the Wilson action, eq. (1.12) of the previous chapter, one can immediately make sure of this exponential scaling of the tunneling time with β. Since the usual local algorithms affect only the plaquettes adjacent to the link being updated, changes in the topological charge are only possible by successive changes of D plaquettes. Hence the probability for one unit of Q_{top} being located on just a few plaquettes is proportional to $\mathrm{e}^{-S_{\mathrm{g}}[U]} \propto \mathrm{e}^{-\beta}$.

The standard assumption in this situation is that all these sectors are implicitly taken into account, and that the effects of the underlying topological structure of the theory are properly included in the expectation values of all physical observables under consideration. Although

no significant contradictions to this statement have been observed so far, it may happen that in the interesting parameter region of the lattice theory the topological observables, in particular Q_{top} and χ_{top} itself, are hampered with so large autocorrelation times that they stay zero (at least within their statistical errors) during every MC run of tolerable length. The idea to overcome this problem, pioneered by Fucito and Solomon in the O(3)–sigma model [71], is to give an instantonic configuration to the system by hand and combine it with the local MC evolution. These so-called instanton hits have then also been used in the XY–model [71], in U(1)–gauge theory in two dimensions [72], and in the Schwinger model [73], where they always turned out to be the essential ingredient for feasible measurements of topological quantities in a numerical simulation.

2.1.1 Implementation

In the two-dimensional U(1)–Higgs model at zero temperature the quite similar prerequisites originate from the fact stressed before that in pure gauge theory the configurations in the various sectors, characterized by Q_{top}, are separated by a potential barrier of height 2β, i.e. the probability amplitude for transitions to configurations with $Q_{\mathrm{top}} \neq 0$ vanishes in the continuum limit $\beta \to \infty$ ($a \to 0$). However, the non-vanishing probability for the topologically non-trivial sectors represents an important physical effect, which should be included in the scaling investigations of the next chapter. Consequently, one would look for a (smooth) deformation of the gauge links $U_{x,\mu}$ leading from a sector with $Q_{\mathrm{top}} = n$ to the neighbouring one with $Q_{\mathrm{top}} = n \pm 1$ via passing at least one point $x \in \Lambda$ with $F_x = \pi$. Surely, this requires $n_x \to n_x \pm 1$ for some vortex configuration $n_x \subset \Lambda$ and will be exploited when recoursing to the instanton hit procedure.

If additionally the Higgs field degrees of freedom are incorporated, it is not surprising as well (and can be seen from the data) that the local updating algorithms — metropolis and overrelaxation in the present case — do not manage to tunnel between the different topological sectors in the space of lattice parameters with $\beta \gtrsim 10.0$ and $\kappa \lesssim 0.5$, which will become evident later to be relevant for the continuum limit of this model. Now the instanton hits appear as an updating in the gauge sector of the model by a certain global proposal of an extended instanton configuration, combined with a metropolis step. They are designed to change the topological charge by one unit and thus to ensure ergodicity of the MC simulation with respect to Q_{top}. A symmetric proposal probability P_{P} and the optimization of the acceptance rate P_{A} of the metropolis decision amounts to choose the interpolating gauge fields independent of the actual configuration, and to provide a change in Q_{top}, which mediates between the minima of two neighbouring sectors as induced by an (Euclidean) instanton.

In the sense of pure gauge theory, these sector minima have a constant field strength of

$$F_x^{(\min)} = \frac{2\pi Q_{\rm top}}{\Omega} \tag{2.1}$$

so that the associated gauge link phases $\Delta A_{x,\mu}$ should comply with

$$\Delta F_x = \pm\frac{2\pi}{\Omega}\,. \tag{2.2}$$

To describe the construction of the needed instanton configuration more precisely, I should emphasize that — owing to gauge invariance — it has to be specified by demanding the gauge invariant, physical quantities to take suitably prescribed values. In pure gauge theory these are the field strengths F_x and the vortex sum (1.49) of section 1.2.2, here $Q_{\rm top} = \sum_x n_x$ over all lattice sites x contributing to such a configuration of quadratic extent with side lengths $1 \leq R_{\rm inst} \leq \min\{L_1, L_2\}$. Therefore, the requirement $F_x = 2\pi/R_{\rm inst}^2$ for all points covered by the instanton, resulting in $Q_{\rm top} = 1$, can be realized in pure gauge theory by arranging the phases $\Delta A_{x,\mu}$ in Lorentz gauge together with the assignments $\tilde{F}_{x;12} = 2\pi/R_{\rm inst}^2$ within the instanton, except for $\tilde{F}_{x;12} = 2\pi(1 - R_{\rm inst}^2)/R_{\rm inst}^2$ in its centre, and zero elsewhere[1].

In adaption to the U(1)–Higgs model, I implemented the instanton hits as follows. Before any thermalization or measurements sweeps a square instanton configuration of extensions $1 \leq R_{\rm inst} \leq \min\{L_1, L_2\}$ in both directions is created. Motivated by the existence of a perturbative vacuum $\rho_x = \langle\rho\rangle$, the once initialized instanton configuration of pure gauge theory is cooled with the full U(1)–Higgs lattice action, where the scalar field degrees of freedom in the gauge invariant κ–term (1.22) are set to $\rho_x = \langle\rho\rangle$, eventually being adjusted after trial simulations, and the gauge is fixed by the requirement $\omega_x = 0$. This corresponds to update proposals, which only shift the gauge field. Thereby it is achieved that, starting from the perturbative vacuum in unitary gauge, the configuration evolves to the classical configuration in the topological sectors $Q_{\rm top} = \pm 1$, with the fluctuations in the scalar field length ρ_x around $\langle\rho\rangle$ assumed to be sufficiently small. The cooling procedure, during which all updating algorithms accept only those proposals lowering the action, finally produces a smooth instanton configuration with minimized action for $\rho_x = \langle\rho\rangle$ and a vortex sitting in its centre as displayed in figures 2.1 and 2.2.

The instanton hits themselves, which are element of the thermalization as well as the measurement sweeps, consist of

$$U_{x,\mu} \to U'_{x,\mu} : A_{x,\mu} \to A'_{x,\mu} = A_{x,\mu} \pm \Delta A_{x,\mu}\,, \quad \varphi_x \to \varphi'_x = \varphi_x\,, \tag{2.3}$$

[1]The $2R_{\rm inst}^2$ phases $\Delta A_{x,\mu}$ are uniquely determined, if the gauge invariant sums $t_\mu = \frac{1}{R_{\rm inst}^2}\sum_x \Delta A_{x,\mu}$, the so-called lattice torons, are also imposed to have some definite values. Of course, one ambiguity still remains and lies in the vortices n_x, which may sum up to the same value of $Q_{\rm top}$, because it is only unique modulo compensating vortex-antivortex pairs. In view of gauge fixing, this substantiates the Gribov copies of the gauge orbit.

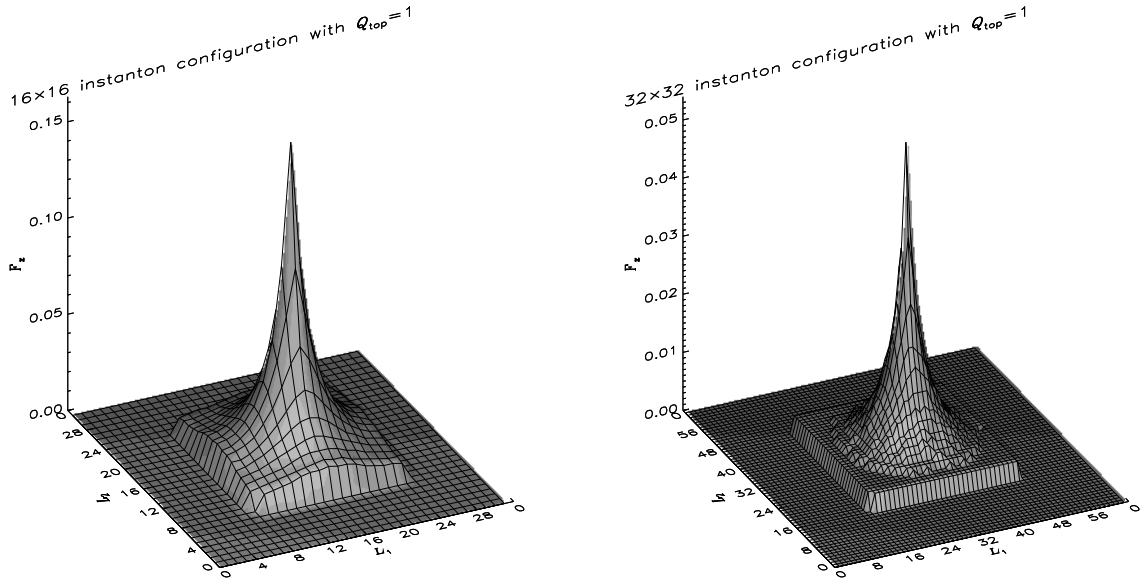

Figure 2.1: *Two typical instanton configurations after* 10^4 *cooling sweeps with* $\omega_x = 0$ *and* $\rho_x = \langle\rho\rangle$ *as proposed in the instanton hits. The figures show the corresponding distributions of the field strengths* F_x *on a* 32×32 *(left) and a* 64×64 *lattice (right).*

which fulfills the detailed balance condition

$$P_{\mathrm{P}}(\{U,\varphi\} \to \{U',\varphi'\}) = P_{\mathrm{P}}(\{U',\varphi'\} \to \{U,\varphi\})\,, \tag{2.4}$$

if the signs of $\Delta A_{x,\mu}$ in eq. (2.3) are proposed with equal probabilities. The acceptance probability of the subsequent metropolis decision within the $R_{\mathrm{inst}} \times R_{\mathrm{inst}}$ sublattice is

$$P_{\mathrm{A}}(\{U,\varphi\} \to \{U',\varphi'\}) = \min\{1, \mathrm{e}^{-\Delta S}\}\,, \quad \Delta S = S[U',\varphi'] - S[U,\varphi]\,. \tag{2.5}$$

Together with the instanton size R_{inst} it determines the cost of the algorithm so that $P_{\mathrm{A}}/R_{\mathrm{inst}}^2$ has to be maximized in practice. Since the instanton hit procedure, in which

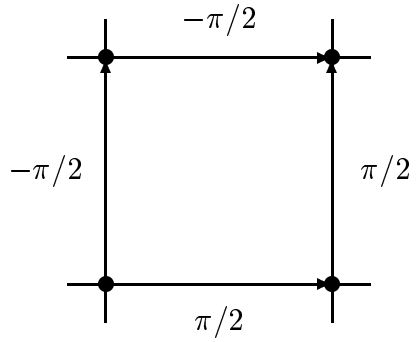

Figure 2.2: *The centre of an instanton configuration is given by a vortex, characterized by the shown values of the* φ*–link phases* $B_{x,\mu} = -\omega_{x+\hat{\mu}} + A_{x,\mu} + \omega_x$.

the randomly chosen reference point of the instanton runs over the whole lattice with increments $R_{\mathrm{inst}}/2$, may be repeated N_{inst} times, the absolute number of proposals per sweep is $N_{\mathrm{iabs}} = 4\Omega N_{\mathrm{inst}}/R_{\mathrm{inst}}^2$. As can be verified from the simulation results, the inclusion of the instanton hits now cures the prohibitively large tunneling times and is sufficient to move through the charge sectors with a reasonable acceptance rate.

2.1.2 Optimization and checks

Some refinement of these hits can be achieved by appropriate choices of the instanton size R_{inst}, their absolute number N_{iabs} per sweep, and — in principle — the number of cooling sweeps N_{cool} for the generation of the instanton configuration to be proposed. Useful criteria in this context are a reasonable acceptance rate P_{A} surviving in the continuum limit and tolerable autocorrelation times, particularly for χ_{top}. To simplify the notation for the symmetric lattices under consideration, I abbreviate $L_1 = L_2 = L$ for the moment.

The qualitative behaviour of P_{A} in dependence of R_{inst} is quite obvious. As it was already visualized in figure 2.1, the cooling procedure favours to strangle the initial instanton configuration in such a way that the field variables give significant contributions to the Boltzmann factor in the functional integral only in a localized region of extensions lower than R_{inst}. Consequently, there will always be a certain instanton size, below which P_{A} begins to decrease as R_{inst} is diminished, until it breaks down for very small R_{inst}–values typically of the order of a few lattice spacings, because then the field strength is so strongly peaked in the relevant region that the related change in the action would hardly ever be accepted. On the other hand, large instanton configurations with $R_{\mathrm{inst}} \lesssim L$ almost extending over the whole lattice imply just marginal influence on the field variables far away from the instanton centre, and thus constitute an superfluous computational overhead.

The optimization of the instanton hits — and above all of their size — generically depends on the lattice parameters β, λ, and κ. I examined the parameter range, which refers to lines of constant physics in the model described later, and after a series of short test runs with $N_{\mathrm{cool}} = 10^4$ cooling sweeps, I came to the conclusion that $R_{\mathrm{inst}} = L/2$ is the best choice here. If only the lattice size at otherwise unchanged couplings is enlarged, the once specified instanton hit parameters can be kept without modifications. N_{inst} and thereby N_{iabs} were fixed by the requirement that the total computational cost of the instanton hits in a simulation should be roughly the same as for all other updating algorithms together. During the optimization it was frequently checked that apart from the autocorrelation times and the acceptance rate P_{A}, the numerical results were not affected by the different instanton hit parameters.

For an illustration P_{A}, the topological susceptibility χ_{top}, and its autocorrelation times τ_{int} calculated from formula (A.30) of appendix A.3 for several choices of R_{inst} and N_{iabs} are collected in table 2.1. In the upper three rows the expenditure for the hits per sweep,

R_{inst}	N_{iabs}	$N_{\mathrm{iabs}}R_{\mathrm{inst}}^2/\Omega$	$P_{\mathrm{A}} \cdot 10^3$	$a^2\chi_{\mathrm{top}} \cdot 10^4$	$\tau_{\mathrm{int}}[\chi_{\mathrm{top}}]$
8	192	12	0.255(5)	0.540(15)	4
16	**48**	**12**	**0.840(8)**	**0.531(8)**	**4**
32	12	12	0.906(23)	0.523(25)	12
16	192	48	0.847(12)	0.527(12)	2

Table 2.1: *Effect of the instanton hit parameters on the numerical data from a simulation in* $\beta = 40.0$, $\lambda = 0.0025$, *and* $\kappa = 0.25885$ *on a* 32×32 *lattice. The line in boldface corresponds to the optimal choice as explained in the text.*

quantified by the combination $N_{\mathrm{iabs}}R_{\mathrm{inst}}^2/\Omega$, has been taken to be the same. Therefore, the maximum of $P_{\mathrm{A}}/R_{\mathrm{inst}}^2$ gets equivalent to a minimal τ_{int}. This minimum is reached while going from $R_{\mathrm{inst}} = 32$ to $R_{\mathrm{inst}} = 16$, where one observes that the acceptance rate P_{A} still stays approximately unchanged. If R_{inst} is lowered to $R_{\mathrm{inst}} = 8$, the autocorrelation time is maintained, but P_{A} already drops as fast as R_{inst}^{-2} increases, and this decrease of P_{A} will finally overstrip the increase of R_{inst}^{-2} for even lower values of R_{inst}. A variation of the instanton size when shifting the instanton proposals over the lattice leads to no further improvement. This confirms the choice of the instanton hit parameters mentioned above, i.e. in the example $R_{\mathrm{inst}} = 16$ for $L = 32$. Increasing N_{iabs} by a factor of four at equal R_{inst} and constant P_{A} yields a further gain in τ_{int}, even though the arising costs from the simultaneous growth of the expenditure due to the additional hits seems not justified in balance with the other updating algorithms. Note that in all cases the corresponding values of χ_{top} agree perfectly, whereas the spread of their statistical errors stems from the different statistics in the individual runs of at least 10^5 configurations. All other observables, e.g. the constituents of the lattice action per point (1.26), are completely insensitive against theses alterations in the instanton hits as it should be.

In a last test concerning the correctness of the program code I calculated the instanton action by numerical simulations. For the two-dimensional U(1)–Higgs model in the continuum, the instanton as a finite-energy solution of the classical Euclidean field equations is the Nielsen-Olesen vortex [28]. In singular gauge the spherically symmetric ansatz for it is

$$A_\mu^{(\mathrm{inst})}(x) = \frac{\varepsilon_{\mu\nu}x_\nu}{e_0 r^2}\,[\,A(r) + 1\,]\,, \quad \phi_0^{(\mathrm{inst})}(x) = v_0 f(r) \tag{2.6}$$

with real-valued profile functions $A(r)$, $f(r)$, and boundary conditions

$$\begin{aligned} A(r) &\overset{r\to 0}{\sim} c\,r^2\,, & f(r) &\overset{r\to 0}{\sim} c'r\,, \quad c, c'\text{: constants} \\ \lim_{r\to\infty} A(r) &= -1\,, & \lim_{r\to\infty} f(r) &= 1 \end{aligned} \tag{2.7}$$

to ensure $Q_{\mathrm{top}} = 1$. The Euclidean action of this solution in terms of their derivatives has

the closed form [29, 61]

$$S_{\rm inst} = \pi v_0^2 \int_0^\infty {\rm d}r \left\{ \frac{[\,A'(r)\,]^2}{r m_{W,0}^2} + r[\,f'(r)\,]^2 + \frac{f^2(r)[\,A(r)+1\,]^2}{r} + \frac{r m_{H,0}^2 [\,f^2(r)-1\,]^2}{4} \right\} . \tag{2.8}$$

Here v_0 denotes the bare vacuum expectation value of the scalar field and e_0 the bare gauge coupling entering the continuum action (1.1). This expression is exactly known [29] solely for

$$R_{HW,0} = \frac{m_{H,0}}{m_{W,0}} = 1 : \quad S_{\rm inst} = \pi v_0^2 \, . \tag{2.9}$$

Under the assumption of a variable bare mass ratio $R_{HW,0} \neq 1$, this action is multiplied by a factor a_0, which has been computed analytically (and evaluated numerically) for a wide range of $R_{HW,0}$–values in [61]. There the authors state the continuous relation $a_0(R_{HW,0}) \simeq R_{HW,0}^{0.41}$ which offers the possibility of a direct verification by the lattice approach also for parameters with a $R_{HW,0}$–value via eq. (1.8), which is not explicitly found in [61]. Now the strategy is to start from a one-instanton configuration generated by a single instanton hit with a configuration of definite size and perform the cooling algorithm. Since it accepts only those of the proposed field configurations with a minor action compared to the preceding one, all quantum fluctuations in the system are iteratively eliminated, and one is finally left with a plateau in the action, which can be identified with the lattice instanton action $S_{\rm inst}^{\rm (lat)}$. The results of this procedure, listed for two representative values of $R_{HW,0}$ in table 2.2, reproduce convincingly the continuum numbers, especially in $\kappa = 0.2555$ ($R_{HW,0} = 1.75$), where no interpolation of a_0 in $R_{HW,0}$ has to be done. They are independent of the size of

κ	$R_{HW,0}$	v_0^2	$S_{\rm inst}^{\rm (lat)}/\pi v_0^2$	a_0
0.2555	1.75	2.7594	1.2639	1.2664
0.256	1.747	2.9696	1.2623	1.2570

Table 2.2: *Results for the (classical) instanton action after* 10^4 *cooling sweeps in* $\beta = 40.0$ *and* $\lambda = 0.0025$ *on a* 32×32 *lattice.*

the starting instanton configuration, and their confrontation with the slightly worse estimate of $S_{\rm inst}^{\rm (lat)}/\pi v_0^2 = 1.281$ in $\kappa = 0.2555$ on the coarser 16×16 lattice at $\beta = 10.0$ and $\lambda = 0.01$ suggests that finite-lattice artifacts are nearly absent.

2.1.3 A remark on dislocations

In four-dimensional SU(2)–gauge theory one faces an unwanted lattice effect, conveniently called dislocations, which tends to spoil the scaling behaviour of the topological susceptibility. As topological defect on the scale of the lattice spacing a it is a severe drawback of the geometrical $Q_{\rm top}$–definition together with the use of the ordinary Wilson action. The reason

for this phenomenon is the scale invariance of the instanton solution in the continuum [26], which is entailed by the fact that it contains an arbitrary radius parameter ρ_{inst}. For instance, during cooling it reflects in the observation that gradually shrinking instantons with radius $\rho_{\mathrm{inst}} \lesssim a$ can finally not be resolved by the discretized space-time structure ('instantons falling through the meshes of the lattice'). On the lattice the ambiguity in ρ_{inst} manifests itself in dislocations, which are as low action configurations responsible for a decrease of $S_{\mathrm{inst}}^{(\mathrm{lat})}$, e.g. determined by cooling again, considerably below its classical continuum value $8\pi^2|Q_{\mathrm{top}}|/g^2$, if g denotes the SU(2)-gauge coupling. This feature persists on all scales a in the continuum limit.

The two-dimensional U(1)–Higgs theory, however, does not suffer from such problems, because the classical instanton solution possesses no free radius parameter like ρ_{inst}, of which one can ascertain by inspecting eqs. (2.6) and (2.7). The shape of an lattice instanton is supposed to be resolved increasingly well in the continuum limit $a \to 0$ instead, and hence, possible lattice artifacts in the topological susceptibility should not be ascribed to the existence of dislocations.

2.2 Updating scheme

The MC investigation of the two-dimensional U(1)–Higgs model applies a combination of metropolis and overrelaxation algorithms for the field variables $A_{x,\mu}$, ρ_x, and ω_x, mixed with the instanton hits described before. When estimating the integrated autocorrelation times of the observables defined in section 1.2 from their table of binning errors with eq. (A.30), it turns out that, besides the topological susceptibility, the Higgs field length is the slowest mode of the system. Since this is in close analogy to the the SU(2)–Higgs case, see section 5.3, I adapted the simultaneous φ–overrelaxation in cartesian components as suggested in ref. [179] and summarized in its original setup for the SU(2)–Higgs model in section A.2.2.

2.2.1 Scalar field overrelaxation

To begin with, the complex-valued scalar field φ_x is written as two-component field $\phi_x = \{\phi_{x,l} \in \mathbb{R} \,|\, l = 1,2\}$, which corresponds to the global O(2)–symmetry of the pure scalar sector of the U(1)–Higgs model:

$$\varphi_x = \phi_{x,1} + i\phi_{x,2} = \mathrm{Re}\,\varphi_x + i\,\mathrm{Im}\,\varphi_x\,, \quad |\varphi_x|^2 = \sum_{l=1}^{2} \phi_{x,l}^2 = \rho_x^2\,. \tag{2.10}$$

Along the lines of section A.2.2 in appendix A, i.e. via substituting the previous equation followed by a quadratic completion, the relevant scalar part of the lattice action (1.11) at

site $x \in \Lambda$ is split into a Gaussian (quadratic) and a quartic term

$$\begin{aligned} S_{\phi,x}(\varphi_x) &= -2\kappa \sum_{\mu=1}^{2} \mathrm{Re}\left(\varphi^*_{x+\hat{\mu}} U_{x,\mu} \varphi_x + \varphi^*_x U_{x-\hat{\mu},\mu} \varphi_{x-\hat{\mu}}\right) + \rho_x^2 + \lambda(\rho_x^2 - 1)^2 \\ &= \zeta_x \left(\phi_x - \frac{b_x}{\zeta_x}\right)^2 + \lambda \left[\rho_x^2 - \frac{1}{2\lambda}\left(2\lambda - 1 + \zeta_x\right)\right]^2 + \text{constant}\,, \end{aligned} \tag{2.11}$$

with summation over l in the first term and auxiliary fields, using eq. (2.10) again,

$$\begin{aligned} b_{x,1} &\equiv \kappa \sum_{\mu=1}^{2} \Big[\mathrm{Re}\left(\varphi^*_{x+\hat{\mu}} U_{x,\mu}\right) + \mathrm{Re}\left(U_{x-\hat{\mu},\mu} \varphi_{x-\hat{\mu}}\right) \Big] \\ &= \kappa \sum_{\mu=1}^{2} \Big[\phi_{x+\hat{\mu},1} \mathrm{Re}\, U_{x,\mu} + \phi_{x+\hat{\mu},2} \mathrm{Im}\, U_{x,\mu} \\ &\qquad + \phi_{x-\hat{\mu},1} \mathrm{Re}\, U_{x-\hat{\mu},\mu} - \phi_{x-\hat{\mu},2} \mathrm{Im}\, U_{x-\hat{\mu},\mu} \Big] \end{aligned} \tag{2.12}$$

$$\begin{aligned} b_{x,2} &\equiv \kappa \sum_{\mu=1}^{2} \Big[-\mathrm{Im}\left(\varphi^*_{x+\hat{\mu}} U_{x,\mu}\right) + \mathrm{Im}\left(U_{x-\hat{\mu},\mu} \varphi_{x-\hat{\mu}}\right) \Big] \\ &= \kappa \sum_{\mu=1}^{2} \Big[-\phi_{x+\hat{\mu},1} \mathrm{Im}\, U_{x,\mu} + \phi_{x+\hat{\mu},2} \mathrm{Re}\, U_{x,\mu} \\ &\qquad + \phi_{x-\hat{\mu},1} \mathrm{Im}\, U_{x-\hat{\mu},\mu} + \phi_{x-\hat{\mu},2} \mathrm{Re}\, U_{x-\hat{\mu},\mu} \Big]\,. \end{aligned} \tag{2.13}$$

Now the scalar field components are exactly reflected with respect to the Gaussian (quadratic) part of $S_{\phi,x}$,

$$\phi_{x,l} \;\to\; \phi'_{x,l} = \frac{2}{\zeta_x}\, b_{x,l} - \phi_{x,l}\,, \quad l = 1, 2\,, \tag{2.14}$$

and the quartic remainder is taken into account by an additional Metropolis-like accept-reject step. The optimal compromise between high acceptance rates and a good performance of the algorithm is then realized in the same way as in eqs. (A.17) – (A.19), resulting in the acceptance condition

$$P_{\mathrm{A}}(\phi_x \to \phi'_x) = \min\{1, \mathrm{e}^{-\Delta S_{\phi,x}}\}\,, \quad \Delta S_{\phi,x} = \lambda \left[(\rho_x'^2 - b_x^2)^2 - (\rho_x^2 - b_x^2)^2 \right]\,. \tag{2.15}$$

With Euler's formula $U_{x,\mu} = \mathrm{e}^{iA_{x,\mu}} = \cos A_{x,\mu} + i \sin A_{x,\mu}$, eqs. (2.12) and (2.13) can be easily expressed through the gauge field phases $A_{x,\mu}$, and the scalar field phases ω_x are reconstructed from the backtransformation of polar coordinates[2] $\omega_x = \arctan(\phi_{x,2}/\phi_{x,1})$. The acceptance rates, which essentially depend on the small size of the parameter λ, range from 96 % for $\lambda = 0.01$ up to far above 99 % for $\lambda = 0.00015625$.

[2] Of course, one has to take $\omega_x \to \omega_x + \pi$ for $\phi_{x,1} = \rho_x \cos\omega_x < 0$, because the arctan–function gives only angles modulo π.

2.2.2 Optimization

In order to look for an optimal combination among the set of algorithms at disposal I collected a sample history of 50000 measurements of some representative lattice operators O in a typical point of parameter space and calculated their autocorrelation functions and integrated autocorrelation times $\tau_{\rm int}[O]$ according to eqs. (A.31) and (A.32). The results are displayed in table 2.3 and figure 2.3. Except for the last row in boldface letters, the

metropolis			overrelaxation			$\tau_{\rm int}$ in sweeps			
$A_{x,\mu}$	ω_x	ρ_x	$A_{x,\mu}$	ω_x	φ_x	$P_{\rm pl}$	$\chi_{\rm top}$	ρ^2	L_φ
1	6	1	2	2	-	1.4(2)	6.7(6)	24(2)	24(2)
1	6	1	2	-	2	0.95(5)	4.0(4)	3.1(2)	3.2(2)
1	3	1	2	-	2	1.00(5)	4.1(5)	2.7(1)	2.8(1)
1	1	1	2	-	2	0.96(3)	4.3(4)	2.5(1)	2.6(1)
1	1	1	1	-	3	1.2(1)	4.6(6)	2.2(2)	2.3(2)
1	1	1	1	-	5	1.11(7)	4.1(8)	1.5(1)	1.6(1)
1	**1**	**1**	**1**	**-**	**5**	**1.24(7)**	**2.8(3)**	**1.5(1)**	**1.6(1)**

Table 2.3: *Autocorrelation times with jackknife errors for some representative operators from a simulation in $\beta = 40.0$, $\lambda = 0.0025$, and $\kappa = 0.259$ on a 32×32 lattice. Each updating sweep consists of a sequence of different algorithms as given by the numbers in the left part of the table. The boldface entries give the final updating scheme used. Further comments are found in the text.*

respective simulations were done without any optimizations of the instanton hits — and also omitting the cooling of the initially generated instanton configuration — so that the outcome of the scalar field overrelaxation could be carefully isolated. The elimination of the ω–overrelaxation in favour of the full φ–overrelaxation already shows the most substantial $\tau_{\rm int}$–reduction for ρ^2 and L_φ, both involving the scalar field length ρ_x, but also $\chi_{\rm top}$ gains a factor of about 1.7, which hints at a considerable influence of the scalar background field to the topological instantonic excitations. Since a further variation in the number of Metropolis updates per sweep does not lead to any decisive improvement in $\tau_{\rm int}$, one Metropolis step per sweep for each field variable seems to be sufficient, whereas a raise in the number of φ–overrelaxation steps is still advantageous. This confirms qualitatively the experiences from the SU(2)–Higgs case reported in section section 5.3 of the second part of my work. The last row of table 2.3 (with typical autocorrelation functions in the right diagram of figure 2.3) gives the final updating scheme, which has been used in almost all simulations underlying the data of the next chapters. It includes the supplementary smoothing of the instanton configuration proposed in the hits by cooling with respect to the U(1)–Higgs action and $\omega_x = 0, \rho_x = \langle\rho\rangle$ as explained in section 2.1.1.

I should admit, however, that the autocorrelation times of the topological susceptibility incline to increase with increasing β and lattice volume and end in a drastic growth, together with a breakdown of the acceptance rates of the instanton hits, for $\beta = 640.0$, which is my most continuum-like simulation point. I will return to this problem later in section 3.2 of the next chapter, when discussing the scaling of $\chi_{\rm top}$ in the continuum limit.

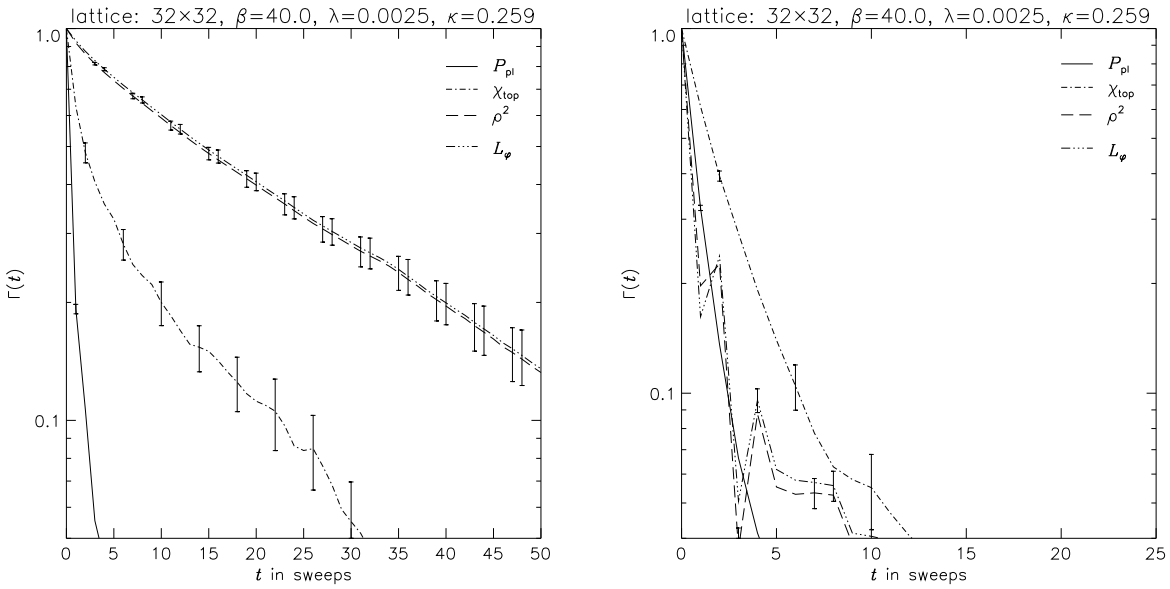

Figure 2.3: *Normalized autocorrelation functions for a simulation with ω–overrelaxation (left) and φ–overrelaxation (right) in the updating sequence corresponding to the first and last rows of table 2.3, respectively. Note the slightly different axis scales for better visualization.*

Chapter 3

Continuum limit and topological susceptibility

Now I arrive at the central chapter of the first part, which is mainly devoted to the numerical computation of the topological susceptibility on the lattice and its scaling behaviour in the continuum limit [64]. This limit is achieved along lines of constant physics in the space of lattice parameters and represents for its own a material result of my work, because it turns out to be qualitatively different from the case with fixed scalar field length.

For the investigations of χ_{top} two courses were pursued. After considering the scaling of its dimensionless ratio to a physical mass squared as directly extracted from the MC simulations, I tried to get more sensitive information about the asymptotic scaling of the topological susceptibility by estimating the slope of $\beta a^2 \chi_{\mathrm{top}}$ as a function of β. It will show up to be the only independent variable parametrizing a given line of constant physics, if the quartic coupling λ and the scalar hopping parameter κ assume suitably prescribed values, which define this line in the space of lattice couplings.

Finally, an instanton-induced confinement mechanism of fractional external charges is reviewed and numerically confirmed by utilizing results of the simulations [64].

3.1 Lines of constant physics

It is one of the basic ingredients of lattice field theory that the continuum limit $a \to 0$ of a lattice model, if existent at all, has to take place in a point of the bare, i.e. lattice parameter space, where the correlation length diverges or, equivalently, the masses am in lattice units vanish while the physical, dimensionful masses $m \equiv m^{(\mathrm{phys})}$ have to remain finite. Treated as a model in statistical mechanics, the systems then exhibits the critical behaviour of a second order phase transition. All observables calculated on the lattice are expected to scale in this limit with the lattice constant a according to their individual dimensions in lattice units.

The continuum limit is realized on lines of constant physics (LCPs), which in general can be looked upon as trajectories in the bare parameter space, for which independent physical — 'renormalized' — quantities, typically couplings and masses, are held fixed and only a is varying.

Consequently, I want to set up the continuum limit of the two-dimensional U(1)–Higgs model with variable scalar field length by the requirement that the masses of the Higgs and vector excitations in lattice units should approach zero in this limit:

$$a \to 0: \quad am_H \to 0\,, \quad am_W \to 0\,, \quad \frac{m_H}{m_W} = \text{constant}\,. \tag{3.1}$$

In order to get an impression of the behaviour of these masses in dependence of β, λ, and κ, I scanned a wide region of lattice parameter space and determined the masses from simulation results on the corresponding timeslice correlation functions as explained in section 1.2 of chapter 1. The emerging qualitative picture can be summarized as follows.

For any fixed λ and $\beta \to \infty$, the vector mass am_W appears to tend to zero, presumably defining a continuum limit in the sense of $a \to 0$, but the Higgs mass am_H stays always finite. This ends up with infinite m_H at $\beta = \infty$ for all (fixed) λ–values and reflects the freezing of the radial mode on large scales in the two-dimensional $\phi^4_{n=2}$–theory [76]. Figure 3.1 illustrates the typical dependence of the Higgs and vector masses on κ. The diagrams on the right hand side, in which solely β has been enlarged by a factor four, support the assertion of a finite Higgs mass in lattice units. The minimal am_H lies above 0.4 for all three parameter sets, whilst am_W scales appropriately with the lattice constant when going from $\beta = 10.0$ to $\beta = 40.0$; the deviation from this behaviour in $\beta = 160.0$ only corroborates the suspicion that a temporal lattice extension of $L_2 = 32$ is too short relative to the typical correlation lengths in the vector channel for such high β–values. By the way, the scaling of am_W with β like $\sqrt{2\kappa/\beta}$ for large enough but fixed κ, remember the classical relation (1.24), was also confirmed in the fixed length case $\lambda = \infty$, where the Higgs mass am_H from correlations of the operator L^+_φ does not become small either. The continuum limit $\beta = \infty$ will then be qualitatively the same as for fixed $\lambda < \infty$.

Instead, the crucial observation is now that it is possible to make both am_H and am_W small by taking the simultaneous limits $\beta \to \infty$ and $\lambda \to 0$ as shown in figure 3.2. There I find a change in the behaviour of the mass spectrum around the crossover κ–value $\bar{\kappa}$, which I define temporarily at the minimal vector mass am_W in lattice units as extracted from correlation functions of the operator L^-_φ. The fact these am_W–estimates are only consistent with those from plaquette (F or $\sin F$) correlations for $\kappa > \bar{\kappa}$, and the similar dependence of am_H and am_W on κ, are two striking analogies to the four-dimensional U(1)–Higgs model [87, 88], whose discussion is postponed to section 4.1 in chapter 4. However, the masses from the operators L^+_φ and ρ^2 in the Higgs channel agreed with each other inside their statistical errors in the whole κ–range examined. Figures 3.1 and 3.2 also contain the relations of the bare continuum, i.e. classical masses to the lattice parameters according to eqs. (1.24) and

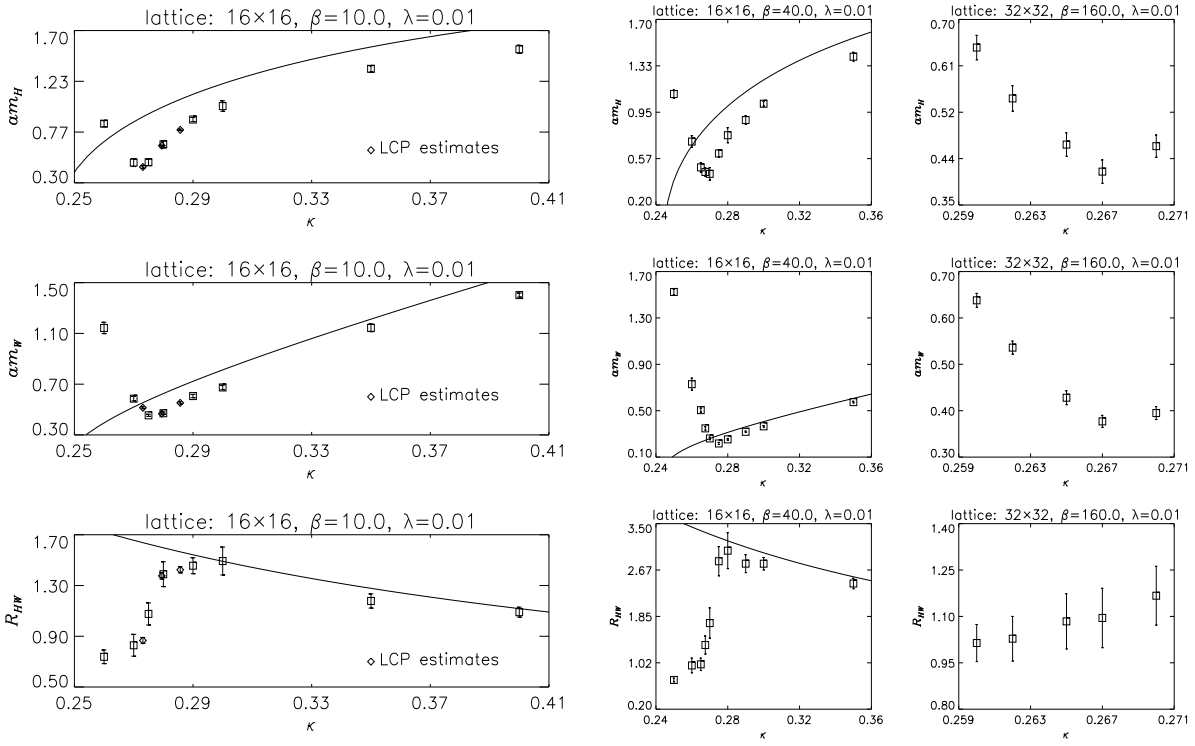

Figure 3.1: *Higgs, vector masses, and their ratios from correlations of the operators L_φ^+ or ρ^2 and L_φ^-, respectively. From left to right the parameter β was scaled at fixed λ, and the mass axes have been accommodated properly. The estimates in the LCP points specified by the tables 3.1 and 3.2 are also included, and the solid lines give their classical relations to the lattice parameters.*

(1.25). In contrast to the physical Higgs and vector masses, which are approximated by these curves only for larger κ–values, their ratio $R_{HW} = m_H/m_W$ resembles the classical behaviour with increasing κ already beginning at $\kappa \simeq \bar{\kappa}$. This may be plausible under the viewpoint of perturbation theory in the continuum, since the bare Higgs field vacuum expectation value, which involves the only primitive divergence of the model and is thought to be divergent for the renormalization procedure, cancels in the bare ratio $R_{HW,0}$ of eq. (1.8), and its finite perturbative corrections are smaller than for the masses themselves.

In the spirit of the just made observations I characterize the LCPs of the model more quantitatively. First one has to specify, which dimensionless physical quantities should be held fixed along these lines to define the required renormalization conditions. I decided to take the physical Higgs to vector boson mass ratio R_{HW} and the renormalized vacuum expectation value of the scalar field v_R defined in eq. (1.30) of section 1.2. Then the demands $am_H \to 0$ and $am_W \to 0$ are accomplished by the conditions

$$v_R = \sqrt{2\kappa}\,\langle\rho\rangle = \overline{v}\,, \quad R_{HW} \equiv \frac{m_H}{m_W} = \overline{R} \tag{3.2}$$

with fixed numbers $\overline{v}$ and $\overline{R}$ for a given LCP in bare (lattice) parameter space. With a

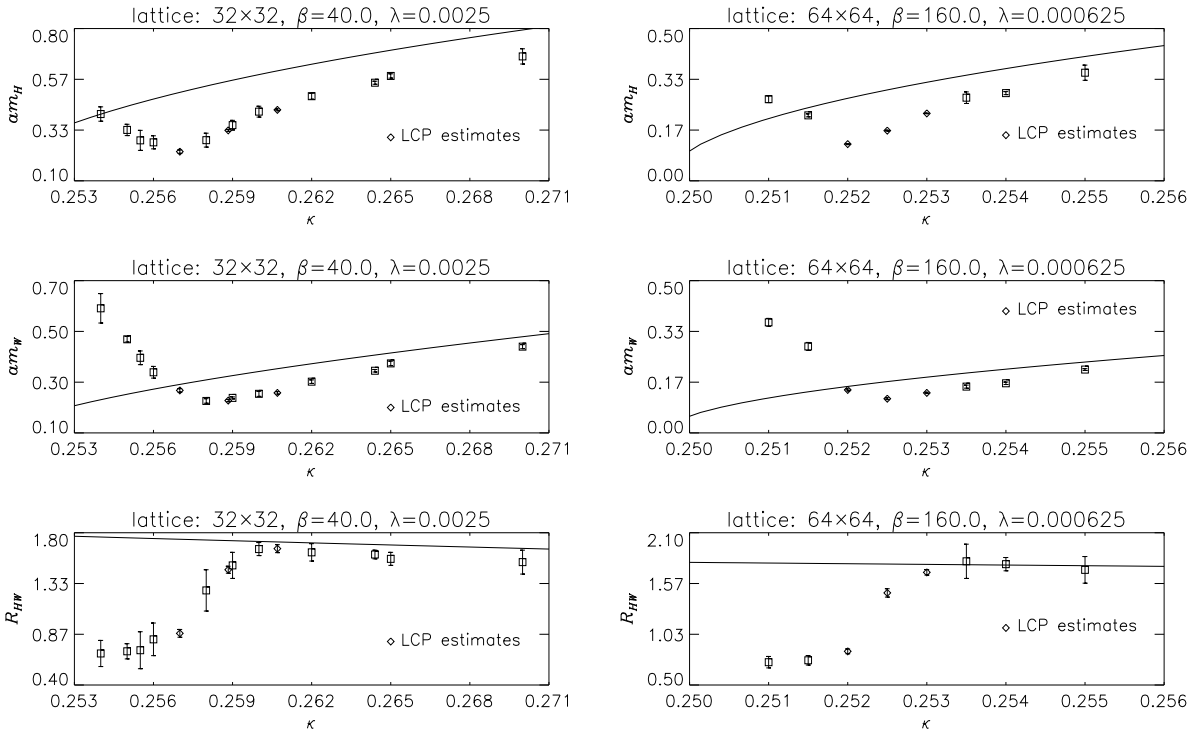

Figure 3.2: *Higgs, vector masses, and their ratios from correlations of the operators L_φ^+ or ρ^2 and L_φ^-, respectively. From left to right the parameters β and λ were scaled at fixed product $\beta\lambda$, and the mass axes have been accommodated properly. The estimates in the LCP points specified by the tables 3.1 and 3.2 are also included, and the solid lines give their classical relations to the lattice parameters.*

proper tuning of the hopping parameter κ this can be achieved by the limits

$$\beta \to \infty\,, \quad \lambda \to 0\,, \tag{3.3}$$

which are realized for large enough β as

$$\beta \to \infty\,, \quad \beta\lambda = \text{constant}\,. \tag{3.4}$$

All simulated points in the space of lattice parameters, together with measured values of v_R and the R_{HW}–data from results of the corresponding mass fits, are collected in tables 3.1 and 3.2. I have $\beta\lambda = 0.1$, except for two points at $\beta = 10.0$, where a slight increase of λ was necessary to get the desired R_{HW}–values by inducing larger Higgs masses, and κ was adjusted until the renormalization conditions (3.2) were simultaneously fulfilled within errors. Thus the approach to the continuum limit proceeds by moving along the LCPs from a point in parameter set A via B and C to a point in set D. The physical lattice volume $V = a^2 L_1 L_1$ stays constant during this limit, because the reduction of the lattice constant by a factor $\sqrt{\beta'/\beta}$ in the step $\beta \to \beta' > \beta$, is accompanied by scaling up the lattice extensions

with the same amount $\sqrt{\beta'/\beta}$. As can be verified from table 3.2, the choice $\beta\lambda \simeq 0.1$ gives a satisfactory scaling behaviour of the Higgs and vector masses in lattice units — actually a decrease by a factor about $\sqrt{\beta'/\beta} \simeq 2$ as expected — and leads automatically to the validity of the second condition in eq. (3.2) within errors. The renormalized vacuum expectation

set	lattice	β	λ	κ	sweeps	v_R
D	128×128	640.0	0.00015625	**0.250815**	200000	**1.8757(6)**
D	128×128	640.0	0.00015625	**0.25069**	400000	**1.6197(13)**
D	128×128	640.0	0.00015625	**0.25055**	300000	**1.2747(9)**
C	64×64	160.0	0.000625	**0.253**	800000	**1.8772(1)**
C	64×64	160.0	0.000625	**0.2525**	400000	**1.6146(5)**
C	64×64	160.0	0.000625	**0.252**	200000	**1.2746(5)**
B	32×32	40.0	0.0025	**0.2607**	1000000	**1.8751(1)**
B	32×32	40.0	0.0025	0.25883	600000	1.6140(2)
B	32×32	40.0	0.0025	**0.258835**	600000	**1.6150(2)**
B	32×32	40.0	0.0025	0.25885	600000	1.6170(2)
B	32×32	40.0	0.0025	**0.257**	200000	**1.2757(5)**
A_1	16×16	10.0	0.01	0.2857	1000000	1.8736(1)
A_2	16×16	10.0	0.013	**0.2937**	1000000	**1.8736(1)**
A_3	16×16	10.0	0.015	0.2987	1000000	1.8724(1)
A_1	16×16	10.0	0.01	0.2795	500000	1.6186(2)
A_2	16×16	10.0	0.013	**0.2858**	500000	**1.6144(2)**
A_3	16×16	10.0	0.015	0.2899	500000	1.6161(2)
A_1	16×16	10.0	0.01	**0.2731**	200000	**1.2739(5)**

Table 3.1: *All parameter sets of the simulation points for the LCP investigations in this and later sections. For the fits of secondary quantities, their full samples of measurements were divided into 50 subsamples. The right column gives the the measured values of the renormalized vacuum expectation value of the Higgs field with binning errors, and the boldface numbers belong to the final LCP data. Note that the LCPs were initialized in set C and then traced back with proper parameter tuning towards coarser lattices, while the extension to the most continuum-like set D has been done thereafter.*

values of the Higgs field in the first condition of (3.2) are then matched through the fine-tuning of κ thereafter. By inspecting the numbers of parameter set B in tables 3.1 and 3.2 one should notice in this context that v_R, which is accessible in the MC simulation with high statistical accuracy, reacts quite sensitive on changes in κ, but the resulting R_{HW}–values are not significantly affected by these changes, in particular compared to the typical

set	κ	am_H	am_W	R_{HW}
D	**0.250815**	**0.1115(4)** 0.1118(5)	**0.0686(12)** 0.0703(13)	**1.625(34)** 1.589(37)
D	**0.25069**	**0.0841(7)** 0.0828(3)	**0.0619(57)** 0.0576(8)	**1.36(14)** 1.437(25)
D	**0.25055**	**0.0676(5)** 0.0675(4)	**0.0807(53)** 0.0837(22)	**0.838(61)** 0.807(26)
C	**0.253**	**0.2214(10)** 0.2229(8)	**0.1315(22)** 0.1387(23)	**1.684(29)** 1.607(26)
C	**0.2525**	**0.1648(16)** 0.1685(16)	**0.1123(30)** 0.1184(20)	**1.468(44)** 1.424(27)
C	**0.252**	**0.1206(18)** 0.1200(23)	**0.1412(33)** 0.1416(59)	**0.854(25)** 0.847(42)
B	**0.2607**	**0.4262(43)** 0.4377(21)	**0.2578(49)** 0.2687(51)	**1.654(37)** 1.629(34)
B	0.25883	0.3375(47) 0.3396(48)	0.2284(49) 0.2311(72)	1.478(41) 1.469(48)
B	**0.258835**	**0.3320(43)** 0.3269(41)	**0.2274(45)** 0.2213(61)	**1.460(32)** 1.477(45)
B	0.25885	0.3299(51) 0.3246(45)	0.2275(54) 0.2307(73)	1.450(42) 1.407(45)
B	**0.257**	**0.2342(79)** 0.2258(60)	**0.2675(70)** 0.2622(95)	**0.875(36)** 0.861(37)
A_1	0.2857	0.7865(74) 0.7986(61)	0.5524(89) 0.5514(70)	1.424(24) 1.448(23)
A_2	**0.2937**	**0.8824(41)** 0.9055(66)	**0.5401(83)** 0.556(13)	**1.634(25)** 1.628(40)
A_3	0.2987	0.927(14) 0.9421(69)	0.5469(89) 0.5625(61)	1.695(39) 1.675(21)
A_1	0.2795	0.6420(44) 0.625(25)	0.4667(82) 0.4847(84)	1.376(26) 1.289(50)
A_2	**0.2858**	**0.692(11)** 0.701(14)	**0.4770(92)** 0.483(27)	**1.451(37)** 1.451(83)
A_3	0.2899	0.744(13) 0.762(15)	0.4769(86) 0.4844(80)	1.561(40) 1.573(36)
A_1	**0.2731**	**0.446(11)** 0.446(11)	**0.5139(78)** 0.530(16)	**0.867(23)** 0.842(37)

Table 3.2: *Results and jackknife errors of the masses in lattice units for the simulation points of table 3.1, determined from fits of correlation functions as described in the text. The two columns in each particle channel correspond to decay masses at spatial momenta $p_1 = 0$ and $p_1 = 2\pi/aL_1$, the latter converted via the lattice dispersion relation. The boldface numbers are regarded as the final estimates.*

sizes of their statistical errors[1]. The boldface numbers in the tables correspond to the final parameter choices and to their numerical results for the three LCPs under study from now on.

I also want to stress that the renormalization conditions (3.2) on v_R and R_{HW} are equivalent to a fixing of the renormalized scalar quartic coupling λ_R and the renormalized

[1]The fact that the central value of the $p_1 = 0$ mass ratio R_{HW} in the middle data point of parameter set D lies somewhat lower than expected does not yet stand in real contradiction to this 'rule', since there v_R differs by about three standard deviations from the other data on v_R around 1.615 for the corresponding coarser lattices. This is due to an unfortunately too high choice for κ. By the way, R_{HW} at these parameters is still compatible with the other R_{HW}–values inside its large error, which is dominated by the statistical error of the — admittedly very small — vector mass am_W.

gauge coupling e_R introduced according to the bare relations (1.7) and (1.8) as

$$m_H^2 = \frac{\lambda_R v_R^2}{3}\,, \quad m_W^2 = e_R^2 v_R^2\,, \quad R_{HW}^2 = \frac{\lambda_R}{3e_R^2}\,, \tag{3.5}$$

if one of the renormalized couplings is independently determined, e.g. ae_R from the static potential derived from Wilson loops in section 3.4.

All mass estimates displayed in figures 3.1, 3.2, and table 3.2 were obtained by least squares fits to exponential shapes of the type (1.59) with state of the art methods; for more informations the reader may consult section B.2 in appendix B or references given therein. Especially in the simulation points on the LCPs, which establish a starting point for the further investigations in this and the following chapter, and where rather high statistics had been accumulated, I used a combination of correlated and uncorrelated fits with statistically independent data subsamples. This guarantees a careful choice of the optimal fit intervals from the results of correlated fits incorporating the full correlation matrix, whereas the final numbers listed in the table 3.2 come from ordinary uncorrelated fits on these distinguished fit intervals. Conveniently, I took the largest fit intervals with still clear signal to noise ratios in their tails. For a squared deviation χ^2 between fit and data of $\chi^2/\mathrm{dof} \simeq 1$, which served as yardstick for the goodness of the correlated fits, some of the smallest time distances had to be omitted from the correlation functions in both particle channels. The compatible Higgs masses from the operators L_φ^+ and ρ^2 were always averaged to a single estimate, and the statistical errors of the masses and their ratios R_{HW} come from jackknife analyses with the data subsamples. The moderate errors of the latter (below 5 % except for parameter set D, where the statistic is lower) hint at only small correlations between the two channels. On the contrary, in all other mass determinations, which rather were intended to give a qualitative guideline for their dependencies on the lattice parameters, I used uncorrelated fits alone. The larger error bars are owing to the lower statistics of the MC data and to the (quite conservative) method of error determination with normally distributed random data and error propagation in R_{HW}. I also measured correlation functions at higher spatial momenta, and the lattice dispersion relation (1.60) was fulfilled inside the mass errors with only few exceptions. For all the LCP data this can be read off once more from table 3.2.

Finally, it has to be emphasized that the continuum limit (3.4), which amounts to send $\kappa \to 1/4$ at the same time, see the tables above and figure 3.3 in the next section, should not be confused with the Gaussian limit. The important point to keep in mind here is that the relation between the dimensionful bare continuum couplings e_0 and λ_0 and the lattice parameters is $\beta = 1/a^2 e_0^2$ and $\lambda \propto a^2 \lambda_0$ from eqs. (1.13) and (1.10). Hence, $\lambda \to 0$ at constant product $\beta\lambda$ does not imply $\lambda_0 \to 0$ for $a \to 0$ as it would correspond to the Gaussian (trivial) fixed point in the terminology of renormalization group.

3.2 Scaling behaviour of χ_{top}

I numerically determined the topological susceptibility χ_{top}, defined geometrically in eqs. (1.48) and (1.50) of the first chapter through the topological charge as the sum over the projected plaquette angles,

$$\chi_{\mathrm{top}} = \frac{1}{V}\left\langle Q_{\mathrm{top}}^2 \right\rangle , \quad Q_{\mathrm{top}} = \frac{1}{2\pi}\sum_{x\in\Lambda} F_x , \quad U_{\mathrm{p},x} = \mathrm{e}^{\,iF_x} , \quad F_x \in [-\pi,\pi) ,$$

by direct measurements in the MC simulations on the LCPs just settled. The results are listed in table 3.3 and illustrated in figure 3.3. For the sake of completeness, the final

LCP	set	κ	R_{HW}	v_R	$a^2\chi_{\mathrm{top}}\cdot 10^4$	$\chi_{\mathrm{top}}/m_H^2\cdot 10^4$
L1	A_2	0.2937	1.634(25)	1.8736(1)	0.1050(40)	0.135(6)
	B	0.2607	1.654(37)	1.8751(1)	0.0302(15)	0.166(12)
	C	0.253	1.684(29)	1.8772(1)	0.01050(70)	0.214(16)
	D	0.250815	1.625(34)	1.8757(6)	0.0006(5)	0.05(4)
L2	A_2	0.2858	1.451(37)	1.6144(2)	1.624(21)	3.39(15)
	B	0.258835	1.460(32)	1.6150(2)	0.5331(77)	4.84(20)
	C	0.2525	1.468(44)	1.6146(5)	0.1811(43)	6.67(29)
	D	0.25069	1.36(14)	1.6197(13)	0.0576(78)	8.1(1.2)
L3	A	0.2731	0.867(23)	1.2739(5)	14.83(9)	74.6(4.1)
	B	0.257	0.875(36)	1.2757(5)	4.116(25)	75.0(5.5)
	C	0.252	0.854(25)	1.2746(5)	1.205(9)	82.9(3.1)
	D	0.25055	0.838(61)	1.2747(9)	0.344(24)	75.3(6.4)

Table 3.3: *Topological susceptibility by direct measurements in the LCP simulation points of the previous section. The statistical errors of χ_{top} come from the plateau in the binning table. In point D on LCP L1 its available statistic is far too low for quoting significant estimates and errors. For comparison, the values $a^2\chi_{top}^{(PGT)}$ in pure gauge theory are $25.33\cdot 10^{-4}$, $6.333\cdot 10^{-4}$, $1.583\cdot 10^{-4}$, and $0.396\cdot 10^{-4}$.*

estimates of the fixed renormalized quantities R_{HW} and v_R are also included in the table.

In general I observed a rapid breakdown of the topological susceptibility around the crossover κ–value $\bar{\kappa}$ at minimal vector mass am_W, introduced in the previous section. Moreover, within the chosen parameter sets χ_{top} varies by orders of magnitude. One can see a contraction of the κ–region, which is limited by a still measurable susceptibility, i.e. $a^2\chi_{\mathrm{top}} \geq c$ with c arbitrarily small but strictly non-zero, from above and by the line L3 from below. Note that this LCP already lies close to the pure gauge theory, where through eq. (1.53) the β–dependence $a^2\chi_{\mathrm{top}}^{(\mathrm{PGT})} \simeq 1/4\pi^2\beta$ for large β and volumes Ω is analytically known, i.e. $\chi_{\mathrm{top}} \leq c'\chi_{\mathrm{top}}^{(\mathrm{PGT})}$ with c' near but strictly below one. These numbers are confronted with

the MC data in the caption of table 3.3, and one can make sure that their agreement gets better when moving towards point D on L3. These constraints on $\chi_{\rm top}$, in addition to the desired decrease of the masses in lattice units, was the real motivation for the chosen positions of the LCPs in lattice parameter space.

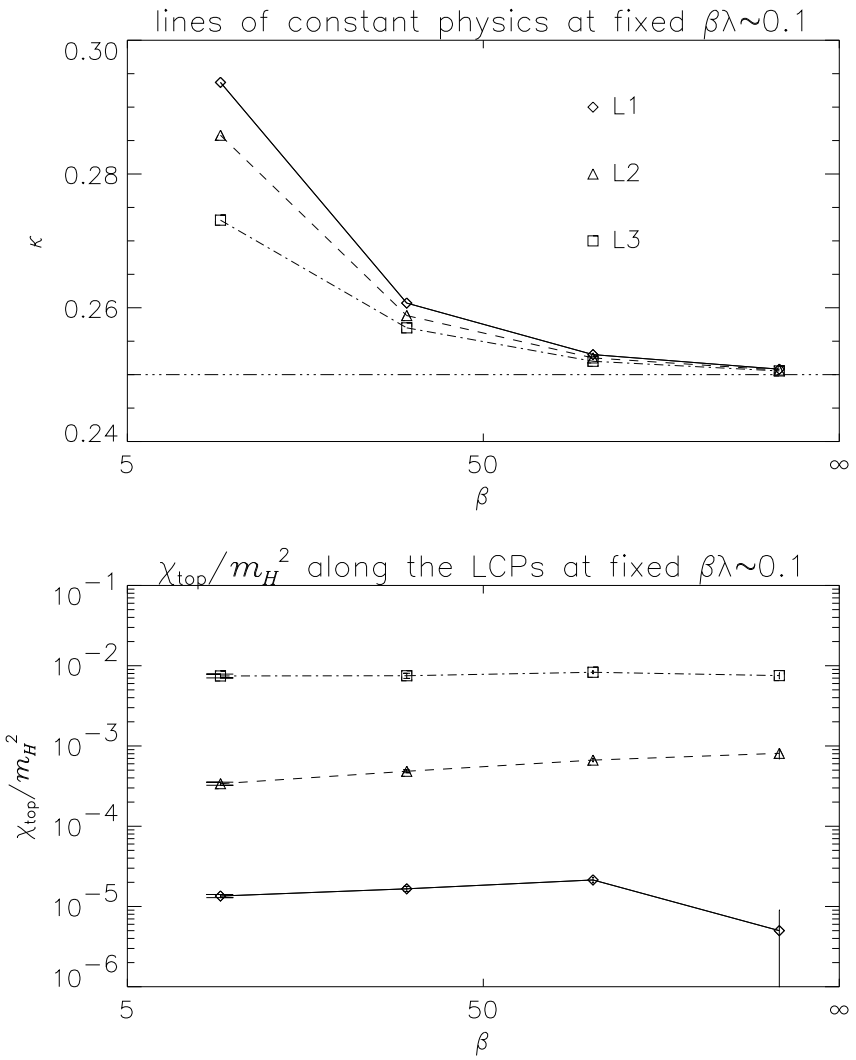

Figure 3.3: *Scaling behaviour of the topological susceptibility along the LCPs, which are curves $\kappa = \kappa(\beta)$ at fixed $\beta\lambda$ in lattice parameter space as shown in the upper plot. The lines are only meant to guide the eye. The quality of the scaling of the ratio χ_{top}/m_H^2 is rather good on L3 (near pure gauge theory) and deteriorates towards L2 and L1. In the lower right data point the statistic is too bad for a reliable estimate.*

From the results on the topological susceptibility by direct measurements I arrive at the conclusion that the scaling of its dimensionless ratio $\chi_{\rm top}/m_H^2$ to the Higgs mass m_H squared is rather poor, although in spite of the relatively high statistics for the parameter sets A to C its statistical errors, caused by propagation of the errors on $\chi_{\rm top}$ into the ratios $\chi_{\rm top}/m_H^2$,

is yet quite large. The only exception is the pure gauge theory like LCP L3, which appears to have only negligible scaling violations compared to the lines L1 and L2.

Since the topological susceptibility is a volume-independent quantity by definition, possible finite-volume effects manifest in a suppression of χ_{top}, if the physical volumes considered were too small, and thus it should increase noticeably with increasing volumes. I examined these effects under two aspects by rescaling both lattice extensions at otherwise identical parameters so that the corresponding lattice resolutions, set through β, remain unchanged. In the first place some simulations in the LCP points B and C on 48×48 and 96×96 lattices resulted in estimates for χ_{top}, which coincided inside their statistical errors with those in table 3.3, hence significant finite-volume effects can be safely ruled out. In respect of such artifacts arising on lattices smaller than the ones of table 3.1 utilized here, it was confirmed indeed that minimally these volumes were necessary for a trustworthy determination of χ_{top}. Secondly, it may be interesting, whether the finite-volume effects themselves have scaling violations of roughly the same size as χ_{top} computed on the original lattices. As exemplarily proven for the points B, C, and D of L2 on lattices with halved extensions, this is actually true, because there it turned out that $a^2\chi_{\mathrm{top}}$ decreases again by factors around three instead of $\beta'/\beta = 4$, which would be expected in the case of ideal asymptotic scaling with β. Consequently, an explanation for the bad scaling behaviour of χ_{top}, especially in L1 and L2, must carefully be detached from any finite-volume effects.

Of course, one has to ask for the systematic errors on the topological susceptibility, which are induced by the statistical uncertainties in the renormalization conditions (3.2). The sensitivity of χ_{top} on the fixing of the renormalized vacuum expectation value has already indirectly been addressed in table 3.1 of section 3.1, where for the parameter set B of L2 three neighbouring v_R–values with nearly constant mass ratios R_{HW} are given. There an uncertainty in v_R of approximately 0.2 % leads to spreads in $a^2\chi_{\mathrm{top}}$ and $\chi_{\mathrm{top}}/m_H^2$, which are estimated to be below 5 % for the former and below 10 % for the latter. This indicates that a matching of v_R outside its last significant digit is more or less sufficient in regard of the — quite large — statistical errors of $a^2\chi_{\mathrm{top}}$ and $\chi_{\mathrm{top}}/m_H^2$, particularly since an exact tuning of the very accurate v_R–values is very rarely or at best incidentally possible in most cases. However, the response of $a^2\chi_{\mathrm{top}}$ to a variation of R_{HW} within its statistical errors at constant v_R is quite more substantial and has also been quantified in point B of the middle LCP. The necessary shifts in $R_{HW} = m_H/m_W$ are achieved by choosing slightly different values of the scalar self-coupling λ, which essentially influences the size of the Higgs mass in lattice units am_H, while it leaves the vectors mass am_W almost unchanged. Then the renormalization condition on v_R is fulfilled by an adjustment of the hopping parameter κ as before, and the results of such an analysis can be found in table 3.4. These numbers are to be combined with the statistical error taken from table 3.3 and yield $\chi_{\mathrm{top}}/m_H^2 = 4.84(20 + 1.35) \cdot 10^{-4}$ for the representative LCP point B on L2. Therefore the total errors of the dimensionless ratios $\chi_{\mathrm{top}}/m_H^2$ are obviously dominated by the systematic errors due to the reachable numerical

λ	κ	R_{HW}	v_R	$a^2\chi_{\rm top}\cdot 10^4$	$\chi_{\rm top}/m_H^2\cdot 10^4$
0.0022	0.25797	1.345(66)	1.6143(3)	0.606(10)	6.24(30)
0.0025	0.258835	1.460(32)	1.6150(2)	0.5331(77)	4.84(20)
0.0030	0.26025	1.546(33)	1.6155(2)	0.4459(86)	3.54(20)

Table 3.4: *Results on χ_{top} and χ_{top}/m_H^2, if the renormalized mass ratio R_{HW} in point B of LCP L2 from table 3.3 (middle row) takes the values, which are maximally allowed by its absolute error. These data are from 400000 measurements at $\beta = 40.0$ on a 32×32 lattice.*

precision in the renormalization conditions on R_{HW}, which in turn are limited through the statistical uncertainties in the determination of the masses.

Nevertheless, the scaling of the ratio $\chi_{\rm top}/m_H^2$ from A to C on the LCPs is deficient, except for the line L3 close to pure gauge theory. Superficially, one could imagine that these difficulties with the topological susceptibility have to do with the existence of dislocations. But the relevance of this objection for the computation of $\chi_{\rm top}$ is rather unlikely, since it was already argued in section 2.1.3 that dislocations of the type as in four-dimensional non-abelian gauge theories are absent in the two-dimensional U(1)–Higgs model[2]. Under these aspects, the LCP simulations in the three points with parameter set D were intended to make closer contact with continuum physics by 'brute force', so let me comment on them now.

The statistical errors of the quantities in tables 3.1 – 3.3 are considerably larger because of the lower statistic in these points. This is distinct above all for the topological susceptibility and seems to be intimately connected to the fact that the acceptance rate $P_{\rm A}$ of the instanton hits does unfortunately not survive in the continuum limit. As table 3.5 reflects, $P_{\rm A}$ drops rapidly when going from point C ($\beta = 160.0$) to point D ($\beta = 640.0$) by factors roughly between 42 for L1 and 227 for L3, and as a consequence, the integrated autocorrelation times $\tau_{\rm int}$ of $\chi_{\rm top}$ suddenly jump by factors roughly between 9 and 130. In order to account for this dramatic increase of $\tau_{\rm int}$ and to exclude the related severe thermalization effects, I skipped 25000 measurements (instead of usually 10000 else) from the beginning of the simulations on a cold start configuration to obtain the estimates on $a^2\chi_{\rm top}$ in the points D of table 3.3. But these numbers as well as those of $\chi_{\rm top}/m_H^2$ in the same table either do not give any new insight into the scaling behaviour of the topological susceptibility or are actually even meaningless as in the case of simulation point D on LCP L1.

From additional runs on smaller lattices with identical parameters and their qualitatively similar results one can guess, that the large value $\beta = 640.0$ alone is responsible for the problems, which plague the simulations with parameter set D. In my opinion, the fol-

[2]Although some authors [58, 63] speak of dislocations also in the present model, they should be better interpreted as ordinary lattice artifacts, which — in principle — will vanish in the continuum limit.

LCP	set	β	κ	$P_{\mathrm{A}} \cdot 10^5$	$\tau_{\mathrm{int}}[\chi_{\mathrm{top}}]$
L1	A_2	10.0	0.2937	5.5(1)	2
	B	40.0	0.2607	3.7(1)	4
	C	160.0	0.253	2.5(1)	8
	D	640.0	0.250815	0.06(2)	68
L2	A_2	10.0	0.2858	113(1)	2
	B	40.0	0.258835	84.2(1)	3
	C	160.0	0.2525	55.8(1)	8
	D	640.0	0.25069	0.94(7)	220
L3	A	10.0	0.2731	2098(9)	1
	B	40.0	0.257	1309(6)	2
	C	160.0	0.252	704(4)	3
	D	640.0	0.25055	3.1(1)	390

Table 3.5: *Acceptance rates of the instanton hit routine and integrated autocorrelation times of the topological susceptibility along the LCPs as estimated from formula (A.30). The statistics of the points D is not large enough for a plain error plateau in the binning table of χ_{top}. Other observables do not show this dramatic increase of their autocorrelation times.*

lowing explanation for this might be nearest at hand. Namely, the instanton configurations representing the minima of the topological charge sectors are more subtle than those proposed in the updating procedure by the instanton hits as described in section 2.1 of the last chapter. These instanton configurations are initialized with the appropriate field strength of pure gauge theory and smoothed by cooling to give the minimal action for a background scalar field with phases $\omega_x = 0$ and lengths $\rho_x \simeq \langle\rho\rangle$. However, just the last assumption is not really justified in the vortex itself, which sits in the centre of the instanton configuration with gauge invariant link phases as e.g. in figure 2.2. In strict sense, one should have $\rho_x = 0$ there, if compatibility with the classical instanton solution in the continuum, see eqs. (2.6) and (2.7), is required. In the continuum limit $a \to 0$ realized as $\beta \to \infty$, the mesh of lattice sites becomes denser and thus, the detailed structure of the instanton configuration is far better resolved compared to smaller β–values, for which the approximation $\rho_x \simeq \langle\rho\rangle \neq 0$ also in the vortex turns out to be sufficiently adequate. For larger β–values this choice of the Higgs field lengths leads to considerable deviations of the proposed instantons from the true configurations with minimal action so that the changes of the total lattice action induced by the instanton hits — finally deciding about their acceptance rates — react very sensitive to these imperfections. As the numerical data presented up to now exemplify, the worse behaviour of the instanton hits sets in during the step from $\beta = 160.0$ to $\beta = 640.0$, and its effects appear in table 3.5 to be strongest for the LCP L3 closest to the pure gauge

theory. This observation I do not understand completely, because on the contrary, I found the problems with P_{A} and χ_{top} in some further simulations at κ–values below the crossover value $\bar{\kappa} \simeq 1/4$ to be declining and to be no longer significant in the vicinity of pure gauge theory ($\kappa \to 0$), which is in agreement with the expectation that gauge and scalar degrees of freedom decouple in this limit.

I did not make any attempts to cure these drawbacks in the instanton hit routine. The main reason was that, even in the case of moderate autocorrelation times $\tau_{\mathrm{int}}[\chi_{\mathrm{top}}]$, the computational cost to get in D statistical errors on $a^2\chi_{\mathrm{top}}$ of orders comparable to the ones in LCP points C by brute force simulations is under normal circumstances too high. This can be inferred from the meaning of the dimensionless product $V\chi_{\mathrm{top}} \ll 1$ as the probability for the occurrence of $\chi_{\mathrm{top}} \neq 0$, which ideally should scale in the continuum limit. If the lattice resolution is increased about a factor two by blowing up β and the lattice extensions by factors four and two, respectively, the computational expenditure also rises with these factors accordingly although the number of lattice points has enlarged, since the related growth of the correlation length in this step does not result in new independent, i.e. uncorrelated field modes, which would improve the statistics of $V\chi_{\mathrm{top}}$.

The whole discussion in this section has revealed that the scaling of the topological susceptibility, which is still quite unclear and eludes any conclusive judgement, deserves further studies from a different point of view as suggested in the next section.

3.3 Criterion for asymptotic scaling of χ_{top}

At first glance, the outcome of the last section concerning the poor scaling behaviour of topological susceptibility in the continuum limit is not very encouraging. There it has been conjectured that with the strong decrease (increase) in the instanton hits acceptance rates (integrated autocorrelation times $\tau_{\mathrm{int}}[\chi_{\mathrm{top}}]$) when going from LCP points C to D one runs into serious problems with a feasible determination of χ_{top} in the MC investigations close to the continuum limit. But it became also apparent that the instanton hits are of vital importance in order to have any realistic chance for direct measurements of χ_{top} in the interesting LCP points at all. This statement, already touched in section 2.1 of the previous chapter, comes from the fact that the simulation points lie in a region of lattice parameter space, where the transitions between non-trivial topological sectors are highly suppressed. Consequently, a simulation of in principle all these sectors without an artificial enhancement of the topological excitations by the instanton hits would always cause the system to be stuck in one sector for a long MC time and result in notoriously large statistical errors on χ_{top}. For these reasons I try to shed a light on the scaling behaviour of the topological susceptibility through another doorway.

3.3.1 Idea and derivation

As opposed to the foregoing section, where the lattice constant a as the physical scale for the investigation of the topological susceptibility was given through the Higgs mass m_H, the aim is here to find a quantitative criterion for asymptotic scaling of $\chi_{\rm top}$. Since the model under study is superrenormalizable and the bare gauge coupling $e_0 = 1/a\sqrt{\beta}$ receives only finite quantum corrections, I take the standpoint that the scale a is simply set by β now[3]. In section 3.1 the continuum limit of the two-dimensional U(1)–Higgs model became evident to be achieved via eqs. (3.3) and (3.4). There the requirement of a constant product $\beta\lambda$ showed up to comply with the renormalization condition on the Higgs to vector mass ratio $R_{HW} = \overline{R} =$ constant in the limit $\beta \to \infty$, at least as far as $\beta \geq 40.0$ in practice. Therefore, it is justified to base the present considerations on the definition of modified renormalization group trajectories in bare parameter space, which coincide with the old LCPs for $\beta \to \infty$ ($\beta \geq 40.0$). Then the assumption is that

$$\beta\lambda = \text{constant} \tag{3.6}$$

does hold exactly on a given LCP. As an important consequence, the determination of the masses and their ratios R_{HW}, which represented a non-negligible source of uncertainties for $\chi_{\rm top}/m_H^2$ in section 3.2, can actually be released. Furthermore, the renormalization condition on the vacuum expectation value of the Higgs field,

$$v_R = \overline{v} = \text{constant}\,, \tag{3.7}$$

uniquely determines the evolution of the scalar hopping parameter κ as a function of β so that along each LCP the scale parameter

$$\tau \equiv \ln\beta \tag{3.8}$$

is the only free variable, on which λ and κ depend.

Of course, it goes without saying that the τ–dependence of these two lattice parameters also carries over to arbitrary expectation values of observables $O = O(\{U,\varphi\})$ along the LCPs. Hence, the method to be applied is the following. Let $O = O^{(\rm phys)}a^{d_O}$ possess the mass dimension d_O and the functional integral representation (A.10) of appendix A.2 for its expectation value:

$$\langle O\rangle_Z = \frac{1}{Z}\int \mathcal{D}[U,\varphi]\,\mathrm{e}^{-S[U,\varphi]}\,O\,, \quad Z = \int \mathcal{D}[U,\varphi]\,\mathrm{e}^{-S[U,\varphi]}\,.$$

[3]This is different from non-abelian gauge theories in $D = 4$, where the scale is conveniently set by the so-called Λ–parameters, which are renormalization scheme dependent and have to be determined non-perturbatively in general. The geometrically defined $Q_{\rm top}$ itself is not renormalized, and $\chi_{\rm top}$ is expected to exhibit logarithmic scaling towards the continuum limit.

If this expectation value is measured on the lattice, the naively sensible constraint on $\langle O \rangle_Z$ to be independent of the physical space-time volume $V = a^2\Omega$ in the continuum limit is equivalent to $\langle O \rangle_Z \propto a^{d_O} \propto \beta^{-d_O/2}$ to depend only on the scale parameter τ at fixed lattice volume Ω. This implies

$$\frac{\mathrm{d}}{\mathrm{d}\tau} \ln \langle O \rangle_Z = \frac{1}{\langle O \rangle_Z} \frac{\mathrm{d}}{\mathrm{d}\tau} \langle O \rangle_Z = \frac{1}{\langle O \rangle_Z} \beta \frac{\mathrm{d}}{\mathrm{d}\beta} \langle O \rangle_Z = -\frac{d_O}{2} , \tag{3.9}$$

whose derivative with respect to τ on the left hand side will translate into derivatives of the couplings in the lattice action, which can be fixed by the modified renormalization conditions for the LCPs claimed in eqs. (3.6) and (3.7). The useful information provided by the identity (3.9) complements the search for asymptotic scaling of the dimensionless combination $\beta^{d_O/2}\langle O \rangle_Z$, because the τ–behaviour of its derivative might enable to diagnose scaling although its values themselves do not yet reflect this feature [66].

More concretely, I decompose the lattice action of the model in eqs. (1.20) – (1.22) of section 1.1 as

$$\begin{aligned} S[U,\varphi] &= \beta \sum_{x\in\Lambda} \Big(1 - \mathrm{Re}\, U_{\mathrm{p},x}\Big) + \lambda \sum_{x\in\Lambda} \big(\rho_x^2 - 1\big)^2 + \kappa \sum_{x\in\Lambda} \left(-2 \sum_{\mu=1}^{2} L^+_{\varphi;x\mu}\right) + \sum_{x\in\Lambda} \rho_x^2 \\ &\equiv \beta S_\beta + \lambda S_\lambda + \kappa S_\kappa + \sum_{x\in\Lambda} \rho_x^2 \\ &= \sum_{c_i\in\mathcal{P}} c_i S_i + \sum_{x\in\Lambda} \rho_x^2 , \quad \mathcal{P} = \{c_1, c_2, c_3\} \equiv \{\beta, \lambda, \kappa\} , \end{aligned} \tag{3.10}$$

the φ–link having been introduced in (1.29) of section 1.2, and the identification of the different pieces S_β, S_λ, and S_κ of the total action is obvious. The set $\mathcal{P}$ of the coupling parameters c_i, $i = 1, 2, 3$, has been introduced for notational simplicity. With these arrangements and the quotient rule, the left hand side of (3.9) may be recasted to

$$\begin{aligned} \frac{\mathrm{d}}{\mathrm{d}\tau} \ln \langle O \rangle_Z &= \frac{1}{\langle O \rangle_Z} \left\{ \frac{1}{Z} \frac{\mathrm{d}}{\mathrm{d}\tau} \int \mathcal{D}[U,\varphi]\, \mathrm{e}^{-S[U,\varphi]}\, O - \frac{1}{Z^2} \frac{\mathrm{d}Z}{\mathrm{d}\tau} \int \mathcal{D}[U,\varphi]\, \mathrm{e}^{-S[U,\varphi]}\, O \right\} \\ &= -\sum_{c_i\in\mathcal{P}} \frac{\mathrm{d}c_i(\tau)}{\mathrm{d}\tau} \left[\frac{\langle O S_i \rangle_Z}{\langle O \rangle_Z} - \langle S_i \rangle_Z \right] = -\sum_{c_i\in\mathcal{P}} \frac{\mathrm{d}c_i(\tau)}{\mathrm{d}\tau} \frac{\langle O S_i \rangle_{\mathrm{c}}}{\langle O \rangle_Z} \end{aligned} \tag{3.11}$$

with the abbreviation

$$\langle O S_i \rangle_{\mathrm{c}} \equiv \langle O S_i \rangle_Z - \langle O \rangle_Z \langle S_i \rangle_Z \tag{3.12}$$

in formal analogy to connected correlation functions. Guided through the observation that the κ–values of the LCPs in the previous sections, see e.g. table 3.3, approximately obey an exponential decay law, I define the auxiliary variable

$$h = h(\tau) \equiv \ln\big[\, 4\kappa(\tau) \,\big] . \tag{3.13}$$

It depends through κ on τ and allows to write the evolution of κ on a given LCP in integral form as

$$h(\tau) = h(\tau_0) \exp\left\{ -\int_{\tau_0}^{\tau} \mathrm{d}\tau'\, \gamma(\tau') \right\} \tag{3.14}$$

with a function $\gamma = \gamma(\tau)$ and a value $h(\tau_0)$ at some initial argument τ_0. Thus when using $\mathrm{d}/\mathrm{d}\tau = \beta\,\mathrm{d}/\mathrm{d}\beta$ and the constant product $\beta\lambda$ as well as the last equation, the derivatives of the lattice parameters with respect to τ in (3.11) give

$$\frac{\mathrm{d}c_1(\tau)}{\mathrm{d}\tau} = \frac{\mathrm{d}\beta(\tau)}{\mathrm{d}\tau} = \beta\,\frac{\mathrm{d}\beta}{\mathrm{d}\beta} = \beta \tag{3.15}$$

$$\frac{\mathrm{d}c_2(\tau)}{\mathrm{d}\tau} = \frac{\mathrm{d}\lambda(\tau)}{\mathrm{d}\tau} = \beta\,\frac{\mathrm{d}\lambda(\beta)}{\mathrm{d}\beta} = -\lambda \tag{3.16}$$

$$\frac{\mathrm{d}c_3(\tau)}{\mathrm{d}\tau} = \frac{\mathrm{d}\kappa(\tau)}{\mathrm{d}\tau} = \frac{\mathrm{d}}{\mathrm{d}\tau}\,\frac{\mathrm{e}^{h(\tau)}}{4} = \frac{\mathrm{e}^{h(\tau)}}{4}\,\frac{\mathrm{d}h(\tau)}{\mathrm{d}\tau} = -\gamma(\tau)\cdot\kappa\ln(4\kappa)\,. \tag{3.17}$$

Summing together, eqs. (3.9) and (3.11) lead to the central relation

$$\frac{\mathrm{d}}{\mathrm{d}\tau}\ln\langle O\rangle_Z = \frac{1}{\langle O\rangle_Z}\Big[\,-\beta\langle OS_\beta\rangle_{\mathrm{c}} + \lambda\langle OS_\lambda\rangle_{\mathrm{c}} + \gamma(\tau)\cdot\kappa\ln(4\kappa)\cdot\langle OS_\kappa\rangle_{\mathrm{c}}\Big] = -\frac{d_O}{2}\,, \tag{3.18}$$

which now expresses scaling along the modified trajectories in the continuum limit.

This is directly applied to the topological susceptibility χ_{top} as the expectation value

$$\chi_{\mathrm{top}} = \frac{1}{V}\langle k^2\rangle_Z \quad\Leftrightarrow\quad a^2\chi_{\mathrm{top}} = \frac{1}{\Omega}\langle k^2\rangle_Z\,, \tag{3.19}$$

while $Q_{\mathrm{top}} = k \in \mathbb{Z}$ in the corresponding topological sectors, and the right hand side being measured on the lattice has mass dimension $d_{\chi_{\mathrm{top}}} = 2$. Inserting this together with (3.12) and $V = a^2\Omega$ into (3.18), I arrive at

$$\begin{aligned} O^{(\chi)}[\gamma] &\equiv \frac{\mathrm{d}}{\mathrm{d}\tau}\ln\left(a^2\chi_{\mathrm{top}}\right) \\ &= \frac{1}{V\chi_{\mathrm{top}}}\Big\{-\beta\left\langle k^2\,S_\beta\right\rangle_{\mathrm{c}} + \lambda\left\langle k^2\,S_\lambda\right\rangle_{\mathrm{c}} + \gamma(\tau)\cdot\kappa\ln(4\kappa)\cdot\left\langle k^2\,S_\kappa\right\rangle_{\mathrm{c}}\Big\} \\ &= \frac{1}{a^2\chi_{\mathrm{top}}}\Big\{-\beta\left[\left\langle\frac{k^2}{\Omega}\,S_\beta\right\rangle_Z - a^2\chi_{\mathrm{top}}\langle S_\beta\rangle_Z\right] + \lambda\left[\left\langle\frac{k^2}{\Omega}\,S_\lambda\right\rangle_Z - a^2\chi_{\mathrm{top}}\langle S_\lambda\rangle_Z\right] \\ &\quad + \gamma(\tau)\cdot\kappa\ln(4\kappa)\left[\left\langle\frac{k^2}{\Omega}\,S_\kappa\right\rangle_Z - a^2\chi_{\mathrm{top}}\langle S_\kappa\rangle_Z\right]\Big\}\,, \end{aligned} \tag{3.20}$$

and perfect scaling of the topological susceptibility is now equivalent to the condition

$$O^{(\chi)}[\gamma] = -1\,. \tag{3.21}$$

The so far unknown, τ–dependent decay constant γ in eqs. (3.14) and (3.20) can be extracted in two ways. Either by exponential fits of κ as functions of τ for each LCP, or, what is surely more elegant, by repeating the steps, which led to eq. (3.18), but now for the renormalization condition of constant $v_R = \sqrt{2\kappa}\,\langle\rho\rangle = \overline{v}$ along the LCPs. This is the natural choice, since it has not explicitly been used yet. From (3.9) I get for an arbitrary prefactor κ^c, $c \in \mathbb{R}$, in front of an observable O of mass dimension zero

$$\begin{aligned} 0 &= \frac{\mathrm{d}}{\mathrm{d}\tau}\ln\langle\kappa^c\,O\rangle_Z = \frac{\mathrm{d}}{\mathrm{d}\tau}\Big(c\ln\kappa + \ln\langle O\rangle_Z\Big) \\ &= c\,\frac{1}{\kappa}\,\frac{\mathrm{d}\kappa(\tau)}{\mathrm{d}\tau} + \frac{\mathrm{d}}{\mathrm{d}\tau}\ln\langle O\rangle_Z = -c\gamma(\tau)\cdot\ln(4\kappa) + \frac{\mathrm{d}}{\mathrm{d}\tau}\ln\langle O\rangle_Z \end{aligned} \tag{3.22}$$

with the first derivative term as in (3.17). In the second derivative term I employ eqs. (3.11) and (3.18) again to find for $O = \rho$ and $c = 1/2$ the closed form

$$\begin{aligned} \gamma(\tau) &= \frac{1}{\ln(4\kappa)} \frac{\beta\langle O S_\beta\rangle_{\rm c} - \lambda\langle O S_\lambda\rangle_{\rm c}}{\kappa\langle O S_\kappa\rangle_{\rm c} - c\,\langle O\rangle_Z} \\ &= \frac{1}{\ln(4\kappa)} \frac{\beta\langle \rho\, S_\beta\rangle_{\rm c} - \lambda\langle \rho\, S_\lambda\rangle_{\rm c}}{\kappa\langle \rho\, S_\kappa\rangle_{\rm c} - \frac{1}{2}\langle\rho\rangle_Z}\,, \end{aligned} \tag{3.23}$$

which is assumed to be inserted into eq. (3.20).

Alternatively one can consider instead of $O^{(\chi)}[\gamma]$ in (3.20) an analogous quantity, which is obtained on similar footing. Denoting with Z_k the partition function of the topological sector with $Q_{\rm top} = k \in \mathbb{Z}$, i.e.

$$Z = \sum_{k=-\infty}^{\infty} Z_k = Z_0 + 2\sum_{k=1}^{\infty} Z_k\,, \quad Z_k = \int \mathcal{D}[U,\varphi]\, {\rm e}^{-S[U,\varphi]}\, \delta_{Q_{\rm top},k}\,, \tag{3.24}$$

I introduce

$$z_k \equiv \frac{Z_k}{Z} = \left\langle \delta_{Q_{\rm top},k}\right\rangle_Z\,, \quad \langle O\rangle_{Z_k} = \frac{1}{Z_k}\int \mathcal{D}[U,\varphi]\, {\rm e}^{-S[U,\varphi]}\, O\, \delta_{Q_{\rm top},k}\,, \tag{3.25}$$

where the latter means an expectation value in the topological sector k. The counterpart of eqs. (3.11) and (3.18) after substituting (3.15) – (3.17) is here

$$\begin{aligned} \frac{\rm d}{{\rm d}\tau}\ln Z_k(\tau) &= \frac{1}{Z_k(\tau)}\frac{\rm d}{{\rm d}\tau} Z_k(\tau) \;=\; -\sum_{c_i\in\mathcal{P}} \frac{{\rm d}c_i(\tau)}{{\rm d}\tau}\,\langle S_i\rangle_{Z_k} \\ &= -\beta\langle S_\beta\rangle_{Z_k} + \lambda\langle S_\lambda\rangle_{Z_k} + \gamma(\tau)\cdot\kappa\ln(4\kappa)\cdot\langle S_\kappa\rangle_{Z_k}\,, \end{aligned} \tag{3.26}$$

and for a dilute gas of instantons and large volumes, compare with eq. (1.51) in section 1.2, the topological susceptibility (3.19) is the sector sum

$$a^2\chi_{\rm top} = \frac{1}{\Omega}\,\langle k^2\rangle_Z = \frac{1}{\Omega}\,\frac{1}{Z}\,\sum_{k\in\mathbb{Z}} k^2 Z_k = \frac{2}{\Omega}\,\frac{\sum_{k=1}^{\infty} k^2 Z_k}{Z_0 + 2\sum_{k=1}^{\infty} Z_k} \tag{3.27}$$

in terms of Z_k. From eq. (3.9) and $d_{\chi_{\rm top}} = 2$ it holds

$$\frac{\rm d}{{\rm d}\tau}\,\ln\left(a^2\chi_{\rm top}\right) = -1 \tag{3.28}$$

as before, and bearing in mind that Ω is independent of τ, some straightforward manipulations with the logarithms of the sums in (3.27) end in the scaling condition

$$\begin{aligned} O_K^{(\chi)}[\gamma] &\equiv \frac{1}{\sum_{k=1}^K k^2\tilde{z}_k}\sum_{k=1}^K k^2\tilde{z}_k\,\frac{\rm d}{{\rm d}\tau}\ln Z_k(\tau) - \sum_{k=0}^K \tilde{z}_k\,\frac{\rm d}{{\rm d}\tau}\ln Z_k(\tau) \\ &= -1\,, \quad \tilde{z}_k \equiv \begin{cases} z_0 & , k=0 \\ 2z_k & , k>0 \end{cases}\,, \end{aligned} \tag{3.29}$$

in which the derivatives with respect to τ have to be evaluated via eq. (3.26). Strictly speaking, the sum over k is infinite as in (3.27), however, in the numerical simulation there is only a finite number of sectors with non-vanishing incidence probability, over which the sum extends. The observable $O_K^{(\chi)}[\gamma]$ with $K \geq 1$ the maximally contributing sector is absolutely identical to $O^{(\chi)}[\gamma]$ in (3.20), and it turned out in the simulations that this was always true when truncating the sum at $K = 4$.

3.3.2 Numerical analysis and discussion

In the sequel I restrict myself to the middle LCP L2. The reasons are that this line is well separated from the pure gauge theory regime, where as best as the data of section 3.2 admitted the scaling of $\chi_{\rm top}$ is most pronounced, and that the emerging κ–values are still small enough to accumulate sufficient statistics with conclusive estimates in a tolerable amount of computer time. In order to compensate for a possible lack of information through the omission of the most continuum-like point D, the two intermediate points $\mathrm{I_{AB}}$ and $\mathrm{I_{BC}}$ between A and C were included in the investigations. So I measured the expectation values entering eqs. (3.20) and (3.23) in the all these LCP points on L2 as listed in table 3.6. The matching of the renormalized vacuum expectation value of the scalar field v_R required by the condition (3.7) was realized by a proper adjustment of κ in the manner of section 3.1.

set	lattice	β	λ	κ	sweeps	v_R
$\mathrm{A_1}$	16×16	10.0	0.01	0.27942	1000000	1.6147(1)
$\mathrm{I_{AB}}$	24×24	22.5	0.004444	0.264695	2000000	1.6144(1)
B	32×32	40.0	0.0025	0.258835	6000000	1.6146(1)
$\mathrm{I_{BC}}$	48×48	90.0	0.001111	0.2542405	2000000	1.6146(2)
C	64×64	160.0	0.000625	0.2525	3000000	1.6148(1)
$\mathrm{A_1}$	24×24	10.0	0.01	0.27942	500000	1.6149(2)
$\mathrm{I_{AB}}$	32×32	22.5	0.004444	0.264695	1000000	1.6143(1)
$\mathrm{I_{AB}}$	48×48	22.5	0.004444	0.264695	600000	1.6143(1)

Table 3.6: *Parameters and statistics of the simulation points on the middle LCP, where two new parameter sets I_{AB} and I_{BC} have been included. As previously, the product $\beta\lambda$ is fixed to 0.1, and κ is tuned to fulfill the renormalization condition on v_R.*

As it is clear from their definitions, $O^{(\chi)}[\gamma]$ and $\gamma(\tau)$ are functions of primary averages and thus secondary quantities, which can not be combined appropriately in the simultaneous MC runs, so that the full histories of the measurement samples of all relevant observables were blocked into subsamples to be averaged already during the simulations. The numerical computation of $O^{(\chi)}[\gamma]$ and $\gamma(\tau)$ according to eqs. (3.20) and (3.23) was done in jackknife

set	κ	$a^2\chi_{\rm top}\cdot 10^4$	$\gamma(\tau)$	$O^{(\chi)}[\gamma]$	stat. error	syst. error
A_1	0.27942	2.070(17)	0.7896(8)	-1.180	0.057	0.010
I_{AB}	0.264695	0.8959(65)	0.8474(10)	-0.964	0.062	0.013
B	0.258835	0.5488(37)	0.8806(14)	-0.874	0.052	0.018
I_{BC}	0.2542405	0.2824(26)	0.9050(13)	-0.759	0.143	0.018
C	0.2525	0.1847(15)	0.9161(16)	-0.744	0.143	0.022
A_1	0.27942	2.047(21)	0.7894(10)	-1.017	0.071	0.012
I_{AB}	0.264695	0.9216(90)	0.8508(10)	-0.795	0.099	0.013
I_{AB}	0.264695	0.9242(61)	0.8475(13)	-1.107	0.140	0.016

Table 3.7: *Results for the observables, which characterize the quality of the scaling behaviour of the topological susceptibility. The estimates and their statistical errors come from jackknife analyses with independent subsamples from the data of table 3.6. In $\kappa = 0.258835$ (set B) the estimates on χ_{top} and $\gamma(\tau)$ are only from $3\cdot 10^6$ and 10^6 configurations, respectively.*

analyses within the jackknife samples calculated from these subsamples as for all other secondary quantities on the LCPs too, and the results together with their statistical jackknife errors and the systematic errors owing to the statistical uncertainties in the determinations of $\gamma(\tau)$ are presented in table 3.7.

The dependence of the logarithm of the dimensionless product $\beta a^2\chi_{\rm top}$ on the scale parameter τ is depicted in the upper diagram of figure 3.4. In addition to the discrete data points, its derivatives with respect to τ,

$$\frac{\mathrm{d}}{\mathrm{d}\tau}\ln\left(\beta a^2\chi_{\rm top}\right) = \frac{\mathrm{d}}{\mathrm{d}\tau}\ln\beta + \frac{\mathrm{d}}{\mathrm{d}\tau}\ln\left(a^2\chi_{\rm top}\right) = 1 + O^{(\chi)}[\gamma]$$

from eqs. (3.8) and (3.20), are recorded as slopes of the corresponding 'tangents' as well. One can easily see that the estimates on $\beta a^2\chi_{\rm top}$ from direct measurements show the behaviour as prescribed by the tangents in these points, which unfortunately do not have the tendency to approximate an horizontal slope on their passage from A to C. This is substantiated further by the lower diagram in the same figure, where $\ln h = \ln h(\tau)$ and its derivatives,

$$\frac{\mathrm{d}}{\mathrm{d}\tau}\ln h(\tau) = \frac{1}{h}\frac{1}{\kappa}\frac{\mathrm{d}\kappa(\tau)}{\mathrm{d}\tau} = -\gamma(\tau)$$

from eqs. (3.13) and (3.17), are illuminated in dependence of τ. After a subtraction of the contributions linear in τ, almost no discrepancies between the derivatives in the individual points given by the slopes of the tangents and the finite differences $\Delta\ln h(\tau)/\Delta\tau$ contained in the polygon connecting the points A to C are visible. Hence the evolutions of $\beta a^2\chi_{\rm top}$ and κ with τ on the LCP, the latter being inferred from the demand to keep v_R constant, are to a certain degree consistent with the evolutions of their derivatives. Both observations are conform with the scaling violations along the LCPs of section 3.1 made for $\chi_{\rm top}/m_H^2$ before.

The error on the numerical fixing of v_R via the renormalization condition (3.7) is the only intrinsic uncertainty left in this method. A rather conservative estimation of its influence on $a^2\chi_{\rm top}$ and $\gamma(\tau)$ leads to the result that for a variation of v_R about 0.2 %, which is more than five times larger than the absolute spread of all v_R–values in table 3.6 around their median $\overline{v}_R = 1.6146$, the induced changes in $a^2\chi_{\rm top}$ and $\gamma(\tau)$ are below 5 % and 0.1 %, respectively, and therefore without any measurable influence on the scaling criterion provided by $O^{(\chi)}[\gamma]$. Since a — though not extraordinarily marked — discrepancy between $\beta a^2\chi_{\rm top}$ and its derivative with respect to τ is still recognizable in points A_1, I_{AB}, and B on the smallest lattices used, it is near at hand to look for possible finite-size effects at least in the first two points by repeating the MC runs on larger lattices at otherwise identical parameters. The results of simulations with lattice extensions scaled by a factor 3/2 are displayed in the lower two rows of tables 3.6, 3.7, and in figure 3.5, where they have been combined with the unchanged data in points B, I_{BC}, and C. Owing to the slight shifts of $a^2\chi_{\rm top}$ and $\gamma(\tau)$ in I_{AB} outside their statistical errors compared to the smaller volume, the asymptotic scaling of $\beta a^2\chi_{\rm top}$ seems to have somewhat improved, but this effect is not significant enough to suspect a contradiction between its failure and the conceptionally perhaps more successful scaling criterion based on the behaviour of its derivatives. In a final check I increased the lattice volume in I_{AB} again by a factor $(3/2)^2$, see the last row of table 3.6, and as can be verified from the corresponding entries of the results in table 3.7, finite-size effects on $a^2\chi_{\rm top}$, $\gamma(\tau)$, and $O^{(\chi)}[\gamma]$ are now negligible or even absent.

Joining all these informations together, I necessarily must state that within these findings the dimensionless observable $\beta a^2\chi_{\rm top} = \chi_{\rm top}/e_0^2$ does not seem to scale in the continuum limit $\beta \to \infty$ along LCP L2 either. So far, of course, the statistical accuracy of the data do not already exclude a more optimistic possibility: In contrast to the fact that $\beta a^2\chi_{\rm top}$ does not approach a constant value when passing from simulation points A to C, its slope could still vanish in the continuum limit and hint at asymptotic scaling of this quantity, if the trajectory defined by the renormalization conditions (3.6) and (3.7) were followed beyond the points considered here. At the moment, however, such an interpretation may be rather improbable and would need further explanation from some deeper insight into the problem, which is actually not available. Finite-volume effects for $a^2\chi_{\rm top}$ as well as for its derivative with respect to the scale parameter $\tau = \ln\beta$, implicitly determined by $O^{(\chi)}[\gamma]$, can not definitely be ruled out, but there is no fear (or better: hope) that they could change this conclusion qualitatively. Moreover, I expect the topological susceptibility to enjoy a quite similar, unclear behaviour on the LCPs L1 and L3 too, once the statistical and therewith numerical precision in these points would become proportionate to the data of L2.

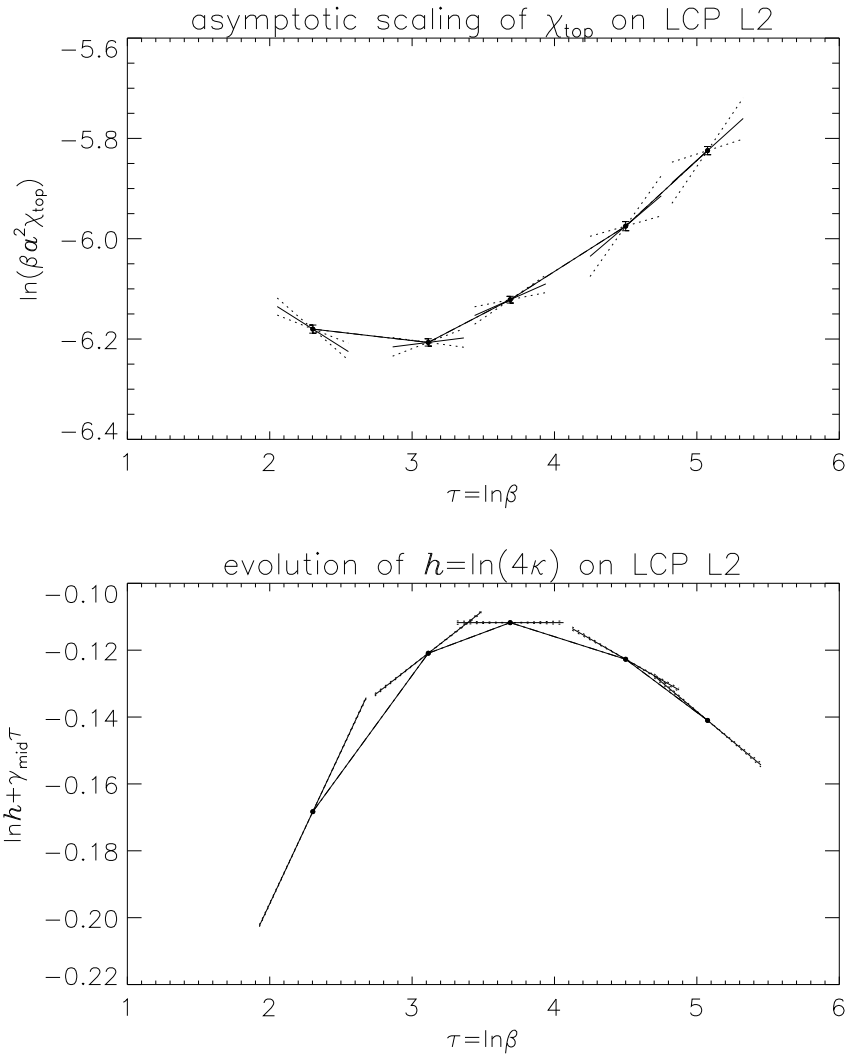

Figure 3.4: *Asymptotic scaling of χ_{top} on the middle LCP L2.* ***Upper plot:*** $\ln(\beta a^2\chi_{top})$ *as a function of τ. Its tangents in the discrete simulation points of table 3.6 have slopes $1+O^{(\chi)}[\gamma]$. The dotted lines correspond to the sum of statistical and systematic errors on this quantity.* ***Lower plot:*** $\ln h$ *as a function of τ, whose tangents have slopes $-\gamma(\tau)$. Its linear part has been partly removed by a shift with $\gamma_{mid}\tau$, $\gamma_{mid}\equiv\gamma(\tau)\,|_{set=B}$ for better visualization. A more thorough discussion is found in the text.*

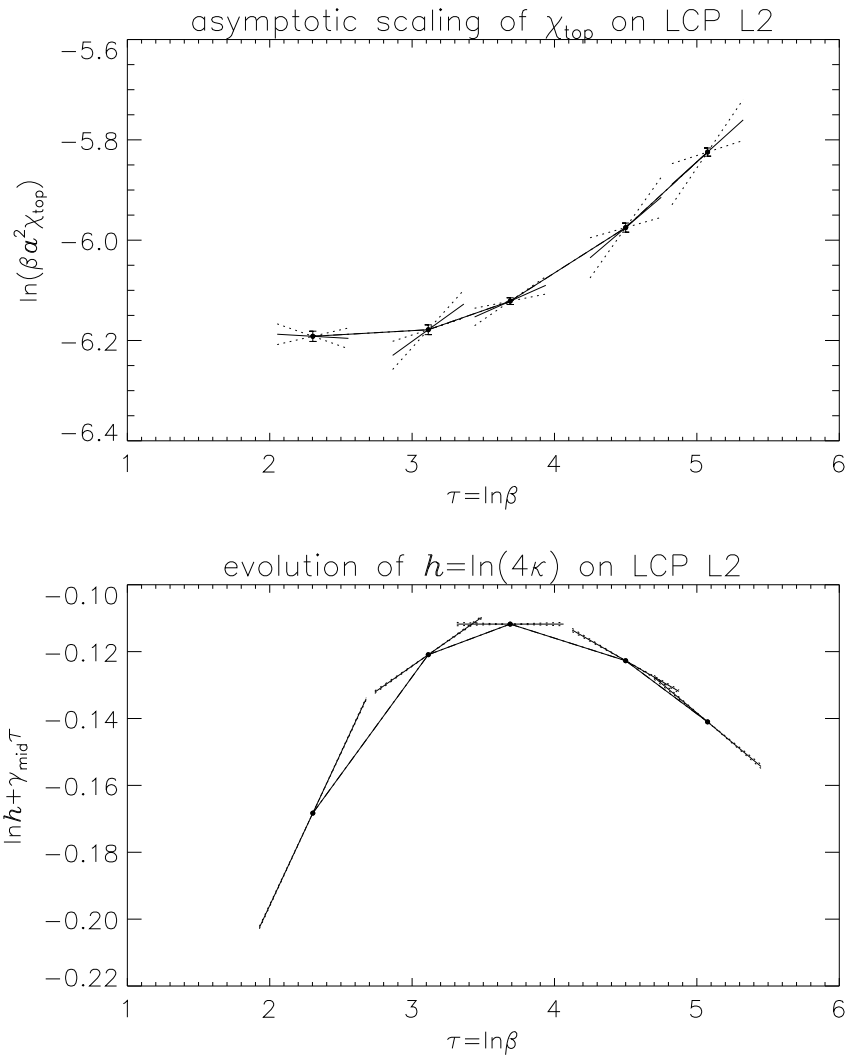

Figure 3.5: *The same as in figure 3.4, but with the left two points A_1 and I_{AB} substituted by the results of the two forelast rows in table 3.7 coming from the larger lattices. While χ_{top} tends to have small finite-volume effects, $h = \ln(4\kappa)$ appears to stay less affected.*

3.4 Confinement by instantons

This section is devoted to a nice confinement mechanism for fractional charges in the two-dimensional abelian Higgs model, which goes back to refs. [77, 78] and can be attributed to instantons in the dilute gas approximation. Recently, it has also been worked out that this phenomenon is an analogue of the Aharonov-Bohm effect in three- and four-dimensional abelian Higgs models [80].

The force between an external pair of static quarks is most conveniently investigated by means of the static quark-antiquark potential extracted from large Wilson loops, which were introduced in section 1.2 of chapter 1 as a measure for the response of the gauge field to an external quark-like source passing around his perimeter. For the pure gauge theory in two dimensions it has been mentioned before that this potential is linear in the spacelike distance R for any charges, i.e. the Wilson loops obey the area law, and the force, which as derivative (gradient) of the potential with respect to R is constant in this case, confines the external quark-antiquark pair. In the presence of a Higgs field in the fundamental representation of the gauge group it is generally known [22] that the confinement concept gets obscured by the fact that an external source can always be screened by fluctuations of the Higgs field. So even if the energy between the static sources starts increasing as they separate, it becomes perhaps favourable to pop a scalar particle-antiparticle pair out of the vacuum, which shields the gauge charge of the sources and prevents the energy to grow further. But the long-range characteristics of the static potential depends crucially on the modulus q of the external charges in units of the charge of the elementary scalar field modes e_0, and one has to distinguish between integer ($q/e_0 = 1$) and non-integer[4] values ($q/e_0 = 1/2$). The emerging qualitative scenario may be elucidated in reference to the continuum action of section 1.1, where the sign of the bare mass squared m_0^2 decides about the 'phases' of the theory. For integer q one always expects screening behaviour. The Wilson loop obeys a perimeter law, and the force between the external charges should fall off exponentially. The intuitive reason is that the charges of the dynamical scalar field, which can materialize as a particle-antiparticle pair out of the ground state, are integer, and as a consequence, an arbitrarily wide separation of the external test charges gets energetically possible and will probably end in subsequent processes like 'hadronization' with the screening scalar charges themselves. The situation changes for a non-integer charges q. Owing to the distance independent, confining Coulomb force in the case $m_0^2 > 0$ it is now impossible to separate particles and antiparticles, and all resulting bound states are stable, because they can not decay through the emission of — in two dimensions non-existent — photons. In the Higgs phase with $m_0^2 < 0$, on the other hand, one would expect free external charges, which again feel the screening effect of the massive vector boson in the same fashion as for integer charges.

[4]Since in the definitions of gauge field $A_{x,\mu}$ and field strength F_x the charge e_0 is absorbed, see chapter 1, these two cases translate on the lattice into $q = 1$ and $q = 1/2$, respectively.

However, in this context it is a special feature of the present model that instantons are exclusively responsible for confinement of fractional charges also in the Higgs region, i.e. the long-range force between external particles with $q = 1/2$ stays independent of their separations. To begin with, I will sketch the argument in the continuum first and discuss the numerical results from the lattice simulations later.

3.4.1 Derivation in the continuum

Here I orientate myself by refs. [5, 79], which the reader should consult for more details about instantons and their rôle in quantum mechanics and field theory, apart from the literature quoted in the introduction.

Suppose that there is a dilute gas of widely separated, non-interacting instantons and antiinstantons in a finite volume V with extensions L_i, $i = 1, \ldots, D$. This approximation — the dilute gas approximation — presumes an instanton density, which is small enough for the mean distance between instantons and antiinstantons in the system to be so large against the correlation length as the typical interaction range of their attractive potential that the interactions of instantons with antiinstantons can readily be neglected. Then a saddlepoint expansion of the functional integral around the stationary point of the Euclidean action, i.e. the instanton solution of the classical field equations, gives for the semiclassical instanton transition rate in the continuum

$$\begin{aligned} \Gamma_{\mathrm{inst}} &= \prod_{i=1}^{D} \left[\left(\frac{S_{\mathrm{inst}}}{2\pi} \right)^{\frac{1}{2}} L_i \right] \mathcal{D}^{-\frac{1}{2}} \, \mathrm{e}^{-S_{\mathrm{inst}}} , \quad \mathcal{D} \equiv \left| \frac{\det'[\phi_{\mathrm{inst}}]}{\det\,[\overline{\phi}]} \right| \\ &= K V_s T \, \mathrm{e}^{-S_{\mathrm{inst}}} , \quad K \equiv \left(\frac{S_{\mathrm{inst}}}{2\pi} \right)^{\frac{D}{2}} \mathcal{D}^{-\frac{1}{2}} \end{aligned} \tag{3.30}$$

with V_s denoting the spatial volume and S_{inst} the classical instanton action, which already appeared in section 2.1.2 of chapter 2. The fluctuation determinant $\mathcal{D}$, which implicitly contains divergent quantum corrections to be regularized, depends on the instanton configuration $\phi_{\mathrm{inst}}(x)$ and the stable minimum $\overline{\phi}(x)$ of the classical scalar potential. Each zero mode due to translational invariance in the space-time directions contributes a portion $(S_{\mathrm{inst}}/2\pi)^{1/2}$ to the pre-exponential factor K, and its vanishing eigenvalues, besides the negative one from the saddlepoint solution itself, have to be omitted for the evaluation of the primed determinant in the numerator. In the two-dimensional case with $V = V_s T = RT$ considered here the instanton transition rate reads

$$\Gamma_{\mathrm{inst}} = K V \, \mathrm{e}^{-S_{\mathrm{inst}}} , \quad K = \frac{S_{\mathrm{inst}}}{2\pi} \, \mathcal{D}^{-\frac{1}{2}} . \tag{3.31}$$

The central point for the following is to establish a relation between the topological susceptibility and this semiclassical rate:

$$\chi_{\mathrm{top}} = \frac{2\,\Gamma_{\mathrm{inst}}}{V} . \tag{3.32}$$

This may be demonstrated by writing the path integral representation of the time evolution in a periodic potential, whose minima are associated with the vacua of different topological charge sectors, as a dilute-gas sum over n instantons and $\bar{n}$ antiinstantons. If H is the Hamilton operator of the system and $\mathrm{e}^{\eta} \equiv \Gamma_{\mathrm{inst}}$ for the moment, the relevant matrix element for a tunneling transition between an initial state $|k_{\mathrm{i}}\rangle$ with $Q_{\mathrm{top}} = k_{\mathrm{i}}$ to a final state $|k_{\mathrm{f}}\rangle$ with $Q_{\mathrm{top}} = k_{\mathrm{f}}$ and $k_{\mathrm{f}} - k_{\mathrm{i}} = k \in \mathbb{Z}$ is, modulo a constant factor,

$$\langle k_{\mathrm{f}}|\mathrm{e}^{-HT}|k_{\mathrm{i}}\rangle = \sum_{n=0}^{\infty}\sum_{\bar{n}=0}^{\infty} \frac{1}{n!\bar{n}!}\,\mathrm{e}^{\eta n}\,\mathrm{e}^{\eta\bar{n}}\,\delta_{n-\bar{n},k}\,. \tag{3.33}$$

If I define the function

$$z(x) \equiv \sum_{k\in\mathbb{Z}}\sum_{n=0}^{\infty}\sum_{\bar{n}=0}^{\infty} \frac{1}{n!\bar{n}!}\,\mathrm{e}^{(\eta+x)n}\,\mathrm{e}^{(\eta-x)\bar{n}}\,\delta_{n-\bar{n},k}\,, \tag{3.34}$$

its second derivative and the δ–function,

$$\begin{aligned}\frac{\mathrm{d}^2}{\mathrm{d}x^2}\,z(x) &= \sum_{k}\sum_{n,\bar{n}} \frac{1}{n!\bar{n}!}\,(n-\bar{n})^2\,\mathrm{e}^{(\eta+x)n}\,\mathrm{e}^{(\eta-x)\bar{n}}\,\delta_{n-\bar{n},k} \\ &= \sum_{k} k^2\,\Big[\sum_{n,\bar{n}} \frac{1}{n!\bar{n}!}\,\mathrm{e}^{(\eta+x)n}\,\mathrm{e}^{(\eta-x)\bar{n}}\,\delta_{n-\bar{n},k}\Big]\,,\end{aligned}$$

yield the expectation value of the squared topological charge in analogy to eq. (3.27) as

$$\langle k^2\rangle_Z = \frac{\sum_{k\in\mathbb{Z}} k^2\,\langle k_{\mathrm{f}}|\mathrm{e}^{-HT}|k_{\mathrm{i}}\rangle}{\sum_{k\in\mathbb{Z}}\langle k_{\mathrm{f}}|\mathrm{e}^{-HT}|k_{\mathrm{i}}\rangle} = \frac{1}{z(0)}\,\frac{\mathrm{d}^2}{\mathrm{d}x^2}\,z(x)\,\Big|_{x=0}\,. \tag{3.35}$$

On the other hand the series

$$\begin{aligned}z(x) &= \sum_{k\in\mathbb{Z}}\sum_{n,\bar{n}} \frac{1}{n!\bar{n}!}\,\left(\mathrm{e}^{\eta+x}\right)^n\left(\mathrm{e}^{\eta-x}\right)^{\bar{n}}\,\delta_{n-\bar{n},k} \\ &= \sum_{k\in\mathbb{Z}} \delta_{n-\bar{n},k}\,\exp\left\{\mathrm{e}^{\eta+x}+\mathrm{e}^{\eta-x}\right\}\end{aligned}$$

is a product of two exponentials so that

$$\frac{\mathrm{d}^2}{\mathrm{d}x^2}\,z(x) = \Big[\left(\mathrm{e}^{\eta+x}+\mathrm{e}^{\eta-x}\right) + \left(\mathrm{e}^{\eta+x}+\mathrm{e}^{\eta-x}\right)^2\Big]\,z(x)\,,$$

and eq. (3.35) together with (3.27) and $\mathrm{e}^{\eta} = \Gamma_{\mathrm{inst}}$ becomes

$$V\chi_{\mathrm{top}} = \langle k^2\rangle_Z = \frac{1}{z(0)}\,\frac{\mathrm{d}^2}{\mathrm{d}x^2}\,z(x)\,\Big|_{x=0} = 2\,\mathrm{e}^{\eta} = 2\,\Gamma_{\mathrm{inst}}\,, \tag{3.36}$$

and eq. (3.32) is proven.

The non-zero probability amplitudes for transitions through finite-energy barriers between homotopically inequivalent gauge-rotated vacua, which has been employed in this

calculation, expresses the well accepted fact that the true ground state of quantum gauge theories is infinitely degenerate. Thus it can be written as a superposition[5] of all these vacua,

$$|\theta\rangle = \sum_{k\in\mathbb{Z}} \mathrm{e}^{\,ik\theta}\,|k\rangle\,, \tag{3.37}$$

and the winding number $k \in \mathbb{Z}$ labelling the homotopy classes is equal to the topological charge considered so far. Except for a phase factor, the so-defined true vacuum $|\theta\rangle$ is invariant under 'large' gauge transformations, which interpolate non-continuously between states in different homotopy classes. When inserting the Fourier representation of the δ–function

$$\delta_{nk} = \frac{1}{2\pi}\int_0^{2\pi} \mathrm{d}\theta\,\mathrm{e}^{\,-i(n-k)\theta}$$

into eq. (3.33) and using the exponential series, Euler's formula, and eq. (3.31) in the last step of

$$\begin{aligned}
\langle k_\mathrm{f}|\mathrm{e}^{\,-HT}|k_\mathrm{i}\rangle &= \frac{1}{2\pi}\sum_{n,\bar n}\frac{1}{n!\bar n!}\,(\Gamma_\mathrm{inst})^n\,(\Gamma_\mathrm{inst})^{\bar n}\int_0^{2\pi}\mathrm{d}\theta\,\mathrm{e}^{\,-i(n-\bar n)\theta}\,\mathrm{e}^{\,ik\theta} \\
&= \frac{1}{2\pi}\int_0^{2\pi}\mathrm{d}\theta\,\mathrm{e}^{\,ik\theta}\Big[\sum_n\frac{1}{n}\left(\Gamma_\mathrm{inst}\,\mathrm{e}^{\,-i\theta}\right)^n\Big]\Big[\sum_{\bar n}\frac{1}{\bar n}\left(\Gamma_\mathrm{inst}\,\mathrm{e}^{\,i\theta}\right)^{\bar n}\Big] \\
&= \frac{1}{2\pi}\int_0^{2\pi}\mathrm{d}\theta\,\mathrm{e}^{\,ik\theta}\,\exp\{\,2\,\Gamma_\mathrm{inst}\cos\theta\,\} \\
&= \frac{1}{2\pi}\int_0^{2\pi}\mathrm{d}\theta\,\mathrm{e}^{\,ik\theta}\,\exp\left\{\,2KV_sT\mathrm{e}^{\,-S_\mathrm{inst}}\cos\theta\,\right\}\,,
\end{aligned}$$

one recognizes that there is a continuum of energy eigenvalues $E(\theta)$ with

$$\langle k_\mathrm{f}|\mathrm{e}^{\,-HT}|k_\mathrm{i}\rangle \overset{T\to\infty}{\sim} \mathrm{e}^{\,-E(\theta)\,T} \quad\Leftrightarrow\quad E(\theta) = -2KV_s\,\mathrm{e}^{\,-S_\mathrm{inst}}\cos\theta\,, \tag{3.38}$$

which has to be identified as the energy of the true vacuum eigenstate $|\theta\rangle$ in eq. (3.37). Hence, the topological susceptibility as well as the Euclidean functional integral involving the action $S = S[A,\phi_0]$ of the theory

$$\int\mathcal{D}[A,\phi_0]\,\mathrm{e}^{\,-S}\,\mathrm{e}^{\,ik\theta} \;\propto\; \langle\theta|\mathrm{e}^{\,-HT}|\theta\rangle \;\propto\; \exp\left\{\,2KV_sT\mathrm{e}^{\,-S_\mathrm{inst}}\cos\theta\,\right\} \tag{3.39}$$

could be expressed via the partition function of a dilute gas of instantons in terms of the semiclassical instanton transition rate Γ_inst in eqs. (3.30) or (3.31).

After these preparations the energy shift of the vacuum, caused by two static charges q in units of e_0 with opposite sign brought into the system, is deduced from the expectation value $\langle\theta|W_q|\theta\rangle$ of a rectangular Wilson loop $W_q = W_q[\mathcal{A}]$ of area $\mathcal{A}$ with side lengths R and T, which is the contour integral

$$W_q = \mathrm{Re}\,\exp\left\{iq\oint_{\partial\mathcal{A}}\mathrm{d}x_\mu A_\mu(x)\right\} = \mathrm{Re}\,\exp\left\{2\pi ik\,\frac{q}{e_0}\right\} \tag{3.40}$$

[5] This is very similar to the Bloch-wave functions in the quantum mechanical treatment of the electronic band structure in crystals with periodic potentials.

over its boundary $\partial\mathcal{A}$ and, in regard of eq. (1.48) of subsection 1.2.2, related to the topological charge

$$k = Q_{\text{top}} = \frac{e_0}{4\pi}\int_{\mathcal{A}} \mathrm{d}^2x\,\epsilon_{\mu\nu}F_{\mu\nu}(x) = \frac{e_0}{2\pi}\oint_{\partial\mathcal{A}} \mathrm{d}x_\mu A_\mu(x) \tag{3.41}$$

inside the loop so that eq. (3.39) with $V_s = R$ in two dimensions can be replaced by

$$\begin{aligned}\int \mathcal{D}[A,\phi_0]\,\mathrm{e}^{-S}\,W_q\,\mathrm{e}^{ik\theta} &= \int \mathcal{D}[A,\phi_0]\,\exp\left\{-S + ik\left(\theta + \frac{2\pi q}{e_0}\right)\right\} \\ &= \exp\left\{2KRT\,\mathrm{e}^{-S_{\text{inst}}}\cos\left(\theta + \frac{2\pi q}{e_0}\right)\right\}\,. \end{aligned}\tag{3.42}$$

If the dilute-gas sum over instantons and antiinstantons, which led to these approximations of the relevant functional integrals, is split into sums over objects lying inside and outside the Wilson loop, while configurations overlapping the loop are neglected at the same time, one obtains

$$\begin{aligned}\ln\langle\theta|W_q|\theta\rangle &= \ln\left\{\frac{\int \mathcal{D}[A,\phi_0]\,\mathrm{e}^{-S}\,W_q\,\mathrm{e}^{ik\theta}}{\int \mathcal{D}[A,\phi_0]\,\mathrm{e}^{-S}\,\mathrm{e}^{ik\theta}}\right\} \\ &= 2K\,\mathrm{e}^{-S_{\text{inst}}}\left\{\Big(R'T' - RT\Big)\cos\theta + RT\cos\left(\theta + \frac{2\pi q}{e_0}\right) - R'T'\cos\theta\right\} \\ &= -2KRT\,\mathrm{e}^{-S_{\text{inst}}}\left\{\cos\theta - \cos\left(\theta + \frac{2\pi q}{e_0}\right)\right\}\,,\end{aligned}$$

where the space-time region outside the loop was assumed to be bordered by some larger (in principle infinite) Wilson loop of extensions R' and T', the first two terms come from the inside and outside portions of the numerator in its representation (3.42), and the last one from the denominator according to (3.39). Therefore, the resulting contribution to the static potential

$$\begin{aligned}\Delta V_q(R) &= -\lim_{T\to\infty}\frac{1}{T}\,\ln\langle\theta|W_q|\theta\rangle \\ &= 2KR\,\mathrm{e}^{-S_{\text{inst}}}\left\{\cos\theta - \cos\left(\theta + \frac{2\pi q}{e_0}\right)\right\}\end{aligned}\tag{3.43}$$

is proportional to the separation R between the external charges, thus linear in R with a force of constant strength. As it stands, this equation has the interesting property that the charges of the external test particles are completely screened by the charge of the Higgs condensate only for integer q, whereas for non-integer q the contribution ΔV_q signals confinement with a strength proportional to the topological susceptibility χ_{top}. To see this, I take $\theta = 0$, which is just the situation one encounters in the numerical analysis on the lattice of the next paragraph, because in the MC simulations I average over all topological charge sectors without any weighting with the corresponding phase factors $\mathrm{e}^{ik\theta}$. Then (3.43) together with eqs. (3.31) and (3.32) give indeed

$$\Delta V_q(R) = 2KR\,\mathrm{e}^{-S_{\text{inst}}}\left\{1 - \cos\left(\frac{2\pi q}{e_0}\right)\right\} = \chi_{\text{top}}\,R\left\{1 - \cos\left(\frac{2\pi q}{e_0}\right)\right\}$$

$$= \begin{cases} 0 & , q/e_0 = 1 \\ 2\,\chi_{\rm top}\,R & , q/e_0 = \frac{1}{2} \end{cases} . \tag{3.44}$$

To summarize, non-integer external charges in the two-dimensional U(1)–Higgs model are confined in both the symmetric phase ($m_0^2 > 0$) and the Higgs phase ($m_0^2 < 0$), but with the major difference that opposed to the former case, where the long-range force — coming from the ordinary linear Coulomb potential — is proportional to these charges, the force is exponentially small in the latter due to the prefactor in eq. (3.43), which is the typical mark of an instanton effect. It is also worthwhile to emphasize again that the linear Coulomb potential in the normal (1+1)–dimensional non-Higgs electrodynamics has to be expected even classically, i.e. the quantum result will survive in the limit $\hbar \to 0$, if I had retained the explicit $\hbar$–dependence in the derivation. However, as then the exponential factor in (3.43) would become $\mathrm{e}^{-S_{\rm inst}} \to \mathrm{e}^{-S_{\rm inst}/hbar}$, the linear confining potential of fractional charges in the abelian Higgs model — caused by instantons — is very much a non-perturbative quantum effect.

Finally, I should point out that this confinement mechanism essentially relies on the two-dimensionality of the model and does not work in four dimensions. An heuristic explanation found in refs. [77, 79] is based on the boundary conditions for the instanton solution in this case, which require the gauge fields in the limit of large spatial distances to approach pure gauges plus pieces falling off too fast to affect the Wilson loop integral, whose gauge invariance then solely allows non-contributing instantons in the always existing directions perpendicular to the loop.

3.4.2 Numerical analysis on the lattice

In order to examine, whether the saturation of the functional integral with instantons is reproduced by the non-perturbative numerical lattice simulations, I measured Polyakov loop correlations $P_q(R)$ in the LCP parameter sets of table 3.1. They were introduced in eqs. (1.41) and (1.43) of section 1.2 as Wilson loops for arbitrary external charges $q = 1$ and $q = 1/2$ with extensions $1 \leq R \leq L_1/2$ and $T = L_2$, i.e.

$$P_q(R) = W_q(R,T)\Big|_{T=L_2}, \quad W_q(R,T) = \left\langle \mathrm{e}^{\,iq\sum_{x\in\mathcal{A}_{R,T}} F_x} \right\rangle , \quad F_x \in [-\pi,\pi) ,$$

with $\mathcal{A}_{R,T} \subset \Lambda$ the area of the respective Wilson loop, and the static potential was computed from these expectations values as claimed in eq. (1.45) of subsection 1.2.1:

$$V_q(R) = -\frac{1}{q^2 L_2} \ln P_q(R) .$$

Because of the choice of Polyakov loop correlations as Wilson loops of maximal temporal extensions, the substitution of the limit $T \to \infty$ in the original potential definitions (1.34) or (3.43) by this prescription is warrantable.

The static potentials obtained in this way were fitted with uncorrelated least-squares fits to a modified Yukawa ansatz of the form

$$V_q(R) = V_{\rm yuk}(R) \, + \, \delta_{q,\frac{1}{2}} \, \alpha R \, , \quad V_{\rm yuk}(R) = \frac{e_R^2}{2m_s} \left(1 - {\rm e}^{\, -am_s R} \right) , \tag{3.45}$$

in which the second, linear term takes into account the expected instanton effects in $\Delta V_q(R)$ of the previous paragraph on fractional charges with $q = 1/2$ in the dilute gas approximation. The first part $V_{\rm yuk}(R)$ of this ansatz is the usual Yukawa-like shape and derives in direct analogy to the four-dimensional SU(2)–Higgs case from the assumption that the underlying particle reactions are governed by a massive vector boson exchange, see e.g. subsection 8.2.3 in chapter 8 and refs. [88, 115]. Lowest order (tree-level) perturbation theory in the continuum gives for $m_s > 0$ and $r \equiv Ra > 0$ the relevant contribution

$$\int_{-\infty}^{\infty} \frac{{\rm d}p}{2\pi} \, \frac{{\rm e}^{\, ipr}}{p^2 + m_s^2} = \frac{1}{\pi} \int_0^{\infty} {\rm d}p \, \frac{\cos{(pr)}}{p^2 + m_s^2} = \frac{{\rm e}^{\, -m_s r}}{2m_s} \tag{3.46}$$

after a straightforward application of the residuum theorem. Since $P_q(0) = 1$ holds for the Polyakov loop correlations, the attractive potential has to meet $V_q(0) = 0$, and its asymptotics (1.39) for large spacelike distances R in pure gauge theory leads to the prefactor e_R^2 in the first term of eq. (3.45), which here receives an interpretation as squared renormalized gauge coupling with $ae_R = ae_0 + \mathcal{O}(a^2 e_0^2) = 1/\sqrt{\beta} + \mathcal{O}(a^2 e_0^2)$. Whilst the screening behaviour $\lim_{R\to\infty} V_{\rm yuk}(R) = e_R^2/2m_s$ is compatible with $\lim_{R\to\infty} V(R) =$ constant as it is characteristic for static potentials (1.34) from Wilson loops with perimeter law (1.37), one recovers a nearly linear behaviour $aV_{\rm yuk}(R) \simeq a^2 e_R^2 R/2$ for $am_s \ll 1$ and small enough R. Hence the fit ansatz in eq. (3.45) is appropriate to verify the meaning of the fit parameters ae_R as renormalized gauge coupling, am_s as screening mass, closely connected to the vector boson mass am_W, and α as string tension, which now can be related through eq. (3.44) to the topological susceptibility,

$$q = \frac{1}{2} : \quad \frac{q^2 \alpha}{2} = a^2 \chi_{\rm top} \, , \tag{3.47}$$

in the validity range of the dilute gas approximation.

All fit results of the static potentials in the LCP simulation points are collected in table 3.8. In view of the continuum ansatz (3.45), which does not include any finite-lattice size or spacing corrections, the fit intervals beginning at $R = 1$ could not be extended to $R = L_1/2$. I discarded at least two of the last R–distances in dependence of reasonable values for $\chi^2/{\rm dof}$ at still significant statistical signal to noise ratios, and the physical lengths of the fit intervals on a given LCP were mostly taken to be equal.

The scaling of the fit parameters according to their dimensions in lattice units is generally good, and the theoretically predicted qualitative scenario is confirmed by the data. More precisely, the static potential for integer charges ($q = 1$) shows screening behaviour on all

LCP	set	κ	$q=1$		$q=1/2$		
			am_s	ae_R	am_s	ae_R	$\alpha/8\cdot 10^4$
L1	A_2	0.2937	0.5447(10)	0.3156(1)	0.5394(15)	0.3155(2)	$\simeq 0$
	B	0.2607	0.2660(9)	0.15792(5)	0.2657(15)	0.1577(2)	0.039(30)
	C	0.253	0.1289(11)	0.07892(3)	0.1304(16)	0.0787(2)	0.026(18)
	D	0.250815	0.0642(18)	0.03949(2)	0.643(26)	0.0395(3)	$\simeq 0$
L2	A_2	0.2858	0.4358(15)	0.3183(2)	0.4364(22)	0.3136(3)	1.52(14)
	B	0.258835	0.2053(14)	0.15806(7)	0.2175(27)	0.1540(5)	0.802(89)
	C	0.2525	0.0949(18)	0.07900(4)	0.1001(27)	0.0765(5)	0.241(50)
	D	0.25069	0.0470(18)	0.03953(3)	0.0475(31)	0.0387(8)	0.054(36)
L3	A	0.2731	0.1996(33)	0.3223(4)	0.1878(24)	0.3209(3)	—
	B	0.257	0.0730(16)	0.1582(1)	0.0542(8)	0.1569(2)	—
	C	0.252	0.0255(12)	0.07885(7)	0.0190(6)	0.07854(7)	—
	D	0.25055	0.0057(5)	0.03943(2)	0.0060(17)	0.03943(2)	—

Table 3.8: *Fit results of the Polyakov loop correlations along the LCPs with jackknife errors. The simulated β–parameters correspond to the values 0.3163, 0.1581, 0.0791, and 0.0395 of the bare gauge coupling ae_0. The values of $\alpha/8$ should be compared with $a^2\chi_{top}$ in table 3.3.*

LCPs, and the renormalization of the bare gauge $ae_0 = 1/\sqrt{\beta}$ turns out to be always very small. But unlike the vector boson masses am_W from the L_φ^-–correlations of table 3.2 in section 3.1, which increase for decreasing $\kappa < \bar{\kappa}$, $\bar{\kappa}$ being the κ–value at minimal am_W, the screening masses am_s continue to decrease when going from L2 to L3 too. This is in fact the expected picture of a vanishing screening mass in the limit of pure gauge theory ($\kappa \to 0$), where the influence of the scalar field modes on short distances weakens before the screening effect due to the very small, but still finite screening mass at larger distances sets in again. In this sense, am_s behaves similarly to the plaquette masses, i.e those coming from correlations of the operators F or $\sin F$, which seem to resemble a massless, albeit non-existent, photon in the pure gauge theory limit as will be discussed in the next chapter. On the LCPs L1 and L2, which are both positioned in the Higgs region of the model, the screening masses am_s of table 3.8 and the vector masses am_W of table 3.2 are rather consistent with each other and fulfill $am_s \simeq am_W \simeq ae_R v_R = v_R/\sqrt{\beta} + \mathcal{O}(a^2 e_0^2)$ with v_R from table 3.1 in approximate agreement with eq. (3.5). For a cross-check of the screening dominance in the $q=1$ potentials, I also tried an ansatz with a linear term as in (3.45) with $q=1/2$, however, the vanishing of the coefficient α within its errors sustained that in this case the fit is not sensitive to such an additional degree of freedom.

The static potentials for non-integer external charges ($q=1/2$) possess a more complex structure. On the LCP L3, which lies closest to pure gauge theory and is not yet supposed

to comply with the dilute gas approximation, the three-parameter fits to the shape (3.45) are not able to disentangle the leading linear contribution of the screening part $V_{\rm yuk}(R)$ for $am_s \ll 1$ from the explicit linearity αR so that only a two-parameter fit as for $q = 1$ was suited to get stable fit results. When approaching the Higgs region $\kappa > \bar{\kappa}$, the topological susceptibility $\chi_{\rm top}$ lowers increasingly, and the assumption of a dilute gas of fewer and thus widely separated and weakly coupled instantons and antiinstantons becomes more and more justified. Hence the instanton-induced confinement mechanism described above comes into play now, and the screening behaviour of the potentials should be surpassed by a linear rise at large distances, where the instantons and antiinstantons as collective long-range modes in the system attain their strongest impact. The fit results in table 3.8 corroborate these

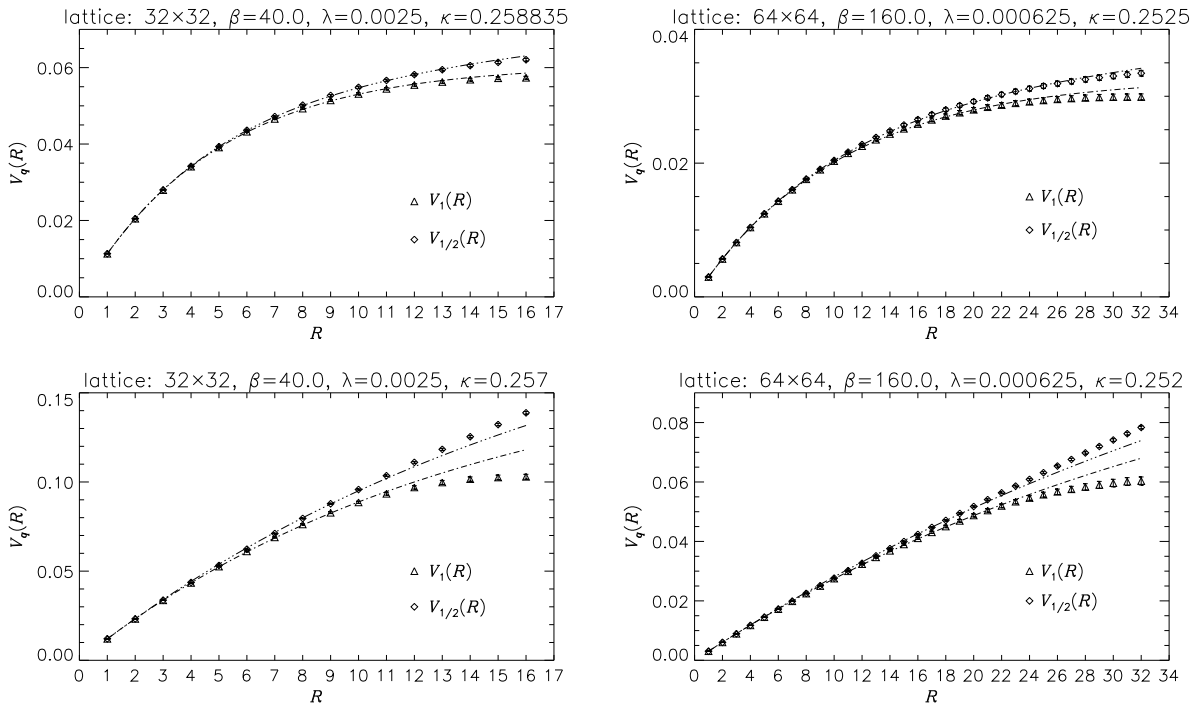

Figure 3.6: *Lattice potentials for external static charges with $q = 1, 1/2$ and their fit curves to the Yukawa ansatz (3.45). The errors of the lattice data are smaller than the plot symbols. The shown data points are representative for the LCPs L2 (upper plots), lying just in the Higgs regime, and L3 (lower plots), which is already close to pure gauge theory, while the parameter sets on the left and on the right correspond to different stages of the continuum limit on these trajectories. Some further comments are given in the text.*

expectations. In addition to the fit parameters ae_R and am_s, which agree quite well with those of the $q = 1$ potentials, it was possible to resolve the string tension α with acceptable statistical accuracy, in particular for the line L2 already lying in the Higgs regime. The corresponding $q = 1/2$ potentials display confinement, and the fit parameters α can be identified with $\chi_{\rm top}$ by using eq. (3.47). From a comparison with the directly measured

results on $\chi_{\rm top}$ in table 3.3 one concludes that the numbers are fairly compatible, although there is a slight quantitative discrepancy, since the values extracted from the Yukawa fits have a trend to be larger than the former ones. This may ascribed to the neglection of any lattice corrections in the continuum-like fit ansatz and, moreover, to the fact that α itself is, especially on L1, a genuinely small quantity, which is the more difficult to isolate from the screening part — and concurrently larger — the more points are left out from the end of the maximal R–extension for the individually chosen fit intervals limited by $L_1/2$.

The analyses of the static potentials from Polyakov loop correlations are exemplarily visualized in figure 3.6 for two parameter sets of the LCPs L2 and L3, respectively, which approach the continuum limit. Whereas the potentials $V_q(R)$ for $q = 1$ show screening in the Higgs region (upper left and right diagrams) as well as in the confinement region close to pure gauge theory (lower left and right diagrams), the linear instanton effect at large spatial separations R for $q = 1/2$ is clearly observable in the Higgs region. This stands in contrast to the confinement region, in which the nearly linear growth of the lattice data starting even at smaller R is produced by very low screening mass values am_s in $V_{\rm yuk}(R)$ of eq. (3.45) and not by instantons. Note that in the case of lower am_s and weaker screening the potentials are afflicted with larger finite-volume effects, tending to flatten them with increasing distance R in the same direction as the pure screening contribution $V_{\rm yuk}(R)$ does. Therefore, I had to discard at least four of the last possible R–distances in the potential fits of the pure gauge theory like line L3. Nevertheless, the numerical confirmation of the intrinsic interplay of the topological excitations with the interactions between the scalar charges in the model and the external static test charges, in particular the preservation of their confining force in the Higgs regime for $q = 1/2$, can be assessed as satisfactory.

Chapter 4

Some phase structure investigations

The following two items, which complete my studies of the lattice U(1)–Higgs model in two dimensions, are keyed to its phase structure and possible similarities as well as differences in comparison with the four-dimensional U(1)–Higgs model, also named compact scalar QED with Higgs field in the fundamental representation, and the fixed length case with $\lambda = \infty$ comprising the two-dimensional XY–model at infinite β. Since both models are comprehensively documented in the literature, see for instance refs. [81, 82, 83, 86, 87, 88] and [4, 67, 68, 70], I will not go into too much technical details here and mainly concentrate on those aspects, which are relevant for the model at hand.

4.1 Comparison with the $D = 4$ model

As anticipated in section 3.1 when discussing the mass spectrum of the model, the vector mass estimates am_W from correlation functions of the φ–link operator L_φ^- and the plaquette operators F or $\sin F$ are only consistent for $\kappa > \bar{\kappa}$. Recall that $\bar{\kappa}$, which will be frequently used from now on, denotes the crossover κ–value defined at the minimal am_W from L_φ^-–correlations. For decreasing $\kappa < \bar{\kappa}$ both the F– and $\sin F$–correlations weaken strongly with likewise worse signal to noise ratios and show a decreasing mass, finally dropping to zero, because the χ^2–fits of the measured correlation functions at spacelike lattice momenta $p_1 = 0$ and $p_1 = 2\pi/aL_1$ to the shapes (1.59) of subsection 1.2.3 give so small prefactors A that their exponential decays are no longer detectable. In view of the fact that in spite of the wrong parity of the spacelike plaquette sums at zero momentum in four dimensions, the plaquette operators at higher non-zero momenta couple to the physical photon [51], the vanishing of the correlations functions of the operators F and $\sin F$ would correspond to a massless photon state in the limit of pure gauge theory ($\kappa \to 0$). Within a non-perturbative MC study this was also found in the Coulomb phase of the four-dimensional lattice U(1)–Higgs model in ref. [88], which there provides the most natural way to distinguish between such a Coulomb

phase and confinement or Higgs phases, where the photon is massive, see below[1]. However, as already pointed out for the continuum model in section 1.1, a massless photon is no physical degree of freedom in a two-dimensional — i.e. spatially one-dimensional — theory, since its interpretation descends from the here missing components transversal to the direction of the gauge field propagation. Besides the qualitatively different behaviour of the L_φ^-–correlations in figures 3.1 and 3.2 — with no noticeable contributions from a massless photon-like state for $\kappa < \bar{\kappa}$ — from the plaquette correlations, the very similar κ–dependence of the Higgs and vector boson masses am_H and am_W as extracted from the respective operators ρ^2, L_φ^+, and L_φ^- compared to the model in four dimensions [88], in particular its characteristic dips, is another exciting observation.

These analogies to the compact lattice U(1)–model in four dimensions, where the inclusion of the radial mode of the scalar field enriches the phase landscape of the model considerably, were the actual motivation for the ensuing investigations in the present case. First, I briefly summarize the phase diagram of the four-dimensional model [86, 87, 88], whose lattice parametrization in terms of the gauge links $U_{x,\mu} \in \mathrm{U}(1)$, $\mu = 1, \ldots, 4$, the complex Higgs doublet field φ_x, and the couplings β, κ, and λ is identical to the two-dimensional one in chapter 1. Emanating from the deconfinement phase transition at $\beta = \beta_c \simeq 1$ in the pure gauge theory ($\kappa = 0$), one has for any fixed $\lambda < \infty$:

- **Coulomb phase ($\beta > \beta_c$ and $\kappa < \kappa_c$)**
  A phase with free, scalar charged states in the spectrum, which are exposed to the long-ranged Coulomb potential ($V(r) \propto -1/r$), and a massless photon as the vector gauge field coupled to the charges. Pairs of these charges can form neutral bound states, so-called scalar- and vector-like bosonium particles.

- **Confinement-Higgs phase ($\beta < \beta_c$ and $\kappa > 0$ or $\beta > \beta_c$ and $\kappa > \kappa_c$)**
  The confinement and Higgs regions are separated by a first oder phase transition only for $\lambda \lesssim \mathcal{O}(0.1)$ and analytically connected for larger λ–values. Both regions contain massive counterparts of the bosonium states in the Coulomb phase, namely the Higgs boson and a massive vector boson (photon). The latter is merged of the massive vector bosonium and the massless photon. The static potential is the short-ranged Yukawa potential ($V(R) \propto -\mathrm{e}^{-m_s r}/r$), prescribed by Wilson loops obeying the perimeter law, with a non-zero screening mass m_s. Moreover, there are still important physical differences:

  - **Confinement region ($\beta < \beta_c$ and $\kappa > 0$)**
    No charged states occur in the physical spectrum. The static charges are screened

[1] As the photon is an excitation in this model, which stays massless to all orders of perturbation theory in both phases, the generation of some non-vanishing photon mass in the confinement-Higgs phase appears a non-perturbative effect.

by a heavy but dynamical constituent field φ, like mesons consisting of heavy quarks in QCD.

– **Higgs region ($\beta > \beta_c$ and $\kappa > \kappa_c$)**
Here the static charges are screened via fluctuations of the scalar matter field φ, which condensates to $\langle \varphi^* \varphi \rangle = \langle \rho^2 \rangle$, associated with the Higgs phenomenon at work.

The transition between the Coulomb phase and the Higgs region, called the Higgs phase transition, is of first order for small λ and weakens for increasing λ and β.

4.1.1 Observables

As the Wilson loop criterion for confinement in the pure gauge theory fails in gauge theories interacting with dynamical matter fields, which are able to screen the confining linear potential in all phases [22], there have been proposed suitable criteria for the existence of free charged states with finite energy [85] and bound states of a charged particle and an external source [84] by means of gauge invariant two-point functions. Restricting to the former one defines

$$G(R,T) \equiv \left\langle \mathrm{Re}\left(\varphi_y^* U_{\mathcal{C}_{R,T}(y,x)} \varphi_x \right) \right\rangle \ , \tag{4.1}$$

which correlates the scalar fields φ_x and φ_y over a product of gauge link variables $U_{\mathcal{C}_{R,T}(y,x)}$ around an open path $\mathcal{C}_{R,T}(y,x) \in \Lambda$ of space- and timelike extensions $R \times T$ and planar distance $|y-x| = T$ in Euclidean time. In analogy to Wilson loops and, as pictorially inferred from figure 4.1, the gauge invariant two-point function $G(R,T)$ measures the response of the coupled system of gauge and matter fields to an external charged source q. For both space- and timelike distances R and T becoming large, this function decays exponentially,

$$G(R,T) \overset{R,T\to\infty}{\sim} \begin{cases} \mathrm{e}^{-am_c T - aE_q(2R+T)} & \text{(Coulomb phase)} \\ \mathrm{e}^{-a\mu(2R+T)} & \text{(confinement-Higgs phase)} \end{cases} , \tag{4.2}$$

with m_c being the mass of a charged particle allowed in the Coulomb phase, and at fixed R it behaves for large T as

$$G(R,T) \overset{T\to\infty}{\sim} c_G(R)\, \mathrm{e}^{-a\mu T} \tag{4.3}$$

with an R–dependent coefficient c_G and μ the lowest energy in the fields screening the point-like charge q. This screening energy is known to be independent of the spatial detour R in the lattice path $\mathcal{C}_{R,T}(y,x)$ and provides a sensitive order parameter exhibiting a discontinuity at the Higgs phase transition [87], if it is compared with the perimeter law behaviour of Wilson loops $W(R,T)$ in eq. (1.37) of subsection 1.2.1 in chapter 1 rewritten to

$$W(R,T) \overset{R,T\to\infty}{\sim} \mathrm{e}^{-aE_q(2R+2T)} , \tag{4.4}$$

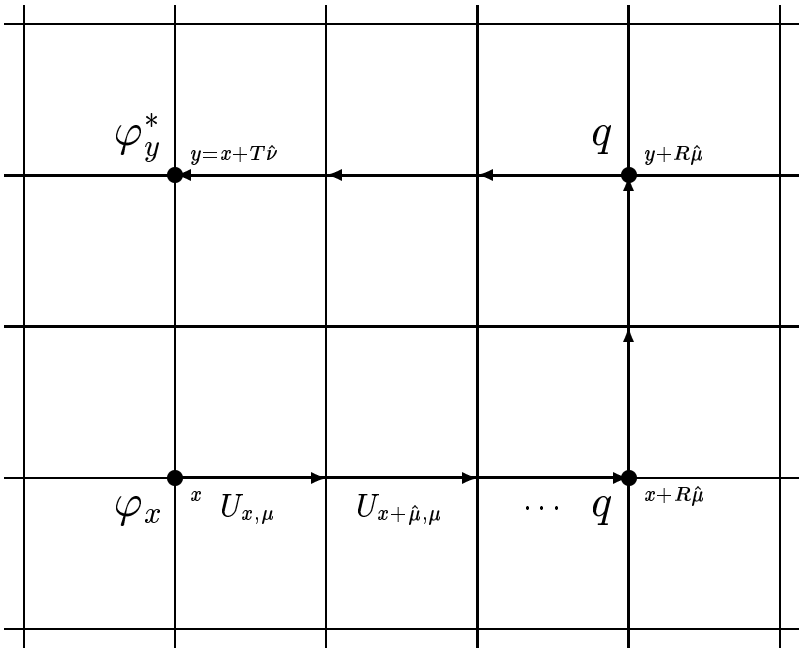

Figure 4.1: *Open lattice path $\mathcal{C}_{R,T}(y,x)$ and the corresponding product $U_{\mathcal{C}_{R,T}(y,x)}$ of parallel transporters (directed links $U_{x,\mu}$) between the scalar fields on sites x and y for the definition of $G(R,T)$ in (4.1), if one supposes an external static charge q to be present at spatial locations $x+R$ and $y+R$ with a separation T in the time direction. In the example it is $R=3$ and $T=2$, and in two dimensions $\mu=1$ and $\nu=2$.*

which holds in the presence of screening matter fields. The quantity

$$E_q = \frac{1}{2}\, V(\infty)\,, \tag{4.5}$$

with $V(\infty)$ denoting the large R limit of the static potential[2]

$$aV(R) = -\lim_{T\to\infty} \frac{1}{T}\, \ln W(R,T) = \lim_{T\to\infty} \left(\frac{2aE_qR}{T} + 2aE_q \right)\,, \tag{4.6}$$

is the lowest energy of the fields around one external charge q, i.e. the energy in the Coulomb field produced by q in the Coulomb phase or the sum of the contributions from the interacting gauge fields and the charged scalar matter fields screening the external source q in the confinement-Higgs phase. Consequently, one expects $\mu = E_q$ in the confinement-Higgs phase, while in the Coulomb phase, where gauge invariant charged states with finite energy belonging to the complex scalar field can exist, one might have $\mu = E_q + m_{\rm c} - E_{\rm b}^{\rm (cq)} > E_q$ with $m_{\rm c}$ the 'dressed' mass of the charged particle and $E_{\rm b}^{\rm (cq)} \geq 0$ its largest binding energy to an external static source q brought into the system.

[2]For scalar fields with unit charge considered here, the subscript q of the Wilson loops and static potentials in the last section of the previous chapter is omitted for shorthand notation, hence $q=1$ is always meant.

Inspired by a ratio of $G(R,T)$ and a proper fractional power of Wilson loops [85], which is aimed to divide out the perimeter law factor also contaminating the decay (4.2) of the former, the authors of ref. [87] now introduce

$$\rho_{\rm AC}(T) \equiv \frac{G(0,T)}{W(T,T)^{1/4}} \stackrel{T\to\infty}{\sim} {\rm e}^{-a(\mu-E_q)T} \tag{4.7}$$

from eqs. (4.3) and (4.4), and predict for its large T limit

$$\rho_{\rm AC}^{\infty} \equiv \lim_{T\to\infty} \rho_{\rm AC}(T) = \begin{cases} \neq 0 & , \mu = E_q \quad \text{(confinement-Higgs phase)} \\ = 0 & , \mu > E_q \quad \text{(Coulomb phase)} \end{cases} . \tag{4.8}$$

Therefore, the order parameter $\rho_{\rm AC}^{\infty}$ distinguishes the confinement and Higgs regions from the Coulomb phase with free charges, because in the former the lowest energy μ of a screened external charge is equal to the lowest energy E_q of an external charge in contrast to the latter, where an external charge can in principle exist in screened (bound) and unscreened states with different energies μ and E_q.

4.1.2 Numerical analysis

Since the observable constructed in this way has been successfully applied in four-dimensional gauge-Higgs theories with SU(2)– or U(1)–gauge symmetry and the scalar field in the fundamental representation [113, 87] to probe the essential properties of its different phases, it is natural to address how $\rho_{\rm AC}^{\infty}$, which tests for confinement or free charges, comes out in the two-dimensional model. To this end, I determined the two-point function $G(R,T)$ for $R = 0$ and the square Wilson loops $W(T,T)$ with extensions $T = 1, \ldots, L_2/2$ during the numerical simulations in the LCP parameters of table 3.1 in section 3.1.

When performing uncorrelated least squares fits of the large T asymptotics of the functions entering eq. (4.7) to the purely exponential shapes

$$f(T) = A\,{\rm e}^{-BT} + C\,, \quad f(T) \in \{G(0,T), W(T,T), \rho_{\rm AC}(T)\} \tag{4.9}$$

with the third, constant fit parameter C only in the case of the ratio $\rho_{\rm AC}(T)$, one identifies the decay constants as $B = a\mu$ for $G(0,T)$ and $B = 4aE_q$ for $W(T,T)$. All the resulting fit parameters are listed in table 4.1, and I also verified the R–independence of $a\mu$ to satisfactory accuracy by a comparison with fits of some data for $G(R,T)$ and $R = 1$. The majority of the fits of the functions $G(0,T)$ and $W(T,T)$, which covered their tails of at least $L_2/4$ points from the end of the total range, were good and had small values of χ^2/dof. The static potential $aV(R)$ at $R = \infty$ originates from the rough plateau region at large R–distances of the potential as it was computed from the Polyakov loop correlation with $q = 1$ in section 3.4 of chapter 3. One can see that the energies $aV(\infty)$, $a\mu$, and aE_q scale appropriately with their mass dimensions in the continuum limit along the LCPs, and in regard of the relatively small

LCP	set	κ	$P(R) : \frac{1}{2} aV(\infty)$	$G(0,T) : a\mu$	$W(T,T) : aE_q$	$\rho_{\rm AC}(T) : \rho_{\rm AC}^{\infty}$
L1	A_2	0.2937	0.0447(1)	0.0462(1)	0.0464(1)	5.294(1)
	B	0.2607	0.0229(1)	0.0239(1)	0.0237(1)	5.698(3)
	C	0.253	0.0118(1)	0.0124(1)	0.0123(1)	5.603(3)
	D	0.250815	0.0059(2)	0.0064(1)	0.0061(1)	5.35(1)
L2	A_2	0.2858	0.0549(2)	0.0587(1)	0.0578(1)	3.754(3)
	B	0.258835	0.0287(2)	0.0310(1)	0.0296(1)	3.837(3)
	C	0.2525	0.0149(2)	0.0168(1)	0.0154(2)	3.596(7)
	D	0.25069	0.0074(3)	0.0087(2)	0.0077(1)	3.33(2)
L3	A	0.2731	0.0930(5)	0.1122(4)	0.0935(4)	1.811(5)
	B	0.257	0.0515(7)	0.0643(3)	0.0523(3)	1.518(7)
	C	0.252	0.0295(6)	0.0393(3)	0.0284(2)	1.100(8)
	D	0.25055	0.023(9)	0.0259(7)	0.015(1)	0.70(1)

Table 4.1: *Fit results with jackknife errors along the LCPs for the observables, which were motivated by investigations in the four-dimensional model. The potential $aV(\infty)$ is taken from the previously computed Polyakov loop correlations for $q = 1$. Its large statistical error in the lower left entry comes from the badly measurable signal of the correlations with time separation $T = L_2 = 128$.*

statistical errors on these quantities, the relation $E_q = V(\infty)/2$ is fulfilled with sufficient accuracy. The reason for aE_q being systematically somewhat larger is that the potential does not yet achieve a really constant value for $R \to L_1/2$ before its distortion by the finite volume, but the agreement gets slightly better, if one inserts the exact limit $V(\infty) = e_R^2/2m_s$ of the large R extrapolation in the continuum fit ansatz (3.45) instead, which typically lies above the lattice estimates.

The quality of $\mu = E_q$, which would imply a vanishing fit parameter $B = a(\mu - E_q) \simeq 0$ and a non-zero constant $C = \rho_{\rm AC}^{\infty} > 0$ for $\rho_{\rm AC}(T)$ as $T \to \infty$, is excellent along L1 in the Higgs region, however, the equality becomes rather moderate for decreasing κ at fixed parameters β and λ towards L3 in the confinement region near pure gauge theory. This is compatible with observations made in section 3.4 for the potential from Polyakov loop correlations as well as in the four-dimensional models [113, 87], because then the screening distance of the static potential, which rises linearly with R due to an area law prevalence for smaller Wilson loops until the shielding quanta of the scalar field flatten it completely, is expected to exceed the maximally available size $L_2/2$ of $W(T,T)$. Thus with decreasing κ the fitted estimates of aE_q are presumably too low on L2 and and especially on L3. In addition, an overestimation of $a\mu$ caused by a slow approach of $G(0,T)$ to its asymptotic behaviour in T is also possible. Both effects should reduce on lattices with larger temporal extensions. As I found stable fits for $\rho_{\rm AC}(T)$ over large T–intervals throwing away only a

few of the smallest T–distances, it is nevertheless remarkable and parallel to the experiences in four dimensions [113, 87] that these ratios reach their asymptotic values $\rho_{\rm AC}^{\infty}$ of table 4.1 already at medium distances around $T \simeq L_2/4$ for all LCPs apart from L3, for which the discrepancies between $a\mu$ and aE_q shift $\rho_{\rm AC}^{\infty}$ to rear T, although the constant tail of $\rho_{\rm AC}(T)$ still appears. These findings are exemplarily underlined by the curves in figure 4.2, where the typical shapes of the gauge invariant ratio $\rho_{\rm AC}(T)$ as a function of T in the different regions of bare parameter space are displayed.

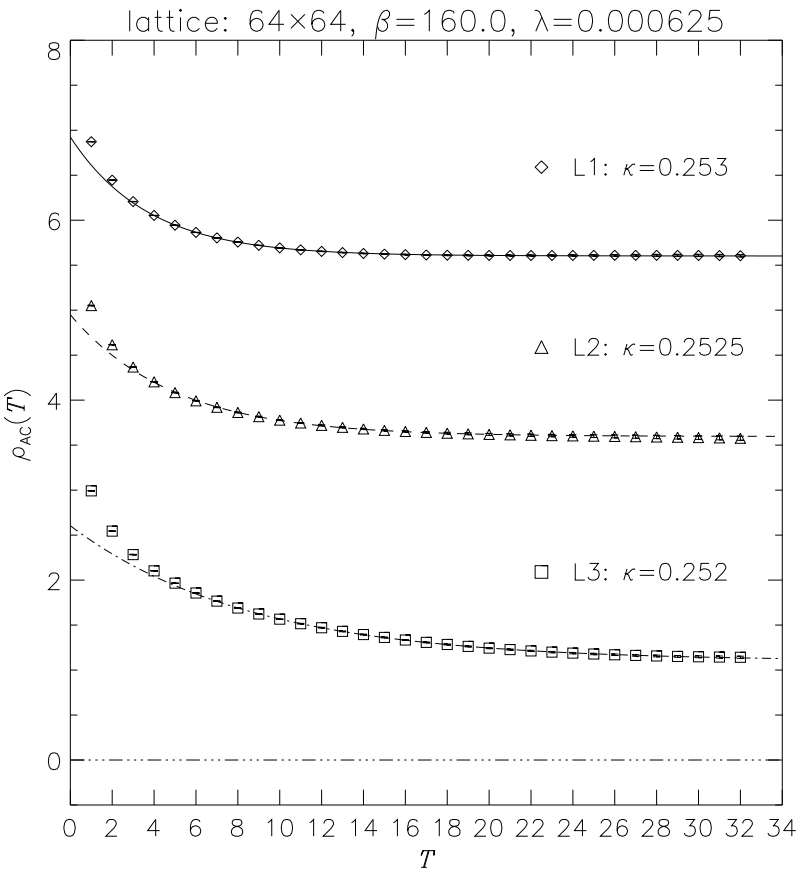

Figure 4.2: *Simulation results and χ^2–fits of $\rho_{AC}(T)$ to the ansatz (4.9) in parameter point C on all three LCPs L1, L2, and L3. The statistical errors of the lattice data are smaller than the plot symbols. Since the $T \to \infty$ extrapolation leads always to values for the order parameter ρ_{AC}^{∞}, which stay definitely larger than zero, there is no hint at a phase transition into a Coulomb-like phase in the two-dimensional model. As emphasized in the text, this was already to be expected from theoretical arguments.*

Referring to the criterion in eq. (4.8), I did not discover any indication in the numerical investigations for a Coulomb-like free charge phase in coupling parameter space, besides the confinement-Higgs phase, where $\rho_{\rm AC}^{\infty} > 0$ is complied strictly. This is fully consistent with the physical belief that in the two-dimensional U(1)–Higgs model, which does contain neither

charged states nor a physical photon, a Coulomb phase as for abelian gauge theories in four dimension is missing [22, 54]. Since the observables in table 4.1 do not show a characteristic discontinuity on the course from the LCPs L1 and L2 in the Higgs region ($\kappa > \bar{\kappa}$) to L3 in the confinement region ($\kappa < \bar{\kappa}$) at fixed β and λ, there are no hints at a phase transition in this model for finite values of the lattice parameters.

4.2 Generalization of the fixed length case

I have outlined in section 3.1 of chapter 3 that the approach to the quantum continuum limit of the two-dimensional U(1)–Higgs model with variable scalar field length might be attained as in eqs. (3.2) – (3.4), namely

$$\beta \to \infty\,, \quad \lambda \to 0\,, \quad \beta\lambda = \text{constant} \tag{4.10}$$

for large enough β, for which the renormalization conditions on the renormalized vacuum expectation value of the Higgs field v_R and the Higgs to vector mass ratio R_{HW}, imposed by a proper tuning of the hopping parameter κ, are

$$v_R = \sqrt{2\kappa}\,\langle\rho\rangle = \overline{v}\,, \quad R_{HW} \equiv \frac{m_H}{m_W} = \overline{R}\,. \tag{4.11}$$

Of course, the concrete values of the constants $\overline{v}$ and $\overline{R}$, e.g. those actually chosen in tables 3.1 and 3.2, decide about the position of the individual LCPs in bare lattice parameter space. This limit has to be carefully distinguished from the limit $\beta \to \infty$ at fixed scalar self-coupling λ, which arrives at the pure two-component $\phi^4_{n=2}$–theory on the lattice with a global U(1)–symmetry and a second order phase transition at a certain $\kappa = \kappa_c$.

4.2.1 Phase structure of both models

If the limit $\lambda \to \infty$ is taken before sending $\beta \to \infty$, the radial mode of the Higgs field freezes to $|\varphi_x| = 1$, and one obtains the XY–model, which deals with two-component classical spins normalized to unit lengths and nearest neighbour interactions. The global symmetry group is O(2). In view of (1.22) of section 1.1, its action on a two-dimensional lattice in terms of the scalar field angles ω_x is

$$S_{\mathrm{XY}} = -2\kappa \sum_{x\in\Lambda} \sum_{\mu=1}^{2} \cos\left(\omega_x - \omega_{x+\hat{\mu}}\right)\,, \tag{4.12}$$

and the underlying continuous field theory describes a free massless scalar field with κ as the inverse temperature $1/T$. This model undergoes the prominent Kosterlitz-Thouless phase transition of infinite order at $\kappa_c \simeq 0.56$ [70], and it is well established by different methods — and was already reviewed in the introduction — that this transition becomes

a smooth and analytic crossover for $\beta < \infty$ inside the phase diagram [22, 54, 56]. The low-temperature phase ($\kappa > \kappa_c$) of the XY–model, treated in the spin wave approximation $-2\kappa\cos(\omega_x - \omega_{x+\hat{\mu}}) \to \kappa(\omega_x - \omega_{x+\hat{\mu}})^2$, is short-range ordered, because the alignment of spins is energetically favoured here. It predicts a power law decrease of the spin-spin correlation function, and free vortices are absent. The physics of the high-temperature phase ($\kappa < \kappa_c$) is different. In a strong coupling expansion the correlations turn out to decay exponentially, and one speaks of a dilute vortex gas as a plasma of weakly coupled vortices and antivortices. This suggests that with increasing temperature the neglection of the periodic character of the angle variables ω_x gets unjustified. More precisely, one may imagine configurations, where the angle between the spin and a fixed direction — followed along a simple closed curve — varies by an integer multiple n of 2π. Such a configuration, a vortex of order n, is a topological invariant when the curve or the configuration changes continuously, and it should be identified with the centre $n_x \subset \Lambda$ of an extended instanton configuration as discussed on the lattice in earlier sections, e.g. in 2.1 and 3.2. The long-range fluctuations of these topological excitations are assumed to combine with the spin wave fluctuations and increase the disorder in the system, finally mediating the phase transition [4, 67, 68].

My investigations in the model with variable length, which yet proves to possess a much simpler phase structure than its four-dimensional pendants, point to a generalization of the situation in the fixed length model. Although the results on the static potentials and order parameters in sections 3.4 and 4.1 as well as the behaviour of the masses am_H, am_W, their ratio R_{HW}, and v_R revealed a qualitative change in the properties of the model with growing κ for fixed $\beta < \infty$ and $\lambda > 0$, none of these quantities reflects any steep increase or another distinct irregularity. Denoting the crossover value $\kappa = \bar{\kappa}$ as before, the physics in the confinement regime at $\kappa < \bar{\kappa}$, which contains the LCP L3, is already similar to the pure gauge theory, whereas the LCPs L2 and L1 are placed in a Higgs regime at $\kappa > \bar{\kappa}$. Integer external charges are always screened. The strength of this effect decreases with vanishing screening mass am_s in the continuum limit, but still persists as long as $\beta < \infty$. Non-integer external charges feel a constant force in the confinement regime and, owing to the disordering influence of a dilute ensemble of instantons and antiinstantons destroying the Higgs mechanism for fractional charges in two dimensions, confinement does also hold in the Higgs regime. Hence, both regions are continuously connected, and no phase transition at finite values of the lattice parameters is to be expected.

This scenario can be made more rigorous by considering the topological susceptibility χ_{top} as a valuable observable most sensitive to the topological nature of the phase transitions in the continuum limit. It is a direct measure for the vorticity, that is the density of vortex-antivortex excitations, if one neglects their short-ranged interactions and is only interested in their long-range bearing, which produces a net topological charge in the system. I have illustrated χ_{top} in dependence of κ, both for the variable and fixed length models, in figure 4.3. In contrast to table 3.3 and figure 3.3 of section 3.2, where its estimates on the LCPs were

given, the paths shown here represent cuts through these lines at fixed values of β and λ in the three-dimensional phase space spanned by the lattice parameters β, λ, and κ. One can recognizes that the κ–range with $\kappa > 1/4$ and $c \leq \chi_{\rm top} \leq c' \chi_{\rm top}^{\rm (PGT)}$, $c > 0$ and $1 - c' > 0$ being arbitrarily small but strictly non-zero, will shrink to zero in the continuum limit (4.10). It is

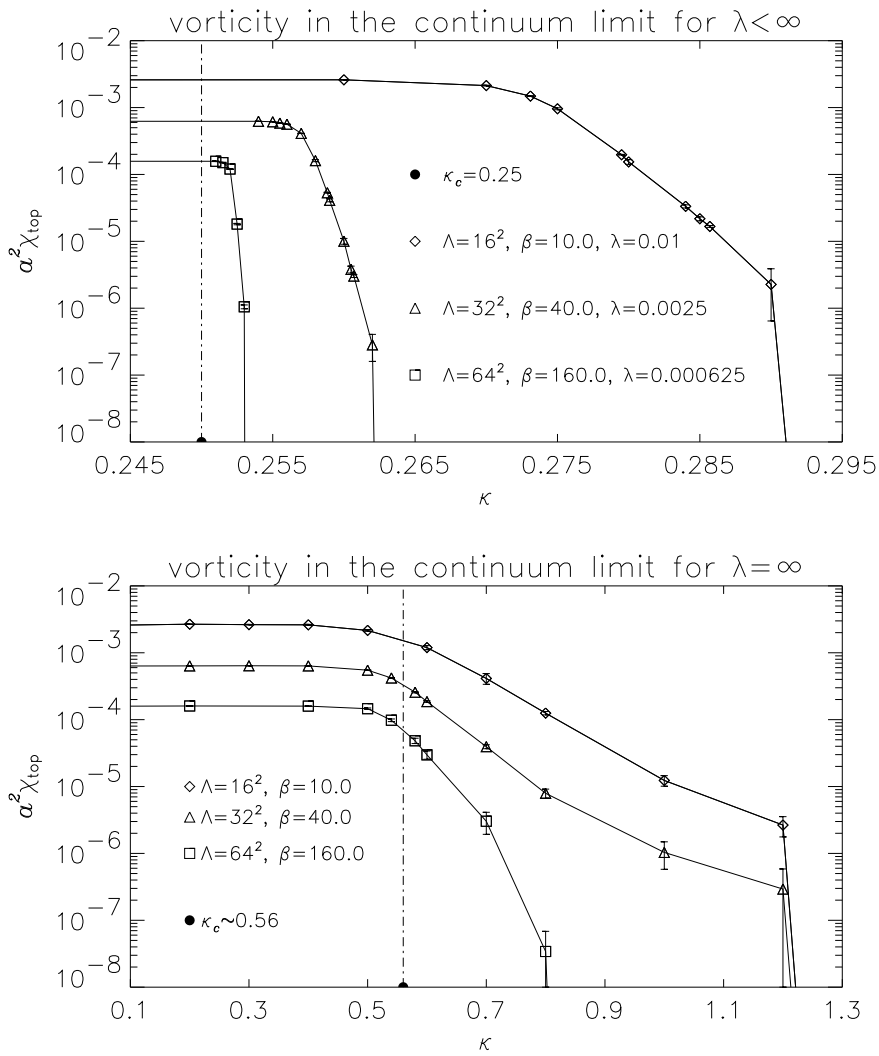

Figure 4.3: *Topological susceptibility in dependence of κ at different stages of the continuum limit in the model with variable ($\lambda < \infty$) and fixed ($\lambda = \infty$) scalar field length. The solid lines, which are only meant to guide the eye, start with the estimate $\chi_{top} = 1/4\pi^2\beta$ at $\kappa = 0$ in pure gauge theory, and they end in a point, where χ_{top} is already zero within its statistical error. The data have different statistics, at least 100000 configurations in the upper diagram and 50000 configurations in the lower one.*

also illustrated that the breakdown of $\chi_{\rm top}$ happens the earlier and the sharper the more one moves in the direction of this limit. The contraction of the parameter domain with $\kappa > 1/4$ and $\chi_{\rm top} > 0$ from above is equivalent to the convergence of the LCPs to the common point

$\kappa = \kappa_c = 1/4$, signalling a phase transition at $\beta = \infty$ and $\lambda = 0$. There the topological susceptibility jumps from $\chi_{\rm top} = \chi_{\rm top}^{\rm (PGT)}$ in a confining phase for $\kappa < \kappa_c$ with pure gauge theory like behaviour to $\chi_{\rm top} = 0$ in a Higgs phase for $\kappa > \kappa_c$ with no free vortices, and thus exhibits a characteristic discontinuity. When confronting this with the corresponding κ–dependence of $\chi_{\rm top}$ for $\lambda = \infty$, see the right plot of figure 4.3, $\kappa_c = 1/4$ resembles the Kosterlitz-Thouless phase transition point $\kappa_c \simeq 0.56$ at $\beta = \infty$ in the fixed length model.

Another important observation inferred from the left plot of figure 4.3, and approximately for the right one as well, is that the decay of $\chi_{\rm top} = \chi_{\rm top}(\kappa)$ at fixed β and λ in the Higgs region proceeds perfectly exponentially. The vortex density does not survive in the continuum limit and causes the vortices and antivortices to become infinitely dilute and irrelevant as $\beta \to \infty$. Once the continuum limit is reached, the theory displays the Higgs phenomenon for fractional charges if $\kappa > \kappa_c = 1/4$, but as long as $\beta < \infty$ one has $\chi_{\rm top} > 0$, and the confining force between them still extends into the Higgs region with an exponential branch. This prevents any phase transition inside the phase diagram and supports the crossover picture found from other quantities before. On these grounds, it is not surprising that the phase diagrams of the abelian Higgs models in two dimensions with variable and fixed scalar field length in figure 4.4 look qualitatively identical.

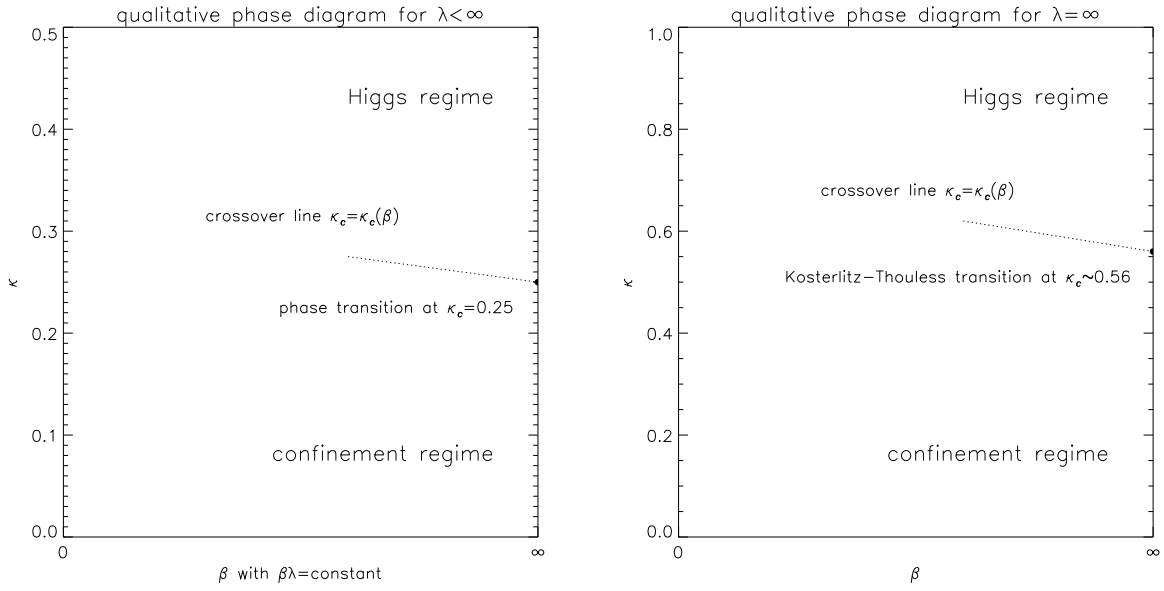

Figure 4.4: *Phase diagram of the lattice abelian Higgs model as recommended by the results of the investigations in this and the foregoing chapter. The evidence for a phase transition in $\kappa_c = 1/4$ at $\beta = \infty$ in the variable length model (left) is analogous to the Kosterlitz-Thouless transition point at $\beta = \infty$ in the fixed length model (right) For notational simplicity, κ_c means here the crossover line inside the phase diagrams too.*

4.2.2 Classical versus quantum continuum limit

In conclusion, I want to emphasize again that in the two-dimensional abelian Higgs model with variable modulus of the scalar field, the LCPs and the evolution of the topological susceptibility with κ at stages increasingly close to the continuum limit give strong evidence for a phase transition in $\kappa_c = 1/4$ at $\beta = \infty$ and for a crossover at $\beta < \infty$. As this limit requires λ to vanish simultaneously, $\kappa_c = 1/4$ is just the solution of eq. (1.10) in section 1.1 of the first chapter,

$$a^2 m_0^2 = \frac{1-2\lambda}{\kappa} - 4 = 0\,, \quad \lambda = 0\,,$$

which relates the bare mass squared of the scalar field in the continuum action (1.3) to the lattice parameters. In this sense κ_c could be understood as the critical point of a classical theory with a symmetric phase for $m_0^2 > 0$ and a broken symmetry Higgs phase for $m_0^2 < 0$. The fact that the continuum limit of the lattice U(1)–Higgs model in two dimensions is settled in the tree-level transition point $\kappa_c = 1/4$ is misleading though, because this limit is by no means approached classically as clarified immediately.

The superrenormalizability of the theory ensures that besides v_0, which involves the only primitive, one-loop divergence in the 1– or 2–point Green function, all field theoretic quantities receive finite renormalizations. In particular, via demanding the tree-level expressions eqs. (1.13) and (1.10) to be valid up to leading order in the continuum limit of the full quantum theory, I can write

$$\frac{1}{a\sqrt{\beta}} = e_0 = \overline{e}_0 + \mathcal{O}(a^2) \tag{4.13}$$

$$\frac{6\lambda}{a^2\kappa^2} = \lambda_0 = \overline{\lambda}_0 + \mathcal{O}(a^2)\,, \tag{4.14}$$

whilst the last equation restates the remark at the end of section 3.1 in chapter 3 that in the present model this limit is not trivial, since the dimensionful self-coupling λ_0 in the continuum yet acquires a non-zero value $\overline{\lambda}_0$. Consequently, the limits $\beta \to \infty$ and $\lambda \to 0$ go with rates proportional to $1/a^2$ and a^2, respectively. The vacuum expectation value of the scalar field, however, does not behave as $v_0^2 = \overline{v}_0^2 + \mathcal{O}(a^2)$, but diverges logarithmically by a formal power counting argument, i.e. together with eq. (1.25) as

$$-\frac{\kappa}{\lambda}\,(1-2\lambda) + \frac{4\kappa^2}{\lambda} = v_0^2 \overset{a\to 0}{\sim} \ln(a^2)\,. \tag{4.15}$$

Inserting now (4.14), I obtain

$$\begin{aligned} v_0^2 &= \frac{6}{a^2\overline{\lambda}_0\,\kappa^2}\left[-\kappa + 4\kappa^2 + \mathcal{O}(a^2)\right] \\ &= \frac{24}{a^2\overline{\lambda}_0}\left[-\frac{1}{4\kappa} + 1 + \mathcal{O}(a^2)\right] \\ &\overset{a\to 0}{\sim} \ln(a^2)\,, \end{aligned} \tag{4.16}$$

and the scalar hopping parameter κ is enforced to converge in the limit $a \to 0$ to

$$\kappa = \kappa_c + \mathcal{O}\Big(a^2 \ln\left(a^2\right)\Big)\,, \quad \kappa_c = \frac{1}{4}\,. \tag{4.17}$$

Therefore, the way towards the continuum limit in lattice parameter space safely develops differently from the behaviour $\kappa = \kappa_c + \mathcal{O}(a^2)$ of a classical theory, in which any of its divergent quantum corrections in higher orders of the loop expansion would be ignored.

Summary

I studied the zero-temperature two-dimensional U(1)–Higgs model by numerical Monte Carlo simulations non-perturbatively on the lattice.

Most emphasis was on those aspects, which were supposed to be related to the variable length of the scalar field as an additional degree of freedom in this model compared to the case of fixed length. As a central new result, I realized the quantum continuum limit along appropriately defined lines of constant physics in the bare lattice parameter space. In fact, I noticed that this limit shows up to be qualitatively different from the analogous limit in those models, where the length of the scalar Higgs field is frozen.

Then I focused on the scaling behaviour of the topological susceptibility in its approach towards the continuum limit by direct evaluation of the corresponding lattice observable originating from the geometrical topological charge definition on the lattice, and by an analysis of its derivative with respect to that coupling of the discretized theory, which parametrizes a given line of constant physics. Whereas no definite statement can be made for the outcome of the former method, I observed an at least partly improved — but still unsatisfactory — scaling of the topological susceptibility, if the latter criterion is taken into account.

Moreover, I addressed the question, whether there is a phase transition line in the lattice model, which extends from the boundary of the phase diagram into its interior while separating physically distinct regions. After an numerical investigation of some possible order parameters and of confinement of external non-integer charges caused by instanton effects, I did not discover any signal for such a transition at finite and non-zero values of the lattice parameters. All the simulation results revealed instead that a smooth crossover between two continuously connected regimes occurs, which display typical characteristics of Higgs- and confinement-like phases of the theory in the continuum.

Finally, as a further striking insight into the physics of the U(1)–Higgs model in two dimensions, the evidence for the absence of a real phase transition can basically be traced back to a similar collective behaviour of its fluctuating topological excitations on both sides beyond the envisaged crossover line, and in this respect one is only able to distinguish rigorously between them, when the continuum limit is reached exactly.

The last conclusions are in general agreement with the already known phase structure of the lattice abelian Higgs model with fixed length of the scalar field.

Part II:
The $4D$ SU(2)–Higgs Model

Chapter 5

The model and its setup for the electroweak phase transition

In this chapter I introduce the conventional continuum and lattice formulations of the model [19, 114, 115], with special emphasis on its use for the numerical investigations of the finite-temperature electroweak phase transition (EWPT) presented in this second part of my work. Since the lattice version of the four-dimensional SU(2)–Higgs model has been subject of numerous publications for many years [112, 113, 117, 118, 119], I will only give a brief survey of the central aspects without any claim to be complete. Formally, the model looks very similar to the two-dimensional one with U(1)–gauge symmetry studied in the first part.

5.1 Continuum and lattice model

As a formal transcription of the two-dimensional model in chapter 1 to the non-abelian case, the continuum action of the four-dimensional SU(2)–Higgs model reads

$$S[A,\Phi] = \int \mathrm{d}^4x\, \mathcal{L}(x) \tag{5.1}$$

with the Lagrange density made up by the pure gauge part and a locally SU(2)–invariant scalar part with quartic self-coupling:

$$\mathcal{L}(x) = \frac{1}{2}\,\mathrm{Tr}\left(F_{\mu\nu}(x)F_{\mu\nu}(x)\right) + D_\mu\Phi^+(x)D_\mu\Phi(x) + \lambda_0\Big(\Phi^+(x)\Phi(x) - v_0^2\Big)^2 . \tag{5.2}$$

Now the Higgs doublet field $\Phi(x)$ is a two-component complex column vector transforming like the fundamental representation of the gauge group SU(2), which interacts through the covariant derivative $D_\mu = \partial_\mu - igA_\mu(x)$, g being the bare gauge coupling, with the gauge field $A_\mu(x) \in \mathrm{SU}(2)$. The field strength is $F_{\mu\nu}(x) = \partial_\mu A_\nu(x) - \partial_\nu A_\mu(x) + [\,A_\mu(x), A_\nu(x)\,]$, $\mu,\nu \in \{1,\ldots,4\}$, and v_0 is the bare, tree-level vacuum expectation value of the Higgs field,

$$v_0^2 = \frac{2\,m_{H,0}^2}{\lambda_0}\,, \quad m_0^2 \equiv -\frac{1}{2}\,m_{H,0}^2\,, \tag{5.3}$$

if $m_0 > 0$ and $m_{H,0} > 0$ denote the bare scalar masses in the symmetric and Higgs phase, respectively[1]. Finally, the bare gauge vector boson mass $m_{W,0}$ in the broken symmetry phase and its dimensionless ratio to the Higgs mass are identified to be

$$m_{W,0}^2 = \frac{v_0^2 g^2}{4}\,, \quad R_{HW,0}^2 \equiv \frac{m_{H,0}^2}{m_{W,0}^2} = \frac{2\lambda_0}{g^2} \tag{5.4}$$

in close analogy to eqs. (1.6) – (1.8) in section 1.1 of the first part.

The lattice action of the model is obtained in analogy to eqs. (1.9) and (1.10) by substituting

$$a\Phi(x) = \sqrt{2\kappa}\,\Phi_x\,, \quad \lambda_0 = \frac{\lambda}{4\kappa^2}\,, \quad a^2 m_0^2 = \frac{1-2\lambda}{\kappa} - 8 \tag{5.5}$$

in the scalar sector, and the complex-valued $2 \otimes 2$ matrices φ_x in electroweak isospin space defined as

$$\Phi_x = \begin{pmatrix} \Phi_{x,1} \\ \Phi_{x,2} \end{pmatrix} = \begin{pmatrix} \Phi_{x,2}^* & \Phi_{x,1} \\ -\Phi_{x,1}^* & \Phi_{x,2} \end{pmatrix} \begin{pmatrix} 0 \\ 1 \end{pmatrix} \equiv \varphi_x \begin{pmatrix} 0 \\ 1 \end{pmatrix} \tag{5.6}$$

represent the Higgs field residing on the lattice sites $x \in \Lambda$. Its four independent real components can be identified from the expansion $\varphi_x = \phi_{x,0}\tau_0 + i\sum_{r=1}^{3}\phi_{x,r}\tau_r$ by the Pauli matrices τ_r, $r = 1, 2, 3$, $\tau_0 \equiv \mathbf{1}_{2\otimes 2}$, and satisfy $\varphi_x^+ = \tau_2 \varphi_x^{\mathrm{T}} \tau_2$. The discretization of the gauge sector involving the link variables $U_{x,\mu} \in \mathrm{SU}(2)$, i.e.

$$U_{x,\mu} = \mathrm{e}^{\,iA_{x,\mu}} = \exp\left\{ iga \sum_{r=1}^{3} A_\mu^r(x)\,\frac{\tau_r}{2} \right\} \tag{5.7}$$

in dependence of the generators $\tau_r/2$ of the Lie algebra of SU(2), is provided by the Wilson action built up from the elementary plaquettes in figure 1.1 with the substitution $U_{x,\mu}^{-1} = U_{x,\mu}^+$,

$$U_{\mathrm{p}} = U_{x;\mu\nu} \equiv U_{x,\mu} U_{x+\hat{\mu},\nu} U_{x+\hat{\nu},\mu}^+ U_{x,\nu}^+ \tag{5.8}$$

to be summed over $x \in \Lambda$ and $1 \le \mu < \nu \le 4$, and the dimensionless coupling

$$\beta = \frac{4}{g^2}\,. \tag{5.9}$$

Hence, the action of the four-dimensional SU(2)–Higgs model on isotropic lattices is

$$S[U,\varphi] \;=\; S_{\mathrm{g}}[U] + S_\phi[U,\varphi] \tag{5.10}$$

$$S_{\mathrm{g}}[U] \;=\; \beta \sum_{\mathrm{p}} \left(1 - \frac{1}{2}\,\mathrm{Tr}\,U_{\mathrm{p}} \right) \tag{5.11}$$

$$S_\phi[U,\varphi] \;=\; \sum_{x\in\Lambda} \left\{ \frac{1}{2}\,\mathrm{Tr}\left(\varphi_x^+\varphi_x\right) + \lambda \left[\frac{1}{2}\,\mathrm{Tr}\left(\varphi_x^+\varphi_x\right) - 1 \right]^2 - \kappa \sum_{\mu=1}^{4} \mathrm{Tr}\left(\varphi_{x+\hat{\mu}}^+ U_{x,\mu}\varphi_x\right) \right\}. \tag{5.12}$$

[1]Here the bare scalar self-coupling λ_0 differs by a factor $4! = 24$ from the conventions used in section 1.1 of the first part.

From $\varphi_x^+ \varphi_x = \phi_x^2 \mathbf{1}_{2\otimes 2} = \rho_x^2 \mathbf{1}_{2\otimes 2}$ it follows that the scalar field can be decomposed into length and angular variables according to

$$\varphi_x = \rho_x \alpha_x \,, \quad \rho_x \in \mathbb{R}^{\geq 0} \,, \quad \alpha_x \in \mathrm{SU}(2) \,, \tag{5.13}$$

which is often useful in the numerical simulations. Then eqs. (5.10) – (5.12) get modified to

$$\begin{aligned} S[U,\varphi] &= \beta \sum_{\mathrm{p}} \left(1 - \frac{1}{2} \operatorname{Tr} U_{\mathrm{p}} \right) \\ &\quad + \sum_{x\in\Lambda} \left\{ \rho_x^2 + \lambda \left(\rho_x^2 - 1 \right)^2 - \kappa \sum_{\mu=1}^{4} \rho_{x+\hat{\mu}} \rho_x \operatorname{Tr} \left(\alpha_{x+\hat{\mu}}^+ U_{x,\mu} \alpha_x \right) \right\} , \end{aligned} \tag{5.14}$$

while the meaning of the lattice parameters β, λ, and the scalar hopping parameter κ is the same as for the abelian case in the previous chapters. This reflects that the lattice theory is entirely formulated in terms of gauge invariant variables, which are the scalar length ρ_x and the link $V_{x,\mu} \equiv \alpha_{x+\hat{\mu}}^+ U_{x,\mu} \alpha_x$. Both of them describe physical degrees of freedom, namely $V_{x,\mu}$ corresponds to the gauge vector boson (W) and ρ_x to the Higgs boson (H).

In the introduction I have argued that at physical Higgs boson masses around 80 GeV and larger, where the first order nature of EWPT gets substantially weaker or even may vanish, the lattice sizes needed for finite-temperature simulations on isotropic lattices are out of the scope of the present numerical resources. Therefore, the simple idea for this range of parameters is to study finite-temperature field theory on anisotropic — sometimes synonymously called asymmetric — lattices with different spacings a_s and a_t in spatial and temporal directions, respectively, characterized by the lattice spacing anisotropy parameter

$$\xi \equiv \frac{a_s}{a_t} \,. \tag{5.15}$$

This method has the additional advantage that it makes an independent variation of the temperature T and the physical volume $V = a_s^3 a_t \Omega$, Ω the total number of lattice points, possible.

On an anisotropic lattice the isotropic action in eqs. (5.10) – (5.14) straightforwardly generalizes to the pieces

$$\begin{aligned} S[U,\varphi] &= \beta_s \sum_{\mathrm{sp}} \left(1 - \frac{1}{2} \operatorname{Tr} U_{\mathrm{sp}} \right) + \beta_t \sum_{\mathrm{tp}} \left(1 - \frac{1}{2} \operatorname{Tr} U_{\mathrm{tp}} \right) \\ &\quad + \sum_{x\in\Lambda} \left\{ \frac{1}{2} \operatorname{Tr} \left(\varphi_x^+ \varphi_x \right) + \lambda \left[\frac{1}{2} \operatorname{Tr} \left(\varphi_x^+ \varphi_x \right) - 1 \right]^2 \right. \\ &\qquad \left. - \kappa_s \sum_{\mu=1}^{3} \operatorname{Tr} \left(\varphi_{x+\hat{\mu}}^+ U_{x,\mu} \, \varphi_x \right) - \kappa_t \operatorname{Tr} \left(\varphi_{x+\hat{4}}^+ U_{x,4} \, \varphi_x \right) \right\} \\ &= \beta_s \sum_{\mathrm{sp}} \left(1 - \frac{1}{2} \operatorname{Tr} U_{\mathrm{sp}} \right) + \beta_t \sum_{\mathrm{tp}} \left(1 - \frac{1}{2} \operatorname{Tr} U_{\mathrm{tp}} \right) \end{aligned}$$

$$+\sum_{x\in\Lambda}\Big\{\rho_x^2+\lambda\left(\rho_x^2-1\right)^2-\kappa_s\sum_{\mu=1}^{3}\rho_{x+\hat{\mu}}\rho_x\mathrm{Tr}\left(\alpha_{x+\hat{\mu}}^{+}U_{x,\mu}\,\alpha_x\right)$$
$$-\kappa_t\rho_{x+\hat{4}}\rho_x\mathrm{Tr}\left(\alpha_{x+\hat{4}}^{+}U_{x,4}\,\alpha_x\right)\Big\}\,, \tag{5.16}$$

in which the link and site variables $U_{x,\mu}$ and φ_x in spatial and temporal directions, as well as the spacelike and timelike plaquettes U_{sp} and U_{tp} have to be distinguished. Since different lattice spacing anisotropies ξ should represent different but equivalent lattice regularizations of the same model, the different coupling parameters in spatial and temporal directions, β_s, β_t, κ_s and κ_t, arise here in a natural way. If one requires the action of the continuum model to be recovered in the classical continuum limit, that is $a_s\to 0$ and $a_t\to 0$ at fixed ξ, one is now led to identify

$$\sqrt{a_s a_t}\,\Phi(x)=\sqrt{2\kappa_s}\,\Phi_x\,,\quad \lambda_0=\frac{\lambda}{4\kappa_s^2\xi}\,,\quad a_s^2m_0^2=\frac{1-2\lambda}{\kappa_s}-6-2\gamma_\kappa^2 \tag{5.17}$$

$$\beta_s=\frac{4}{\xi}\,\frac{1}{g_s^2(\xi)}\,,\quad \beta_t=4\xi\,\frac{1}{g_t^2(\xi)}\,, \tag{5.18}$$

see eqs. (5.5) and (5.9), with $g^2=g_s^2(\xi)=g_t^2(\xi)$ only for $\xi=1$. It is useful to introduce the hopping parameter κ and the inverse gauge coupling squared β as

$$\kappa^2=\kappa_s\kappa_t\,,\quad \beta^2=\beta_s\beta_t\,, \tag{5.19}$$

and again one has the bare gauge coupling g, the bare scalar mass m_0, and the bare quartic scalar self-coupling λ_0 being the parameters of the original continuum theory given through the Lagrangian (5.2). The so-called coupling anisotropies defined as

$$\gamma_\beta\equiv\sqrt{\frac{\beta_t}{\beta_s}}\,,\quad \gamma_\kappa\equiv\sqrt{\frac{\kappa_t}{\kappa_s}} \tag{5.20}$$

are functions of ξ and obey for free fields and thus on the tree-level also for interacting fields the identity

$$\gamma_\beta=\gamma_\kappa=\xi\,. \tag{5.21}$$

However, the anisotropies γ_β and γ_κ receive quantum corrections, which generically might enclose perturbative contributions in higher orders of the loop expansion and non-perturbative effects too. Both will be addressed in chapter 8 of this work.

Eqs. (5.17) – (5.21) yield tree-level relationships between the isotropic and anisotropic couplings via the condition that the naive continuum limits of the corresponding lattice actions (5.14) and (5.16) are the same, which means to satisfy

$$g^2\,|_{\mathrm{iso}}=g^2\,|_{\mathrm{aniso}} \tag{5.22}$$

$$a_t^2m_0^2\,|_{\mathrm{iso}}=\left.\frac{a_s^2m_0^2}{\xi^2}\right|_{\mathrm{aniso}}\,,\quad \lambda_0\,|_{\mathrm{iso}}=\lambda_0\,|_{\mathrm{aniso}}\,. \tag{5.23}$$

When adding proper subscripts for the moment, these relations read

$$\beta_{\mathrm{a}} = \beta_{\mathrm{i}} \tag{5.24}$$

$$\frac{1}{\xi^2}\left[\left(1-\frac{2\lambda_{\mathrm{i}}\kappa_{\mathrm{a}}^2}{\kappa_{\mathrm{i}}^2\xi}\right)\frac{\xi}{\kappa_{\mathrm{a}}} - 6 - 2\xi^2\right] = \frac{1-2\lambda_{\mathrm{i}}}{\kappa_{\mathrm{i}}} - 8\,, \quad \lambda_{\mathrm{a}} = \left(\frac{\kappa_{\mathrm{a}}}{\kappa_{\mathrm{i}}}\right)^2 \frac{\lambda_{\mathrm{i}}}{\xi} \tag{5.25}$$

and can be helpful for a first guess of reasonable anisotropic simulation parameters, if the set of lattice parameters $\{\beta_{\mathrm{i}}, \lambda_{\mathrm{i}}, \kappa_{\mathrm{i}}\}$ referring to an isotropic lattice situation is somehow known in advance. Using eqs. (5.19) – (5.21), the bare Higgs and gauge boson masses in (5.3) and (5.4) translate into expressions in terms of the lattice asymmetry ξ and the anisotropic lattice parameters,

$$m_{H,0}^2 = -2m_0^2 = -\frac{2}{a_s^2}\left[\frac{1-2\lambda}{\kappa}\,\xi - 6 - 2\xi^2\right] \tag{5.26}$$

$$m_{W,0}^2 = \frac{m_{H,0}^2\kappa^2}{2\lambda\xi\beta}\,, \quad R_{HW,0}^2 = \frac{2\lambda\xi\beta}{\kappa^2}\,. \tag{5.27}$$

The vanishing of the former already determines the phase transition point as the value of the critical hopping parameter $\kappa = \kappa_c$ at zeroth order (tree-level) in the couplings. Setting $\xi = 1$ in these equations, everything reduces to the familiar constellation on isotropic lattices with identical lattice spacings $a_s = a_t = a$ in all directions.

5.1.1 Basic observables

In order to introduce the primary quantities, which are relevant for my numerical investigation of the SU(2)–Higgs model, the action (5.16) is together with eqs. (5.17) – (5.20) easily arranged to $S[U,\varphi] = \sum_{x\in\Lambda} S_x$, where the lattice action per site

$$S_x = 6\beta P_{\mathrm{pl},x} + R_x + \lambda Q_x - 8\kappa L_{\varphi,x} \tag{5.28}$$

consists of the length variables of the Higgs field

$$R_x \equiv \tfrac{1}{2}\,\mathrm{Tr}\left(\varphi_x^+\varphi_x\right) = \rho_x^2\,, \quad Q_x \equiv (\rho_x^2-1)^2\,, \tag{5.29}$$

of the weighted sum of the plaquette contributions $U_{x;\mu\nu} = U_{x,\mu}U_{x+\hat{\mu},\nu}U_{x+\hat{\nu},\mu}^+U_{x,\nu}^+$ lying in the space-space and the space-time planes

$$P_{\mathrm{pl},x} = \frac{1}{6}\left(\frac{3}{\gamma_\beta}\,P_{\mathrm{pl},s,x} + 3\gamma_\beta P_{\mathrm{pl},t,x}\right) \tag{5.30}$$

$$P_{\mathrm{pl},s,x} \equiv \frac{1}{3}\sum_{1\le\mu<\nu\le 3}\left(1-\tfrac{1}{2}\,\mathrm{Tr}\,U_{x;\mu\nu}\right), \quad P_{\mathrm{pl},t,x} \equiv \frac{1}{3}\sum_{\mu=1,3\,;\,\nu=4}\left(1-\tfrac{1}{2}\,\mathrm{Tr}\,U_{x;\mu\nu}\right), \tag{5.31}$$

and of the weighted sum of the space- and timelike components

$$L_{\varphi,x} = \frac{1}{4}\left(\frac{3}{\gamma_\kappa}\,L_{\varphi,s,x} + \gamma_\kappa L_{\varphi,t,x}\right) \tag{5.32}$$

$$L_{\varphi,s,x} \equiv \frac{1}{3}\sum_{\mu=1}^{3} L_{\varphi;x\mu}\,, \quad L_{\varphi,t,x} \equiv L_{\varphi;x4} \tag{5.33}$$

of the φ–link operator defined as

$$L_{\varphi;x\mu} \equiv \frac{1}{2}\,\mathrm{Tr}\left(\varphi^{+}_{x+\hat{\mu}} U_{x,\mu} \varphi_x\right) = \frac{1}{2}\,\rho_{x+\hat{\mu}}\rho_x \mathrm{Tr}\left(\alpha^{+}_{x+\hat{\mu}} U_{x,\mu} \alpha_x\right)\,. \tag{5.34}$$

In thermodynamic language the expectation values of the gauge invariant local operators $P_{\mathrm{pl},x}$, Q_x, and $L_{\varphi,x}$ are the densities of those extensive quantities, which are assigned to the bare couplings β, λ, and κ entering the partition function of the lattice system through its action. Eqs. (5.28) – (5.34) also cover most of the observables, whose expectation values are calculated during the program runs[2]. They only have to be averaged over the (eventually space- or timelike) lattice volume before, as sketched in section A.3 of appendix A. For $\xi = \gamma_\beta = \gamma_\kappa = 1$ the action S_x and operators contained in simplify to their well known forms on isotropic lattices. Hence the implication of the extensive discussion concerning the MC simulation of the four-dimensional SU(2)–Higgs model in refs. [135, 137, 139] and partly in section 5.3 carries over directly to the anisotropic lattice case.

The non-perturbatively renormalized masses of the theory are extracted from the exponential decays of correlation functions at zero transverse, i.e. spatial momentum in time direction, whose defining gauge invariant local operators were averaged within each timeslice over the transverse lattice volume first. This has already been drafted in some detail for the two-dimensional U(1)–Higgs model in subsection 1.2.3 of chapter 1, and its general message does apply on principle to the more complicated situation of four dimensions too. With the standard notations adopted there, J: spin, P: parity, and C: charge conjugation parity, the particle spectrum of the model contains the Higgs boson as an isoscalar spin–0 state with quantum numbers $J^{PC} = 0^{++}$ and the gauge vector (W) boson, which is an isovector spin–1 state with quantum numbers $J^{PC} = 1^{--}$. Appropriate operators in the Higgs channel [112, 114, 135] are the site variable $R_x = \rho_x^2$ and the link variable $L_{\varphi;x\mu} = \frac{1}{2}\,\mathrm{Tr}\left(\varphi^{+}_{x+\hat{\mu}} U_{x,\mu} \varphi_x\right)$, where a summation over the — at least three spatial — components of the latter to a scalar operator $L_{\varphi,x}$ as in eq. (5.32) ensures the symmetrization of the spacelike directions. In the vector channel I similarly use the composite link fields [19, 112, 114, 135], constructed from the Pauli matrices as projections onto the three different basis directions in weak isospin space,

$$W_{x;rk} \equiv \frac{1}{2}\,\mathrm{Tr}\left(\tau_r \alpha^{+}_{x+\hat{k}} U_{x,k} \alpha_x\right)\,, \quad r,k = 1,2,3\,. \tag{5.35}$$

While due to lattice symmetry only the diagonal correlators ($r = k$) are non-zero for the isotropic setting and can thus be averaged to $W_x = \frac{1}{3}\sum_{r,k=1}^{3} W_{x;rk}$ before extracting the masses, also the non-diagonal correlators ($r \neq k$) are non-vanishing on anisotropic lattices and will contribute to the W–mass. The correlation functions of these quantities are expected to fall off in the same way as suggested by the fit ansatz (1.59). Unlike the W–boson mass

[2]The traces are conveniently normalized by $\mathrm{Tr}\,\mathbf{1}_{2\otimes 2} = 2$.

am_W, for which a two-parametric form without constant is sufficient thanks to $\langle W_{x;rk} \rangle = 0$, a full three-parameter fit is necessary to calculate the Higgs mass am_H in lattice units.

I also measured planar on-axis Wilson loops, which allow to compute the potential energy of an external static SU(2)–doublet charge pair separated in space by a distance R. Restricting myself to space-time extensions R and T on isotropic lattices for notational reasons, the corresponding formulas in the abelian case in two dimensions, compare with subsection 1.2.1 of chapter 1, read here

$$W(R,T) \equiv \left\langle \frac{1}{2} \operatorname{Tr} U_{\mathcal{C}_{R,T}} \right\rangle , \quad aV(R) = - \lim_{T \to \infty} \frac{1}{T} \ln W(R,T) , \tag{5.36}$$

where $U_{\mathcal{C}_{R,T}}$ stands for the ordered link product around a rectangular closed path $\mathcal{C}_{R,T} \in \Lambda$ with elongations $R \times T$ as it was visualized within figure 1.1 in the same chapter part of this work. The Polyakov loop is the expectation value of the gauge link product along a line of maximal length $L_4 = L_t$ in time direction,

$$L_{\mathrm{P}} \equiv \left\langle \frac{1}{L_1 L_2 L_3} \sum_{\boldsymbol{x}} \frac{1}{2} \operatorname{Tr} \left(\prod_{x_4=1}^{L_4} U_{x,4} \right) \right\rangle , \tag{5.37}$$

and can serve as an order parameter for the phase transition between confinement ($|L_{\mathrm{P}}| = 0$) and the deconfinement phases ($|L_{\mathrm{P}}| \neq 0$) in gauge theories at finite temperature [17, 19].

5.1.2 Finite temperature and phase diagram

The general formalism of finite-temperature field theory [6, 94] relies upon the formal equivalence between Euclidean quantum field theory — originating from a Wick rotation of Minkowski space to imaginary times — and a system of classical statistical mechanics in D dimensions, which substantiates in the representation of thermal expectation values by functional integrals over a finite time extent $1/T$. When translating these concepts to the lattice regularization [19], one has to utilize asymmetric lattices with spacelike extensions much larger than the temporal extension, $L_s \gg L_t$, $s \in \{\mathrm{x}, \mathrm{y}, \mathrm{z}\}$, in order to imitate the thermodynamic limit $L_s \to \infty$ for all L_s. Then the physical temperature is given by the timelike lattice extension as

$$T = \frac{1}{aL_t} , \tag{5.38}$$

and for $L_t \to \infty$ at constant lattice spacing a one recovers $T = 0$ physics. Since the continuum limit of the SU(2)–Higgs model is believed to be trivial, see below, it goes along lines of constant physics (LCPs) approaching the scaling region of the model, where the cutoff effects and potential scaling violations are very small. These are renormalization group trajectories in the bare lattice parameter space, on which dimensionless physical quantities, typically couplings and masses, are held fixed and ideally only a is varying. Therefore the continuum limit at finite temperature is realized as $a \to 0$ with T fixed, which means $L_t \to \infty$

in practice. The temperature in physical units is obtained by relating it to some dimensionful quantity like a particle mass $m^{(\mathrm{phys})}[\mathrm{GeV}]$, whose dimensionless number $am^{(\mathrm{phys})}$ in lattice units should have been calculated from numerical simulation results before:

$$T^{(\mathrm{phys})}[\mathrm{GeV}] = \frac{m^{(\mathrm{phys})}[\mathrm{GeV}]}{am^{(\mathrm{phys})}L_t}\,. \tag{5.39}$$

In the SU(2)–Higgs model the physical mass scale is set by the experimentally known value of the vector boson mass $m^{(\mathrm{phys})}[\mathrm{GeV}] \equiv m_W = 80$ GeV at zero temperature.

For anisotropic lattices with lattice spacing anisotropy parameter $\xi = a_s/a_t$ the identification (5.38) becomes

$$T = \frac{1}{a_t L_t} = \frac{\xi}{a_s L_t}\,, \tag{5.40}$$

which allows for continuous changes of the temperature by varying the lattice spacing anisotropy $\xi > 1$ at fixed temporal extension L_t. Moreover, finite-temperature simulations needing large physical volumes at the same time can be ensured by choosing $\xi > 1$ too, whereas the temperature stays controllable through $L_t \ll L_s$, and the continuum limit is further on achieved as $L_t \to \infty$. This is exactly the situation one encounters in the MC analyses of the EWPT, if scaling investigations, continuum extrapolations, or simulations at large Higgs boson masses around $m_H \equiv 80$ GeV are concerned.

Let me sketch the schematic phase structure of the four-dimensional SU(2)–Higgs model with a fundamental scalar doublet field as it is established by extensive numerical studies. To begin with, I consider zero temperature first [19, 95]. In general there is phase transition surface $\kappa_c = \kappa_c(\beta, \lambda)$ in lattice parameter space spanned by β and λ, which separates the confinement phase at $\kappa < \kappa_c$ from the Higgs phase at $\kappa > \kappa_c$. The limiting cases are identical to those of the U(1)–Higgs model in two dimensions collected in section 1.3 of the first part. For $\kappa = 0$ the model reduces to pure gauge theory with a single confinement phase, and for $\beta = \infty$, i.e. $g^2 = 0$ from eq. (5.9), one is left with pure scalar systems in four dimensions possessing a global O(4)–invariance. These are known as the non-linear sigma model in the fixed length case with $\lambda = \infty$ and as the four-component $\phi^4_{n=4}$–theory for $\lambda < \infty$, which both exhibit a second order phase transition. Assuming $\lambda < \infty$ and $\beta < \infty$ from now on, the symmetric phase ($\kappa < \kappa_c$) and the phase with spontaneously broken symmetry ($\kappa > \kappa_c$) of the $\phi^4_{n=4}$–theory are continued to the interior of the parameter space leading to the just mentioned confinement and Higgs phases, respectively. Resembling QCD, the former is characterized by 'color' gauge fields confining the scalar matter particles ('quarks') into massive singlet bound states, while in the latter, where the Higgs mechanism is at work, the gauge bosons acquire their masses owing to the non-zero vacuum expectation value of the scalar field. This is a non-perturbative phenomenon, which renders the three massless Goldstone modes of the $\phi^4_{n=4}$–theory massive via mixing with — or being 'eaten' by — the gauge vector bosons resulting in the W–boson with mass m_W. The radial degree of freedom of the scalar field gives rise to the Higgs boson with mass m_H.

The transition surface $\kappa_c(\beta, \lambda)$ is of first order with a drastic, thus discontinuous, jump of physical quantities like, for instance, the mass ratio $R_{HW} = m_H/m_W$, and its strength grows for decreasing λ and decreasing but not too small β. For large enough λ and small β the surface has a boundary with (continuous) second order phase transitions. Beyond this edge — and in agreement with [21, 22] — the two phases become analytically connected regions without any local gauge invariant order parameters distinguishing them. Hence, the completely massive particle spectrum and other physical properties below and above $\kappa_c(\beta, \lambda)$ look qualitatively very similar. At these values of β and λ the Higgs and W–boson excitations below $\kappa_c(\beta, \lambda)$ are bound states of scalar constituents, and in strict sense, the confinement and Higgs regimes belong to the same phase of the theory [19, 22], however, quantitative differences still persist.

At high temperatures T raised above the scale of the scalar vacuum expectation value, the spontaneous symmetry breaking disappears so that the symmetry of the vacuum gets restored. The Higgs mechanism is no longer operational, and the symmetry restored confinement phase goes through the electroweak phase transition (EWPT) into the Higgs phase, when the temperature is cooled down below a certain transition temperature T_c. On $T > 0$ lattices with $L_t \ll L_s$, the confinement-Higgs phase transition surface $\kappa_c(\beta, \lambda)$ at finite temperatures slightly shifts towards larger κ–values relative to the transition at $T = 0$. This is illustrated in figure 5.1. The finite-temperature deconfinement phase transition of pure gauge theory ($\kappa = 0$) is of second order and passes to larger β as T is released. For rising $\kappa > 0$ it extends into the phase diagram as a rapid crossover moving to lower β and terminating at some κ deep in the confinement region, long before the confinement-Higgs phase transition line at fixed λ is reached [19, 97, 118]. From the preservation of the $T = 0$ behaviour in dependence of λ and β one may conclude that the EWPT weakens with λ and likewise R_{HW} increasing, if by a proper choice of β a definite value is assigned to the renormalized gauge coupling, and it presumably turns into a smooth crossover.

In order to perform the continuum limit, one has to remove the lattice cutoff by requiring $am \to 0$ for any physical mass m in units of the lattice spacing $a = a(\beta, \lambda, \kappa)$. Since the couplings in the electroweak sector, with the exception of the SU(2)–gauge coupling, are not asymptotically free, the Gaussian fixed point at vanishing couplings is ultraviolet unstable and not suited for the definition of a continuum limit, to which the LCPs of the theory converge. On the other hand, it is well accepted from the non-perturbative lattice investigations that there exists no non-trivial ultraviolet fixed point at non-vanishing couplings to define a non-trivial continuum limit, i.e. the renormalized quartic self-coupling λ_R fulfills $\lim_{a\to 0} \lambda_R(\beta, \lambda, \kappa) = 0$. This implies the continuum limit in the SU(2)–Higgs sector of the standard model to yield a trivial, non-interacting theory. As far as the continuum limit is not yet entirely performed ($am > 0$), one can show that the renormalizability of the theory entails λ_R to have an upper bound going only logarithmically with $a \to 0$ to zero, and consequently, there exist effective theories with non-zero renormalized quartic and

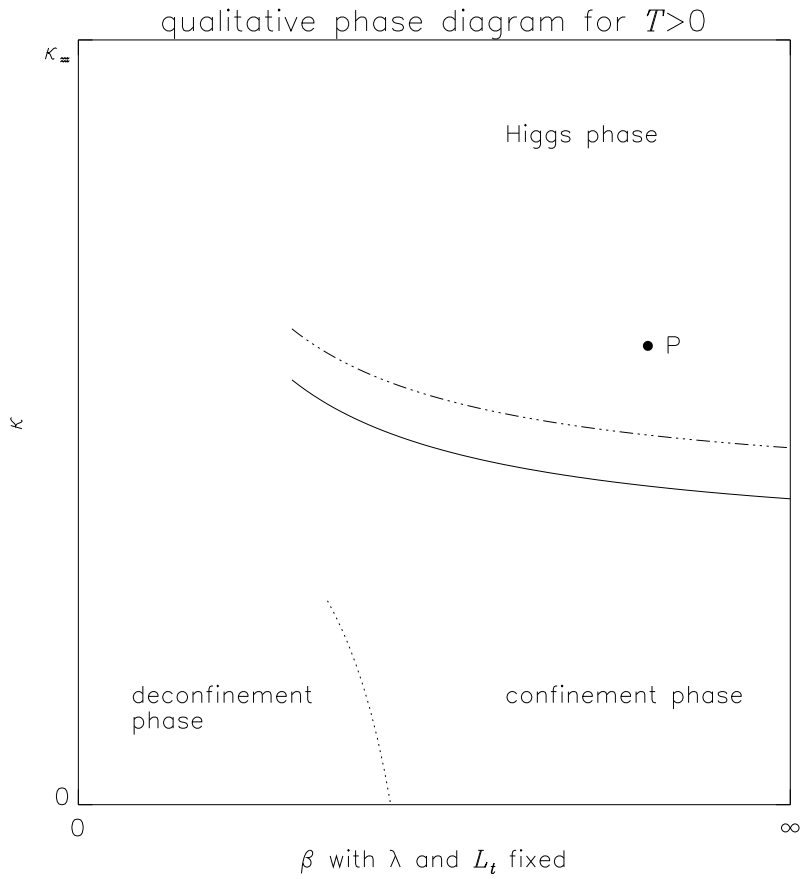

Figure 5.1: *Upwards shift from the full to the dashed line of the first order phase transition between the confinement and the Higgs phase, when switching on finite temperature $T > 0$ on the lattice via $L_s \ll L_t$. The dotted line indicates the position of the deconfinement phase transition, probably only a crossover inside the phase diagram for $\kappa > 0$, and P is a possible physical point at zero temperature with weak gauge coupling in the Higgs phase.*

gauge couplings and very high but finite momentum cutoffs, whose influence on the physics prove to be negligibly small. In the numerical simulations of the SU(2)–Higgs model, the largest tolerable finite-lattice effects at lower cutoffs before the theory looses its sense give an upper triviality bound of $m_H \lesssim 9 m_W$ on the Higgs boson mass [19, 116]. Finally, one should bear in mind that also the Yukawa couplings of the fermions to the Higgs field, which are in principle weak compared to the SU(2)–gauge and scalar quartic couplings and do not change the common picture considerably, provide a cutoff-dependent restriction on the renormalized couplings, originating from radiative corrections generated by them. These enlarge λ_R and imply the so-called vacuum stability lower bound on the Higgs mass depending on the strength of the Yukawa couplings[3]. This manifests itself in the fact that the scalar

[3]Do not confuse it with the positive lower bounds on R_{HW} and λ_R in eq. (5.42), which are a consequence of the Weinberg-Linde bound on the Higgs boson mass in the weak gauge coupling limit $g^2 \to 0$ [19, 124].

vacuum expectation value of the Higgs field appears to be unstable at large scales, hence the instability occurs at the cutoff of the lattice-regularized quantum field theory [19, 123].

5.2 Fixing the parameters

The choice of the bare lattice parameters β, λ, and κ is induced by demanding physical quantities to have some desired values borrowed from the situation faced in nature. This parameter tuning is conventionally done at zero temperature in the Higgs phase, where the numerical simulations and especially the calculation of the particle masses is feasible.

The electroweak SU(2)–gauge coupling $\alpha_W \equiv g_R^2/4\pi$, with g_R the renormalized counterpart of the bare coupling g entering the action (5.2) of section 5.1, is fixed by setting $\beta = 8.0$, which corresponds to $g^2 = 0.5$ in regard of eq. (5.9). It leads to $g^2/4\pi \simeq 0.04$ and $g_R^2/4\pi$ still rather close to the experimentally observed value of $\alpha_W \simeq 0.04$, because the non-perturbative renormalization in g^2 is of roughly $10\,\% - 15\,\%$ upward tendency in the relevant parameter range of interest [115, 134, 135, 137]. Another experimental input is the vector boson mass value of $m_H = 80$ GeV used to convert lattice into physical units. The fixing of the Higgs mass value in lattice units am_H basically amounts to specify the bare quartic coupling λ, and this enables to prescribe the dimensionless Higgs to vector mass ratio

$$R_{HW} \equiv \frac{m_H}{m_W} \tag{5.41}$$

independently. Together with g_R^2 both quantities automatically fix the renormalized quartic coupling λ_R through their relations

$$a^2 m_H^2 = 8\lambda_R v_R^2\,, \quad a^2 m_W^2 = \frac{g_R^2 v_R^2}{4}\,, \quad R_{HW}^2 = \frac{32\lambda_R}{g_R^2} \tag{5.42}$$

to the renormalized vacuum expectation value of the Higgs field v_R in direct analogy to eq. (3.5) of section 3.1 in the abelian case. Since the renormalization at $T = 0$ is, to a good approximation, already achieved by fixing β and λ, a change in the scalar hopping parameter κ mainly reflects in a change of the lattice spacing a and therefore, assuming the physical space volume to be large enough such that its change with a^3 is not important, essentially in the physical temperature $T = 1/aL_t$ on $T > 0$ lattices with $L_s \gg L_t$, if one crosses the phase transition point by varying κ alone.

Hence, the strategy for all finite-temperature studies within the four-dimensional SU(2)–Higgs model may be summarized as follows. In a first step, after fixing the bare couplings β and λ as described above, the critical temperature $T_c > 0$ is imposed via a given temporal lattice extension $L_t = 2, 3, \ldots$ as $T_c = 1/aL_t$, and the system is tuned to reside in $T = T_c$ by determining the phase transition point in $\kappa = \kappa_c$ with one of the methods employed in the next chapters. Then the non-perturbatively renormalized quantities R_{HW} and g_R^2 have to be determined by the results of $T = 0$ simulations in exactly this κ–value on lattices with

geometries $L_t \geq L_s$, i.e. at the phase transition points just gained on the finite-temperature lattices. The masses in both particle channels are extracted from the exponential decays of appropriate correlation functions, see sections 1.2 and 5.1.1, and the renormalized gauge coupling is computed from the (screened) static Yukawa potential of external charges coming from Wilson loops as in refs. [135, 137, 141] and subsection 8.2.3 of chapter 8. In the end, $m_W = 80$ GeV sets the physical scale a for all dimensionless quantities in lattice units.

The procedure is in fact consistent with the (non-perturbative) renormalization at zero temperature in the Higgs phase announced at the beginning, since from the discussion of the phase structure, joined with figure 5.1 in the previous section, it should be clear that the finite-temperature critical points $\kappa = \kappa_c$ at $T = 0$ always belong to the symmetry broken Higgs phase. In this context it is also noteworthy that the use of the physical gauge coupling α_W as input causes the finite-temperature EWPT at $\beta \simeq 8$ to occur between the deconfinement and Higgs regions in the phase diagram. Because of the shift of the deconfinement phase towards larger β–values as $L_t \to \infty$ is taken to reach the continuum limit while keeping the physical situation fixed, the EWPT continues to take place between these two regions and does not interfere with the remnant of the pure gauge theory transition.

As emphasized at several times throughout this work, the continuum limit of quantum field theories on the lattice is taken along LCPs in bare parameter space, which reproduce the same physical theory with increasing accuracy apart from possible scale braking lattice artifacts. Respecting the triviality of the continuum limit in the SU(2)–Higgs model elucidated in the foregoing section, it is to be understood as the approach to the scaling region, where the approximation of an effective continuum cutoff theory is expected to be very good in the low energy regime with momenta $|p| \ll \pi/a$, and where the influence of the finite ultraviolet cutoff is negligible. Since the renormalized couplings vanish only logarithmically with the lattice spacing, the LCPs in this model defining the continuum limit with non-zero renormalized couplings are realized by keeping the values of the two dimensionless and independent physical (renormalized) coupling constants g_R^2 and λ_R, or actually g_R^2 and R_{HW} through eq. (5.42), fixed, and — as thus the ratio $m_W/T_c = am_W L_t$ is constant on a given LCP — the related evolution of the bare couplings g^2 and λ_0 with the lattice spacing a on these paths is parametrized by $\tau \equiv -\ln(am_W)$ characterizing the lattice resolution. Every such LCP with non-zero couplings ends on the boundary of the bare parameter space at some finite $\tau = \tau_{\max}$, but if m_H is not close to the triviality upper limit $9m_W$, the value of $\tau_{\max}$ can be very large, and with the lattice artifacts going to zero by powers of a, the continuum theory is very well approximated [19].

Due to the continuum limit $a \to 0$ being pursued as $L_t \to \infty$, any flow in a has to be compensated by according changes in the parameters β and λ, whose values when moving from L_t to $L_t + 1$ can now be estimated with the aid of the one-loop perturbative renormalization group equations in the continuum [117, 134, 135, 137]. The integration of this system of coupled partial differential equations, which starts at the transition points of the $L_t = 2$

lattices, yields the values of g^2 and λ_0 for the transition points of lattices with temporal extensions $L_t = 3, 4, \ldots$ at distances $\Delta\tau = \ln(am_W)|_{L_t=2} - \ln(am_W)|_{L_t} = \ln(L_t/2)$ in the scale parameter. A perturbative prediction for the change in κ is obtainable through the one-loop perturbative gauge invariant effective potential [135, 137]. However, its relative change along the LCPs is much smaller than for the parameters β and λ, and as shown in refs. [136, 137, 139], a sufficiently precise estimate for the critical point in κ_c is only available by numerical methods, although the κ_c–values resulting from the renormalization group analyses are still useful for guiding the MC simulations.

5.3 Numerical simulation

In my Monte Carlo (MC) simulations of the four-dimensional SU(2)–Higgs model I apply an optimized combination of heatbath and overrelaxation algorithms. Owing to the small values of the scalar self-coupling λ, which actually fix the size of the Higgs mass, large fluctuations of the scalar field modulus ρ_x occurring in the Higgs phase cause the expectation values of the operators ρ^2 and L_φ to have the largest integrated autocorrelations times $\tau_{\rm int}$, whereas observables like plaquette or Wilson loops involving only the gauge links $U_{x,\mu}$ always show the smallest autocorrelations. These are usually much lower in the symmetric phase than in the Higgs phase at the same parameters and lattice extensions.

As shown in refs. [178, 134, 135], the replacement of the ergodic Metropolis steps in the gauge as well as in the scalar sector with the appropriate and more efficient heatbath algorithms for $U_{x,\mu}$ and φ_x, supplemented by an overrelaxation for the Higgs field length ρ_x, already improves the behaviour of the autocorrelations considerably, often by factors up to $\mathcal{O}(1000)$ in some regions of bare lattice parameter space. The latter two algorithms are shortly described in section A.2.2 of appendix A. The optimal ratio among the available heatbath and overrelaxation algorithms called during a complete sweep was suggested in [135] to be the combination given in the upper row of table 5.1. This mixture, which generically depends on the range of the lattice parameters and the lattice size, resulted in minimal $\tau_{\rm int}$–values for the operator $R_x = \rho_x^2$ at a nearly constant amount of CPU time in all parameter set under study. Of course, in the metastability region around the transition point of a first order phase transition at non-zero temperature, where the tunneling rate between the two phases is exponentially suppressed for any local updating algorithm, the autocorrelation times may still grow dramatically beyond those values observed deeper in the symmetric and Higgs phases or at $T = 0$ ('supercritical slowing down').

I want to quantify these statements for the autocorrelations in the applied finite-temperature simulations of two-phase systems discussed in the following chapters [139]. In particular, the introduction of the simultaneous overrelaxation of all four cartesian components of the Higgs field [179], instead of the Higgs field length-overrelaxation as proposed

in [178], see section A.2.2 again, has substantially reduced the integrated autocorrelation time $\tau_{\rm int}$ further. In this way I gained factors of $3-10$ compared to the values previously found in [136] and quoted in section 7.2 of chapter 7. This $\tau_{\rm int}$–behaviour is reflected in table 5.1 and figure 5.2 for the case of a two-phase simulation on isotropic lattices at a low Higgs boson mass of $m_H \simeq 16$ GeV, where as typical examples the autocorrelation functions $\Gamma(t) = \Gamma_{L_\varphi}(t)$ of the φ–link operators $L_\varphi^{(i)}$, $i = 1, 2$, of eq. (5.32) in both phases and their difference ΔL_φ are considered. The observation that this difference has a significantly lower

heatbath		overrelaxation				$\tau_{\rm int}$ in sweeps		
$U_{x,\mu}$	φ_x	$U_{x,\mu}$	α_x	ρ_x	φ_x	$L_\varphi^{(1)}$	$L_\varphi^{(2)}$	ΔL_φ
1	4	3	3	1	-	20(6)	9.4(3.3)	9.2(3.1)
1	1	1	-	-	3	6.3(1.1)	2.2(4)	2.0(4)

Table 5.1: *Autocorrelation times for a 2–κ simulation in $\beta = 8.15$ and $\lambda = 0.00011$ on a $3 \times 24^2 \times 192$ lattice. Each updating sweep consists of a sequence of different algorithms as given by the numbers in the left part of the table. The chosen lattice parameters correspond to a physical Higgs mass of $m_H \simeq 16$ GeV.*

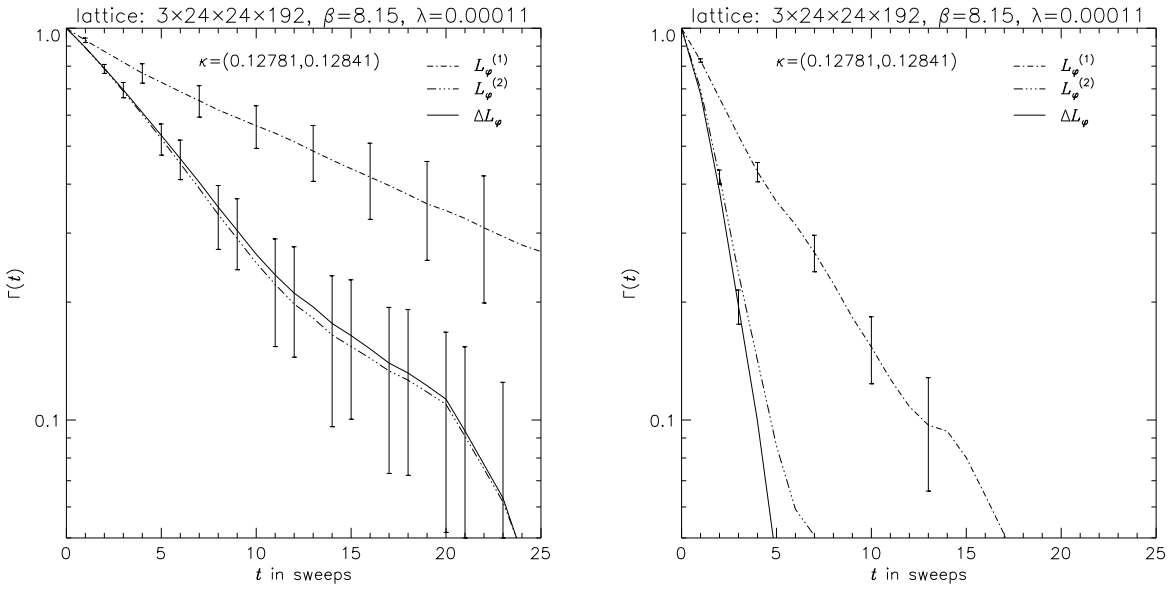

Figure 5.2: *Normalized autocorrelation functions for the 2–κ simulation belonging to table 5.1 with ρ–overrelaxation (left) and φ–overrelaxation (right) in the updating sequence. The autocorrelation functions and integrated autocorrelation times were calculated from a full measurement sample according to the formulas (A.31) and (A.32) of appendix A.3.*

$\tau_{\rm int}$ will become relevant for the determination of the interface tension with the two-coupling method later on.

On zero temperature lattices, the experiences with autocorrelations at $T > 0$ reported here were fully confirmed [137], e.g. the integrated autocorrelation times of the operator ρ^2 typically decreases by factors of $5 - 10$ in dependence of the parameters sets chosen, if the φ–overrelaxation is included as above and $\tau_{\rm int}$ is measured in MC time. The speed-up factor in CPU time can be up to 15, because the algorithm is even simpler. Therefore, the updating scheme per sweep in the lower row of table 5.1, i.e. a sequence of one $U_{x,\mu}$– and one φ_x–heatbath step, succeeded by one $U_{x,\mu}$– and three φ_x–overrelaxation steps, has been taken over without any modifications for the simulations on anisotropic lattices too [140, 141]. However, one should note that the autocorrelation times have the tendency to be somewhat larger on anisotropic lattices than on isotropic ones of the same size.

The program code in FORTRAN77 was developed and optimized for the CRAY Y-MP8 and T90 computers of HLRZ in Jülich, Germany, where most of the large scale numerical simulations presented in the following have been performed. These systems have a vector architecture and offer 64–bit floating point precision. Since the new value of an updated field variable only depends on its old value in the respective site or link and on the values of its direct neighbours, I used a checkered addressing of the lattice in each timeslice with vectorization in both chess-board groups[4]. Then the maximal average performance of up to 650 Mflops per second (T90) was reached on the finite-temperature lattices with $L_t \ll L_{\rm x}, L_{\rm y}, L_{\rm z}$, for which this vectorization gets its largest impact. Smaller lattices were partially simulated on ordinary UNIX and VMS workstations, and a minor portion of the data was also produced on the massively parallel APE-Quadrics computers (with a program version in TAO language) at DESY-IfH in Zeuthen, Germany, which only have single-precision arithmetics. In contrast to some quantities, e.g. the critical hopping parameter or the interface tension from the two-coupling and constrained-simulation methods in $T > 0$ simulations, the 32–bit arithmetics of the APE-Quadrics is sufficient for the calculation of all $T = 0$ quantities, especially for particle masses and the static potential.

The monthly consumed CPU time at HLRZ in Jülich was on average $100 - 120$ hours (referring to one T90 processor with normal priority for the submitted jobs), and the granting of its high performance computer facilities in the years 1994−1997 is gratefully acknowledged.

[4]Note added: For the CRAY version of the program, the vectorized random number generator 'RANF' has been utilized [190], while on the different types of workstations it was 'G05CAF' from the NAG Library [191].

Chapter 6

Thermodynamic quantities

In my treatment of the SU(2)–Higgs model at finite temperature I focus on the phase transition point κ_c, corresponding to the critical temperature T_c of the two-phase system, and on the interface tension σ/T_c^3 between the competing phases. Here I present some methods for the determination of these quantities in the framework of numerical lattice simulations. Most emphasis is on the two-coupling and constrained-simulation methods, which will be applied to physical situations specified by different values of the Higgs boson mass m_H in subsequent chapters.

Another characteristic observable for first order phase transitions is the the latent heat $\Delta\epsilon/T_c^4$. It is defined as the discontinuity of the energy density ϵ at the transition point and can be obtained from the jumps of some order parameters in subsection 5.1.1 of the previous chapter by

$$\frac{\Delta\epsilon}{T_c^4} = L_t^4 \left(8\,\frac{\partial\kappa}{\partial\tau}\,\Delta\langle L_\varphi\rangle - \frac{\partial\lambda}{\partial\tau}\,\Delta\langle Q\rangle - 6\,\frac{\partial\beta}{\partial\tau}\,\Delta\langle P_{\rm pl}\rangle \right) , \tag{6.1}$$

where the partial derivatives with respect to $\tau = -\ln(am_W)$ are to be taken from the one-loop perturbative renormalization group equations, see section 5.1.2 of the same chapter and refs. [134, 135, 137]. In perturbation theory the latent heat derives from the Clausius-Clapeyron equation as $\Delta\epsilon \simeq -\kappa m_H^2 \Delta\langle\rho^2\rangle$ in terms of the discontinuity of the Higgs condensate [107].

For more details about the numerical investigations directed to this quantity, as well as to the mass spectrum in Higgs and symmetric phase neighbouring to the transition temperature, screening length in separated metastable phases, or to the relation between energy density and pressure P, the reader is referred to the publications [135, 137, 144, 146, 147, 150, 152, 122, 149, 153, 145, 154]. Especially the latter has recently become an developing area for numerical studies, because the knowledge of the thermodynamic equation of state, i.e. $\delta(T)/T^4$ with $\delta \equiv \epsilon/3 - P$, is of great interest for the history of the early universe. Only to quote in passing a qualitative result [137], the deviation from the behaviour $\delta = 0$ of a free relativistic, massless photon gas is very small indeed in the high-

temperature confining phase for $T \gtrsim 2T_c$ ('radiation-dominated plasma'), where infrared singularities render the perturbation theory uncertain.

6.1 Critical temperature

A numerical simulation of the SU(2)–Higgs model at finite temperature should start with the determination of the phase transition points. The lattice implementation described in the previous chapter has revealed that in the relevant parameter range any temperature change is triggered by κ at fixed values of β and λ. Therefore, one has to search for the critical scalar hopping parameter κ_c, where the first order phase transition between the spontaneously broken Higgs phase and the phase with restored symmetry occurs. This is an intriguing quantity, because the κ_c–estimate, as well as the uncertainty in its exact position emerging from the individual method employed for its calculation, devolves upon almost all other thermodynamic observables like, for instance, interface tension or latent heat.

As the lattice constant is fixed to $a^{-1} = L_t T_c$ by eq. (5.38) of section 5.1.2, the critical temperature T_c in physical units is then obtained via its ratio $T_c/m_{H,W} = 1/am_{H,W}L_t$ to one of the particle masses am_H and am_W computed from appropriate correlators on zero-temperature lattices.

6.1.1 Effective potential

The most straightforward analytical method to localize the phase transition is the use of the effective potential and its stationary points. This quantity, obtained from the generating functional of the connected Green functions by means of a Legendre transformation, is the momentum independent part of the generating functional of one-particle irreducible Feynman diagrams in the perturbative loop expansion. The physical interpretation of the effective potential becomes more transparent in the field-theoretic language of equilibrium thermodynamics, where it can be identified with the free energy of the quantum system [89]. In perturbation theory the effective potential is evaluated in different gauges. To avoid the difficult task of gauge fixing on the lattice, staying confrontable with results from numerical simulations though, the gauge invariant effective potential has bee devised [106, 107]. As discussed in refs. [107, 135], it offers a conceptually clean perturbative approach to the computation of transition point, interface tension, latent heat, jump of the order parameter, and renormalized masses and couplings. If one performs a proper mass resummation in the Higgs phase, the effective potential in Landau gauge is equivalent to the gauge invariant potential, at least in one-loop order [97, 107].

In the general case of asymmetric lattices a direct perturbative calculation of the lattice-regularized effective potential at finite temperature $V_{\text{eff}}(\Phi) = V_{\text{eff}}(\Phi, T)$ in Landau gauge [19, 138, 141] gives for a constant scalar field $\Phi_x \equiv \Phi$ in one-loop order

$$\begin{aligned} V_{\text{eff}}(\Phi) &= -\frac{m_{H,0}^2}{4}\,\Phi^2 + \lambda_0 \Phi^4 \\ &\quad + \int_k \left\{ \frac{1}{2}\,\ln\left(\hat{k}^2 + 12\lambda_0\Phi^2\right) + \frac{3}{2}\,\ln\left(\hat{k}^2 + 4\lambda_0\Phi^2\right) + \frac{9}{2}\,\ln\left(\hat{k}^2 + \frac{g^2}{4}\,\Phi^2\right) \right\} \end{aligned} \tag{6.2}$$

and the condition

$$\left.\frac{\mathrm{d}^2 V_{\text{eff}}(\Phi)}{\mathrm{d}\Phi^2}\right|_{\Phi=0} = 0 \tag{6.3}$$

leads to the value of the critical hopping parameter κ_c in this order:

$$\kappa_c = \frac{\xi}{2(3+\xi^2)} + \frac{1}{(3+\xi^2)^2}\left[6\xi J_1(\xi,0) - \frac{\xi^2}{(3+\xi^2)}\right]\lambda_0 + \frac{9\xi J_1(\xi,0)}{16(3+\xi^2)^2}\,g^2\,. \tag{6.4}$$

Here the notation for the dimensionless lattice integrals J_n, $n \in \mathbb{N}$, is

$$J_n(\xi, m a_s) = a_s^{4-2n} \int_k \frac{1}{(m^2 + \hat{k}^2)^n}\,, \qquad \int_k \equiv \frac{1}{(2\pi)^4} \int_{-\pi/a_s}^{\pi/a_s} \mathrm{d}^3 k \int_{-\pi/a_t}^{\pi/a_t} \mathrm{d}k_4 \tag{6.5}$$

with $\hat{k}^2 = \sum_{\mu=1}^4 \hat{k}_\mu^2$ and the lattice momenta $\hat{k}_\mu$ defined in eq. (A.8) of appendix A.1. In particular, substituting $p_i = a_s k_i$ and $p_4 = a_t k_4$, one has

$$J_1(\xi,0) = a_s^2 \int_k \frac{1}{\hat{k}^2} = \xi \int_{-\pi}^{\pi} \frac{\mathrm{d}^4 p}{(2\pi)^4}\, \frac{1}{4\left[\sum_{i=1}^3 \sin^2\left(\frac{1}{2}\,p_i\right) + \xi^2 \sin^2\left(\frac{1}{2}\,p_4\right)\right]}\,,$$

and for the special case of symmetric lattice spacings, i.e. $\xi = 1$, these quantum corrections to the critical hopping parameter reproduce the known result of the isotropic SU(2)–Higgs model [117]. Alternatively, one may calculate the one-loop corrections to the bare masses and require the renormalized masses in lattice units to be zero in the limit of zero lattice spacings $a_s \to 0$, $a_t \to 0$, and fixed anisotropy $\xi = a_s/a_t$, while the one-loop renormalized masses are finite in the continuum limit [141]. At the same time, the vacuum expectation value of the scalar field in lattice units $a_s v_0$ will be zero too, marking the phase transition point. For the Higgs mass this amounts to solve

$$a_s^2 m_{H,R}^2 = -a_s^2 m_{H,0}^2 + \left(48\lambda_0 + \frac{9}{2}\,g^2\right) J_1(\xi,0) = 0 \tag{6.6}$$

perturbatively for κ, the bare mass $a_s m_{H,0}$ taken from (5.26), and coincides with the one-loop formula in eq. (6.4). As an instructive check it has been verified that the identical result is obtained starting from perturbation theory in the symmetric phase or imposing zero one-loop renormalized gauge boson mass in lattice units squared, and that it does not depend on the gauge chosen [141]. Since one works on finite lattices with mostly small temporal

extensions ($L_t = 2, 3, \ldots$ for $T > 0$), the lattice integrals should be replaced by finite lattice sums. The transition points predicted by the perturbative one-loop effective potential differ only on the $\mathcal{O}(10^{-4})$ relative scale from the non-perturbative MC values.

But especially the calculation of the interface tension σ by use of the two-coupling method presupposes a more accurate determination of the critical hopping parameter on large lattices. As will become evident in later sections, an estimate for the critical hopping parameter κ_c of the desired precision can then only be attained by recoursing to numerical MC methods.

6.1.2 Order parameters

A popular way to find κ_c in numerical simulations is to look for the maxima in the variances or, equivalently, susceptibilities $\chi(O) \equiv \langle\, (O - \langle O \rangle)^2 \,\rangle$ of some order parameter O and for the minima in their fourth order Binder cumulants $B(O) \equiv 1 - \langle O^4 \rangle / 3 \langle O^2 \rangle^2$ [156, 157, 144, 147, 149, 150, 122], both as functions of the hopping parameter κ, and eventually extrapolated to infinite volume and zero lattice spacing lastly.

Another possible definition of the phase transition point is the equal-area or equal-height criterion of a two-state signal in the probability distributions of O. To this end, one simulates the system in the metastability region at $\kappa \simeq \kappa_c$ near to the expected real transition point and generates an order parameter distribution by collecting a sample history of its measurement values. Since these operators O exhibit a discontinuity at the transition point, two distinct peaks representing the metastable phases with a broad minimum in between might develop in the corresponding histograms for large enough lattice volumes as shown e.g. in figure 9.1 of chapter 9, and the requirement of equal heights or equal areas of the two peaks at $\kappa = \kappa_c$ is conveniently fulfilled by reweighting the distribution to nearby κ–values [147, 149, 150, 152, 188].

Of course, it is tacitly assumed here that the system does frequently undergo tunneling transitions between the two phases during a simulation. But since the tunneling rate is exponentially small in the critical region, these histogram techniques are often pushed ahead by the virtue of multicanonical algorithms [177] to enable tunneling between the phases, and sometimes combined with constrained methods [158] to fight autocorrelations. Such tools invoke an artificial enhancement of the mixed states, which are suppressed due to the additional free energy of the interfaces separating the two phases, and permit to extract the most precise κ_c–estimates. Nevertheless, the observed autocorrelation times are still very large, typically of the order of $\mathcal{O}(10000) - \mathcal{O}(500)$ sweeps in dependence of the lattice sizes and parameters chosen [134, 135].

Although the different definitions of κ_c constitute an inherent uncertainty for its exact value besides the statistical errors of the MC simulations themselves, this uncertainty goes rapidly — in most cases even exponentially — to zero, if the finite spatial volumes grow in

order to come hopefully close to the thermodynamic limit of infinite volume.

The order parameters O under study in the following are ρ^2, $s_{\log}$, i.e. the modified action density

$$s_{\log} = \frac{1}{\Omega} S_{\log} , \quad S_{\log} \equiv S[U,\varphi] - 3 \sum_{x \in \Lambda} \ln \rho_x , \tag{6.7}$$

and the φ–link operator L_φ already defined in eq. (5.34) of subsection 5.1.1. It plays an important rôle in the reweighting procedure [188], which has been used to obtain data in the vicinity of the simulation point from a single MC run, see refs. [135, 136] and section B.3 in appendix B.

6.1.3 Hysteresis

A rather crude and tentative estimate for κ_c is accessible either by the effective potential as explained above or by a hysteresis pattern visible in a thermal cycle of $\langle O \rangle_\kappa$ in dependence of κ, which is readily taken as a characteristic indication for a first order phase transition. It rests on the fact that there exists a secondary minimum of the effective potential $V_{\text{eff}}(\Phi, T)$ in $\Phi = 0$ belonging to the symmetric phase, different from absolute minimum $\Phi = v$ of the broken phase, if the symbol v stands for the thermal expectation value $v(T) \equiv \langle \Phi \rangle$ as an order parameter, in a fixed gauge, exhibiting a discontinuity at the critical point $T = T_c$, where the two minima become degenerate: $V_{\text{eff}}(v(T_c), T_c) = V_{\text{eff}}(0, T_c)$.

In a MC simulation this phenomenon is responsible for hysteresis effects, when the system gets stuck in the wrong minimum and does not flip into the other phase before the transition point is significantly exceeded. Hence, the spatial lattice volume must be large enough in order to have metastability and a vanishingly small tunneling rate, which otherwise would counteract the hysteresis. Representative hysteresis patterns are shown in figures 9.2 and 9.4 of sections 9.1 in the last chapter. Beginning in the symmetric (broken) phase, the hopping parameter κ has been gradually increased (decreased) across the expected transition region until the other phase is reached, while the consecutive simulations were just initialized with the final field configuration of the run at the preceding κ, respectively, and some hundred sweeps were discarded for further equilibration. These curves do not only provide information about the rough position of the transition point in parameter space, but they are also valuable to assign the expectation values $\langle O \rangle_\kappa$ to one of the two phases in question, as it will be useful for the κ_c–determination from two-coupling simulations.

More accurate values of the critical hopping parameter may be achieved by one of the refined methods presented now. They have in common that by appropriate external conditions at least one interface pair is forced to develop within the simulation volume in order to bring the subvolumes of the different phases into thermal contact, and no complete transitions between them as for the multicanonical method must be awaited.

6.1.4 Two-coupling method

If hysteresis effects in thermal cycles are seen at a first order phase transition, the safe and efficient two-coupling method [162] allows to confine the position of the critical hopping parameter κ_c further by exploiting metastability on large volumes.

In determining κ_c with this method, an elongated lattice of geometry $L_{\rm z} \gg L_{\rm x} = L_{\rm y} \gg L_t$ is divided into two halves with different couplings $\kappa_1 < \kappa_2$,

$$\kappa = (\kappa_1, \kappa_2) \equiv (\kappa_1 < \kappa_c \text{ for z} \leq L_{\rm z}/2\,,\ \kappa_2 > \kappa_c \text{ for z} > L_{\rm z}/2)\,, \tag{6.8}$$

which enforces one part to stay in the symmetric phase and the other one in Higgs phase. For long enough z–directions a pair of interfaces will be present[1], which separates these two phases and accommodates the additional free energy shift between them. By equilibrating the configuration in simulations with κ–values far away from the expected transition point — as e.g. estimated by hysteresis runs — the system is achieved to reside in such a two-phase situation with communicating subvolumes. In this configuration the system can sensitively react to free energy differences due to movements of the interfaces and may remain stable against any collapse into a unique phase for many autocorrelation times, as far as κ_c is really enclosed by κ_1 and κ_2. Subsequently, the distance in κ is more and more diminished, and the smallest κ–interval, for which the system still resists to turn over into one single phase, gives lower and upper bounds for the critical hopping parameter. κ_c is then defined as the mean value of the best lower and upper bounds with an error naturally arising as the absolute deviation from these. To discriminate between the two phases during this procedure, a rough knowledge of the κ–dependence of a suitable order parameter at otherwise constant couplings is a helpful information, which can also be gained by hysteresis simulations.

Since the volume-dependent portion of the free energy at nearly unchanged contribution of the interfaces increases when $L_{\rm z}$ is enlarged, very narrow κ–intervals up to $\kappa_2 - \kappa_1 < 10^{-5}$ can be stabilized in the MC simulations. Moreover, after warming up the individual starting configurations appropriately, at each pair of κ the system and its envisaged two-phase structure should be observed for at least 10 autocorrelation times. The observable under consideration to crucially control the conservation (or the breakdown) of the induced two-phase situation has been chosen to be the z–slice expectation value $L_\varphi(\mathrm{z})$ of the φ–link,

$$L_\varphi(\mathrm{z}) \equiv \left\langle \frac{1}{L_{\rm x} L_{\rm y} L_t} \sum_{(\mathrm{x},\mathrm{y},t)} L_{\varphi,x} \right\rangle\,, \quad L_{\varphi,x} = \frac{1}{4}\sum_{\mu=1}^{4} L_{\varphi;x\mu}\,, \quad L_{\varphi;x\mu} = \tfrac{1}{2}\,\mathrm{Tr}\left(\varphi^{+}_{x+\hat{\mu}} U_{x,\mu} \varphi_x\right)\,, \tag{6.9}$$

while $L_{\varphi,x}$ has eventually to be weighted according to eqs. (5.32) – (5.34) in the anisotropic lattice case.

[1] For not too large $L_{\rm z}$ the probability for the appearance of more interface pairs is negligible.

6.1.5 Constrained-simulation method

Here I suggest a new method [136], which in practice is able to give the same and very precise critical hopping parameters κ_c as the multicanonical method, typically with $7-8$ relevant digits accuracy, provided that computer hardware with the required double-point precision (64–bit floating point arithmetics) is available. However, as a considerable benefit, using this method the notoriously large autocorrelation times of the multicanonical simulation can be reduced dramatically.

The method is based on the observation that, for sufficiently large elongated lattices with $L_{\rm z} \gg L_{\rm x} = L_{\rm y} \gg L_t$, a flat and approximately linear regime appears between the peaks in the probability distribution of an order parameter $O = O(\{U,\varphi\})$ [135]. Those peaks in the vicinity of symmetric and Higgs phase expectation values correspond to pure phase configurations. Between the peaks the system is dominated by subvolumes of these configurations and two interfaces perpendicular to the long direction z, i.e. two bulk phases appear. Shifts of the interfaces during the simulation cause the respective subvolumes to increase or decrease, and the linear domain of the histogram ends, when the interfaces touch and a pure phase is met. At the transition point itself the free energy densities of the bulk phases are the same, the ratio of the occupied volumes is arbitrary, and thus the probability distribution becomes flat. By use of the constrained simulation [158] one can artificially enforce that during a simulation in $\kappa \simeq \kappa_c$ an order parameter of the system stays in a given short interval between the peaks. Close to the transition point one then utilizes a reweighting procedure to determine the value of the hopping parameter, at which the distribution is flat.

In regard of the numerical simulation, the MC updating algorithms have to be modified in such a way that only those configurations are generated, which lie in the flat regime between the two peaks of the pure phases. Introducing within this region a lower bound O_- and an upper bound O_+ for the lattice averages of the order parameter $O = O_n = \frac{1}{\Omega}\sum_{x\in\Lambda} O_x$ in a sample of $N_{\rm meas}$ configurations labelled by n, the constraint is realized via replacing the Boltzmann factor in the functional integral by

$$\mathrm{e}^{-S[U,\varphi]} \;\to\; \Theta\Big(O(\{U,\varphi\}) - O_-\Big)\,\Theta\Big(O_+ - O(\{U,\varphi\})\Big)\,\mathrm{e}^{-S[U,\varphi]}\,, \quad \Theta(c) = \begin{cases} 0 & , c<0 \\ 1 & , c\geq 0 \end{cases}\,, \tag{6.10}$$

which translates into action as an additional metropolis decision in the program code. Whenever a proposal of any field variable leads to a O–measurement outside the interval fixed by O_- and O_+, it is rejected[2] so that solely measurement values respecting the condition

$$O \;\in\; [\,O_-\,,\,O_+\,]\,, \quad O = O_n\,, \quad n \in \{1,\ldots,N_{\rm meas}\} \tag{6.11}$$

are allowed. At the same time, the requirement of a flat order parameter histogram in $\kappa = \kappa_c$

[2]Since this metropolis step can be implemented neither vectorized nor parallel, some loss in performance is purchased for the modified algorithms.

is now equivalent to the condition that

$$\langle O \rangle \Big|_{\kappa=\kappa_c} = \frac{1}{2}\,(O_- + O_+) \tag{6.12}$$

holds for the expectation value $\langle O \rangle$ of the order parameter. This relation, which implicitly defines the critical hopping parameter κ_c, can be fulfilled by a κ–reweighting of the measured distribution of O. For the reweighting technique being successfully applicable, credible guesses for κ_c and the order parameter interval $[\,O_-\,,\,O_+\,]$ must be known in advance. These are provided by the two-coupling method for the former, and by individual simulations in the symmetric and Higgs phase for the latter to find their peak positions in the histogram.

In order to get a feeling, whether the lattice system has been simulated within the flat region of the histogram indeed, one should check that separate evaluations with the two parts of the measurement history of O belonging to the lower and upper halves of the interval in eqs. (6.11) and (6.12) yield only such values, which are compatible with the original result from the full history. One should also pay attention to the evolution of the system during the simulation, i.e. it is also recommended to steadily keep under control that the existence of the two-phase equilibrium and the adhering interfaces is preserved. For this purpose one may take again the expectation value of the φ–link operator $L_\varphi(\mathrm{z})$, averaged within each z–slice of the lattice as in eq. (6.9).

The order parameters employed in the following investigations with the constrained-simulation method were $O = s_{\log}$ from eq. (6.7) and $O = \rho^2$, the Higgs modulus squared. In the updating sequence involving the ρ–overrelaxation $s_{\log}$ is the proper choice, since it remains invariant by this algorithm and the α– and U–reflections; only the heatbath algorithms for the scalar field and the gauge links have to be adjusted in this case. If on the other hand the φ–overrelaxation is incorporated instead, the use of ρ^2 is numerically simpler and accelerates the performance. Then the algorithms to be modified are the heatbath and overrelaxation updates for the scalar field φ alone. The achieved acceptance rates of these algorithms was always larger than 98 %, and the observed integrated autocorrelation times typically fall in the range $\tau_{\mathrm{int}} \simeq 20 - 100$ sweeps. Their dependence on the width of the order parameter interval has not been addressed in detail, but it is not surprising that it might noticeably increase for very large intervals or extremely small ones near criticality in T.

As will be sustained in the concrete applications of the next chapter, this method is most precise at moderate computational expense. But I should also notify that confidence can be given to the constrained-simulation method only in those cases, where the pure-phase peaks are well displaced against each other so that the plateau region between them is broad enough to choose a suitable order parameter interval from it. Otherwise, if tunneling events destroy the coexistence of the two phases and the interfaces spanning through the lattice, the method would fail, because then the histograms of the homogeneous phases simulated separately in $\kappa \simeq \kappa_c$ will overlap and the valley between the corresponding peaks will be too narrow to find a flat interval $[\,O_-\,,\,O_+\,]$ there.

This situation is just encountered for a very weak first order phase transition, as it will turn out later to be accomplished for large Higgs masses around 80 GeV. Even when using anisotropic lattices, the their sizes required to separate the peaks of the pure phases sufficiently lie under realistic circumstances beyond the available computer capabilities. Nevertheless, one can still resort to the quite fast and robust two-coupling method of the preceding subsection, which provides κ_c–estimates within an accuracy of $5-6$ digits in dependence of the lattice sizes utilized.

6.2 Interface tension

In the second part of my work I mainly deal with the interface tension σ. This quantity plays a prominent rôle in the course of the EWPT, because it crucially influences the dynamics of the phase transition through the nucleation and expansion of bubbles or droplets [159, 90, 91, 161], finally filling out the whole universe with the new phase. Moreover, the magnitude of σ provides a direct quantitative measure for its strength [160, 93]. The traditional picture, how the first order cosmological EWPT in the early universe — which was not an instant process and whose total duration is of the order of the universe age — has proceeded, may be sketched as follows.

As the universe expands, it cools in the symmetric phase until it reaches the critical temperature T_c, at which the spontaneously broken Higgs phase becomes equally favoured. If $T \simeq T_c$, bubbles of the phase with broken symmetry begin to nucleate. Inside such a bubble the Higgs field has a non-zero thermal expectation value, which renders the W– and Z–bosons massive, and a stable phase of matter exists. In the region outside the bubble wall there is a metastable phase with vanishing Higgs field expectation value and massless vector bosons W and Z, whereas the bubble wall itself interpolates between these stable and metastable phases of matter. However, surface (or in a finite-volume system, interface) tension effects cause these bubbles to shrink immediately so that the universe remains in an approximately homogeneous state. For T somewhat below T_c the bubbles of the Higgs phase nucleate into the symmetric phase, which become sufficiently large so that the curvature of its surfaces decreases and the raised volume pressure from the lower free energy F inside the bubble can overcome the surface tension; otherwise they would disappear again. In a strong enough first order phase transition these so-called critical bubbles grow rapidly until the volume of the universe is completely converted into the stable broken phase, i.e. all of the matter of the universe has finally nucleated through such critical bubbles[3]. At $T = T_c$, the free energy and thus the radius of a critical bubble is infinite. During the phase transition the universe has always supercooled in the high temperature symmetric phase before the transition took place, and within this supercooled and metastable phase bubbles of the

[3]The typical time scale for the formation of a critical bubble is proportional to $\mathrm{e}^{F/T}$.

low-temperature broken phase have formed. Hence the released latent heat has produced a reheating of the electroweak plasma near the nuclei of condensation, resulting in a local departure from thermal equilibrium in the vicinity of the expanding bubble walls, where baryogenesis primarily occurs [159].

To motivate the relevance of the interface tension in this context further, I note that in non-relativistic fluiddynamics the bubble nucleation rate of the Higgs phase in the symmetric phase depends via the relation

$$\Gamma_{\rm nucl} = \Gamma_0 \, {\rm e}^{\,-\Delta F(r_c)/T_c} \,, \quad \Delta F(r) = -\frac{4\pi}{3} \Delta P \, r^3 + 4\pi\sigma r^2 + \mathcal{O}(r) \tag{6.13}$$

exponentially on the free energy difference $\Delta F(r_c)$ between the system with a critical bubble and a pure metastable phase [159]. If the bubble radius r is large compared to the thickness of the bubble or domain wall, the expansion of $\Delta F(r)$ on the right hand side of eq. (6.13) is valid ('thin wall approximation'), where σ is the surface tension of the bubble wall and ΔP the pressure difference between Higgs and symmetric phase. Stating this condition of a thin bubble wall in more physical terms, one would say that the largest correlation length ξ of the system at the phase transition has to be much smaller than the critical bubble radius r_c at the transition temperature itself. The critical bubble radius can be extracted from the maximum of $\Delta F(r)$ as function of r to be $r_c = 2\sigma/\Delta P$, which diverges in $T = T_c$ since $\lim_{T\to T_c} \Delta P = 0$. Now assume that the pressure difference ΔP is sufficiently small, which is equivalent to the requirement $\eta \ll 1$ for the so-called supercooling parameter, here denoted as $\eta \equiv \frac{T_c - T}{T_c}$. Under these prerequisites, ΔP may be expressed to a good approximation by the latent heat $\Delta\epsilon$, which by definition is the discontinuity of the energy density across the phase transition: $\Delta P \simeq \Delta\epsilon \cdot \eta$. Inserting this together with r_c into $\Delta F(r)$ and then into the exponent of $\Gamma_{\rm nucl}$ in (6.13), the bubble nucleation rate is given in the thin wall approximation by [160, 93]

$$\Gamma_{\rm nucl} = \Gamma_0 \exp\left(-\frac{16\pi}{3} \frac{\sigma^3}{(\Delta\epsilon)^2 T_c} \eta^{-2}\right) = \Gamma_0 \exp\left\{-\frac{16\pi}{3} \left(\frac{\sigma}{T_c^3}\right)^3 \left(\frac{\Delta\epsilon}{T_c^4}\right)^{-2} \eta^{-2}\right\} , \tag{6.14}$$

which can also be expressed in terms of the dimensionless ratios of the interface tension and the latent heat with the third and fourth power with the transition temperature T_c, respectively, usually calculated on the lattice. The prefactor Γ_0 can be approximated by T^4 or T_c^4 [104]. If the combination $R_{\rm nucl} \equiv \sigma^3/(\Delta\epsilon)^2 T_c = (\sigma/T_c^3)^3/(\Delta\epsilon/T_c^4)^2$ is large, signalling a strong first order phase transition, a substantial supercooling of the symmetric phase has to be expected, and the temperature, at which the transition really happens, lies substantially below the critical temperature T_c [103]. This would lead to an additional suppression of the sphaleron transition rate, since in the Higgs phase the W–boson mass $m_W = m_W(T)$ — and then, according to eq. (5.4) in section 5.1 of chapter 5, the vacuum expectation value of the Higgs field $v = v(T)$ as well — increases with decreasing temperature. Consequently, as the sphaleron rate in the Higgs phase after the transition has finished is fundamentally

determined by the value of the temperature dependent expectation value $v(T)$ entering the sphaleron energy, see eqs. (13) and (14) in the introduction, an adequate reduction of this rate could in principle prevent the wash-out of any primordial matter-antimatter asymmetry or of an asymmetry directly generated during the EWPT.

To anticipate some results of this work and refs. [135, 136, 137, 139, 142], the ratio $R_{\rm nucl}$, which is a good characterization for the strength of the phase transition, is decreasing from $R_{\rm nucl} \simeq 0.2$ at $m_H \simeq 16$ GeV over $R_{\rm nucl} \simeq 0.005$ at $m_H \simeq 35$ GeV to $R_{\rm nucl} \simeq 0.000005$ at $m_H \simeq 80$ GeV. This means that the EWPT phase transition at $m_H \simeq 80$ GeV becomes extremely weak indeed, and there is at best a minor amount of stabilization of the baryon asymmetry in the universe against a wash-out through supercooling of the symmetric phase.

If the critical bubble radius r_c becomes $r_c \simeq \xi$, ξ the correlation length from above, the thin wall approximation breaks down, and the nucleation rate $\Gamma_{\rm nucl}$ can not be expressed only through the macroscopic parameters σ and $\Delta\epsilon$ of the phase transition at the critical point. In this case the transition is delayed, and the universe is supercooled even more in the symmetry restored phase [93].

The ratio σ/T_c is also decisive in determining the minimal spatial lattice size necessary for an accurate numerical investigation of first order phase transitions. Namely, in order to reach a mixed-phase situation with a well developed double-peak structure in distributions of globally averaged order parameters around the transition region, one should have $L_{\rm x}L_{\rm y}\sigma/T_c = \mathcal{O}(1)$ with the transverse lattice extensions $L_{\rm x}, L_{\rm y}$ being much smaller than $L_{\rm z}$. The lattice in this volume must be fine enough to resolve the interface structure, which becomes thiner for increasing m_H. These physical requirements, which are practically more restrictive than the conditions imposed by the smallness of $\mathcal{O}(a)$–lattice artifacts, imply that the computational gain by using the simplest local three-dimensional action is essentially a factor L_t. Therefore, any extension of the present numerical studies to Higgs boson masses towards $m_H \simeq 80$ GeV will be only modestly easier and less demanding in the framework of dimensional reduction to an effective model in three dimensions [147, 150] than within the full SU(2)–Higgs model in four dimensions.

After this — by no means rigorous — proofs for the importance of σ and $\Delta\epsilon$ to decide about the strength of the EWPT, I will discuss the most convenient methods to determine the electroweak interface tension σ within the SU(2)–Higgs model. Nearly all numerical ones among them rely on its defining relation $A_{\rm I}\,\sigma = \Delta F$ to the difference ΔF in the free energy F of the two phases, if these are separated by an interface (pair) with transverse area $A_{\rm I}$.

6.2.1 Perturbation theory

To be self-contained, I recall the perturbative definition of the interface tension [103], which descents from the effective potential $V_{\rm eff}(\Phi, T)$ introduced in subsection 6.1.1 of chapter 6, whose degenerate minima at the critical temperature represent the metastable states of the

system. To tree-level it reads

$$\sigma = \int_0^{\Phi_c} \mathrm{d}\Phi \, \sqrt{2V_{\mathrm{eff}}(\Phi, T_c)} \tag{6.15}$$

with the location of the broken phase minimum $\Phi_c \equiv \Phi(T_c)$, say in Landau gauge, as the value of the uniform background scalar field $\Phi(T)$ at the critical temperature T_c. More details and analytical results of one- and two-loop resummed perturbation theory can be found in refs. [105, 107].

However, since σ receives contributions from both the broken phase and the symmetric phase with its stringent limitations due to the intrinsic infrared divergences, the perturbative predictions become more and more questionable for increasing Higgs masses and weaker transitions. Therefore, the genuinely bad infrared behaviour of the SU(2)–Higgs effective potential at finite temperature sets the task to work out non-perturbative methods in synthesis with numerical lattice simulations.

6.2.2 Histogram method

The histogram method [163, 164] requires to measure two-peak probability distributions of some order parameter O in finite-volume systems, e.g. for $s_{\log}$ of L_φ as in refs. [134, 135]. During a simulation at $\kappa = \kappa_c$ these two peaks are populated by configurations to be assigned to the pure phases, while the probability for configurations between the peaks, which as mixed states are dominated by contributions from both phases with any bulk phase ratio, are suppressed by a free energy amount associated with the interfaces separating them. Provided that the elongated lattices with $L_{\mathrm{z}} \gg L_{\mathrm{x}} = L_{\mathrm{y}} \gg L_t$ are chosen large enough to ensure the existence of such a thin and non-interacting interface pair with smallest cross-sectional areas $A_{\mathrm{I}} = a_s^2 a_t L_{\mathrm{x}} L_{\mathrm{y}} L_t$, the infinite-volume interface tension[4] is extracted from the ratio of relative thermodynamic weights of pure and mixed phases,

$$\sigma = \lim_{V \to \infty} \frac{1}{2A_{\mathrm{I}}} \ln \frac{p_{\max}}{p_{\min}} \,, \tag{6.16}$$

if κ_c is defined by the equal-height signal in the O–histogram, and $p_{\max}$ and $p_{\min}$ denote the values of this distribution at one of the peak maxima and at the flat, plateau-like minimum in between, respectively. In the case of a strong first order phase transitions at low Higgs masses the usage of multicanonical algorithms is absolutely necessary in order to enhance the tunneling rate from one phase to another and thus to ensure the correct statistical weights for the two phases.

Although the majority of results for the interface tension, especially within the three-dimensional approach of dimensional reduction, has been obtained with this technique [122, 144, 146, 147, 149] or one of its variants [121, 150, 152], it stays very CPU-time consuming

[4] For parametrizations of possible finite-size corrections to σ see [164, 135] and references therein.

in practice due to the large autocorrelations involved, because the metastable system always has do undergo full transitions between the two phases. Another drawback is related to the fact that lattice studies of the EWPT within the minimal standard model for larger and likewise more realistic values of m_H are known to possess a transition, which is very weak and asymmetric in the sense that the fluctuations of properly chosen order parameters are much stronger in the Higgs phase than in the symmetric phase. Therefore, the simplifying assumptions of O–histograms with clear maxima separated by a broad minimum and of a minimal interface distinguishing the pure phases from each other might be hardly valid in this parameter region, and alternative methods are advised.

6.2.3 Two-coupling method

Here I describe the determination of the interface tension σ by means of a suitable variant of the two-coupling method [162], which originally has been invented for Potts models and the finite-temperature QCD phase transition. In the framework of the SU(2)–Higgs model the two-coupling method is performed with the scalar hopping parameter κ, which essentially drives the physical temperature in the four-dimensional lattice model ('2–κ method'), because the latent heat of the system in eq. (6.1) is dominated by the contribution of the φ–link L_φ, which in view of the lattice action (5.28) is thermodynamically conjugated to the hopping parameter κ.

It is a quantitative elaboration of the same method proposed for the estimation of κ_c in subsection 6.1.4, whose fundamental idea is based on a careful extrapolation to the limits $\kappa_c \pm \varepsilon$, $\varepsilon > 0$ sufficiently small, of simulations in two coupled subvolumes supposed to be caught in the respective phases. As a straightforward generalization of the derivation in the isotropic lattice case sketched in refs. [135, 139], I directly turn to the situation with asymmetric lattice spacings $a_s \neq a_t$ in the following; the corresponding formulas for isotropic lattices are then automatically covered by setting $\xi = \gamma_\beta = \gamma_\kappa$ where necessary.

Principle of the method

Let $\Omega = L_{\rm x} L_{\rm y} L_{\rm z} L_t$ denote the number of lattice points and $V = a_s^3 a_t \Omega$ the physical lattice volume, wherein a_s and a_t are the space- and timelike lattice spacings. Now consider one elongated spacelike direction $L_{\rm z} \gg L_{\rm x} = L_{\rm y} \gg L_t$, and suppose as in eq. (6.8) of subsection 6.1.4 that the lattice volume is divided into two equal halves with different κ–values

$$\kappa = (\kappa_1, \kappa_2) \equiv (\kappa_1 < \kappa_c \text{ for z} \leq L_{\rm z}/2\,,\ \kappa_2 > \kappa_c \text{ for z} > L_{\rm z}/2)\,.$$

Hence the lower half is forced in the symmetric phase, the upper one in the Higgs phase, and due to the periodic boundary conditions the system, residing in a mixed-phase state[5],

[5] More precisely and already emphasized before, tunneling processes between the nearly degenerate minima of the effective potential cause Higgs and symmetric phases to be simultaneously present on large enough

gives rise to an interface pair at the phase boundaries $\mathrm{z} \simeq \frac{1}{2} L_\mathrm{z}$ and $\mathrm{z} \simeq L_\mathrm{z}$ perpendicular to the z–direction.

Generically, the interface tension is defined by its relation to the additional free energy ΔF associated with the interfaces via

$$A_\mathrm{I}\, \sigma = \Delta F \,, \tag{6.17}$$

with A_I denoting the area of such an interface. Recall that in the actual setting one has two interfaces of area

$$A_\mathrm{I} = a_s^2 a_t L_\mathrm{x} L_\mathrm{y} L_t \,. \tag{6.18}$$

The connection between the free energy $F \equiv S - \Omega d(s) \equiv \Omega f(s)$, $S = S[U, \varphi]$ the lattice action and $s \equiv S/\Omega$ its density, to the spectral density of states $d(s)$ as a function of s in

$$\mathrm{e}^{\,\Omega d(s)} \equiv \int \mathcal{D}[U, \varphi]\, \delta \left(s - \frac{S}{\Omega} \right) \tag{6.19}$$

implies that the probability distribution of s is $p(s) \propto \mathrm{e}^{\,-\Omega f(s)} = \mathrm{e}^{\,-F}$ [19, 135].

Under the assumption that the time direction of the lattice is orthogonal to the normal vector of the phase surfaces — which is justified for $L_t \ll L_\mathrm{x}, L_\mathrm{y}$ — a thermodynamic argument shows [3, 19] that the interface tensions of the $(3+1)$–dimensional SU(2)–Higgs model and a corresponding 4–dimensional spin model are identical. Consequently, the interface tension σ, as the free energy F per unit area of the walls separating the two phases, is written as

$$\sigma = \frac{1}{2A_\mathrm{I}} \left\{ F(\kappa_1, \kappa_2) - \tfrac{1}{2} F(\kappa_1, \kappa_1) - \tfrac{1}{2} F(\kappa_2, \kappa_2) \right\} , \tag{6.20}$$

and in lattice units

$$\begin{aligned} a_s^2 a_t \sigma &= \frac{1}{2 L_\mathrm{x} L_\mathrm{y} L_t} \left\{ F(\kappa_1, \kappa_2) - \tfrac{1}{2} F(\kappa_1, \kappa_1) - \tfrac{1}{2} F(\kappa_2, \kappa_2) \right\} \\ &= \frac{1}{4 L_\mathrm{x} L_\mathrm{y} L_t} \left\{ \Big[F(\kappa_1, \kappa_2) - F(\kappa_1, \kappa_1) \Big] - \Big[F(\kappa_2, \kappa_2) - F(\kappa_1, \kappa_2) \Big] \right\} . \end{aligned} \tag{6.21}$$

$F(\kappa_i, \kappa_j)$, $i, j = 1, 2$, are the free energies in the whole volume and in the halves, respectively. The non-commutative limits of $\sigma \equiv \sigma(\kappa_1, \kappa_2)$ from the finite-volume situation,

$$\sigma^{(\mathrm{phys})} = \lim_{\kappa_2 \searrow \kappa_c} \lim_{\kappa_1 \nearrow \kappa_c} \Big[\lim_{V \to \infty} \sigma(\kappa_1, \kappa_2) \Big] , \tag{6.22}$$

will ultimately give the physically interesting interface tension.

According to eq. (5.28) in subsection 5.1.1, the lattice action of the anisotropic SU(2)–Higgs model reads

$$S[U, \varphi] = \sum_{x \in \Lambda} S_x \,, \quad S_x = S_{0,x} - 8\kappa L_{\varphi,x} \,, \quad S_{0,x} \text{: independent of } \kappa \,. \tag{6.23}$$

---

lattices.

Here $L_{\varphi,x}$ is the weighted sum of the the space- and timelike components of the φ–link operator $L_{\varphi;x\mu} = \frac{1}{2}\mathrm{Tr}\left(\varphi^{+}_{x+\hat{\mu}} U_{x,\mu} \varphi_x\right)$, see eqs. (5.32) – (5.34),

$$L_{\varphi,x} = \frac{1}{4}\left(\frac{3}{\gamma_\kappa} L_{\varphi,s,x} + \gamma_\kappa L_{\varphi,t,x}\right) , \quad L_{\varphi,s,x} = \frac{1}{3}\sum_{\mu=1}^{3} L_{\varphi;x\mu} , \quad L_{\varphi,t,x} = L_{\varphi;x4} , \tag{6.24}$$

with $\gamma_\kappa \equiv \sqrt{\kappa_t/\kappa_s}$ the coupling anisotropy, $\kappa^2 = \kappa_s\kappa_t$, and κ_s and κ_t as the hopping parameters in space- and timelike directions of section 5.1. Thus, in the 2–κ situation under study, one can decompose this action into

$$S[U,\varphi] = S_0 - \kappa_1 S_1 - \kappa_2 S_2 \tag{6.25}$$

with $S_i = \frac{\Omega}{2}\, s_i$, and the action densities of both phases in terms of the corresponding φ–links $L^{(i)}_{\varphi,x}$ are

$$s_i = 8 L^{(i)}_{\varphi} , \quad L^{(i)}_{\varphi} \equiv \frac{2}{\Omega}\sum_{x\in\Lambda/2} L^{(i)}_{\varphi,x} , \quad i = 1,2\,. \tag{6.26}$$

Although the expectation values $L^{(i)}_{\varphi}(\kappa_1,\kappa_2)$, $i = 1,2$, of $L^{(i)}_{\varphi}$ are measured by averaging in both halves separately, they of course depend on both κ–values, because these are responsible for the position as well as for possible fluctuations and shifts of the interfaces during the simulation.

In order to relate these expectation values at given κ_1 and κ_2 to the free energies in eq. (6.21), one should observe that

$$\frac{\partial F(\kappa_1,\kappa_2)}{\partial \kappa_i} = -\langle S_i\rangle_{\kappa_1,\kappa_2} = -4\Omega\, L^{(i)}_{\varphi}(\kappa_1,\kappa_2) , \quad i = 1,2 \tag{6.27}$$

in the thermodynamic limit and with eq. (6.26). This yields

$$\begin{aligned} a_s^2 a_t \sigma &= \frac{1}{4 L_{\mathrm{x}} L_{\mathrm{y}} L_t}\left\{\int_{\kappa_1}^{\kappa_2} \mathrm{d}\kappa\, \langle S_1\rangle_{\kappa,\kappa_2} - \int_{\kappa_1}^{\kappa_2} \mathrm{d}\kappa\, \langle S_2\rangle_{\kappa_1,\kappa}\right\} \\ &= L_{\mathrm{z}}\left\{\int_{\kappa_1}^{\kappa_2} \mathrm{d}\kappa\, L^{(1)}_{\varphi}(\kappa,\kappa_2) - \int_{\kappa_1}^{\kappa_2} \mathrm{d}\kappa\, L^{(2)}_{\varphi}(\kappa_1,\kappa)\right\} . \end{aligned} \tag{6.28}$$

For κ–pairs with appropriately small deviations $\Delta\kappa \equiv |\kappa_i - \kappa_c|$ from the critical hopping parameter κ_c, the integrals can be well replaced by the sum of the two trapezium areas

$$a_s^2 a_t \sigma \simeq L_{\mathrm{z}}\,(\kappa_2 - \kappa_1)\left[\frac{L^{(1)}_{\varphi}(\kappa_1,\kappa_2) + L^{(1)}_{\varphi}(\kappa_2,\kappa_2)}{2} - \frac{L^{(2)}_{\varphi}(\kappa_1,\kappa_2) + L^{(2)}_{\varphi}(\kappa_1,\kappa_1)}{2}\right] . \tag{6.29}$$

This corresponds to a linear approximation of the $L^{(i)}_{\varphi}(\kappa_1,\kappa_2)$ as functions of κ in the interval $[\kappa_1,\kappa_2]$. If one further identifies the integrands at equal arguments with the φ–link expectation values in the pure phases, their contributions can be assumed to cancel, and

the systematic errors due to these two approximations nearly compensate [135]. Taking all together, one finally arrives at

$$a_s^2 a_t \sigma = \frac{1}{2} \lim_{\kappa_2 \searrow \kappa_c} \lim_{\kappa_1 \nearrow \kappa_c} \left\{ (\kappa_1 - \kappa_2) \lim_{L_z \to \infty} L_z \cdot \Delta L_\varphi(\kappa_1, \kappa_2) \right\} , \tag{6.30}$$

where $\Delta L_\varphi(\kappa_1, \kappa_2) = L_\varphi^{(2)}(\kappa_1, \kappa_2) - L_\varphi^{(1)}(\kappa_1, \kappa_2)$, and which substitutes eq. (6.22) in later applications.

Since for the physical interface tension of interest the limit $\Delta\kappa \to 0$ has to be performed, I propose the phenomenological $(N+2)$–parametric Laurent ansatz

$$L_\varphi^{(i)}(\kappa_1, \kappa_2) = -\frac{c_i}{\kappa_i - \kappa_c} + \sum_{j=0}^{N} \gamma_i^{(j)} (\kappa_i - \kappa_c)^j + \mathcal{O}\left(|\kappa_i - \kappa_c|^{N+1} \right) , \quad i = 1, 2 , \tag{6.31}$$

which leads to the finite-volume estimator for the interface tension

$$a_s^2 a_t \hat{\sigma} = L_z \, (c_1 + c_2) \, . \tag{6.32}$$

The origin of the leading inverse-linear term in (6.31) is motivated by the fact that for $\Delta\kappa \ll 1$ the free energy difference between the two phases behaves as $\Delta F \simeq \mathcal{O}(\Delta\kappa)$. Therefore, the interfaces can penetrate into neighbouring domains with constant κ, and if the change in κ is at $z = z_0$, one infers from eq. (6.19) that the probability p for an interface being at $z > z_0$ is essentially given by $\exp\{-\text{const} \cdot \Delta\kappa(z - z_0)\}$, so $\int dz \, p \simeq 1/\Delta\kappa$. As the numerical data show indeed, the z–slice distribution $L_\varphi(z)$ of the φ–link as function of z has an exponential shape in the critical κ–region.

With $a_t T_c = 1/L_t$ from eq. (5.40) in section 5.1.2 and the lattice spacing anisotropy parameter being $\xi = a_s/a_t$, one obtains its dimensionless ratio to the critical temperature via

$$\frac{\hat{\sigma}}{T_c^3} = \frac{a_t^2}{a_s^2} L_t^3 L_z \, (c_1 + c_2) = \frac{L_t^3 L_z \, (c_1 + c_2)}{\xi^2} \, . \tag{6.33}$$

If the chosen κ–intervals in the numerical simulations for this analysis are symmetric with respect to κ_c, an ansatz identical to (6.31) for ΔL_φ, but in terms of $\kappa_2 - \kappa_1$ and primed parameters, can be used as well. Then the right hand side of (6.33) will simply translate into

$$\frac{\hat{\sigma}}{T_c^3} = \frac{L_t^3 L_z \, c'}{2\xi^2} \, . \tag{6.34}$$

In summary — provided that the anisotropic lattice action is parametrized as in eqs. (5.28) or (6.23) — the only modifications in the determination of σ with the two-coupling method compared to the isotropic case in refs. [134, 135, 136, 139] are 1.) to measure and fit the weighted φ–link operators (6.24) of both z–halves and 2.) the factor $1/\xi^2$ in the previous equations for $\hat{\sigma}/T_c^3$.

Remarks on the realization in practice

- As described in section 6.1.4, the same method does also provide a powerful tool to determine the critical hopping parameter κ_c itself.

- Concerning the $L_{\rm z}$–limit in (6.30) one has to keep in mind that a change in $L_{\rm z}$ is irrelevant for the σ–determination, if the interfaces do not significantly influence or even touch each other within the simulation volume, which would express in deviations of $L_\varphi^{(i)}(\kappa_1, \kappa_2)$ from the corresponding expectation values of the pure, i.e undisturbed phases. So it is sensible to choose $L_{\rm z}$ minimally with respect to the condition that the interfaces do not interact with each other for the smallest κ–interval. Then the $L_{\rm z}$–factors in (6.32) and (6.27) should compensate, and $\hat{\sigma}/T_c^3$ becomes independent of $L_{\rm z}$. A safe monitoring of the phases in equilibrium and the two interfaces is provided once more by the z–slice profiles $L_\varphi({\rm z})$ of the operator $L_{\varphi,x}$, and in addition by the χ^2–values of fits to the ansätze in eq. (6.31).

- The extrapolation to $\Delta\kappa = 0$ by means of the $\kappa_{1,2}$–limits in formula (6.30) may be delicate, and the intervals in κ_1 and κ_2, which can not be taken arbitrarily small for given (spacelike) lattice extensions, must be chosen carefully: Too small differences in the free energy density of the two phases would favour tunneling transitions, and the interfaces disappear. However, since these differences grow proportional to $\mathcal{O}(L_{\rm x}L_{\rm x}\Delta\kappa)$, the larger the lattice volume the narrower and closer to κ_c can the individual κ–intervals be chosen [135, 139], readily of the order $\Delta\kappa \simeq \mathcal{O}(1/L_{\rm x}L_{\rm y})$ or well below. This will show up to be important for the analysis at $m_H \simeq 80$ GeV on anisotropic lattices in chapter 9, where the first order transition is extremely weak albeit detectable.

- The errors on the interface tension from this method quoted in the next chapters consist of

  - the uncertainty in κ_c by repeating the least-squares fits with $\kappa_c \to \kappa_c \pm \Delta\kappa_c$ in (6.31) to estimate the resulting mean deviation in $\hat{\sigma}/T_c^3$, and
  - statistical errors from the $L_\varphi^{(i)}(\kappa_1, \kappa_2)$–fits by adopting a bootstrap error analysis, see section B.1.2 of appendix B, because owing to shifts of the interfaces in the course of the simulation, the φ–links in both phases are correlated, which affects their expectation values and error as well; since this effect cancels in the φ–link differences to a great extent and the ΔL_φ–averages themselves are thus uncorrelated, a statistical error for the fit of this quantity based on normally distributed random data is adequate.

- In general, reasonable χ^2–values (divided by the number of degrees of freedom) serve as a stringent criterion for the quality of the fits to eq. (6.31). Moreover, for a reliable estimate of the interface tension one should take into account

- the sensitivity to the number of fitted data points within the set of available κ–pairs, which were simulated, and
- the significance of the inclusion of an additional, higher-order fit parameter, e.g. by inspecting its bootstrap error compared to its value.

Under these aspects is not imperative to insist on a certain number of necessary fit parameters for all choices of the simulation parameters. If contributions of the higher Laurent coefficients will turn out to have more influence on the slopes at larger κ–intervals, this number can definitely increase. As to be expected intuitively, this is indeed the case when going to enlarged physical volumes, where the phase transition — if present — gets relatively more marked, e.g. in a study of scaling behaviour in the continuum limit $L_t = 2 \to 3 \to \cdots$, or in investigations on anisotropic lattices with extensions comparable to isotropic ones.

6.2.4 Vacuum tunneling in finite volumes

In contrast to the histogram and two-coupling methods, which deduce the interface tension from changes of (sub)volume-averaged observables in mixed-phase systems with minimal interfaces, there is a third method to extract σ from a tunneling correlation length at the phase transition [165, 167]. Now the emphasis is on correlations due to different phases in coexistence in dependence on the geometry of the system, and σ will arise as a finite-size effect.

Namely, in infinite volumes the electroweak symmetry is spontaneously broken, and the ground states of the Hamiltonian are degenerate. However, this phenomenon does not reflect in lattice simulations, since in a finite volume the symmetry is never broken. In this case a small energy splitting E_0 appears between the ground state and the first excited state, which vanishes in the infinite-volume limit. The appearance of E_0 at finite volume is due to the tunneling effect between the symmetric and the Higgs phase. On lattices with geometries $L_{\rm z} \gg L_{\rm x} = L_{\rm y} \gg L_t$ different domains can then be observed in the z–direction, with domain walls between them. The associated interface energy determines the tunneling mass or inverse tunneling correlation length E_0 via the approximate finite-size scaling law

$$a_s E_0 = C \cdot \exp\Big(- A_{\rm I}\, \sigma \Big) , \quad A_{\rm I} = a_s^2 a_t L_{\rm x} L_{\rm y} L_t \tag{6.35}$$

and may be identified with the lowest excitation in the spectrum of the transfer matrix [19, 166, 167]. In general, the prefactor C of eq. (6.35) can depend on $L_{\rm xy} \equiv L_{\rm x} = L_{\rm y}$; but in the present case the leading contribution is $L_{\rm xy}$–independent.

The tunneling or transfer matrix method has been used to determine, for instance, the interface tension of the four-dimensional Ising model in the broken phase [166], to calculate the interface tension in three-dimensional ϕ^4–theory by semiclassical as well as numerical

methods [167], and to determine the interface tension of the finite-temperature confinement-deconfinement phase transition of the pure SU(3)–gauge theory [168]. Within the MC studies of the finite-temperature SU(2)–Higgs model it has been applied to the full four-dimensional theory in refs. [179, 136], and recently within the framework of dimensional reduction to three dimensions in [151], also discussing possible corrections to the pre-exponential factor in (6.35).

To briefly summarize the realization of this technique on principle, one has to simulate the system at given L_t in the previously determined transition points $\kappa = \kappa_c$ on lattices with growing spatial transverse extensions $L_{\rm xy}$, spanning the interface through the lattice. Simultaneously, correlation functions in the orthogonal z–direction are measured in the Higgs channel, whose exponential descents allow to extract the splitting energy $a_s E_0$ for each $L_{\rm xy}$ by least-squares fits in the usual manner. Then the interface tension σ can directly be read off as the slope of the fitted line, which parametrizes $-\ln(a_s E_0)/L_t$ as a function of the transverse area $L_{\rm xy}^2$ in eq. (6.35).

For higher values of the Higgs mass m_H near 80 GeV — and this stays true even on anisotropic lattices — the tunneling method is mostly inhibited by the enormous amount of computer time, which would incur, if the necessary simulations on several large lattices with increasing size were performed. Another point of criticism in this context might be that the implicitly underlying assumption of a much larger tunneling correlation length compared to the typical correlation lengths of the pure phases in equilibrium always sets a lower limit on reliable transverse sizes $L_{\rm xy}$, which will rise with m_H.

Chapter 7

Simulations on isotropic lattices

This chapter comprises my results from numerical simulations of the SU(2)–Higgs model on isotropic lattices at low and intermediate values of the Higgs boson mass. These were obtained by applying some of the method presented comprehensively in the foregoing chapter.

The main topics are the critical hopping parameters and interface tensions at MC parameters, which were chosen to correspond to Higgs masses about 16 GeV and 35 GeV, respectively. In particular, the former analysis addresses the important question, whether and to what extent the interface tension can be affected by scaling violations in comparison with previous studies for $L_t = 2$ lattices.

Finally, the continuum limit extrapolation of T_c/m_H at $m_H \simeq 35$ GeV is designated to hint at possible discrepancies between results from the four-dimensional lattice approach used here and from resummed perturbation theory or simulations of the effective theory in three dimensions.

7.1 Critical κ and interface tension for $m_H \simeq 16$ GeV

To begin with, I determine the interface tension of the finite-temperature electroweak phase transition in a numerical investigation of the SU(2)–Higgs model on a four-dimensional lattice with temporal extension $L_t = 3$. In the following I use a low value of the Higgs boson mass, where the phase transition is quite strong. For the determination of σ the two-coupling method (subsection 6.2.3) in the scalar hopping parameter is employed. Compared to transfer-matrix techniques (subsection 6.2.4) and histogram methods (subsection 6.2.2), it gives an optimal ratio between desired accuracy and required CPU-time for the SU(2)–Higgs model [134, 135, 136, 139].

A suitable observable for the interface tension is the density of the φ–link operator $L_{\varphi;x\mu}$, which is conjugate — in the thermodynamic sense — to the hopping parameter κ and is itself an order parameter of the phase transition. From eqs. (5.32) – (5.34) it reads in the

isotropic case:

$$L_\varphi = \frac{1}{4\Omega} \sum_{x \in \Lambda} \sum_{\mu=1}^{4} L_{\varphi;x\mu} \,, \quad L_{\varphi;x\mu} = \frac{1}{2} \mathrm{Tr} \left(\varphi^+_{x+\hat{\mu}} U_{x,\mu} \varphi_x \right) \,. \tag{7.1}$$

In the spirit of thermal field theory as briefly reviewed in section 5.1.2 of chapter 5, I extend the measurement of σ at $a^{-1} = 2T_c$ in ref. [135] to $a^{-1} = 3T_c$ with the purpose of gaining control over possible lattice artifacts. The parameters in the former analysis were $\beta = 8.0$ and $\lambda = 0.0001$, leading to a renormalized gauge coupling of $g_R^2 \simeq 0.56$ and a Higgs mass of $m_H \simeq 16$ GeV. The physical mass scale is set by the vector boson mass value $m_W = 80$ GeV at $T = 0$ in lattice units. A two-coupling simulation on a lattice of size $2 \times 16^2 \times 128$ resulted in a phase transition point at $\kappa_c = 0.12830(5)$ and a finite-volume estimator for the interface tension of $\hat{\sigma}/T_c^3 = 0.84(16)$.

When passing over to smaller lattice spacings, I have to scale all lattice extensions accordingly in order to keep the physical volume constant. In the case of low Higgs mass this is possible with an acceptable demand of computer resources. With increasing m_H the situation becomes worse, because the phase transition weakens and thus one needs larger physical volumes to obtain a stable two-phase situation. Therefore, I choose a lattice of size $3 \times 24^2 \times 192$ with the changed parameters $\beta = 8.15$ and $\lambda = 0.00011$. They have been obtained by an integration of the one-loop perturbative renormalization group equations with the transition point of the $L_t = 2$ lattice as a starting value [135], see also section 5.2 of chapter 5. But as shown in refs. [134, 135, 137] and motivated in this work before, a sufficiently precise estimate for the critical point in κ_c is only available by numerical methods.

7.1.1 Numerical results

The calculation of the phase transition point and the interface tension is done by a modified version of the two-coupling method [162]. Since this method, which has been used in the SU(2)–Higgs model in refs. [121, 134, 135, 136, 139], is already described and critically discussed in the chapter before, I have not to repeat it here in detail.

By taking a periodic lattice with one elongated spacelike direction, i.e. $L_\mathrm{z} \gg L_\mathrm{x} = L_\mathrm{y} \gg L_t$, the corresponding lattice volume is divided into two halves with different hopping parameters $\kappa_1 < \kappa_2$, forced in symmetric and Higgs phase, respectively. If the transverse directions L_x and L_y are sufficiently large, the system resides in a mixed-phase state, and an interface pair at the phase boundary perpendicular to the z–direction is induced. In a first step one initializes a two-phase situation by a simulation with κ–values far enough from the transition point, whose location was roughly determined by hysteresis runs. Subsequently, the distance in κ is shrunk, and the smallest κ–interval until a unique turn over into one single phase defines the lower and upper bounds for the critical κ. On the $3 \times 24^2 \times 192$

lattice I obtained in this way the estimate

$$\kappa_c = 0.128110(3)\,, \tag{7.2}$$

whose accuracy required the 64–bit floating point precision of the hardware architecture utilized.

For the interface tension σ one proceeds in a similar way as for the κ_c–determination, but due to practical limitations on L_z, one has to prevent the interfaces from touching each other by a choice of somewhat larger κ–intervals. This avoids tunneling events to take place, which would destroy the coexistence of the two bulk phases during the simulation. Figure 7.1 displays typical two-phase structures from the 2–κ method. Note that the plateaus become narrower for smaller κ–intervals, especially in the broken phase, but the phases are still clearly developed, and the interfaces continue to exist.

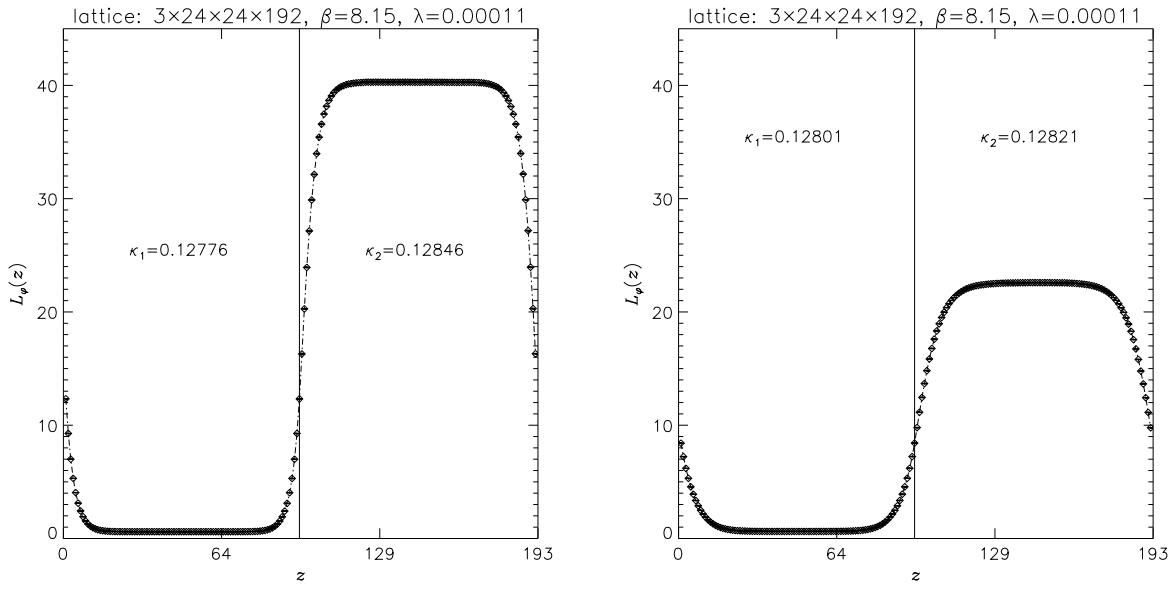

Figure 7.1: *Two-phase profiles of the z–slice expectation value $L_\varphi(z)$ of L_φ for my largest and smallest κ–intervals.*

The results of my simulations are presented in table 7.1. Owing to correlations between $L_\varphi^{(1)}$ and $L_\varphi^{(2)}$, the statistical errors on ΔL_φ are usually smaller than those of $L_\varphi^{(2)}$. This was already suggested by the autocorrelations in figure 5.2 from section 5.3 in chapter 5 and is caused by shifts of the interfaces during the simulation, which cancel out in ΔL_φ to some extent.

In order to give a reliable estimate for the statistical error when fitting these φ–link averages to the functions in eq. (7.3) below, I take their correlations into account by a bootstrap analysis [183]. The characteristic ingredient is to calculate secondary quantities from bootstrap subsamples randomly taken with repetition from the original measurements,

κ_1	κ_2	sweeps	$L_\varphi^{(1)}$	$L_\varphi^{(2)}$	ΔL_φ
0.12776	0.12846	5000	1.5161(24)	37.8216(70)	36.3055(67)
0.12781	0.12841	5000	1.5149(26)	34.7287(68)	33.2138(60)
0.12786	0.12836	5000	1.5285(29)	31.5085(77)	29.9799(76)
0.12791	0.12831	10000	1.5398(19)	28.1144(55)	26.5746(57)
0.12796	0.12826	10000	1.5616(30)	24.5264(76)	22.9648(71)
0.12801	0.12821	20000	1.6019(32)	20.5877(66)	18.9858(59)

Table 7.1: *Results for $L_\varphi^{(1)}$, $L_\varphi^{(2)}$, and ΔL_φ on a $3 \times 24^2 \times 192$ lattice. The errors are obtained by binning.*

which itself can be interpreted as the empirical probability distribution of the observables under consideration. The errors of the fit parameters are extracted as half of the central 68.3%–interval of their distributions from fits performed on these sample averages. A more extensive description of the method in this context and some further references are contained subsection B.1.2 of appendix B.

The interface tension is now computed along the recipe of formulas (6.30) – (6.33), i.e.

$$\begin{aligned} a^3\sigma &= \frac{1}{2} \lim_{\kappa_2 \searrow \kappa_c} \lim_{\kappa_1 \nearrow \kappa_c} \left\{ (\kappa_1 - \kappa_2) \lim_{L_z \to \infty} L_z \cdot \Delta L_\varphi(\kappa_1, \kappa_2) \right\} \\ L_\varphi^{(i)}(\kappa_1, \kappa_2) &= -\frac{c_i}{\kappa_i - \kappa_c} + \gamma_i^{(0)} + \gamma_i^{(1)}(\kappa_i - \kappa_c) + \gamma_i^{(2)}(\kappa_i - \kappa_c)^2 + \mathcal{O}\left((\Delta\kappa)^3\right), \quad i = 1, 2 \\ a^3\hat{\sigma} &= L_z(c_1 + c_2), \quad \frac{1}{T_c} = aL_t \end{aligned} \tag{7.3}$$

with $\Delta L_\varphi(\kappa_1, \kappa_2) = L_\varphi^{(2)}(\kappa_1, \kappa_2) - L_\varphi^{(1)}(\kappa_1, \kappa_2)$ and $\Delta\kappa = |\kappa_i - \kappa_c|$. I quote my final result for two four-parameter fits with χ^2–values of 2.58 and 0.82, which are depicted in figure 7.2. Using (7.3), I find

$$\left(\frac{\hat{\sigma}}{T_c^3}\right)_{L_\varphi} = 0.764(52 + 47), \tag{7.4}$$

while $aT_c = 1/L_t = 1/3$ in lattice units. The error consists of two parts, coming from a bootstrap analysis with 10000 iterations and the uncertainty of κ_c in eq. (7.2).

At this place some explanations about the number of necessary fit parameters are in order. In the examinations of $L_t = 2$ lattices [135, 136], see also the next section, a three-parameter fit was sufficient to give a reliable value for the interface tension; an inclusion of higher order terms gave no improvement. The situation for $L_t = 3$ seems to be different for the following reason: Basically, one has to keep in mind that the expansion of $L_\varphi^{(i)}(\kappa_1, \kappa_2)$ in eq. (7.3) is only a phenomenological ansatz and no prescribed form, which has to be obeyed as e.g. in the case of exponentially shaped correlation function. Furthermore, the lattice volume Ω has increased, and the phase transition, which in a strict sense is only present in

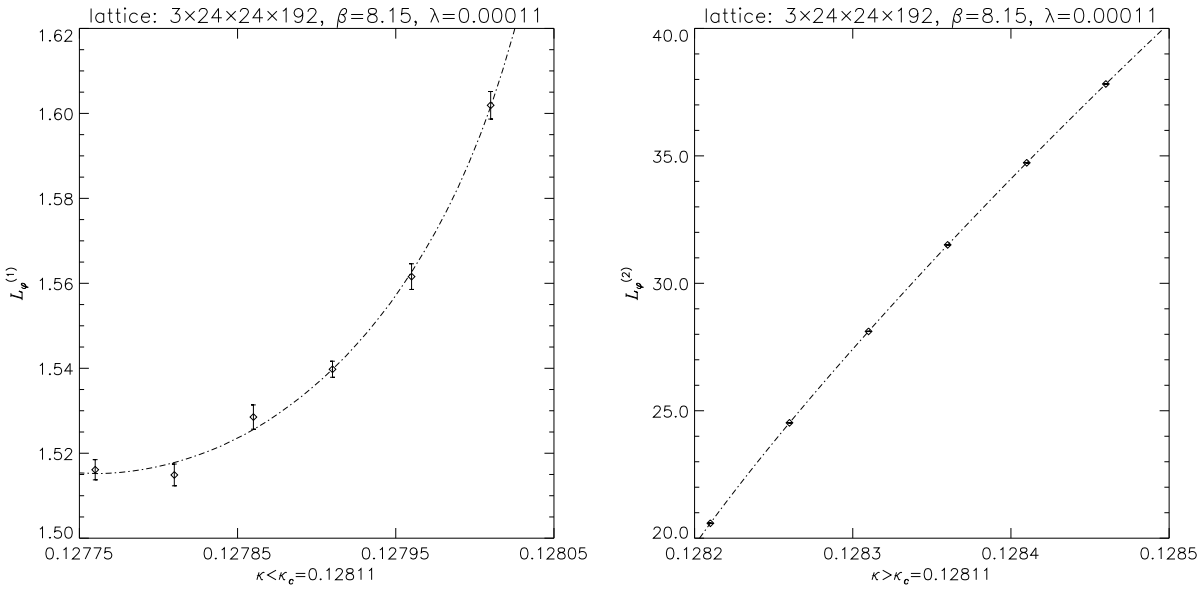

Figure 7.2: *Four-parameter least-squares fits of* $L_\varphi^{(i)}$, $i = 1, 2$, *separately in each phase.*

infinite volumes, is more pronounced. Consequently, the contribution of the higher Laurent coefficients becomes more important for the slopes at larger κ–intervals.

In fact, the three-parameter fit has no satisfactory χ^2, above all in the broken phase, and varies beyond its error, if one or more data points are left out. A five-parameter fit gives $\hat{\sigma}/T_c^3 = 0.85(20 + 5)$ and χ^2–values equal to 1.42 and 0.82. This is compatible to (7.4) within errors, but fairly sensitive to the number of fitted data points. A more careful inspection of the bootstrap calculations reveals that the last fit parameter is not very significant in such cases, where its bootstrap error is roughly as large as its value; this holds true for the five-parameter fits and also the four-parameter fit in the symmetric phase. So for the sake of completeness, I combined the three-parameter fit in the symmetric phase with the four-parameter fit in the broken phase (i.e. the corresponding c_i–values) to $\hat{\sigma}/T_c^3 = 0.793$, although I am nevertheless convinced of the four-parameter fit in both phases to lead to the most reasonable result.

The preceding remarks on the φ–link correlations should have made clear that ΔL_φ is the most natural variable for estimating the interface tension via eq. (7.3). As emphasized in subsection 6.2.3, this requires that the chosen κ–intervals are exactly symmetric with respect to κ_c and, after arranging all factors appropriately, $\hat{\sigma}/T_c^3$ can immediately identified with the residuum of the fitted φ–link difference $\Delta L_\varphi(\kappa_1, \kappa_2)$ surviving in the extrapolation $\kappa_2 - \kappa_1 = 2\Delta\kappa \to 0$. A four-parameter fit to an ansatz similar to that in (7.3) for ΔL_φ was evaluated to yield

$$\left(\frac{\hat{\sigma}}{T_c^3}\right)_{\Delta L_\varphi} = 0.767(53) \tag{7.5}$$

with $\chi^2 = 0.39$, and it is illustrated in figure 7.3. Here I only quote the statistical error, which now comes from 1000 normally distributed random data, since the different ΔL_φ–averages are uncorrelated. Note the perfect agreement of this result, and especially of its error, with the numbers in eq. (7.4) above.

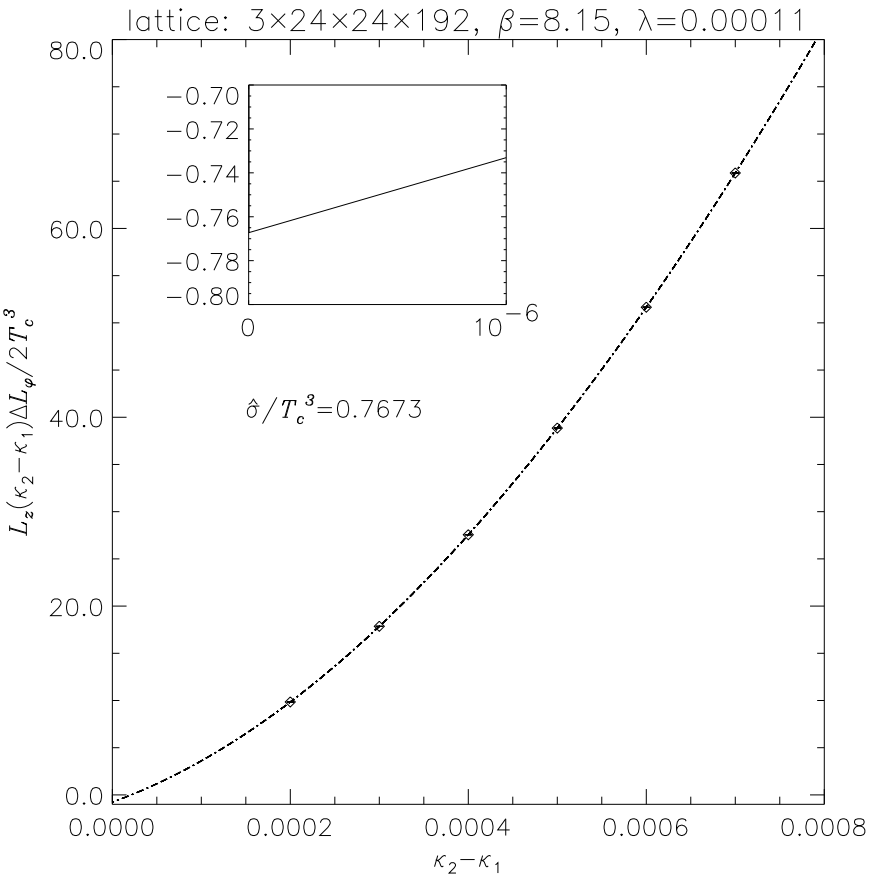

Figure 7.3: *Four-parameter least-squares fit of ΔL_φ as a function of $\kappa_2 - \kappa_1$. An extrapolation to $\kappa_2 - \kappa_1 = 0$ gives the interface tension.*

7.1.2 Conclusion

I have determined the interface tension of the four-dimensional SU(2)–Higgs model with the two-coupling method. All estimates from acceptable fits with a reasonable number of parameters show a very good consistency.

To my knowledge this is the first attempt to supply information about the scaling of σ when going over to a finer lattice. Compared to the $L_t = 2$ results

$$\left(\frac{\hat{\sigma}}{T_c^3}\right)_{2-\kappa} = 0.84(16)\,, \quad \left(\frac{\sigma}{T_c^3}\right)_{\text{hist}} = 0.83(4) \tag{7.6}$$

from refs. [134, 135] — the second number referring to the histogram method — the accuracy of the 2–κ estimate has been improved to the value $\hat{\sigma}/T_c^3 = 0.76(10)$ in eq. (7.4). The observed small deviation between $L_t = 2$ and $L_t = 3$ confirms the smallness of scaling violations, as e.g. also found recently for the critical temperature in [137, 140].

Finally, I confront the result with the perturbative estimate [105, 107] up to order $\mathcal{O}(g^4, \lambda_0^2)$,

$$\left(\frac{\sigma}{T_c^3}\right)_{\text{pert}} = 0.78(1)\,, \tag{7.7}$$

with an error coming from the uncertainties in the renormalized parameters on the lattice. As expected, the agreement with perturbation theory on a quantitative level in this range of the Higgs boson mass is excellent.

7.2 Critical κ and interface tension for $m_H \simeq 35$ GeV

The goal of the present section is to compute the interface tension of the finite-temperature electroweak phase transition at some larger value of the Higgs boson mass. Whereas the determination of σ proceeds completely analogous to the $m_H \simeq 16$ GeV case and can be copied without any further comments, the critical hopping parameter is obtained by use of the constrained simulation method as proposed in subsection 6.1.5 of the foregoing chapter and ref. [136]. An even more detailed presentation of the latter will be given in the last section.

In my finite-temperature simulations I have used elongated lattices with $\Lambda = L_t \times L_{\rm x} \times L_{\rm y} \times L_z$, where $L_t = 2$ and $L_{\rm x} = L_{\rm y} \ll L_z$. Keeping the bare parameters $\beta = 8.0$, $\lambda = 0.0003$ and $L_t = 2$ fixed, the hopping parameter κ was tuned to its critical value. After measuring and fitting the required $T = 0$ correlation function in the Higgs and vector channel, these parameters were found to correspond to a Higgs boson mass of roughly 35 GeV at zero temperature.

7.2.1 Numerical results

In this version of the constrained-simulation method $s_{\log}$ in eq. (6.7), i.e. the density of the subtracted action $S_{\log} = S[U,\varphi] - 3\sum_{x\in\Lambda} \ln \rho_x$, was taken as the order parameter. The lattice size under study was $2 \times 24^2 \times 256$. In a series of two short runs without any bounds on $s_{\log}$ the position of the two peaks, belonging to the pure phases, was estimated. As a consequence, the interval $s_{\log} \in [\,4.90\,,\,4.95\,]$ has been chosen to determine the critical point in κ_c. The MC simulation was carried out at $\kappa = 0.12865$, which is the κ_c–estimate from the two-coupling method applied earlier, and a statistic of 18000 measuring sweeps was collected. Every proposal of the updating algorithms leading to expectation values of $s_{\log}$ outside the selected order parameter interval is rejected. The integrated autocorrelation times turned

out to be $\tau_{\rm int} = 21(2)$ sweeps for $s_{\rm log}$ and L_φ. This value is much smaller than a typical autocorrelation time for a multicanonical simulation, and the reason is the following. In the case of a multicanonical simulation the system must completely go from one phase to the other in order to obtain an independent configuration. In the constrained-simulation method only the ratio of the bulk phases changes slightly, which is, however, sufficient to tell whether the free energy densities of the two phases are the same or not.

The transition point is defined by the implicit relation for κ_c,

$$\langle s_{\rm log} \rangle \Big|_{\kappa=\kappa_c} = \frac{1}{2} \left(s_{\rm log,-} + s_{\rm log,+} \right) \equiv s_{\rm log,mid} \,, \tag{7.8}$$

with $s_{\rm log,-} = 4.90$ and $s_{\rm log,+} = 4.95$ denoting the bounds on $s_{\rm log}$. This definition is equivalent to the condition that at $\kappa = \kappa_c$ the distribution of the measured history of $s_{\rm log}$–values is flat in the given interval. It can be ensured by using the reweighting technique [188] in κ in order to get results on $\langle s_{\rm log} \rangle |_{\kappa=\kappa_c}$ in the vicinity of the point $\kappa = 0.12865$.

For the determination of the statistical error on $\langle s_{\rm log} \rangle |_{\kappa=\kappa_c}$ the results of a bootstrap procedure with 3000 iterations and 30 independent subsamples were adopted, see the next subsection. The final result of this analysis is

$$\kappa_c = 0.1286565(7) \,, \tag{7.9}$$

while the error $\Delta\kappa_c$ in parentheses represents the total spread in κ, which complies with $\langle s_{\rm log} \rangle |_{\kappa=\kappa_c \pm \Delta\kappa} \in [\, s_{\rm log,mid} - \Delta_{s_{\rm log}} \,,\, s_{\rm log,mid} + \Delta_{s_{\rm log}} \,]$, if $\Delta_{s_{\rm log}}$ denotes the statistical errors of the reweighted expectation values $\langle s_{\rm log} \rangle_\kappa$. Within the error bars it agrees with the result $\kappa_c = 0.128658(1)$ from the $2 \times 16^2 \times 256$ lattice by using the equal-height criterion for the peaks in the $s_{\rm log}$–histogram. Thus the finite-size effects of κ_c beyond $L_{\rm x} = L_{\rm y} = 24$ are expected to be small. The above calculation gives the same κ_c for the upper half and for the lower half of the $s_{\rm log}$–interval. This fact can be considered as an additional check that the system was in the flat regime, and via monitoring the z–slice profiles of L_φ the configurations could be frequently tested to contain two bulk phases and two interfaces in between. As a further non-trivial cross-check of the method I should mention that for $\lambda = 0.0001$ ($m_H \simeq 18$ GeV) some results of [134, 135] obtained by the multicanonical method have been reproduced with this new procedure.

Since the basic ideas of the σ–determination with the two-coupling method [162, 135, 136, 139] should be well known in the meantime, I only recall here that a halved lattice with z–extension $L_{\rm z}$ much larger than the others is chosen to have $\kappa_1 < \kappa_c$ in the part with lower z–coordinates and $\kappa_2 > \kappa_c$ in the complementary one. By a suitable initialization of the configurations, a mixed state with two interfaces is obtained. Let $L_\varphi^{(i)}(\kappa_1, \kappa_2)$, $i = 1, 2$, denote the expectation value of L_φ from eq. (7.1) in the part with hopping parameter κ_i, $\Delta L_\varphi(\kappa_1, \kappa_2) = L_\varphi^{(2)}(\kappa_1, \kappa_2) - L_\varphi^{(1)}(\kappa_1, \kappa_2)$ their difference, and $\Delta\kappa = |\kappa_i - \kappa_c|$. Then the

interface tension may be extracted from the expressions (6.30) – (6.33) of subsection 6.2.3,

$$\begin{aligned} a^3\sigma &= \frac{1}{2}\lim_{\kappa_2\searrow\kappa_c}\lim_{\kappa_1\nearrow\kappa_c}\left\{(\kappa_1-\kappa_2)\lim_{L_z\to\infty} L_z\cdot\Delta L_\varphi(\kappa_1,\kappa_2)\right\} \\ L_\varphi^{(i)}(\kappa_1,\kappa_2) &= -\frac{c_i}{\kappa_i-\kappa_c}+\gamma_i^{(0)}+\gamma_i^{(1)}(\kappa_i-\kappa_c)+\mathcal{O}\left((\Delta\kappa)^2\right)\,, \quad i=1,2 \\ a^3\hat{\sigma} &= L_z\,(c_1+c_2)\,, \quad \frac{1}{T_c}=aL_t\,, \end{aligned} \tag{7.10}$$

which illustrate that σ depends only on the φ–link difference $\Delta L_\varphi(\kappa_1,\kappa_2)$.

In table 7.2 the results for $L_\varphi^{(1)}$, $L_\varphi^{(2)}$, and ΔL_φ from simulations on a $2\times 24^2\times 200$ lattice are listed. The statistical errors quoted in the table are obtained by binning. Unfortunately,

κ_1	κ_2	sweeps	$L_\varphi^{(1)}$	$L_\varphi^{(2)}$	ΔL_φ
0.12845	0.12885	10000	1.0607(30)	7.9042(91)	6.8435(83)
0.12849	0.12881	10000	1.0614(32)	7.007(10)	5.9461(92)
0.12853	0.12877	10000	1.0587(41)	6.058(12)	4.999(10)
0.12855	0.12875	12000	1.0684(38)	5.581(12)	4.513(11)
0.12857	0.12873	14000	1.0678(42)	5.035(12)	3.967(11)

Table 7.2: *Results for $L_\varphi^{(1)}$, $L_\varphi^{(2)}$, and ΔL_φ on a $2\times 24^2\times 200$ lattice. The errors are obtained by binning.*

the actually chosen κ–intervals do not lie symmetrically around the best κ_c–value (7.9) from the constrained simulation so that the fits of $L_\varphi^{(i)}$ had to performed independently for $i=1,2$. I estimated the integrated autocorrelation time from the quotient of true and naive statistical errors as implied by formula (A.32) in appendix A.3. For $L_\varphi^{(1)}$ and $L_\varphi^{(2)}$ the autocorrelation time is always found to be smaller than 50 sweeps, however, it still refers to the situation with the ρ–overrelaxation in the updating scheme. As exemplarily stressed in section 5.3 of chapter 5 for the $m_H\simeq 16$ GeV case at $L_t=3$ realized in the previous investigation, these numbers reduce considerably, if the cartesian φ–overrelaxation is used for the MC updates instead.

Again, the statistical errors of ΔL_φ are always smaller than those of $L_\varphi^{(2)}$. This is due to a kind of shift of the interfaces during the simulation; for instance, in the case of an interface moving from the region with κ_2 into the one with κ_1, both expectation values $L_\varphi^{(i)}$ will increase, but the difference between them is not that much affected. Hence there is a strong correlation between the two $L_\varphi^{(i)}$–values obtained on the same configuration. This has to be taken into account when estimating statistical errors for the interface tension, and is achieved by a bootstrap analysis [183]. The bootstrap method — already used before — is shortly discussed in subsection 7.1.1 and more exhaustively in subsection B.1.2 of appendix B. Supposed that the reader is already familiar with the general procedure, I

would only like to mention that in order to eliminate the influence of autocorrelations I have combined 200 measurements to bins for each κ–pair. (E.g. for the first three rows of table 7.2 the bin averages provide $N = 50$ independent values for the quantities $L_\varphi^{(1)}$ and $L_\varphi^{(2)}$; the last rows have $N = 60$ and $N = 70$.) My data are not obtained in a single MC run, but in five different runs for different κ–pairs, so for each κ–pair I generated a bootstrap sample, and in the so-obtained data samples I averaged to $L_\varphi^{(i)}$, $i = 1, 2$, as functions of κ. Using the form of the Laurent ansatz in eq. (7.10), I performed for these functions two independent χ^2–fits within each bootstrap sample. This procedure has been repeated 10000 times, and the statistical error has been determined from the distribution, i.e. from its median containing 68.3 % of the $\hat{\sigma}$–values calculated from the fit parameters.

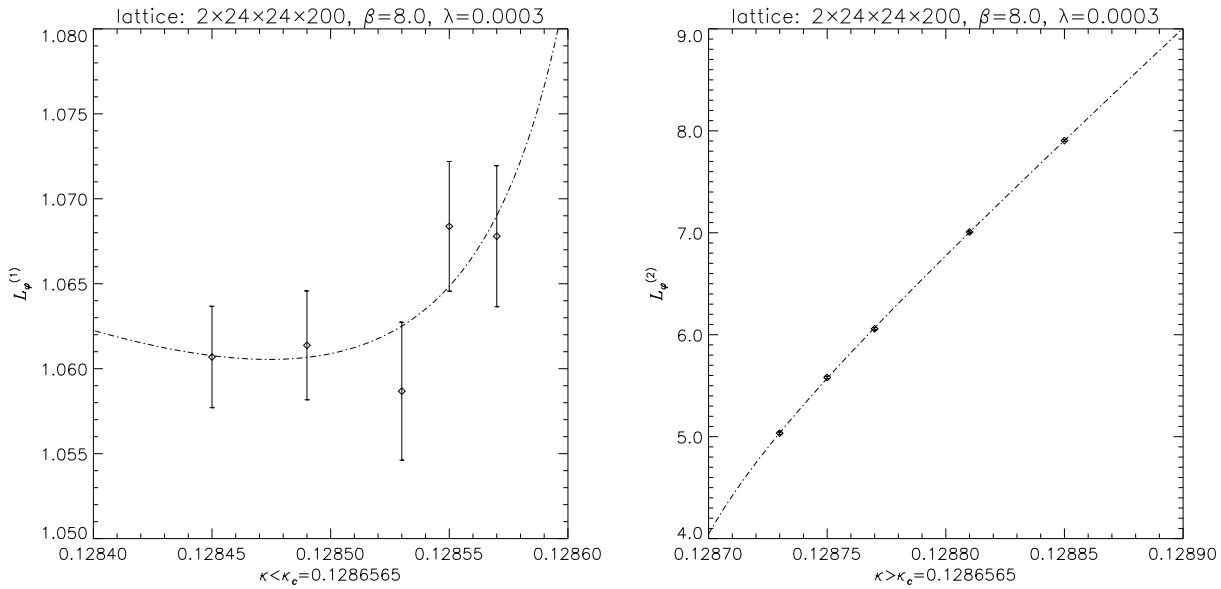

Figure 7.4: *Three-parameter least-squares fits for the determination of $\hat{\sigma}$ from the two-coupling method. The χ^2–values are $\chi_1^2 = 1.88$ and $\chi_2^2 = 1.50$, respectively.*

Figure 7.4 contains the combined data points with the corresponding fits. With $aT_c = 1/L_t = 1/2$ in lattice units this yields

$$\left(\frac{\hat{\sigma}}{T_c^3}\right)_{L_\varphi} = 0.065(9+1)\,. \tag{7.11}$$

The first number in the parenthesis is the statistical error, the second one stands for the uncertainty in the critical hopping parameter. For the individual fits I have $c_1 = 0.00000277(290+5)$ and $c_2 = 0.0000378(61+7)$ with $\chi_1^2 = 1.88$ and $\chi_2^2 = 1.50$, respectively. The error on $c_2 \cdot L_z/T_c^3$ is even larger than that of $\hat{\sigma}/T_c^3$, which is an indication that the correlations have been taken into account correctly. This does also reflect in table 7.2, where this error ratio approximately equals the ratio of statistical errors between $L_\varphi^{(2)}$ and ΔL_φ. In order to check the error estimate based on the bootstrap procedure, a jackknife

error analysis with 80 independent jackknife samples has been performed [1]. The results of the two different methods were in complete agreement.

An additional check, whether the measured curvature of $L_\varphi^{(i)}(\kappa_1, \kappa_2)$ as a function of κ_i, $i = 1, 2$, is really described by eq. (7.10), is supplied by trying also a three-parametric quadratic fit ansatz without any inverse-linear term. The corresponding result has $\chi_1^2 = 1.85$ and $\chi_2^2 = 4.15$, and the value of χ_2^2 shows that the data can not be well described by such a quadratic fit. Due to the large error bars in the symmetric phase (see figure 7.4), the squared deviation between fit and data χ_1^2 is not very sensitive to the proposed fit function. A four-parameter fit with a quadratic term supplementing the Laurent ansatz in (7.10) results in $\chi_1^2 = 1.85$ and $\chi_2^2 = 1.49$. Since the χ^2–values are nearly unchanged compared to (7.11), the fourth parameter does not seem to represent a new degree of freedom, and the estimate for $\hat{\sigma}/T_c^3 = 0.063$ does not deviate significantly from the former.

It is also possible to determine $\hat{\sigma}$ by using the ΔL_φ–values of table 7.2 together with the rough estimate $\kappa_c = 0.12865(1)$ for the transition point, around which the available κ–intervals are centred. It has has been obtained through the two-coupling method in advance. In this case one gets $(\hat{\sigma}/T_c^3)_{\Delta L_\varphi} = 0.075(11)$ with $\chi^2 = 0.77$; the error comes from 1000 normally distributed random data and the uncertainty in κ_c has not been considered. With individual fits for both $L_\varphi^{(i)}$ as described previously, the result is $(\hat{\sigma}/T_c^3)_{L_\varphi} = 0.075(11)$ for $\kappa_c = 0.12865(1)$ with $\chi_1^2 = 1.89$ and $\chi_2^2 = 1.54$. From this agreement I conclude that the correlations between the expectation values $L_\varphi^{(i)}$ are treated similarly in both methods. However, the difference between this result and that of eq. (7.11) emphasizes the importance of a precise κ_c–determination.

7.2.2 Conclusion

The interface tension of the SU(2)–Higgs model has been determined anew by means of the two-coupling method. Within the error bars the result $\hat{\sigma}/T_c^3 = 0.065(10)$ in eq. (7.11) agrees well with the $L_t = 2$ estimate from the tunneling method sketched in section 6.2.4,

$$\left(\frac{\sigma}{T_c^3}\right)_{\text{tunnel}} = 0.053(5)\,, \tag{7.12}$$

where the error contains the statistical error and an estimate of the systematics, the latter being obtained from the difference between the results of the two different operators $L_{\varphi,x}$ and $R_x = \rho_x^2$ used in the Higgs channel correlators [136]. In this calculation the elongated extension was $L_z = 128$, and the size of the transverse lattice directions ranged from $L_{xy} = 4$ to $L_{xy} = 16$. The impressive conformity of the two results from these conceptually distinct methods strengthens the confidence in the correctness of the determination of σ.

[1] For the readers convenience, this technique, which has also often been used elsewhere in this work, is shortly summarized in subsection B.1.1 of appendix B.

The prediction of the perturbative approach [105] is

$$\left(\frac{\sigma}{T_c^3}\right)_{\rm pert} = 0.060(6)\,, \tag{7.13}$$

and the error displayed here comes from the uncertainties in the lattice determination of the renormalized masses and coupling [107]. Despite the huge corrections found for the interface tension in two-loop resummed perturbation theory, the agreement with this analytical tool is remarkable too.

Finally, I want to add that in this intermediate range of the Higgs boson mass there exist also estimates for σ from the histogram method within the dimensionally reduced SU(2)–Higgs model in three dimensions [147]. For confronting these with the present ones, a mapping of the different (perturbative versus non-perturbative) renormalization schemes is necessary before, in order to afford a physical situation comparable to that fixed by the parameters of the four-dimensional theory. After a suitable interpolation of the results in ref. [147] to the pole mass $m_H = 34.0(5)$ GeV and the renormalized gauge coupling $g_R^2 = 0.585$, the author of ref. [148] finds $(\sigma/T_c^3)_{\rm hist}^{D=3} = 0.050(12)$ so that all results show fairly good consistency. In comparison with the corresponding estimates for $m_H \simeq 16$ GeV, the interface tension has decreased by about one order of magnitude, signalling that the first order phase transition has weakened rapidly towards this value of the Higgs boson mass.

When comparing the errors, it should be kept in mind that the product of the lattice volume and the number of sweeps, thus CPU-time, is an order of magnitude smaller in the case of the two-coupling method. Together with the results of refs. [134, 135], in which the histogram method has been used with multicanonical simulations, see subsection 6.2.2 of chapter 6, in total three different approaches for the measurement of the interface tension were studied. As already suggested in the previous section, no significant systematic discrepancies among the results of these methods beyond their statistical errors has been observed, and therefore, the two-coupling method turns out to be the most robust and economic way to estimate the interface tension. Moreover, since this method generically requires the greatest lattice volumes and has typically larger statistical errors in its results too, it seems rather pointless to extrapolate them to infinite volume.

7.3 Continuum limit of T_c/m_H for $m_H \simeq 35$ GeV

Numerical MC investigations of the SU(2)–Higgs model in four dimensions, which is deduced from first field-theoretic principles, are genuinely non-perturbative ab initio and do not contain any further conceptual approximations. By comparing the data from numerical simulations for this model with those from other approaches like perturbation theory or three-dimensional effective theories, one can not only hope to achieve an unambiguous understanding of the finite-temperature EWPT, but also to identify non-perturbative features

and possible sources of systematic errors, which may be difficult to control in one of the latter. In particular, such a comparison is of great interest in practice, because it allows to quantify the intrinsic uncertainty in the dimensional reduction step and possible deviations from resummed perturbation theory in the continuum.

Since most of the $4D$–results on the thermodynamic quantities σ/T_c^3 (interface tension) and $\Delta\epsilon/T_c^4$ (latent heat) were only obtained on lattices with temporal extensions $L_t = 2, 3$ and have typically $\mathcal{O}(10\%)$–errors [134, 135, 136, 139], one should consider the critical temperature T_c in units of the Higgs boson mass m_H, which both are relatively easy to measure on the lattice with ideally quite small errors. After its careful extrapolation to the continuum limit, the dimensionless ratio T_c/m_H can be compared with the available results from one-loop and two-loop perturbation theory in four dimensions [105, 107] and from the dimensionally reduced SU(2)–Higgs model in three dimensions [147].

However, as pointed out before, the uncertainties of the critical hopping parameter κ_c contributes to the errors of many other physical quantities. In view of the promising opportunity for a comparison with the approaches addressed above, this is most severe just in the case of the ratio T_c/m_H, while the transition temperature is $aT_c = 1/L_t$ in lattice units and the Higgs mass am_H is calculated on $T = 0$ lattices in $\kappa = \kappa_c$, which must have been determined independently on $T > 0$ lattices with temporal extensions $L_t = 2, 3, \ldots$ in advance:

$$\frac{T_c}{m_H} = \frac{1}{am_H L_t}\,. \tag{7.14}$$

In contrast to the renormalized parameters $R_{HW} = m_H/m_W$ and g_R^2, where the κ_c–errors cancel to a large extent, the errors of the numerical simulations for the quantity T_c/m_H are dominated by the uncertainties in κ_c. Therefore, if computer hardware with 64–bit floating point arithmetics is accessible, it is desirable to improve the precision of κ_c as far as possible.

The lattice parameters assumed for the following investigation, which constitutes an extension of some existing results in refs. [137, 140], correspond to a Higgs boson mass of $m_H \simeq 35$ GeV. As clarified in earlier publications [137, 148], recent reviews [96, 97], and in this work as well, the agreement of other quantities with two-loop perturbation theory and MC results from simulations of the three-dimensional effective theory is still rather good in this region of medium-sized Higgs masses. Using the one-loop renormalization group β–functions to describe the flow of the bare couplings β and λ along a given line of constant physics (LCP) in lattice parameter space, see section 5.2 of chapter 5 and [135, 137], the simulation points with increasing L_t ($\Leftrightarrow a \to 0$) in these studies were chosen such that the non-perturbatively renormalized quantities $R_{HW} = m_H/m_W$ and g_R^2 should be constant. Then a careful analysis was performed to extract the true statistical errors of the masses and the static potential, and to control systematic errors like finite-volume effects and lattice artifacts. The results could be extrapolated to infinite volumes reliably, and there it was already found that the non-perturbatively determined masses scale properly by $1/L_t$ within

errors, with lattice discretization errors expected to be of the order $\mathcal{O}(1/L_t^2)$, and that the physical shape of the static potential scales too. For instance, the magnitude of lattice artifacts in R_{HW} and g_R^2 on $L_t = 5$ lattices is at the level of a few parts per thousands. Hence, the size of the lattice artifacts turns out to be surprisingly small, and once the statistical errors of the relevant quantities become sufficiently small, the extrapolation to the continuum limit from $L_t = 2$ to $L_t = 5$ seems feasible.

7.3.1 Critical hopping parameter at $L_t = 3$

To begin with, I want to illustrate again — but in some more detail — the determination of the critical hopping parameter κ_c by employing the efficient constrained-simulation method, whose merits and limitations have been discussed in subsection 6.1.5 of the foregoing chapter. The simulation point under consideration has $L_t = 3$ as temporal lattice extension, and the bare parameters are $\beta = 8.15$ and $\lambda = 0.00031$. A two-coupling simulation on a $3 \times 32^2 \times 512$ lattice [137] gave the estimate $\kappa_c = 0.128355(5)$ and has been used a starting point for the constrained simulation. Scaling up the lattice extension used for the corresponding $L_t = 2$ analysis of the previous section, a lattice of size $3 \times 36^2 \times 384$ has to be utilized. I apply the general procedure of subsection 6.1.5, but now, unlike in section 7.2, to the order parameter $O = \rho^2$, because the cartesian φ–overrelaxation algorithm was used in the MC updating scheme. The central lesson to be learned there was that the critical point in κ_c, at which the histogram of the order parameter is flat, can be implicitly defined through the equation

$$\left\langle \rho^2 \right\rangle \Big|_{\kappa=\kappa_c} = \rho^2_{\rm mid} \,, \quad \rho^2_{\rm mid} \equiv \frac{1}{2}\left(\rho^2_- + \rho^2_+\right) \,, \tag{7.15}$$

if the individual measurements ρ^2, conceived as being averaged over the lattice volume in each sweep, are constrained to carry only those values, which comply with

$$\rho^2 \;\in\; [\,\rho^2_- \,,\, \rho^2_+\,] \,. \tag{7.16}$$

The condition (7.15) is fulfilled by reweighting the full distribution of the measured ρ^2–history to κ–values κ' in the vicinity of the simulation point [136, 188]. This numerical tool, which allows to determine the dependence of global quantities (averages) on κ in a single run, is briefly reviewed in section B.3 of appendix B. It works well, if the κ–shifts are so small that the induced shifts of the measured quantities are smaller than their variances; otherwise the technique of Taylor series projection is necessary [137]. The statistical errors $\Delta_{\rho^2} = \Delta_{\rho^2,\kappa'}$ of the expectation values $\langle\rho^2\rangle_{\kappa'}$ from the reweighted distribution in $\kappa' \neq \kappa$ were always obtained by jackknife or bootstrap methods, which are also summarized in appendix B.

The first step was to select a reasonable interval $[\,\rho^2_- \,,\, \rho^2_+\,]$, to which the measurements of the order parameter ρ^2 should be constrained. It has to lie safely between and well separated from the peaks of the pure homogeneous phases, which could be isolated by two short simulations in $\kappa = 0.128355$ on configurations equilibrated deep in the symmetric phase (at

$\kappa = 0.12815$) and in the broken Higgs phase (at $\kappa = 0.12855$) beforehand. Unfortunately, after some constrained-simulation runs with various ρ^2–intervals, it turned out that this κ_c–value, obtained by the 2–κ method from a lattice of different size, does rather fall into the border of the metastable region and tends readily to flip via tunneling in the Higgs phase. However, at the slightly lower hopping parameter $\kappa = 0.128353$ the two-phase equilibrium was more stable, see the left plot of figure 7.5, and an evaluation of all measurements with $\rho^2 \in [\,3.15\,,\,3.20\,]$, taken from a thermalized ρ^2–sample of 6000 sweeps with the constraint $\rho^2 \in [\,3.0\,,\,3.2\,]$ before, gave the tentative value $\kappa_c = 0.1283493(4)$. Using this estimate and

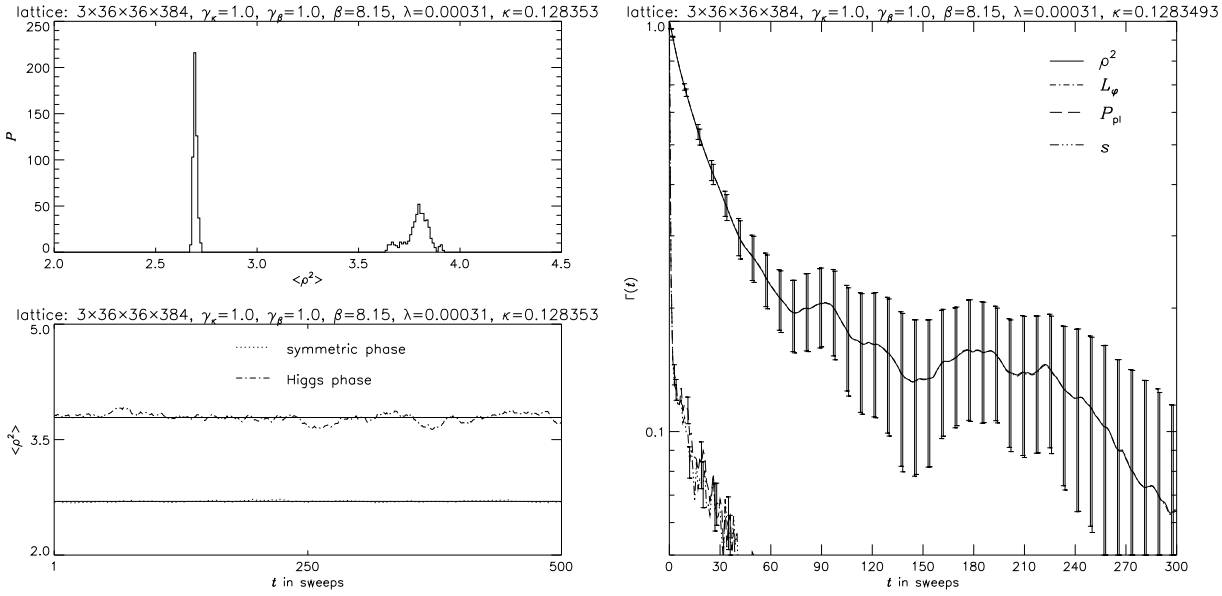

Figure 7.5: ***Left:*** *Positions of the pure-phase peaks in the histogram of the order parameter ρ^2 at $\kappa = 0.128353$ in the metastable region to select its interval for the constrained simulation. Both parts of the histogram have been simulated separately (500 warmup and 500 measurement sweeps each), while the respective starting configurations were first equilibrated at $\kappa = 0.12815$ in the symmetric and at $\kappa = 0.12855$ in the Higgs phase.* ***Right:*** *Autocorrelation functions $\Gamma(t)$, t in sweeps, of some representative lattice operators from the constrained simulation in $\kappa = 0.1283493$. The statistical errors of these functions, as well as those of the integrated autocorrelation times extracted from them, were obtained by jackknife analyses with 25 jackknife samples. The exponential autocorrelation time, which governs the decay of $\Gamma(t)$, was $\tau_{exp} \simeq 30$ sweeps for ρ^2, which is conform with experiences from similar simulations in other points of lattice parameter space.*

its field configuration for a refined analysis in $\kappa = 0.1283493$ with higher statistic, I accumulated — after 3500 warmup sweeps — a history of 20000 ρ^2–measurements constrained to the order parameter interval $\rho^2 \in [\,3.1\,,\,3.2\,]$. The autocorrelation functions and the integrated autocorrelation times in this simulation, which were calculated for some representative operators from their full samples of measurements with the aid of formulas (A.31) and

(A.32) in appendix A.3, are visualized in the right plot of figure 7.5. The autocorrelation time $\tau_{\rm int}[\rho^2] = 75(27)$ sweeps of the constrained order parameter is a bit larger than the typical times observed in section 7.2 and ref. [136]. This may be explained by the fact that, in regard of the tiny κ–shift to the result (7.17) below, the simulation point was already very near to the critical hopping parameter, where generically larger autocorrelation times have to be faced. In order to keep track, whether the two domains associated with the pure metastable phases and separated by a pair of interfaces, have settled in the system and do persist during the whole simulation, I periodically considered the z–slice profile of the φ–link expectation value $L_\varphi(\mathrm{z})$ introduced in eq. (6.9) of section 6.1.4, as exemplarily reproduced in figure 7.7. Since the lattice geometry is such that the transverse directions have extensions much smaller than the elongated z–extension, only interfaces perpendicular to the z–direction are probable.

The reweighting of the data sample of constrained ρ^2–measurements in $\kappa = 0.1283493$ to comply with eq. (7.15) leads to the result

$$\kappa_c = 0.12834938(22)\,. \tag{7.17}$$

An estimation of the statistical error as quoted in parentheses is offered by the condition (7.15) too, if it is required to hold for the upper and lower bounds on the statistical error interval $\langle\rho^2\rangle_\kappa \pm \Delta_{\rho^2}$ of $\langle\rho^2\rangle_\kappa$:

$$\left\langle\rho^2\right\rangle\Big|_{\kappa=\kappa_c-\Delta\kappa_c} + \Delta_{\rho^2} = \rho^2_{\rm mid}\,, \quad \left\langle\rho^2\right\rangle\Big|_{\kappa=\kappa_c+\Delta\kappa_c} - \Delta_{\rho^2} = \rho^2_{\rm mid}\,. \tag{7.18}$$

As the graphical construction suggested in the left plot of figure 7.6 illustrates, this gives a lower bound $\kappa_c - \Delta\kappa_c$ and an upper bound $\kappa_c + \Delta\kappa_c$ for the statistical error on the critical hopping parameter determined from the constrained-simulation method. Thanks to the larger number of lattice points used and the elimination of the ρ–reflection in favour of the φ–reflection to reduce autocorrelations, the accuracy, which was achieved for the value at $L_t = 2$ in eq. (7.9) of section 7.2 (and which is also contained in refs. [136, 137] and table 7.3), has significantly increased.

As a control that the system really has been simulated in the flat regime, the evaluation along eqs. (7.15) and (7.16) has been repeated with the ρ^2–histories restricted to the lower and upper interval halves $[\,\rho^2_-\,,\,\rho^2_{\rm mid}\,]$ and $[\,\rho^2_{\rm mid}\,,\,\rho^2_+\,]$, respectively. The corresponding estimates $\kappa_c = 0.12834905(30)$ and $\kappa_c = 0.12834950(32)$ are consistent with the result (7.17), even though they possess larger statistical errors as expected. In addition, I also checked on a possible lack of thermalization, which in principle could affect the κ_c–analysis. But when omitting some portions of several thousand ρ^2–measurements from the beginning of the statistic, I found only numbers, which were compatible with the statistical error of the best estimate in eq. (7.17), so that any systematic influence of thermalization effects is absent. Finally, the right plot in figure 7.6 shows the sensitivity of the reweighted histograms against

a variation of the critical hopping parameter about one standard deviation in both directions.

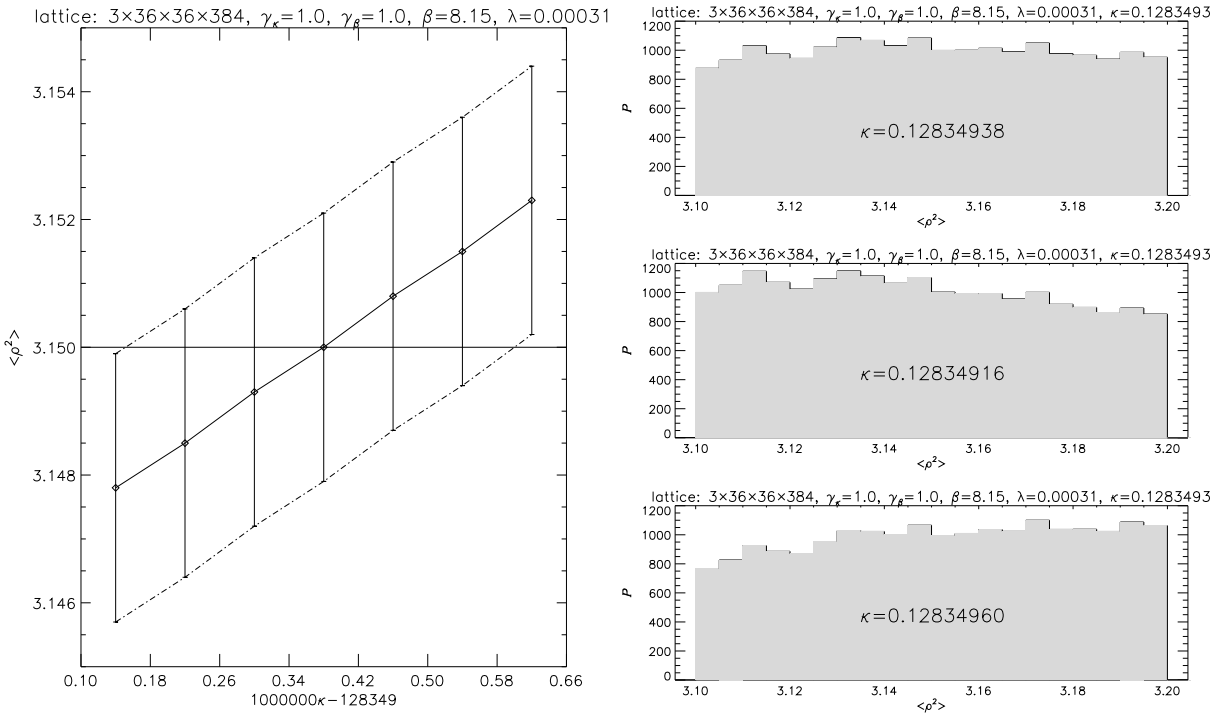

Figure 7.6: ***Left:*** *The full line connects the expectation values of the order parameter ρ^2 as a function of the hopping parameter, computed by reweighting, and the dashed lines give the range of their statistical errors. This sets the error on κ_c as the width of that κ–interval, which is bounded by the intersection points of these dashed lines with the horizontal line at $\langle\rho^2\rangle = \rho^2_{mid}$. From $3.1 \leq \rho^2 \leq 3.2$ and $\rho^2_{mid} = 3.15$ the result $\kappa_c = 0.12834938(22)$ is obtained.* ***Right:*** *Reweighted histograms of the ρ^2–distribution from the simulation in $\kappa_c = 0.1283493$. In the lower two diagrams κ is varied according to $\kappa_c \mp \Delta\kappa_c$, if $\Delta\kappa_c$ denotes the standard deviation of κ_c in eq. (7.17), whose histogram is depicted on the top. The latter is pretty flat indeed, while the other two already show some descent (ascent), which characterizes an approach to the border of the metastable region. This provides a further test for the correct curvature of the order parameter distribution in κ_c.*

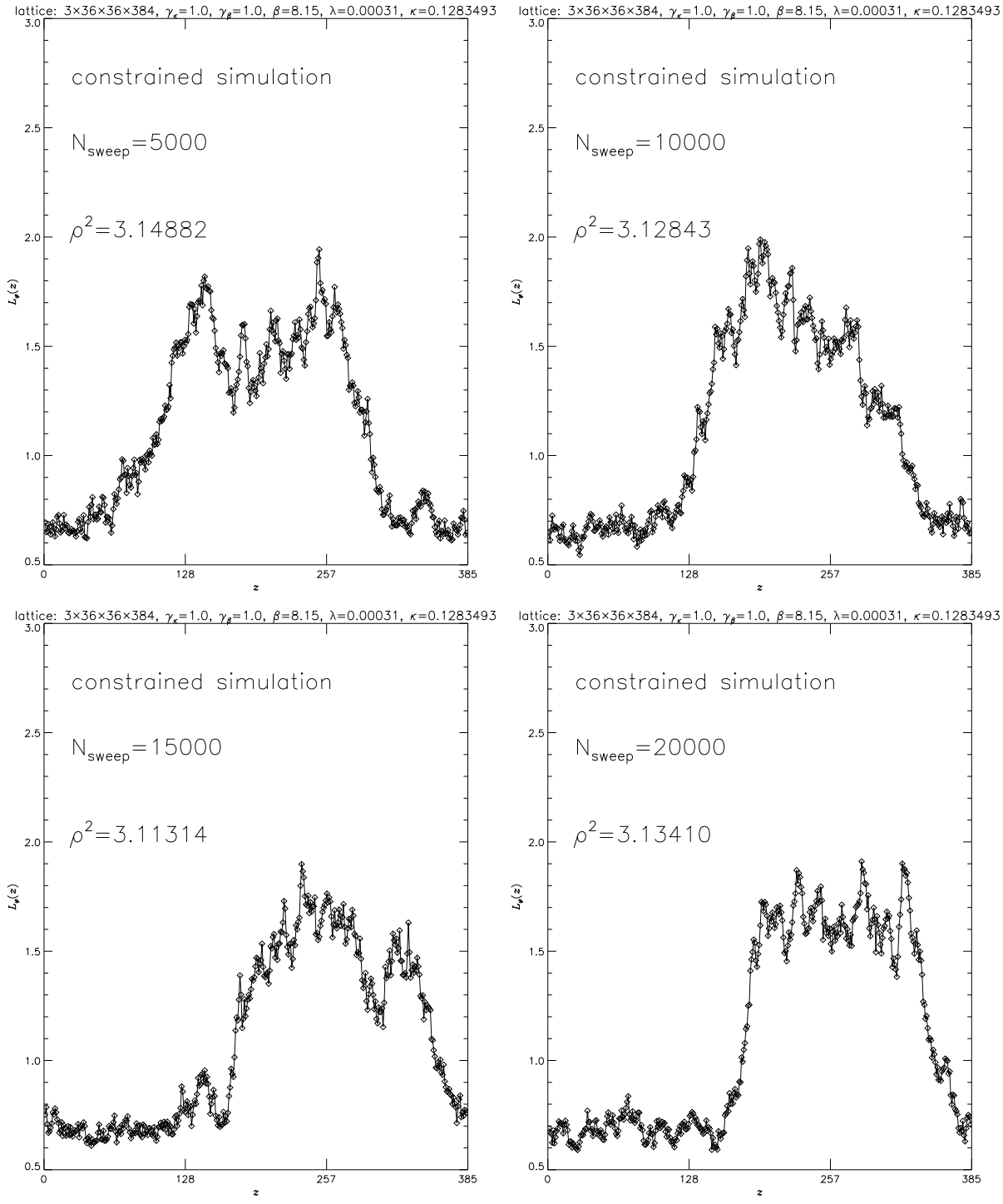

Figure 7.7: *The z–slice expectation value $L_\varphi(z)$ of the φ–link during a constrained simulation in $\kappa \simeq \kappa_c$, monitored at stages marching on with MC time. The two phases and the interfaces separating them are clearly visible. But in contrast to a two-coupling simulation, where the phase boundaries are (ideally) fixed by the choice of different κ–values in the two z–halves, they can freely move along the z–direction in the present case. In view of the dynamical picture of bubble nucleation during the EWPT, see section 6.2 of the previous chapter, these shapes may also be interpreted as the profile of a bubble, which develops in numerical simulations near criticality of the system in T. The spatial thickness of its wall along the z–direction can also be identified.*

7.3.2 Continuum extrapolation and discussion

Since the critical temperature in lattice units is prescribed via the periodicity of the lattice in time direction as $aT_c = 1/L_t$, it can be expressed in physical units, if its dimensionless ratio to a renormalized mass at zero temperature — extracted from the exponential decays of suitable timeslice correlation functions — is known. In the present case I am interested in the critical temperature T_c in units of the Higgs mass m_H.

Technically, the $T = 0$ Higgs mass has been determined by a linear extrapolation of the nearby values $am_H = 0.1587(14)$ in $\kappa = 0.128355$ and $am_H = 0.1796(40)$ in $\kappa = 0.128405$ at $L_t = 3$, published in [137] for a $24^3 \times 32$ lattice, to the more precise κ_c of eq. (7.17). In regard of the typical size of the statistical errors on the masses, this is correct within the small κ–range encountered. The result is $T_c/m_H = 1/am_H L_t = 2.132(22)$, where now the error has been computed from the errors of the input data incorporating both the statistical error $\Delta\,(am_H)$ of the extrapolated mass $am_H = am_H(\kappa)$ and the error $\Delta\kappa_c$ of the critical hopping parameter itself. Namely, the total error consists of $\Delta^{\rm tot}\,(am_H) = \Delta\,(am_H) + \Delta^{\kappa_c}\,(am_H)$, where the influence of the κ_c–uncertainty $\Delta^{\kappa_c}\,(am_H)$ on the Higgs mass can be estimated as

$$\Delta^{\kappa_c}\,(am_H) = \Delta\kappa_c \,\frac{\partial}{\partial\kappa}\, am_H(\kappa)\,\Big|_{\kappa=\kappa_c} \simeq \Delta\kappa_c \left|\, \frac{am_H(\kappa') - am_H(\kappa_c)}{\kappa' - \kappa_c} \,\right| , \qquad (7.19)$$

if $\kappa' = \kappa_c \pm \Delta\kappa_c$. Then, as usual, the error sum $\Delta^{\rm tot}\,(am_H)$ propagates into the inversion to the ratio $T_c/m_H = 1/am_H L_t$, and its value is recorded together with the other numbers at different L_t from the same paper in table 7.3. Presupposing the leading scaling violation

lattice	β	λ	method	κ_c	T_c/m_H
$2 \times 24^2 \times 256$	8.0	0.0003	constrained	0.1286565(7)	2.026(11)
$3 \times 36^2 \times 384$	8.15	0.00031	**constrained**	**0.12834938(22)**	**2.132(22)**
$4 \times 44^2 \times 512$	8.25	0.000315	two-coupling	0.128235(5)	2.087(48)
$5 \times 56^2 \times 570$	8.33	0.000319	two-coupling	0.128170(5)	2.21(10)

Table 7.3: *Simulation points and its results for the critical hopping parameter and the dimensionless ratio T_c/m_H of the critical temperature to the $T = 0$ mass in the Higgs channel along the LCP at $m_H \simeq 35$ GeV. The boldface numbers are new compared to refs. [137, 140]. As described in the text, the statistical uncertainty in the determination of κ_c has been taken into account for the error of T_c/m_H as well.*

of the non-perturbative Higgs mass to be of order $\mathcal{O}(a^2)$, I subsequently performed a linear fit in $(aT_c)^2 = 1/L_t^2$ to these T_c/m_H–data in similar way, using again error propagation to calculate the error of the extrapolated quantity. This fit is displayed in figure 7.8, together with the simulation results of table 7.3 and the predictions of four-dimensional resummed perturbation theory in the continuum [105, 107]. Note that the one-loop and two-loop

results almost coincide at $m_H \simeq 35$ GeV, which hints at good convergence properties and the credibility of the perturbation series for the quantity T_c/m_H in this parameter region.

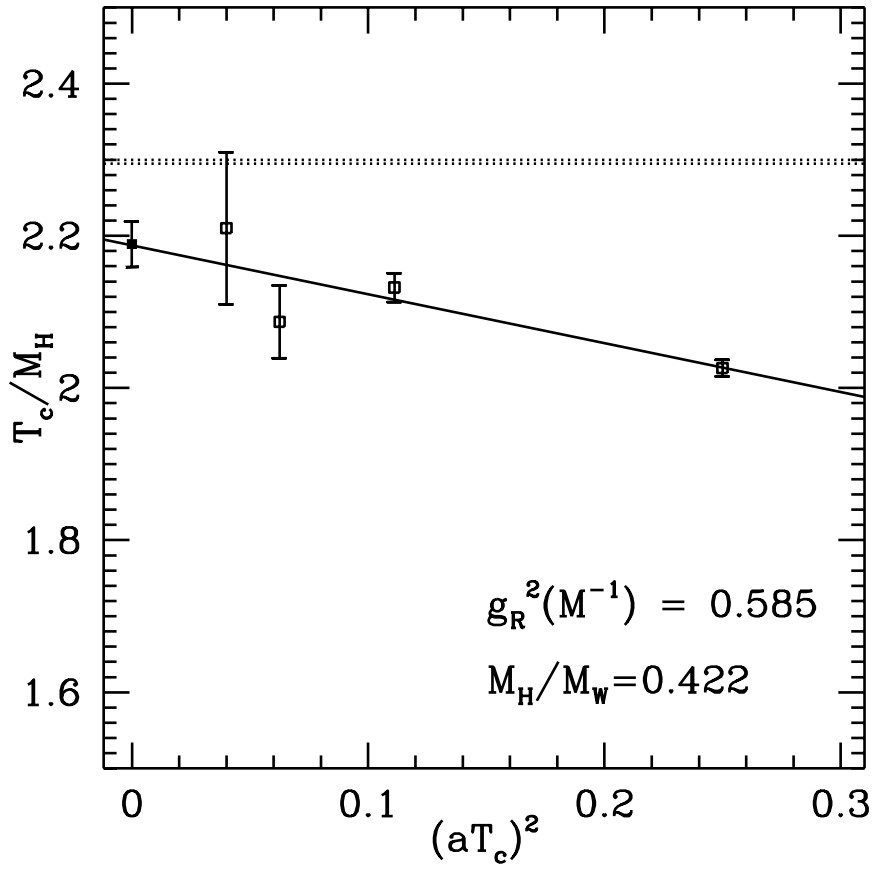

Figure 7.8: *Numerical results for the transition temperature in units of the Higgs boson mass, here $m_{H,W} \equiv M_{H,W}$. Assuming $\mathcal{O}(a^2)$–lattice artifacts, the straight line is the $a \to 0$ extrapolation, which has been made with respect to $(aT_c^2) = 1/L_t^2$ and gave the continuum limit value (7.20) shown by the filled symbol. The errors on the T_c/m_H–entries with $a^{-1} \geq 4T_c$ are dominated by the uncertainties in the critical hopping parameters from the 2–κ simulations with single-precision (32–bit) arithmetics. The dashed horizontal lines are the perturbative predictions [105, 107] at order g^3 (upper) and g^4 (lower). They correspond to fixed values of R_{HW} and g_R^2 (with M being the screening mass of the Yukawa potential, see the next chapter), which characterize the LCP under consideration.*

The final result of the fitting procedure reads

$$\frac{T_c}{m_H} = 2.189(34)\,, \quad T_c = 73.9(1.2)\ \text{GeV} = 8.58(14) \cdot 10^{14}\ \text{K}\,, \tag{7.20}$$

while the critical temperature in physical units refers to $R_{HW} = 0.422$ and $m_W = 80$ GeV. It resembles the limit of the continuum extrapolation $a \to 0$ ($L_t \to \infty$) including the new, error-reduced κ_c–value at $L_t = 3$ computed numerically above, and in this sense it should

be regarded as more reliable than that quoted in refs. [137, 140]: $T_c/m_H = 2.147(40)$. The quality of the fit for the T_c/m_H at different L_t is very good, also when including the $L_t = 2$ point in the extrapolation, which is supported by its sum of squares per degree of freedom $\chi^2/\mathrm{dof} = 1.23$ and the smallness of scale breaking lattice artifacts found in [135, 137, 139]. By the way, the value at $L_t = 2$ is about 7 % smaller. This relatively small deviation is much better than the expectation based on lattice perturbation theory, for instance, the authors of ref. [147] give an estimate of scaling violations between 20 % and 30 % for $L_t = 2$.

For further discussion I use the values $R_{HW} = 0.422(11)$ and $g_R^2 = 0.585(10)$ established in ref. [137] as a perturbative reference point for the LCP considered here. This is under the mild assumption that corrections due to the different renormalization conditions for the gauge coupling g_R and the order parameter ρ on the lattice and in the continuum, which are expected to be of relative order $\mathcal{O}(g_R^2)$, can be neglected. Compared to the value $T_c/m_H = 2.147(40)$, obtained there with the κ_c–estimate at $L_t = 3$ from the 2–κ method, the continuum limit (7.20) has lifted a bit. Although this number comes now somewhat closer to the prediction $(T_c/m_H)_{\mathrm{pert}} \simeq 2.29$ of two-loop resummed perturbation theory [105, 107], figure 7.8 indicates that the T_c/m_H–value extrapolated to the continuum limit still differs by about three standard deviations from the perturbative result.

The estimate from MC simulations of the effective SU(2)–Higgs theory after dimensional reduction to three dimensions is $(T_c/m_H)_{a\to 0}^{D=3} = 2.227(15)$. It has been obtained from extrapolations of the phase transition points, mostly determined by different numerical methods, to a common limit of infinite volumes and zero lattice spacings [147] and, as in the case of the interface tension before, after converting it via a suitable interpolation to the physical parameters $m_H = 34.0(5)$ and $g_R^2 = 0.585$ of the $4D$–theory. Varying the renormalized gauge coupling like $g_R^2 = 0.585 \pm 0.015$, the result does not yet change outside its error [148]. This number, which is consistent with the $4D$–results inside the errors, has higher precision and lies a little closer to the prediction of two-loop resummed perturbation theory. Nevertheless, provided that the systematic errors in the parameter matching of ref. [148] are negligible, there is also a discrepancy downwards of more than two standard deviations from the perturbative result. The new estimate $T_c/m_H = 2.189(34)$ of eq. 7.20) has decreased the relative difference between the lattice MC results for the models in four and three dimensions from approximately 4 % to 2 %. Even now this is definitely larger than those valuations [146, 147], which claim the intrinsic uncertainty involved in the successive perturbative steps of dimensional reduction and lattice regularization to be in the optimal — but surely too optimistic — case to be smaller than 0.1 %.

Consequently, in my opinion one has to suspect that there are some non-negligible higher-loop contributions and/or non-perturbative effects, which may only show up in the full four-dimensional theory, since it does not contain any approximation at all. It is possible that deviations of similar magnitude will emerge in other quantities (e.g. interface tension or latent heat) as well, once the precision would become similar there. In order to furnish

this statement further and to arrive at a final conclusion, a refined κ_c–determination also at $L_t = 4, 5, \ldots$ is indispensable. But the obvious obstacle of memory restrictions for the today accessible computers, related to the very large lattice sizes required at these L_t–values, can only be overcome by the use of anisotropic lattices.

An often heard objection to the confrontation of the lattice SU(2)–Higgs model in four dimensions with its three-dimensional counterpart or continuum perturbation theory made here is that the definitions of the renormalized gauge couplings in the different approaches are not the same. Whereas the lattice definition in four dimensions $g_R = g_R^{(V)}$ derives from the static potential $V(R)$, the perturbative calculations in the continuum — also adapted for the effective theory to express the parameters of the three-dimensional model through those of the original one in four dimensions — refer to the conventional $\overline{\rm MS}$–renormalization scheme: $g_R = g_R^{(\overline{\rm MS})}$. So strictly speaking, the influence of these distinct definitions can be reasonably estimated only, if at least a perturbative first order relation between between $g_R^{(V)}$ and $g_R^{(\overline{\rm MS})}$ is known, whose coefficient must not necessarily be small. This is an important — albeit missing — prerequisite, which would enable to convert the renormalized parameters into each other and to prepare comparable physical situations for both cases. Of course, unless such a relation is not available, every direct comparison between results from the four-dimensional model and from the three-dimensional reduced theory or continuum perturbation theory retains some non-assessable uncertainty, upon which one could always fall back to explain the perhaps arising discrepancies.

Chapter 8

Quantum corrections to the coupling anisotropies

This chapter is devoted to the perturbative as well as the non-perturbative determination of the quantum corrections to the coupling anisotropies of the SU(2)–Higgs model on lattices with asymmetric lattice spacings.

The $\mathcal{O}(g^2, \lambda)$–results, which were obtained in ref. [138] by a one-loop calculation requiring the rotational invariance of the gauge and Higgs boson propagators in the continuum limit, are confirmed with high accuracy in a non-perturbative investigation by means of numerical simulations of the model on appropriate lattices. It is demonstrated that rotational invariance is also restored for the static potential computed from space-space and space-time Wilson loops, when the perturbatively determined coupling anisotropies are used in the simulations [141]. As already stated before, the anisotropic lattice approach is indispensable to reach the physically more realistic Higgs mass range of $m_H \simeq 80$ GeV or larger within the SU(2)–Higgs model in four dimensions.

8.1 Perturbative analysis

Here is a condensed outline of the essential steps in the perturbative first order calculation and its main results [138, 140]. More technical details of this analysis, e.g. about the contributing one-loop graphs and their evaluation in Feynman gauge, can be found in ref. [141].

- The aim is to access the first order quantum corrections to the tree-level identity $\gamma_\beta = \gamma_\kappa = \xi$ in the loop expansion

$$\gamma_\beta = \gamma_\beta(\xi) = \xi\,\eta_\beta(\xi)\,, \quad \gamma_\kappa = \gamma_\kappa(\xi) = \xi\,\eta_\kappa(\xi) \tag{8.1}$$

  with functions η_β and η_κ, formally double-expanded in the squared bare gauge coupling

$g^2 = 4/\beta$ and the lattice scalar quartic self-coupling λ as

$$\eta_\beta^2(\xi) = 1 + c_\beta(\xi) g^2 + b_\beta(\xi)\lambda + \mathcal{O}(g^4, \lambda^2) \tag{8.2}$$

$$\eta_\kappa^2(\xi) = 1 + c_\kappa(\xi) g^2 + b_\kappa(\xi)\lambda + \mathcal{O}(g^4, \lambda^2)\,. \tag{8.3}$$

A formal power counting argument suggests $\lambda \sim g^2$. The perturbative analysis of $\gamma_\beta(\xi)$ and $\gamma_\kappa(\xi)$ is based on the idea that the Higgs and gauge boson correlation lengths in physical units are required to be the same in the different directions [132].

- When elaborating perturbation theory and its Feynman rules for the present model, one may follow the usual steps [19, 117] with the only complication that one has to keep track of the different lattice spacings and couplings. More precisely, the elementary vertices of the theory are easily read off from the various pieces of lattice action (5.16) in chapter 5 translated into its continuum notation after some tedious rearrangements. The corresponding propagators of the fields are written down from the parts of the action quadratic in the fields. In momentum space the inverse tree-level propagators, which are of zeroth order in g^2 and λ, have for Higgs and W–boson the form

$$\tilde{\triangle}_{H,0}(p)^{-1} = \sum_{i=1}^{4} \hat{p}_i^2 + m_{H,0}^2\,, \quad \tilde{\triangle}^{ab}_{W,0,\mu\nu}(p)^{-1} = \delta^{ab}\delta_{\mu\nu}\left[m_{W,0}^2 + \sum_{i=1}^{4} \hat{p}_i^2 \right], \tag{8.4}$$

with isospin indices $a, b \in \{1, 2, 3\}$, and analogously for the three Goldstone bosons and the Fadeev-Popov ghost field. Taking into account the two-point interaction vertices arising as a consequence of the anisotropy, the momentum squared sums modify to

$$\sum_{i=1}^{4} \hat{p}_i^2 \longrightarrow \sum_{i=1}^{3} \hat{p}_i^2 + \frac{\gamma_\kappa^2}{\xi^2}\,\hat{p}_4^2\,, \tag{8.5}$$

where the momenta $\hat{p}_\mu$, $\mu \in \{1, \ldots, 4\}$, are defined in eq. (A.8) of appendix A.1. Exceptionally, a more complex structure is inherent in the gauge boson inverse propagator, because it already contains a part of the perturbative corrections due to the lattice anisotropy.

- Another point to remember from subsection 6.1.1 of chapter 6 is that one must perform perturbation theory near the critical line of the SU(2)-Higgs model. This means first the determination of the mass-counterterms, generated by loop corrections, and then to tune the bare parameters — essentially the scalar hopping parameter to its critical value κ_c — in a way that the one-loop renormalized masses m_R, $m_R \in \{m_{H,R}, m_{W,R}\}$, are finite in the continuum limit while, however, their values in lattice units $a_s m_R$ vanish. The coupling ratios γ_β and γ_κ are still free parameters and can be fixed by two additional conditions, namely by demanding rotational (Lorenz) invariance for the scalar and gauge boson propagators.

- The physical particle propagators receive self-energy corrections, among which those to eq. (8.4), i.e.

$$\tilde{\triangle}_{H,1}(p)^{-1} = \tilde{\triangle}_{H,0}(p)^{-1} + \Sigma_{H,1}(p) \tag{8.6}$$

$$\tilde{\triangle}^{ab}_{W,1,\mu\nu}(p)^{-1} = \tilde{\triangle}^{ab}_{W,0,\mu\nu}(p)^{-1} + \Sigma^{ab}_{W,1,\mu\nu}(p)\,, \tag{8.7}$$

  are needed to calculate the one-loop corrections of the anisotropy parameters γ_β and γ_κ. According to ref. [132], rotational symmetry restoration for these two propagators in the continuum limit $a_s, a_t \to 0$ at constant lattice spacing anisotropy $\xi = a_s/a_t$ on the one-loop level is achieved by satisfying the conditions

$$1 + \frac{1}{2}\,\frac{\partial^2 \Sigma_{H,1}(p)}{\partial p_i^2}\bigg|_{p=0} = \frac{\gamma_\kappa^2}{\xi^2} + \frac{1}{2}\,\frac{\partial^2 \Sigma_{H,1}(p)}{\partial p_4^2}\bigg|_{p=0}, \quad i = 1,2,3 \tag{8.8}$$

$$1 + \frac{1}{2}\,\frac{\partial^2 \Sigma_{W,1,ii}(p)}{\partial p_j^2}\bigg|_{p=0} = \frac{\gamma_\beta^2}{\xi^2} + \frac{1}{2}\,\frac{\partial^2 \Sigma_{W,1,ii}(p)}{\partial p_4^2}\bigg|_{p=0}, \quad i \neq j = 1,2,3\,, \tag{8.9}$$

  which leads to a cancellation of the corrections to the anisotropies in the kinetic parts of eqs. (8.6) and (8.7) with the kinetic parts of the self-energies $\Sigma_{H,1}(p)$ and $\Sigma_{W,1,ii}(p)$. This ensures that the two-point functions with one-loop corrections have the same shape in the z– and t–directions and determines at the same time the — a priori unknown — functions $c_\beta(\xi)$, $c_\kappa(\xi)$, $b_\beta(\xi)$, and $b_\kappa(\xi)$ in the expansions (8.2) and (8.3). As two non-trivial constraints to be checked, the final expressions for these functions do fulfill gauge independence and a relation similar to (8.9) via equating $\tilde{\triangle}_{W,1,13}(p)$ and $\tilde{\triangle}_{W,1,14}(p)$.

- Important features of the final result to be mentioned:

  - Since the use of the one-loop renormalized masses ($a_s m_{H,R} = a_s m_{W,R} = 0$) in the propagators instead of the bare ones leads to changes of higher order in g^2 and λ, all results are given at those bare parameters, for which the renormalized masses vanish, in full consistency with the general perturbative procedure on the lattice.
  - The functions $b_\beta(\xi)$, $b_\kappa(\xi)$, and thus the $\mathcal{O}(\lambda)$–corrections to the anisotropy parameters vanish. This feature may be qualitatively understood from the well-known fact that the ϕ^4–theory does not have any wave function renormalization up to first order in the scalar self-coupling[1].
  - Evaluating the one-loop diagrams, which exclusively emerge from the pure gauge theory sector, one reproduces the $\mathcal{O}(g^2)$–corrections of the result in ref. [129]. The inclusion of the scalar particles then causes only small changes, i.e. the relative difference between the $c_\beta(\xi)$–functions for the pure SU(2)–gauge theory and the SU(2)–Higgs model is typically a few %.

[1] In the pure Higgs (ϕ^4) sector of the theory only graphs with two or more scalar self-interaction vertices have a non-trivial dependence on the external momentum.

– The perturbative contributions to the hopping parameter yield a correction to γ_κ of the same sign and order of magnitude than that of the gauge anisotropy parameter γ_β. It is possible to combine the anisotropies to $c'_\beta(\xi) = c_\beta(\xi) - c_\kappa(\xi)$, and for this choice in the gauge sector with $\gamma_\kappa = \xi$ the rotational invariance can be restored on the one-loop level, giving identical masses in both directions, if the lattice spacing asymmetry a_s/a_t is adjusted appropriately. However, the obtained asymmetry will then slightly differ from the original ξ–value:

$$\begin{aligned} \xi \;=\; \xi^{(\mathrm{initial})} \;\to\; \xi^{(\mathrm{p})} \;&\equiv\; \left(\frac{a_s}{a_t}\right)_{\mathrm{pert}} \\ &=\; \xi\left(1 - \frac{c_\kappa(\xi)}{2}\,g^2\right)\Bigg|_{\xi=\xi^{(\mathrm{initial})}} + \mathcal{O}(g^4, \lambda^2)\,. \end{aligned} \tag{8.10}$$

The quantitative result for $\xi = \xi^{(\mathrm{initial})} = 4$ becoming relevant in the MC analysis of the next section is:

$$\gamma_\kappa \equiv \xi^{(\mathrm{initial})} = 4\,, \quad \gamma_\beta^{(\mathrm{p})} = 3.919\,, \quad \xi^{(\mathrm{p})} = 4.052\,. \tag{8.11}$$

After this short excursion to the perturbative corrections to the coupling anisotropies, I will now prove by numerical simulations on lattices with anisotropic lattice spacings that the perturbative coupling asymmetries remain unchanged for the practically reasonable parameters of the SU(2)–Higgs model [140, 141].

8.2 Non-perturbative analysis

The second part of this chapter deals with my non-perturbative determination of the anisotropy parameters by means of numerical simulations. Besides a mere confirmation of the one-loop calculations in the previous part, it could give estimates of possible corrections, which go beyond perturbation theory. This is an important step towards future studies of the finite-temperature electroweak phase transition in the framework of the four-dimensional SU(2)–Higgs model on anisotropic lattices. Namely, if the deviation from the perturbative results turns out to be so small that its influence on expectation values in a numerical simulation is negligible within their typical statistical errors, the one-loop perturbative anisotropies γ_β, γ_κ, and ξ can be used without any further non-perturbative fine-tuning. At first sight this may not seem very surprising, because the zero-temperature theory is weakly coupled ($g^2 \simeq 0.5$), e.g. compared to QCD ($g^2 = 6/\beta \simeq 1.0$). But owing to the fact that the corrections in the parameter λ — entering only at two-loop level — whose size essentially determines the value of the Higgs boson mass, are not exactly known, such an investigation is nevertheless necessary, particularly in view of Higgs masses around 80 GeV or larger.

As already discussed before, the tree-level values of the anisotropies receive quantum corrections, of course, with not necessarily purely perturbative contributions, which in general

have to be determined non-perturbatively. A physically motivated idea for their estimation is to impose the restoration of the space-time interchange symmetry as a remnant of Lorentz invariance after discretization of the continuum theory. In practice this is to be realized by the requirement that Higgs and gauge boson correlation lengths in physical units should be equal in space- and timelike directions. The static potentials deriving from space-time and space-space Wilson loops allow for an alternative determination of the lattice spacing anisotropy ξ.

The forthcoming subsections describe my numerical studies in more detail. After some brief remarks on the simulation techniques and parameters used, I present the results on the physical observables under consideration and propose, how they can serve to extract the coupling and lattice spacing anisotropies non-perturbatively. Finally, the values obtained in this way are confronted with perturbation theory.

8.2.1 Simulation and its parameters

In the MC simulations I applied the same combination of heatbath and overrelaxation algorithms, whose implementation for the model on isotropic as well as on anisotropic lattices has been extensively discussed in sections 5.1.1 and 5.3 of chapter 5 and in refs. [135, 137, 139, 141]. The updating scheme per sweep was a sequence of one $U_{x,\mu}$– and one φ_x–heatbath step, followed by one $U_{x,\mu}$– and three φ_x–overrelaxation steps, which has been adopted from refs. [137, 139] without changes. There it was observed that the inclusion of the overrelaxation algorithms [178, 179] reduced the autocorrelation times substantially, in particular for the operators ρ^2 and L_φ, whose expectation values show the largest autocorrelations.

As pointed out in the introduction to this chapter, the anisotropic version of the SU(2)–Higgs model is believed to provide quantitative insights into the electroweak phase transition at large Higgs boson masses of $m_H \gtrsim 80$ GeV, at which the typical excitations with small masses (i.e. large correlation lengths) would demand very large isotropic lattices exceeding any presently accessible computer resources. In principle a rough resolution in the spatial directions by moderate lattices combined with accordingly large lattice anisotropies ξ could handle this situation. However, for $T > 0$ a small temporal extension L_t sets the — very large — temperature scale through $T = 1/a_t L_t$, and hence it is more sensible to ensure a large enough lattice cutoff by employing $\xi \simeq L_t$, thus in my numerical work I take[2]

$$\xi = 4\,. \tag{8.12}$$

Since this makes the correlation lengths in time direction smaller than in space directions,

[2] This argument is perturbative one: At $T > 0$ the simulations should take into account two energy scales, namely T and gT (the 'Debye screening mass'). Thus it is necessary that the lattice cutoff $1/a_s = 1/\xi a_t = T_c L_t/\xi$ does not become too small, i.e. $1 < \xi \lesssim L_t$ at least.

it seems to be reasonable to fulfill $L_t \simeq \xi L_z$ in order to restore the symmetry of the physical extensions and to enable a precise mass determination. I consider two lattices of sizes $8^2 \times 12 \times 48$ and $8^2 \times 16 \times 64$, where the spatial correlation lengths in lattice units are still of order $\mathcal{O}(1)$ and the finite-volume effects are expected to be small.

The $T = 0$ simulations are generically intended to fix the physical parameters, i.e. renormalized couplings and masses, of the theory at $T > 0$. Consequently, the lattice parameters in this study are chosen to reach the interesting region of $m_H \simeq 80$ GeV or a Higgs to gauge boson mass ratio of

$$R_{HW} \equiv \frac{m_H}{m_W} \simeq 1 \tag{8.13}$$

with the experimental input $m_W = 80$ GeV setting the overall physical scale. This is — at least approximately — achieved by the values $\beta = 8.0$ and $\lambda = 0.000178$. The scalar hopping parameter, which has to comply with the condition that the $T > 0$ system is at a phase transition point for a certain temporal lattice extension, is calculated from the discretized version of the anisotropic one-loop effective potential in Landau gauge[3] via eqs. (6.3) and (6.4) of subsection 6.1.1 in chapter 6. Referring to $L_t = 4$, this amounts to $\kappa = 0.10662$. The non-perturbative corrections usually tend to decrease the tree-level mass ratio

$$R_{HW,0} \equiv \frac{m_{H,0}}{m_{W,0}} = \sqrt{\frac{2\lambda\xi\beta}{\kappa^2}} \tag{8.14}$$

and, as can be verified from the entries in the tables below, these bare parameters lead to a (on-shell) Higgs mass of $m_H = 72(5)$ GeV[4] and a (non-perturbatively) renormalized gauge coupling squared of $g_R^2 = 0.577(15)$.

My strategy for the determination of the coupling anisotropies is as follows. In the previous section I have reviewed the calculation of the quantum corrections η_β and η_κ in $\gamma_\beta(\xi) = \xi\,\eta_\beta(\xi)$ and $\gamma_\kappa(\xi) = \xi\,\eta_\kappa(\xi)$, see eqs. (8.2) and (8.3), up to one-loop order in perturbation theory, as it was carried out in ref. [138]. In the numerical simulation, however, one prefers to pursue the inverse way of thinking, i.e. I have to find those couplings of the lattice action eq. (5.16), for which at a given initial ξ–value the space-time symmetry is restored. Therefore, I fix one of the coupling anisotropies to its tree-level value, ignoring its quantum corrections, and tune the other one to produce identical ratios of (decay) masses in space- and timelike directions for a set of two or more (particle) channels. The mass ratios determine the actual lattice anisotropy, which will then slightly differ from the original ξ in (8.12) and which must in principle be known when converting dimensionless lattice quantities into physical units. In this spirit I choose three pairs of coupling anisotropies, denoted as 'tree',

[3] The knowledge of the more accurate, non-perturbative value of the critical hopping parameter, which has to be determined numerically as in the previous chapters, is not relevant here.

[4] In order to get closer to $R_{HW} = 1$, the λ–value will be shifted a bit to 0.000192 in the $T > 0$ investigations of the next chapter.

'low' and 'perturbative',

$$\begin{aligned} \mathrm{t}: &\qquad \gamma_\kappa = 4.0\,, \quad \gamma_\beta = 4.0 \\ \mathrm{l}: &\qquad \gamma_\kappa = 4.0\,, \quad \gamma_\beta = 3.8 \\ \mathrm{p}: &\qquad \gamma_\kappa = 4.0\,, \quad \gamma_\beta = 3.919\,, \end{aligned} \tag{8.15}$$

and calculate the corresponding lattice spacing anisotropies from different physical quantities as described comprehensively in the subsequent sections. Assuming that they depend linearly on γ_β in this small interval, I can interpolate to a matching point $(\gamma_\beta^{(\mathrm{np})}, \xi^{(\mathrm{np})})$, at which all ξ–values coincide within errors. These estimates are quoted as my non-perturbative results.

The numerical simulations have been done independently on the APE-Quadrics computers at DESY-IfH in Zeuthen, Germany, and — to a smaller degree — on the CRAY Y-MP8 and T90 of HLRZ in Jülich, Germany. As mentioned in chapter 5, the 32–bit floating point precision of the former is sufficient for the calculation of all $T = 0$ quantities involved here.

8.2.2 Correlation functions and masses

I now turn to the determination of the Higgs and gauge boson masses. As in refs. [135, 137], they were obtained from suitable correlation functions of gauge invariant, local operators at zero momentum, integrated over time and space slices, respectively. Those are R_x and $L_{\varphi;x\mu}$ for the Higgs channel, and the composite link fields

$$W_{x;rk} \equiv \frac{1}{2}\,\mathrm{Tr}\left(\tau_r \alpha^+_{x+\hat{k}} U_{x,k} \alpha_x\right)\,, \quad \tau_r\text{: Pauli matrices}\,, \quad r,k = 1,2,3 \tag{8.16}$$

for the gauge (W–boson) channel, which have been introduced already in eq. (5.35) of section 5.1.1.

The connected correlation functions Γ_O of these operators have been measured in the timelike and in one spacelike direction. For the Higgs mass m_H the functions $\Gamma_O(t)$ and $\Gamma_O(z)$ were calculated from t– and z–slice averages of R_x and the weighted φ–link $L_{\varphi,x}$ of eq. (6.24). Since these functions can not be regarded as uncorrelated, I have averaged them — after an appropriate normalization of the correlations at distance zero — before performing the mass fits. The same prescription holds for the gauge boson mass m_W, but with two major differences: Firstly, the t– and z–slice correlation functions of $W_{x;rk}$ have been measured separately for all combinations of r and k, and secondly, in place of $k = 3$ in (8.16) actually I have to take $k = 4$ for the correlations in z–direction (i.e. all directions in $W_{x;rk}$ are orthogonal to the direction of propagation). Again the individual correlation functions are averaged to one function per direction as in the Higgs channel.

As lowest energies, the particle masses are extracted from one-exponential least squares fits to shapes of the form

$$\Gamma_O(\ell) = A\left[\mathrm{e}^{-M\ell} + \mathrm{e}^{-M(L-\ell)}\right] + C\,, \quad \ell = 0,1,\ldots,\frac{L}{2}\,, \quad L \in \{L_t, L_z\} \tag{8.17}$$

with $M \in \{a_t m_{H,t}, a_t m_{W,t}\}$ or $M \in \{a_s m_{H,s}, a_s m_{W,s}\}$, respectively. The constant terms in the vector channel are highly suppressed so that a two-parameter fit is mostly sufficient. Each full data sample has been divided into subsamples, and the statistical errors on the masses originate from jackknife analyses. All simulation parameters and lattice sizes are collected in table 8.1.

index	lattice	γ_κ	γ_β	correlation functions		Wilson loops	
				sweeps	subsamp.	subsamp.	indep. sweeps
t1	$8^2 \times 12 \times 48$	4.0	4.0	100000	50	50	100
l1	$8^2 \times 12 \times 48$	4.0	3.8	100000	50	50	100
p1	$8^2 \times 12 \times 48$	4.0	3.919	576000	192	—	—
t2	$8^2 \times 16 \times 64$	4.0	4.0	192000	64	64	150
l2	$8^2 \times 16 \times 64$	4.0	3.8	192000	64	64	150
p2	$8^2 \times 16 \times 64$	4.0	3.919	704000	256	128	150

Table 8.1: *Summary of the numerical simulations for the mass and static potential computations on anisotropic lattices. The other parameters are* $\beta = 8.0$, $\lambda = 0.000178$, *and* $\kappa = 0.10662$.

My fitting procedure consists of correlated fits, sometimes with eigenvalue smoothing, and simple uncorrelated fits. For the former I use the Michael-McKerrel method [187], whose features and application in the SU(2)-Higgs model have been sketched in ref. [137]. The method has also been applied to the mass determinations in the context of the two-dimensional U(1)–Higgs model in the first part of my work, and a short description of this technique can be found in subsection B.2 of appendix B. Its main purpose is to select the most reasonable fit interval in data sets, which are strongly correlated in the fitted direction. Uncorrelated fits, which genuinely ignore these correlations, are often plagued with very small values of χ^2 per degree of freedom (dof) for nearly all fit intervals in question, whereas in correlated fits the emergence of $\chi^2/\mathrm{dof} \simeq 1$ for some fit intervals represents a safe criterion to settle upon reasonable fit intervals. This also works well for data sets of lower statistics, if the smallest eigenvalues of the correlation matrix are smeared via replacing them by their average. All resulting mass estimates in lattice units are shown in tables 8.2 and 8.3. I chose the largest fit interval with a reasonable χ^2/dof from the correlated fit and the results of the uncorrelated fit along this interval as the final fit parameters. Both fits were always consistent within errors, and other fit intervals with comparable or even lower χ^2/dof did not cause any significant changes.

As emphasized above, the space-time symmetry restoration, which implicitly establishes $\xi^{(\mathrm{np})}$, becomes apparent in equal physical correlation lengths $a_s \xi_s = a_t \xi_t$ of the theory. Thus

I introduce anisotropy parameters in the Higgs and vector channels by calculating the ratios

$$\xi_H \equiv \frac{a_s m_{H,s}}{a_t m_{H,t}}, \quad \xi_W \equiv \frac{a_s m_{W,s}}{a_t m_{W,t}} \tag{8.18}$$

within the jackknife samples of the space- and timelike masses. These are displayed again in tables 8.2 and 8.3. Due to the compatibility of the results from the two lattices one

quantity	t1	l1	p1
$a_t m_{H,t}$	$4-18$: 0.1408(22)	$4-22$: 0.1370(27)	$4-24$: 0.1387(15)
$a_s m_{H,s}$	$0-6$: 0.5635(31)	$1-6$: 0.5611(62)	$1-6$: 0.5603(30)
ξ_H	4.002(67)	4.097(86)	4.041(55)
$a_t m_{W,t}$	$8-24$: 0.1523(13)	$8-22$: 0.1538(13)	$8-24$: 0.1554(25)
$a_s m_{W,s}$	$1-6$: 0.6225(29)	$2-6$: 0.6066(40)	$2-6$: 0.6307(22)
ξ_W	4.091(30)	3.945(32)	4.059(44)
$R_{HW,t}$	0.925(15)	0.891(20)	0.892(18)
$R_{HW,s}$	0.905(6)	0.925(12)	0.888(7)

Table 8.2: *Fit intervals, Higgs and gauge boson masses in time- and spacelike directions, and the resulting lattice spacing anisotropies for the smaller lattice.*

quantity	t2	l2	p2
$a_t m_{H,t}$	$4-32$: 0.1408(22)	$4-32$: 0.1370(27)	$4-32$: 0.1378(11)
$a_s m_{H,s}$	$1-8$: 0.5590(42)	$1-7$: 0.5586(40)	$1-8$: 0.5550(40)
ξ_H	3.969(73)	4.080(80)	4.027(36)
$a_t m_{W,t}$	$8-32$: 0.1499(31)	$8-30$: 0.1599(42)	$6-32$: 0.1525(15)
$a_s m_{W,s}$	$1-8$: 0.6318(40)	$3-8$: 0.607(11)	$2-8$: 0.6133(27)
ξ_W	4.23(10)	3.80(13)	4.021(48)
$R_{HW,t}$	0.940(24)	0.857(26)	0.904(11)
$R_{HW,s}$	0.885(8)	0.921(20)	0.905(5)

Table 8.3: *The same quantities as in table 8.2 for the larger lattice.*

concludes that the finite-size effects are quite small. Furthermore, I should stress that ξ_H decreases with increasing γ_β, whilst ξ_W behaves just in the opposite way. This is an indication that by an interpolation in γ_β it will be possible to find the non-perturbative lattice spacing anisotropy, and one can yet recognize that ξ_H and ξ_W, as well as $R_{HW,t}$ and $R_{HW,s}$, are almost identical in the perturbative point.

8.2.3 Wilson loops and static potentials

Another approach to the ξ–determination is based on the static potential, which has the physical interpretation as the energy of an external pair of static charges brought into the system. To this end, I have measured rectangular on-axis Wilson loops $W_{ij}(R_i, R_j)$ of extensions $1 \leq R_i \leq L_i/2$ and $1 \leq R_j \leq L_j/2$, lying in space-time and space-space planes. The gauge configuration was transformed to temporal gauge for space-time and to $A_3^r(x) = 0$ gauge for space-space Wilson loops, and every loop with two sides in t– or z–direction, respectively, was included in the statistics.

As a generalization of the isotropic lattice case I distinguish between static potentials

$$V_{ij}(R_i) = -\lim_{R_j \to \infty} \frac{1}{a_j R_j} \ln W_{ij}(R_i, R_j) \tag{8.19}$$

in spacelike ($ij = st, ss$) and timelike ($ij = ts$) directions, according to the $R_j \to \infty$ extrapolation in the second argument of W_{ij}, which is supposed to be done first. The shape of the potential, which is governed by a massive W–boson exchange [115, 127], is known to be Yukawa-like, and calculating along the lines of refs. [125, 126], lowest order (tree-level) lattice perturbation theory yields

$$V_{ij}(R_i) = \frac{3g^2}{2} \prod_{n \neq j} \int_{-\pi/a_n}^{\pi/a_n} \frac{\mathrm{d}k_n}{2\pi} \frac{\sin^2\left(\frac{R_i a_i k_i}{2}\right)}{\sum_{n \neq j} \hat{k}_n^2 + m_{W,0}^2} + \mathcal{O}(g^4), \tag{8.20}$$

with lattice momenta $\hat{k}_n = 2a_n^{-1} \sin(a_n k_n/2)$, $n = 1, \ldots, 4$. In the continuum limit this expression reflects the usual screening behaviour, i.e. modulo a constant,

$$-\frac{3g^2}{4} \frac{\mathrm{e}^{-m_{W,0} r}}{4\pi r}, \quad r \equiv R_i a_i, \tag{8.21}$$

independent of i and j. After substituting $p_n = a_n k_n$ with $p_n = 2\pi l_n / L_n$ and $l_n = 0, 1, \ldots, L_n - 1$ on a finite lattice, one obtains from eq. (8.20)

$$a_i V_{ij}(R_i) = \frac{3g^2}{16\pi} \Big[I_{ij}(M_{ij}, 0) - I_{ij}(M_{ij}, R_i) \Big] + \mathcal{O}(g^4), \tag{8.22}$$

where $M_{ij} = a_i m_{W,0} \equiv a_i m_{V,ij}$, and I_{ij} denotes the lattice sum

$$I_{ij}(M_{ij}, R_i) \equiv \frac{2\pi}{L_i L_k L_l} \sum_{p_i, p_k, p_l} \frac{\cos(R_i p_i)}{\frac{a_k a_l}{a_i^2} M_{ij}^2 + \sum_{n \neq j} \frac{4 a_k a_l}{a_n^2} \sin^2\left(\frac{1}{2} p_n\right)}, \tag{8.23}$$

where k and l are different from each other and from i and j. Since $g^2 = g_R^2 + \mathcal{O}(g_R^4)$, the simulation results for V_{ij} are fitted with the Yukawa ansatz

$$a_i V_{ij}(R_i) = -\frac{A_{ij}}{R_i} \mathrm{e}^{-M_{ij} R_i} + C_{ij} + D_{ij} G_{ij}(M_{ij}, R_i), \tag{8.24}$$

where G_{ij} is a term correcting for finite-lattice (size and spacing) artifacts, and A_{ij}, M_{ij}, C_{ij}, D_{ij} are the parameters to be fitted. The screening mass in lattice units M_{ij} is closely

related but not exactly equal to the physical vector boson mass $a_i m_{W,i}$ determined from the correlation functions in the previous subsection[5]. The distance- and mass-dependent contribution G_{ij} describes the difference between the continuum potential and the finite-lattice version to lowest order and reads for on-axis R_i:

$$G_{ij}(M_{ij}, R_i) = \frac{1}{R_i}\, \mathrm{e}^{-M_{ij}R_i} - I_{ij}(M_{ij}, R_i)\,. \tag{8.25}$$

By definition, the 'global' renormalized coupling is obtained by identifying the coefficient of the contribution relevant at short distances,

$$g_R^2 = \frac{16\pi}{3}\, A_{ij}\,. \tag{8.26}$$

Note that M_{ij}/a_i and also g_R^2 as determined from Wilson loops with different indices have to be independent of the indices for properly chosen coupling anisotropies.

In a first step of the analysis I performed multi-exponential fits $W_{ij}(R_i, R_j) = \sum_{n=0}^{N} c_n\, \mathrm{e}^{-V_n R_j}$ in order to get the potential for fixed R_i as the ground state energy V_0 from the large R_j asymptotics of the Wilson loops in (8.19). Starting at distances $R_j = 8 - 11$ or $R_j = 1, 2$ in dependence of the available range in the fitted direction, a sum of two exponentials gave always stable fits with an optimal compromise between acceptable χ^2/dof and statistical errors, and with V_0 well separated from higher excitations by a large energy gap. Subsequently, the resulting potentials[6] were carefully fitted to eq. (8.24), and the values of the best fit parameters with its errors from jackknife analyses of the data subsamples are listed in table 8.4. I only used uncorrelated fits in the present context, because the size of the Wilson loop extensions does not admit much variation in the fit intervals. In some cases the smallest distances $R_i = 1$ or $R_i = 1, 2$ were omitted to have a satisfactory χ^2/dof. This supports the experiences from earlier work [137] that the lattice correction G_{ij} may be not adequate enough for the data. A more thorough inspection of the fit results hints at a renormalization of $g^2 = 0.5$ on the $\mathcal{O}(15\%)$–level, and from the validity of $A_{ij} \simeq D_{ij}$ one can judge, how good the assumption of a one-gauge boson exchange really is [127]. The spacelike potentials from W_{st} and W_{ss} lead to consistent numbers, but the discrepancy between the screening masses $M_{ij} \in \{a_s m_{V,st}, a_s m_{V,ss}, a_t m_{V,ts}\}$ and the gauge boson masses of the preceding section is often larger than expected. When comparing the two lattices, I observe only small finite-volume effects in g_R^2, although the M_{ij} still differ outside their — even larger — standard deviations. However, as one will see below, these effects seem to cancel to a great extent in the mass ratios I am mainly interested in.

[5] Note that the lowest-order relation between the physical W–boson mass as the decay mass of a two-point function and the mass m of the propagator is $am_W = 2\ln\left(\sqrt{1 + a^2m^2/4} + am/2\right) + \mathcal{O}(g_R^2, \lambda_R)$, where the perturbative lattice corrections might be significant [115].

[6] More precisely, the potentials have to be rendered dimensionless before, i.e. in view of eqs. (8.19) and (8.24) one has to attach a factor a_i/a_j.

index	A_{ij}	$m_{V,ij}$	D_{ij}	C_{ij}	$g_R^2 \equiv \frac{16\pi}{3} A_{ij}$	$g_R^2(1/M_{ij})$
t1, W_{st}	0.0335(12)	0.626(67)	0.044(10)	0.0832(4)	0.561(19)	0.575(38)
t1, W_{ts}	0.0346(3)	0.1479(55)	0.0401(15)	0.02763(6)	0.5800(43)	0.605(17)
t1, W_{ss}	0.0358(7)	0.639(27)	0.0238(81)	0.1105(2)	0.600(12)	0.592(20)
l1, W_{st}	0.0354(8)	0.593(37)	0.0292(68)	0.0873(4)	0.592(14)	0.582(28)
l1, W_{ts}	0.0351(3)	0.1651(41)	0.0372(7)	0.02768(5)	0.5881(50)	0.603(20)
l1, W_{ss}	0.0360(7)	0.623(29)	0.0269(56)	0.1111(2)	0.602(12)	0.597(21)
t2, W_{st}	0.0336(2)	0.594(26)	0.0332(65)	0.0833(1)	0.5622(35)	0.562(15)
t2, W_{ts}	0.0343(1)	0.1401(19)	0.0390(9)	0.02776(2)	0.5739(14)	0.5932(78)
t2, W_{ss}	0.0345(3)	0.594(13)	0.0346(29)	0.1110(1)	0.5781(54)	0.5781(72)
l2, W_{st}	0.0347(2)	0.555(19)	0.0284(56)	0.0878(1)	0.5821(29)	0.570(14)
l2, W_{ts}	0.0338(1)	0.1429(12)	0.0342(9)	0.02792(2)	0.5657(11)	0.5621(64)
l2, W_{ss}	0.0344(4)	0.557(16)	0.0303(28)	0.1117(2)	0.5761(69)	0.574(12)
p2, W_{st}	0.0339(1)	0.576(13)	0.0322(36)	0.0851(1)	0.5679(21)	0.5645(92)
p2, W_{ts}	0.0343(1)	0.1428(11)	0.0362(2)	0.02780(1)	0.5742(12)	0.5845(50)
p2, W_{ss}	0.0345(3)	0.5810(98)	0.0307(19)	0.1112(1)	0.5780(43)	0.5756(77)

Table 8.4: *All Yukawa fit parameters with jackknife errors of the static potentials, calculated from space-time ($ij = st$ and $ij = ts$) and space-space ($ij = ss$) Wilson loops. The renormalized coupling $g_R^2(1/M_{ij})$ is explained in the text.*

For the sake of completeness, I also discuss a 'local' definition of the renormalized gauge coupling, which goes back to refs. [115, 128] and has been applied to the isotropic SU(2)–Higgs model in [135, 137]. Since the short-distance potentials turn out to deviate from a pure Yukawa ansatz, I set

$$g_R^2(R_i) \equiv \frac{16\pi}{3} \frac{a_i V_{ij}(R_i) - a_i V_{ij}(R_i - d)}{I_{ij}(M_{ij}, R_i - d) - I_{ij}(M_{ij}, R_i)} \tag{8.27}$$

at distance R_i with M_{ij} as screening masses from the large-distance fits to the eq. (8.24). The distance R_i is the solution of the equation

$$\frac{1}{R_i}\, \mathrm{e}^{-M_{ij}R_i} \left[\frac{1}{R_i} + M_{ij} \right] = \frac{I_{ij}(M_{ij}, R_i - d) - I_{ij}(M_{ij}, R_i)}{d} \tag{8.28}$$

and is interpolated to the physical scale $R_{0,ij} \equiv 1/M_{ij}$, giving the typical interaction range of the potential. Eq. (8.28) is motivated by requiring the force as the gradient of the static potential $\frac{\mathrm{d}}{\mathrm{d}R_i} a_i V_{ij}(R_i)$ in the continuum limit (8.21) to be equal to the finite difference $\left[\, a_i V_{ij}(R_i) - a_i V_{ij}(R_i - d) \,\right]/d$ as would follow from (8.22). This improves the naive choice $R_i - \frac{1}{2} d$ to tree-level [128], because it compensates for lattice artifacts of order $\mathcal{O}(a_i^2/r_i^2)$. The results for $d = 1$ are collected in the last column of table 8.4 and agree with g_R^2 from the global definition. The errors contain the statistical errors of the potentials, the (ever

dominating) uncertainties in the screening masses, and systematic errors by accounting for the sensitivity to a quadratic $R_{0,ij}$–interpolation with three neighbouring points instead of a linear one with only two points.

Rotational symmetry now implies that the renormalized gauge coupling and $M_{ij}/a_i = m_{V,ij}$ should be independent of i and j. For g_R^2 this is obviously true, and in analogy to eq. (8.18) a further kind of lattice spacing anisotropy from the ratios of screening masses is

$$\xi_V \equiv \frac{a_s m_{V,st}}{a_t m_{V,ts}} \quad \text{or} \quad \xi_V \equiv \frac{a_s m_{V,ss}}{a_t m_{V,ts}} \,. \tag{8.29}$$

Its values in all simulation points are quoted in table 8.5. In contrast to the entering masses, they show rather good consistency and are hardly affected by the finite volume.

quantity	t1	l1	t2	l2	p2
$\xi_V = a_s m_{V,st}/a_t m_{V,ts}$	4.23(47)	3.56(26)	4.24(18)	3.88(14)	4.033(96)
$\xi_V = a_s m_{V,ss}/a_t m_{V,ts}$	4.32(24)	3.76(20)	4.24(12)	3.89(13)	4.068(80)
ξ_V via matching	4.250(77)	3.923(62)	4.179(38)	3.915(52)	4.028(31)

Table 8.5: *Errors for the lattice spacing anisotropy obtained as ratios of the corresponding screening masses, which are computed from their jackknife samples. The direct matching of the potentials is described in the text.*

The errors of ξ_H, ξ_W, and ξ_V are relatively large. This is caused by the fact that they are determined as ratios of masses with individual statistical errors. The jackknife errors quoted are obtained from the jackknife samples for the mass ratios themselves, and calculating the errors from the mass errors using error propagation would result in even larger error estimates. Inspired by a method found in refs. [131, 133], one can obtain even smaller errors, if ξ is directly determined by a matching of the space- and timelike secondary quantities, without any reference to the correlation lengths extracted from them afterwards. I have realized this proposal for the static potentials in space (V_{st}) and time (V_{ts}) direction. To begin with, I calculated the corresponding continuum potentials

$$V_{\mathrm{cont},ij}(R_i) \equiv V_{ij}(R_i) - C_{ij} - D_{ij} G_{ij}(M_{ij}, R_i) \,, \tag{8.30}$$

since the lattice sum I_{ij} in (8.23) is only sensible for integer R_i. Constant and lattice correction term in lowest order are found from eqs. (8.22) and (8.24) to be

$$C_{ij} + D_{ij} G_{ij}(M_{ij}, R_i) = \frac{3 g_R^2}{16\pi} \left[I_{ij}(M_{ij}, 0) - I_{ij}(M_{ij}, R_i) + \frac{1}{R_i} \, \mathrm{e}^{-M_{ij} R_i} \right] \,, \tag{8.31}$$

while solely in the subtraction step g_R^2 and $M_{ij} = a_i m_{V,ij}$ were taken from table 8.4. Hence, the matching condition reads

$$V_{\mathrm{cont},st}(R_s) = c \cdot V_{\mathrm{cont},ts}(R_t/\xi) \,, \quad \xi_V \equiv \xi \,. \tag{8.32}$$

It was fulfilled by fitting the spacelike continuum potential to a Yukawa shape $-A\,\mathrm{e}^{-mx}/x+C$ in imitation of (8.21), equating the fit function at arguments R_t/ξ with the timelike potential data times a constant, and solving every possible equation pair for ξ and c. The final ξ_V–values given in the last row of table 8.5 are averages over all such solutions along that R_i–interval, in which the two potentials have their characteristic slopes, and interchanging the rôles of $V_{\mathrm{cont},st}$ and $V_{\mathrm{cont},ts}$ in eq. (8.32) always enabled a useful cross-check. As exemplarily reflected in the perturbative simulation parameters on the larger lattice in figure 8.1, the deviation between the curves then becomes uniformly minimal in their whole range. The

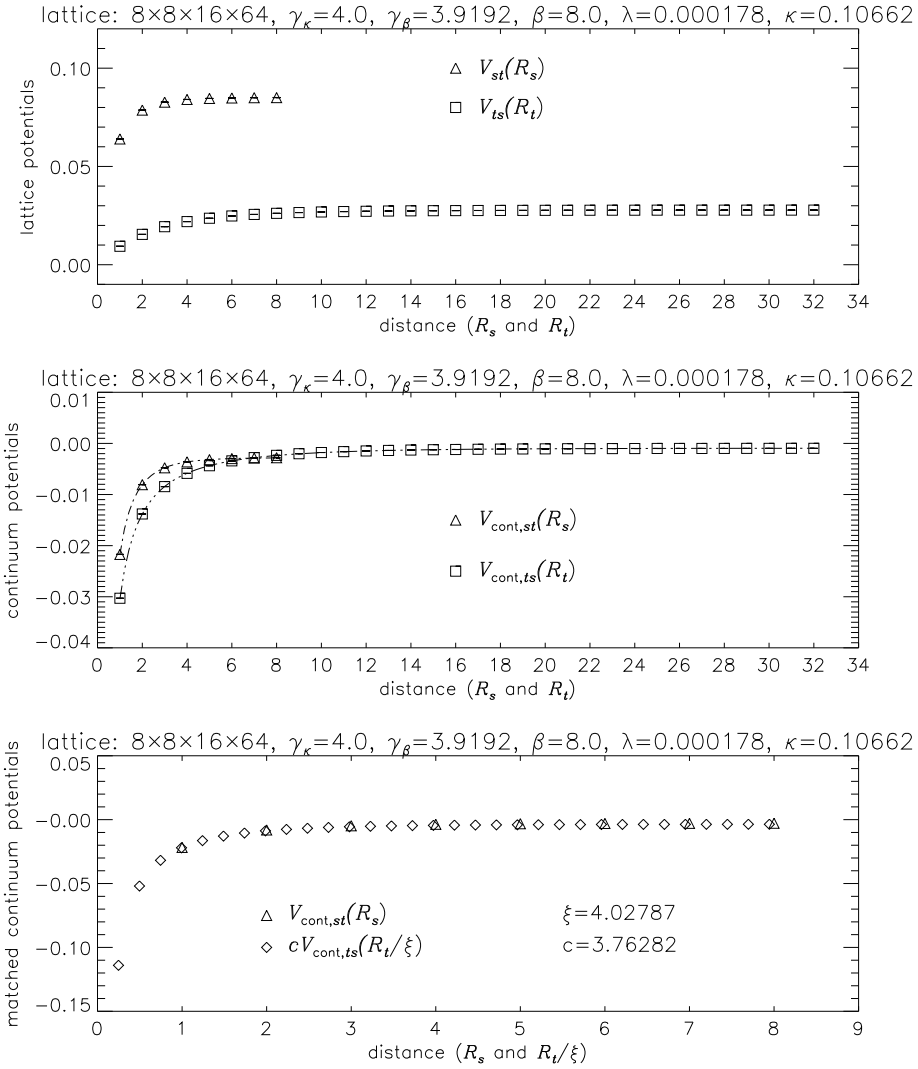

Figure 8.1: *Matching of the (properly subtracted) lattice potentials at the perturbative parameters from the larger lattice. The error bars are smaller than the symbols, and the matching condition (8.32) to restore the rotational symmetry of the static potential is perfectly met.*

lattice spacing anisotropies of this potential matching resemble the screening mass ratios,

but the errors from a repetition of this procedure with 1000 normally distributed random data are indeed smaller. Moreover, ξ_V is fully compatible with ξ_H and ξ_W in the previous subsection at the perturbative values of the coupling anisotropies.

8.2.4 Numerical results and discussion

I have determined the lattice spacing anisotropies ξ_i from Higgs ($i = H$) and gauge boson ($i = W$) correlation functions and static potentials ($i = V$) at different pairs of coupling anisotropy parameters. Since γ_κ has been held fixed, each ξ_i is looked upon as a function of γ_β, and the requirement of space-time symmetry restoration suggests the existence of a unique coupling anisotropy $\gamma_\beta^{(\mathrm{np})}$, where all ξ_i possess the same value $\xi^{(\mathrm{np})}$. This defines the non-perturbative anisotropy parameters.

Therefore, I linearly interpolate the numbers $\xi_{ij} \equiv \xi_i(\gamma_{\beta,j})$ at the three values $\gamma_{\beta,j}$ of eq. (8.15) within their errors $\Delta\xi_{ij}$ to a matching point $(\gamma_\beta^{(\mathrm{np})}, \xi^{(\mathrm{np})})$ by minimizing the sum of squares

$$\chi^2 = \sum_i \sum_j \left\{ \frac{\xi_{ij} - (\, \xi^{(\mathrm{np})} + c_i \, [\, \gamma_{\beta,j} - \gamma_\beta^{(\mathrm{np})} \,] \,)}{\Delta\xi_{ij}} \right\}^2 \tag{8.33}$$

with respect to c_i and the common fit parameters $\gamma_\beta^{(\mathrm{np})}$ and $\xi^{(\mathrm{np})}$. I obtain the final results

$$\begin{aligned} 8^2 \times 12 \times 48 : \qquad & \gamma_\beta^{(\mathrm{np})} = 3.911(43) \, , \quad \xi^{(\mathrm{np})} = 4.040(35) \\ 8^2 \times 16 \times 64 : \qquad & \gamma_\beta^{(\mathrm{np})} = 3.920(19) \, , \quad \xi^{(\mathrm{np})} = 4.040(26) \end{aligned} \tag{8.34}$$

with $\chi^2/\mathrm{dof} \simeq 1$ and statistical errors coming from 5000 normally distributed random data around the measured mean values and their variances as input. Figure 8.2 illustrates that both points agree with the simulated ξ_i at the perturbative γ_β–value as well as with the perturbative point itself, and finite-size effects appear to be remarkably small. It remains to be mentioned that (8.34) includes the ξ_V–values — which incidentally were not available at $\gamma_\beta = 3.919$ for the smaller lattice — from the matching of the potentials. Using for each point the weighted averages of the two screening mass ratios in table 8.5 instead, I get the similar results $\gamma_\beta^{(\mathrm{np})} = 3.921(38)$, $\xi^{(\mathrm{np})} = 4.038(29)$, and $\gamma_\beta^{(\mathrm{np})} = 3.921(19)$, $\xi^{(\mathrm{np})} = 4.038(26)$, respectively.

All estimates signal a perfect confirmation of the perturbative results $\gamma_\beta^{(\mathrm{p})} = 3.919$ and $\xi^{(\mathrm{p})} = 4.052$ as quoted in eq. (8.11) of the first section of this chapter and calculated in refs. [138, 140, 141]. There is no evidence that the unknown higher-order corrections in g^2 and λ could lead to any visible modifications, which would make the applicability of one-loop perturbation theory to the anisotropy parameters doubtful. In conclusion, the non-perturbative contributions can not be resolved within the intrinsic errors of numerical simulations, and as a consequence, the perturbative choice of the anisotropy parameters in investigations with the anisotropic SU(2)-Higgs model, also for Higgs masses $m_H \gtrsim 80$ GeV, is justified.

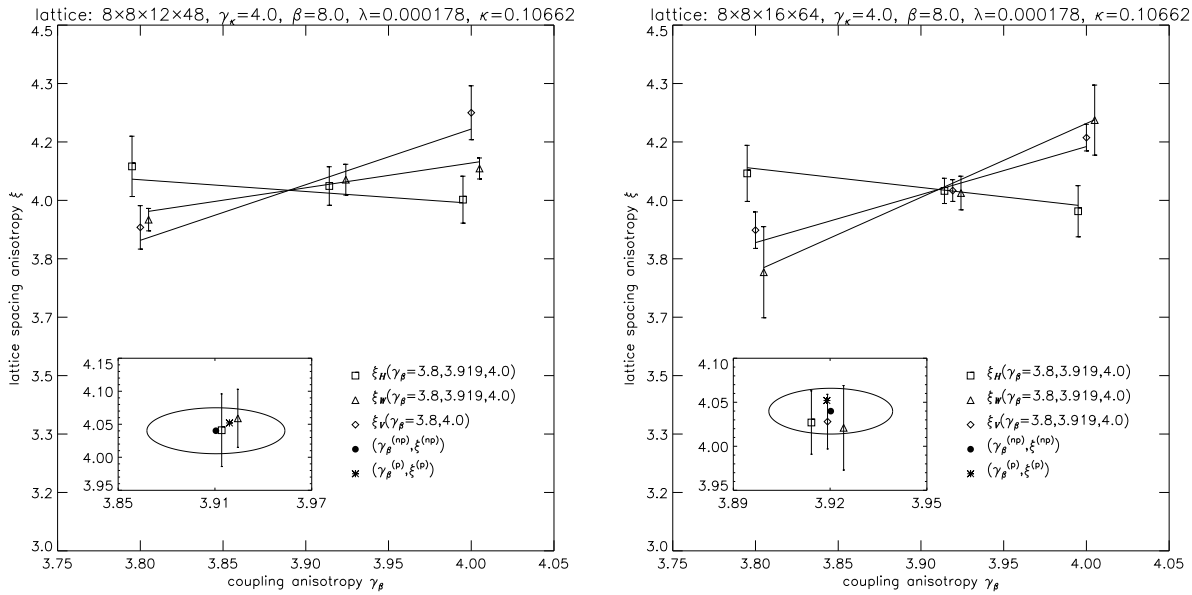

Figure 8.2: *Final ξ–evaluation for both lattices from the three simulation points, whose equal abscissas are slightly displaced for better visualization. The inserts show the average matching points and its error ellipses, which enclose both the numerical estimates at $\gamma_\beta =$ 3.919 and the perturbative result.*

8.3 Conclusion

In summary, performing numerical simulations, I have found strong evidence that the perturbative coupling asymmetries of the SU(2)–Higgs model on lattices with anisotropic lattice spacings, which were determined in one-loop lattice perturbation theory in ref. [138], do not change appreciably, i.e. non-perturbative effects are small. In fact, rotational symmetry is restored within the MC errors using the perturbative anisotropies both in the Higgs and W–masses computed from time and space correlation functions. I have also investigated space-time and space-space Wilson loops and obtained the appropriate scaling behaviour of the static potential in space and time directions.

The results show that for the physically interesting range of couplings, perturbative results on the coupling anisotropies may be taken to coincide with their non-perturbatively determined counterparts. Thus studying the phase transition on lattices with anisotropic lattice spacings is straightforward, the coupling anisotropies are known, and the one-loop perturbative approach to these parameters seems to be satisfactory. This opens the possibility to simulate the SU(2)–Higgs model for Higgs masses around and above 80 GeV, as it has been done in the last chapter of this work.

Chapter 9

Simulations on anisotropic lattices

Now, as the study of the four-dimensional SU(2)–Higgs model and its thermodynamics on anisotropic lattices are well defined and completely controllable, I arrive at the numerical results on the EWPT from finite-temperature simulations on such lattices. As pointed out several times before, the main goal of the anisotropic lattice regularization it to reach interesting Higgs boson masses of the physical reality around $m_H \simeq 80$ GeV, using practicable lattice sizes and moderate computer resources to analyze the phase transition.

In this context I report on the interface tension at a relatively rough lattice resolution of $a_t^{-1} = 2T_c$. Owing to the still quite large volumes, which are necessary to infer the character of the transition, it has been determined by the — quite robust and economic — two-coupling method. All results will confirm the picture of a very weak first order EWPT for this large Higgs mass value, which may be already considered as a strong indication against electroweak baryogenesis scenarios within the minimal standard model.

At an earlier stage of my investigations, in order to establish the anisotropic lattice approach and gain experience with its applicability to the present model, I also reproduced some of its known properties at low and medium Higgs boson masses, which I want to summarize first. Hence, the underlying numerical simulations were rather meant as a generic scan over the possibilities than as a thorough high statistics study.

9.1 Some tests and qualitative observations

The general intention of this exploratory study of the finite-temperature SU(2)–Higgs model on anisotropic lattices was to verify some typical signals of a first order phase transition, for instance two-peak structures and hysteresis patterns, at different Higgs boson masses. With the knowledge of suitable values for the lattice parameters in the isotropic case [135, 136, 137] it was straightforward to estimate, by using eqs. (5.20) – (5.25) in section 5.1 of chapter 5, just those sets of anisotropic lattice parameters, to which some given Higgs mass approximately

corresponds.

The MC simulations were always started in the perturbative predictions for the critical hopping parameter. These are obtainable from the one-loop effective potential as outlined in subsection 6.1.1 of chapter 6. E.g. for a parameter point with tree-level anisotropies $\gamma_\kappa = \gamma_\beta = \xi = 2.0$ and $m_H \simeq 20$ GeV ($\beta = 8.0$, $\lambda = 0.00005$, $R_{HW,0} = 0.27$) this gives $\kappa_c^{(\mathrm{p})} = 0.14622$ for the transition point, in which the typical jump of an order parameter like ρ^2, L_φ, or the action density s happens. At the particularly convenient value $\gamma_\kappa = \gamma_\beta = \xi = 4.0$ and $m_H \simeq 35$ GeV ($\beta = 8.0$, $\lambda = 0.00005068$, $R_{HW,0} = 0.53$) a similar calculation yields $\kappa_c^{(\mathrm{p})} = 0.10702$. Then a non-perturbative fine-tuning in κ was carried out to search for long living metastable phases in coexistence in form of two-peak structures in distributions (histograms) of different observables. As illustrated in figure 9.1, the smallest volumes, where this could be achieved, were $2 \times 2^2 \times 4$ and $2 \times 4^2 \times 32$ lattices, respectively, resulting in $\kappa_c \simeq 0.14620$ and $\kappa_c \simeq 0.10709$. Both diagrams exhibit nice two-state signals in

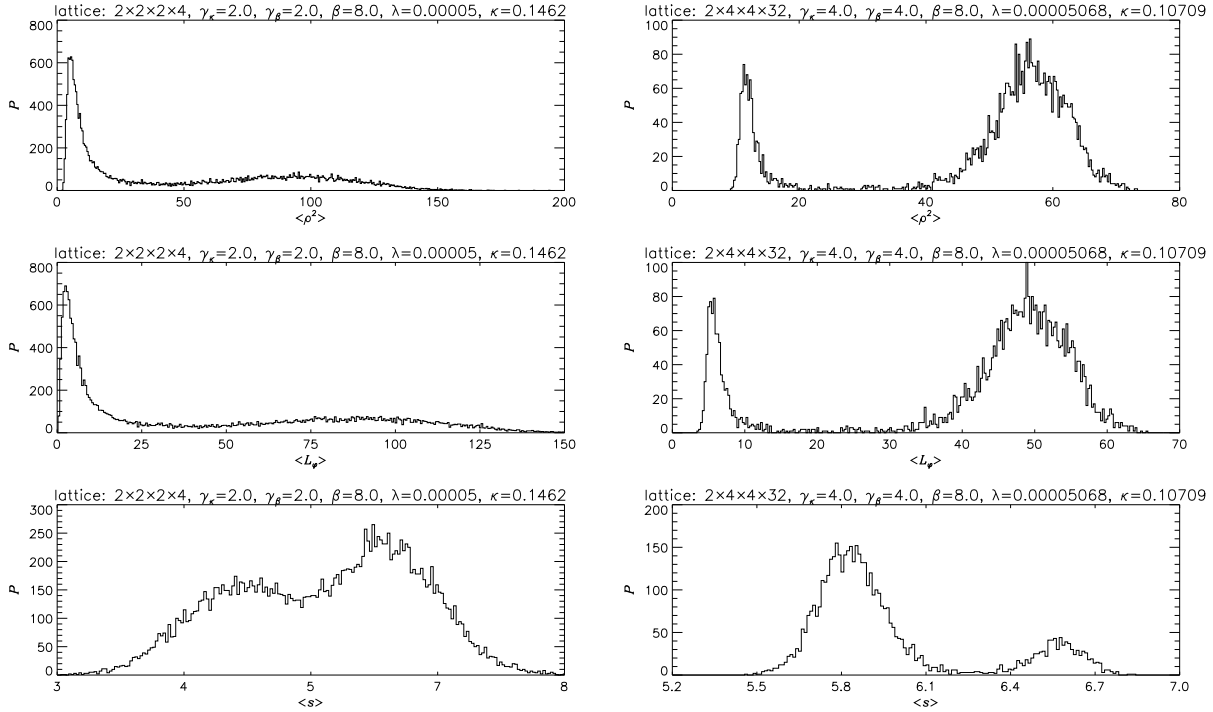

Figure 9.1: *Typical two-peak structures in the probability distributions of some order parameters from simulations in $\kappa \simeq \kappa_c$ on anisotropic lattices. The chosen parameters correspond to $m_H \simeq 20$ GeV (left: 20000 sweeps), $m_H \simeq 35$ GeV (right: 5000 sweeps), and the tree-level relation $\gamma_\kappa = \gamma_\beta = \xi$ has been assumed. The sharp maximum on the left corresponds to the symmetric phase, the broader one on the right to the Higgs phase of broken symmetry.*

the histograms of the order parameters considered, which is in complete agreement with the expectation that for these Higgs mass values the relatively strong first order nature of the phase transition should already be observable on small or medium-sized lattices.

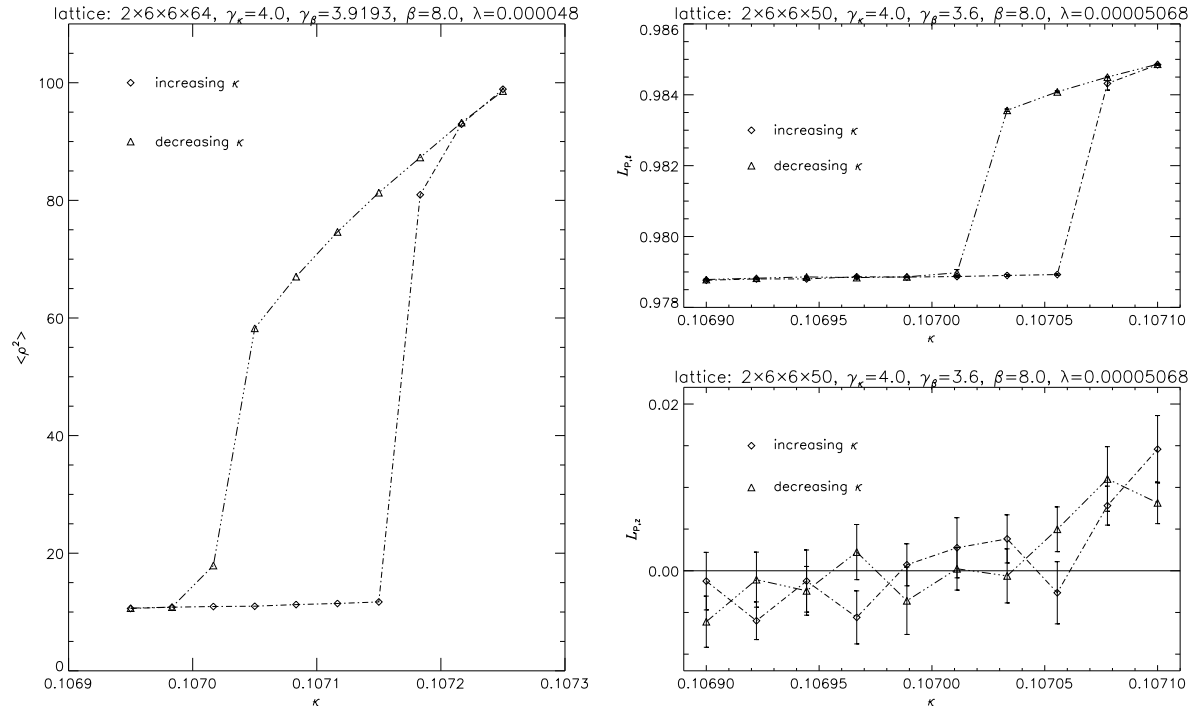

Figure 9.2: *Thermal cycles for the Higgs condensate $\langle\rho^2\rangle$ (left: 100 warmup and 250 measurement sweeps) and the Polyakov loops $L_{P,t}$ and $L_{P,z}$ in t– and z– directions, respectively (right: 500 warmup and 4000 measurement sweeps), both at $m_H \simeq 35$ GeV. An interpretation for the latter is given in the text.*

Again for $m_H \simeq 35$, but this time at slightly different values for the coupling anisotropies, hysteresis patterns developed too, see figure 9.2. To comment the right diagram in more detail, I should mention that the Polyakov lines in t– and z–directions have been calculated in temporal gauge as the Wilson loops before (i.e. $A_4^r(x) = 0 \Leftrightarrow U_{x,4} = \mathbf{1}_{2\otimes 2}$, or $A_3^r(x) = 0 \Leftrightarrow U_{x,3} = \mathbf{1}_{2\otimes 2}$ for the spacelike sublattice). In this gauge they simply equal the expectation value of the last, non-unit link in t– and z–direction. Since the Polyakov loop enjoys the property to be an order parameter for the confinement-deconfinement phase transition, see section 5.1.1 of chapter 5 or ref. [17, 19], a natural explanation for the observed shapes of the time- and spacelike Polyakov lines $L_{\mathrm{P},t}$ and $L_{\mathrm{P,z}}$ in dependence of κ is the following. The system at finite temperature is always in the deconfinement phase ($|L_{\mathrm{P},t}| > 0$), showing the usual hysteresis effect around the transition region, whereas within the zero-temperature spatial sublattice of extensions $6^2 \times 50$ a transition between confinement behaviour ($|L_{\mathrm{P,z}}| = 0$) in the symmetric phase and deconfinement behaviour ($|L_{\mathrm{P,z}}| > 0$) in the Higgs phase takes place.

As an exemplary quantitative check, I also redetermined the interface tension with the two-coupling method for $m_H \simeq 35$ GeV. In accordance with the isotropic simulation parameters of the analogous analysis in section 7.2 of chapter 7 and ref. [136], the interface tension

could be resolved on a $2 \times 6^2 \times 50$ lattice with tree-level coupling ratios $\gamma_\kappa = \gamma_\beta = \xi = 4.0$ at $\beta = 8.0$ and $\lambda = 0.00005068$. Using six κ–pairs in the range $\kappa = (0.106840, 0.107340)$ to $\kappa = (0.107040, 0.107140)$ symmetrically around the critical one with a statistic of at least 20000 sweeps each, I obtained from a four-parameter least-squares fit (with $\chi^2 = 0.31$ and a statistical error from 1000 normally distributed random data) of the measured expectation values of the φ–link difference $\Delta L_\varphi(\kappa_1, \kappa_2)$ to the Laurent ansatz (6.31) the result

$$\kappa_c = 0.10709(1) : \quad \left(\frac{\hat{\sigma}}{T_c^3}\right)_{\Delta L_\varphi} = 0.083(22)\,. \tag{9.1}$$

In fact, this number is in fairly good agreement with the estimate $\hat{\sigma}/T_c^3 = 0.065(10)$, which was found for the case of an isotropic lattices.

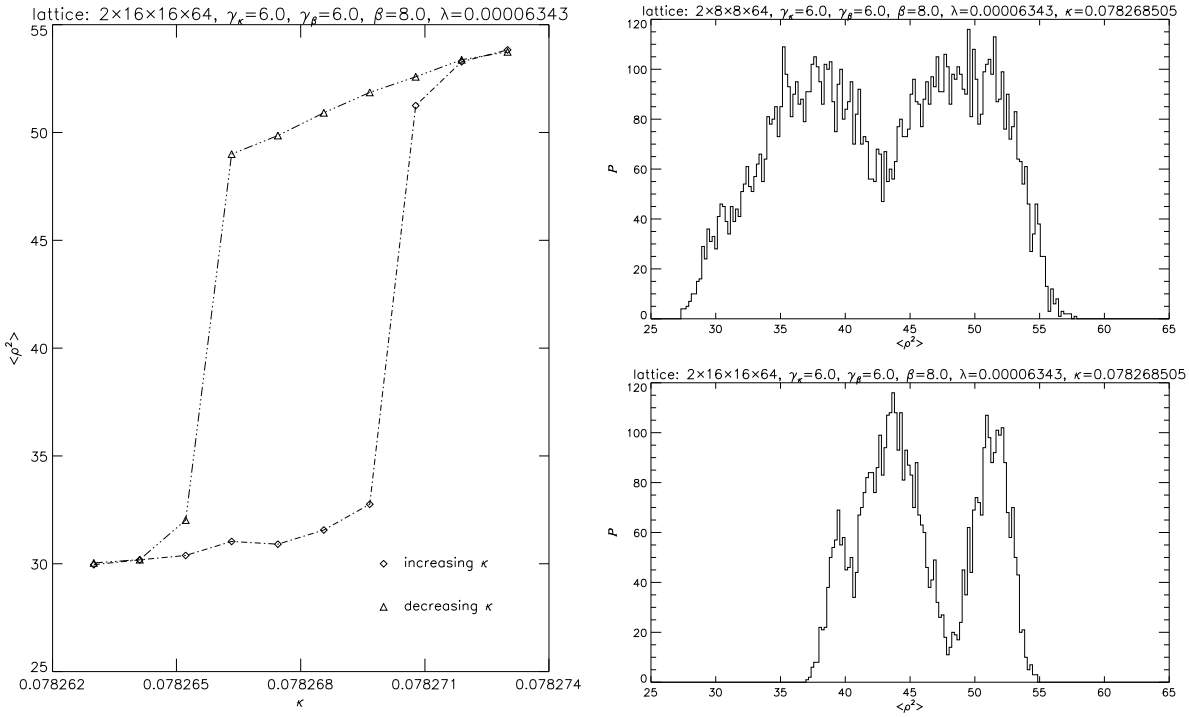

Figure 9.3: *Hysteresis (left: 500 warmup and 2500 measurement sweeps) and two-peak histograms (right: 10000 and 5000 sweeps, respectively) of* $\langle\rho^2\rangle$. *The lattice parameters and tree-level anisotropies* $\gamma_\kappa = \gamma_\beta = \xi = 6.0$ *lead to a bare Higgs to vector boson mass ratio of* $R_{HW,0} \simeq 1$, *see eq. (5.27) or (8.14), i.e.* $m_H \simeq 80$ *GeV.*

In expectation of an extremely weak first order EWPT in the experimentally relevant Higgs mass regime of $m_H \simeq 80$ GeV [120, 121, 135, 149], much larger physical volumes will be necessary to analyze the transition there. When choosing the tree-level anisotropies $\gamma_\kappa = \gamma_\beta = \xi = 6.0$ together with $m_H \simeq 80$ GeV ($\beta = 8.0$, $\lambda = 0.00006343$, $R_{HW,0} = 1.00$) and adjusting the scalar hopping parameter κ appropriately, clear two-peak structures and a hysteresis appeared in the expectation value of the Higgs condensate ρ^2, both depicted in

figure 9.3. As the two-state signal in $\kappa \simeq \kappa_c$ persists for increasing spatial lattice size, is seems unambiguous that the metastability in the system with sufficiently large tunneling rate and mixed states — hinting at a first order character of the phase transition — is actually inherent at these parameters and not an artifact of the finite volume.

In the next section I will calculate the interface tension at those bare parameters, which were already used in the $T = 0$ simulations of the previous chapter, besides a small variation in λ to ensure $m_H = 80$ GeV within errors. Thus one has $\xi = 4.0$, the perturbative values for the coupling anisotropies, and a pole mass of $m_H = 78(4)$ GeV ($\beta = 8.0$, $\lambda = 0.000192$, $\kappa = 0.107791$, $R_{HW,0} = 1.03$). The required lattice sizes employed in figure 9.4 to resolve the transition and its interface tension later were $2 \times 24^2 \times 192$ and $2 \times 32^2 \times 288$. In

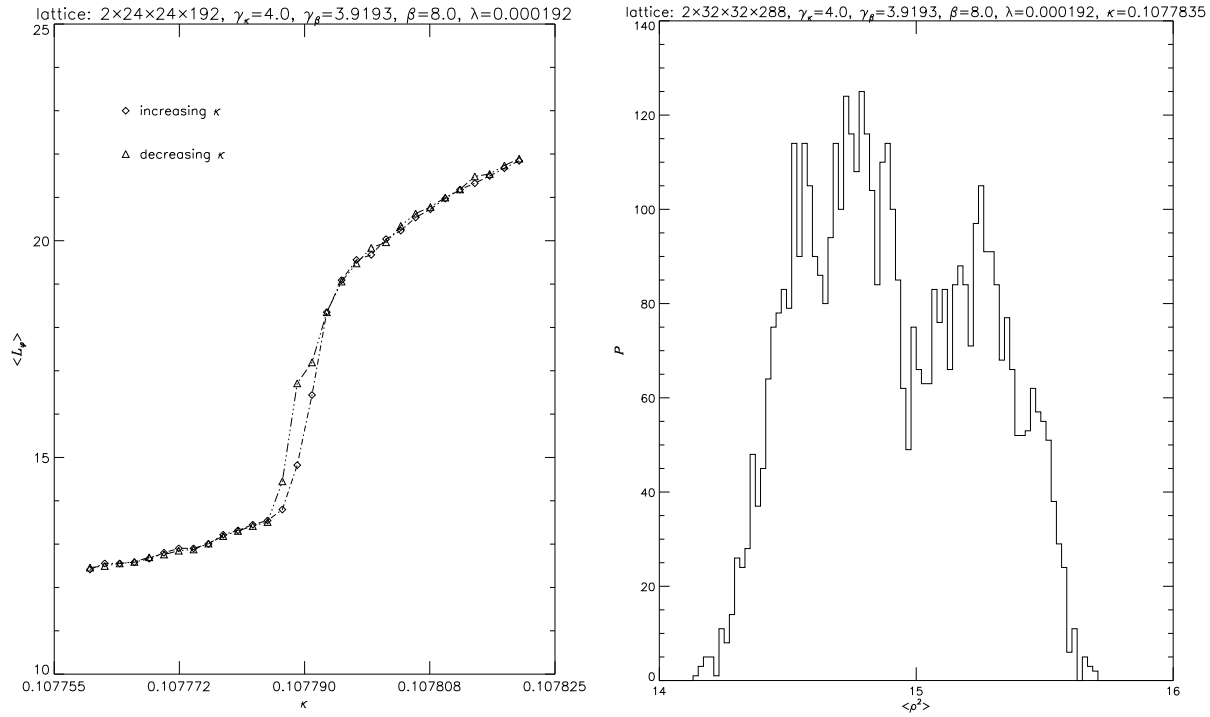

Figure 9.4: *Hysteresis of $\langle L_\varphi \rangle$ (left: 250 warmup and 500 measurement sweeps) and a two-peak histogram (right: 2500 sweeps) of $\langle \rho^2 \rangle$ on lattices of different sizes. For the coupling anisotropies I used the perturbative values of the previous chapter, and the physical pole mass of the Higgs boson at these parameters comes out to be $m_H = 78(4)$ GeV.*

the left diagram a strong increase of the expectation value of the order parameter L_φ can be detected, and a slight hysteresis effect is preserved, even outside the statistical errors, which are suppressed in the plot for reasons of pictorial simplification. But compared to the hysteresis at $m_H \simeq 35$ GeV in the left plot of figure 9.2, the jump of the order parameter is significantly smaller now. Note that the exact position (9.2) of the critical hopping parameter κ_c obtained with the two-coupling method below lies inside the open domain of the hysteresis as it should be. Finally, as reflected in the right diagram of figure 9.4, metastability does also

hold in the critical hopping parameter (9.3) of the larger lattice. Here the order parameter distribution consists of two overlapping ρ^2–histograms, which were generated by simulating the system in $\kappa = \kappa_c$ on configurations equilibrated deep in the symmetric and Higgs phase, respectively.

All these qualitative features reveal that, at least as far as $L_t = 2$ is concerned, the first order nature of the phase transition for $m_H \simeq 80$ GeV is still visible, although the characteristic signals in the order parameters under inspection have become less pronounced, and the strength of the transition has weakened substantially. This hypothesis is corroborated further by the quantitative analysis presented immediately.

9.2 Critical κ and interface tension for $m_H \simeq 80$ GeV

A sensible determination of the interface tension σ from simulation results at such a large value of the Higgs boson mass is supplied by the two-coupling method [162, 135, 136, 139]. I have applied this method again, because it has been argued in chapter 6 to be under the actual computer (i.e. memory and time) restrictions the sole one, at least within the four-dimensional model, which is supposed to work well also in the case of an extremely weak first order phase transition, one is confronted with here. As outlined in subsection 6.2.3, the generalization of the two-coupling method to a situation with anisotropic lattices is straightforward.

Based on the findings of chapter 8, where the one-loop quantum corrections to the anisotropy parameters have been confirmed non-perturbatively in this parameter region, I declare that the rotational symmetry of the asymmetric lattice is restored through the perturbative choice $\gamma_\kappa = 4.0$ and $\gamma_\beta = 3.9193$ for the coupling anisotropies. The related tiny shift in the lattice spacing anisotropy $\xi = a_s/a_t$, possibly entering the final expressions for physical quantities in lattice units, is then neglected as an higher-order effect; I always assume $\xi = 4.0$ in the following. The other bare parameters are $\beta = 8.0$ and $\lambda = 0.000192$, and the lattice size under study is $2 \times 24^2 \times 192$. After measuring on a $T = 0$ lattice of size $8^2 \times 16 \times 64$ at $\kappa = \kappa_c = 0.107791$ the timeslice correlation functions in the Higgs and vector channel together with the Wilson loops needed to compute the static potential, the non-perturbatively renormalized quantities come out in the standard manner as $R_{HW} = 0.975(50)$ and $g_R^2 = 0.539(16)$. The former corresponds to a physical pole mass of $m_H = 78(4)$ GeV and does also include an estimation of the uncertainty in κ_c from additional simulations in $\kappa = \kappa_c \pm 0.000005$ around the critical hopping parameter of eq. (9.2). At the same time this gives $T_c/m_H = 1/a_t m_{H,t} L_t = 1.884(47)$ for the dimensionless ratio of the critical temperature to the Higgs mass, which will be commented in the discussion of the results later.

According to eq. (6.8) I have different hopping parameters $\kappa = (\kappa_1, \kappa_2)$ in the two halves along the z–direction, while in the light of eqs. (5.24) and (5.25) in section 5.1,

the corresponding space- and timelike couplings are now to be deduced from the coupling anisotropy γ_κ as $\kappa_{1s} = \kappa_1/\gamma_\kappa, \kappa_{1t} = \kappa_1\gamma_\kappa$ and $\kappa_{2s} = \kappa_2/\gamma_\kappa, \kappa_{2t} = \kappa_2\gamma_\kappa$. For a properly chosen initial κ–interval, which brings the symmetric and the broken phases in thermal contact, a pair of interfaces spans through the lattice, and, as illustrated in figure 9.8, the usual procedure of gradually shrinking its width resulted in the estimate

$$\kappa_c = 0.107791(3) \tag{9.2}$$

for the critical hopping parameter. In figure 9.5 I show typical two-phase distributions of z–slices for the φ–link expectation value $L_\varphi(\mathrm{z})$, defined in subsection 6.1.4 of chapter 6. An

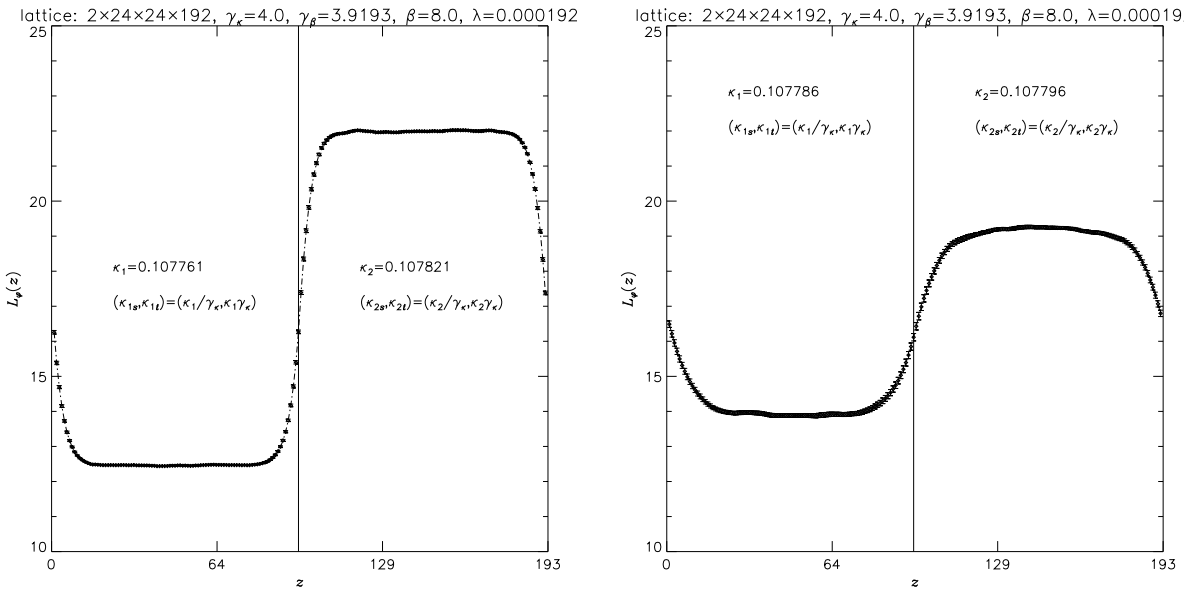

Figure 9.5: *Two-phase profiles of the z–slice expectation value $L_\varphi(z)$ of L_φ for the largest and smallest κ–intervals on the $2 \times 24^2 \times 192$ lattice.*

interface pair has developed, and the plateaus marking the pure-phase expectation values $L_\varphi^{(i)}(\kappa_1, \kappa_2)$, $i = 1, 2$, are flat and broad enough to ascertain that the coexisting phases are stable against any turn-over into the other phase. The integrated autocorrelation times in sweeps for these simulation points, which were calculated from the full data samples of $L_\varphi^{(i)}$–measurements as described in section A.3 of appendix A, range from $\tau_{\mathrm{int}}[L_\varphi^{(1)}] = 22(1), \tau_{\mathrm{int}}[L_\varphi^{(2)}] = 18(2)$ to $\tau_{\mathrm{int}}[L_\varphi^{(1)}] = 159(17), \tau_{\mathrm{int}}[L_\varphi^{(2)}] = 93(17)$, and from $\tau_{\mathrm{int}}[\Delta L_\varphi] = 14(1)$ to $\tau_{\mathrm{int}}[\Delta L_\varphi] = 113(12)$ for the difference $\Delta L_\varphi = L_\varphi^{(2)} - L_\varphi^{(1)}$ of these quantities[1].

As a check for possible finite-volume effects I also produced some data on a larger lattice of size $2 \times 32^2 \times 288$ at otherwise unchanged parameters and couplings, where a lower statistic was sufficient to attain trustworthy expectation values and absolute errors of roughly the

[1]The statistical errors of the integrated autocorrelation times emerged from a jackknife analysis with 25 samples.

same precision. In this case the two-coupling estimate for the critical point in κ_c is

$$\kappa_c = 0.1077835(25)\,. \tag{9.3}$$

All simulation data, which were gathered in $\kappa = (\kappa_1, \kappa_2)$ centred symmetrically around κ_c for the determination of the interface tension σ from these two lattices, are listed in table 9.1. Compared to the previous analyses on isotropic lattices for stronger first order

κ_1	κ_2	sweeps	$L_\varphi^{(1)}$	$L_\varphi^{(2)}$	ΔL_φ
0.107761	0.107821	40000	*12.7856(73)*	*21.5913(92)*	8.8057(90)
0.107766	0.107816	40000	12.944(11)	21.1656(99)	8.2217(95)
0.107771	0.107811	60000	13.1186(89)	20.7117(90)	7.593(11)
0.107776	0.107806	60000	13.3410(90)	20.215(13)	6.874(12)
0.107781	0.107801	70000	13.711(15)	19.599(16)	5.888(20)
0.107786	0.107796	80000	14.316(39)	18.773(25)	4.457(37)
0.107757	0.107810	10000	12.6839(58)	21.146(12)	8.462(13)
0.107762	0.107805	10000	12.8446(97)	20.708(11)	7.863(13)
0.107767	0.107800	10000	13.026(12)	20.194(19)	7.168(20)
0.107772	0.107795	10000	13.293(17)	19.592(25)	6.299(23)
0.107777	0.107790	10000	13.620(20)	18.752(33)	5.132(31)
0.107780	0.107787	5000	14.075(46)	18.107(54)	4.032(72)

Table 9.1: *Results for $L_\varphi^{(1)}$, $L_\varphi^{(2)}$, and ΔL_φ on the two lattices of sizes $2 \times 24^2 \times 192$ (upper data) and $2 \times 32^2 \times 288$ (lower data). The errors are obtained by binning as before. In order to obtain acceptable χ^2–values, the entries in italics were only omitted for the individual fits of $L_\varphi^{(i)}$ in each phase.*

transitions at lower Higgs masses, the κ–intervals have now been chosen closer to each other and to κ_c as well, while it was ever verified that — as e.g. in figure 9.5 — the distinct phases were well separated by a pair of interfaces and that no tunneling into the other phase had occurred. The reason is that for a very weak transition, as encountered at these lattice parameters, the diverging of the $L_\varphi^{(i)}(\kappa_1, \kappa_2)$, $i = 1, 2$, when κ_1 and κ_2 approach κ_c from below and above, respectively, sets in later and will be far less violent than for $m_H \lesssim 50$ GeV. Therefore, the curvatures in the shapes of the two φ–links as functions of κ and particularly their residua, which in view of the Laurent ansätze (9.4) determine the interface tension, should be modelled more accurately in the present case.

The interface tension can be computed once more along the recipe of formulas (6.30) – (6.33) from subsection 6.2.3, including the obvious modifications in the anisotropic lattice case,

$$a_s^2 a_t \sigma \;=\; \frac{1}{2} \lim_{\kappa_2 \searrow \kappa_c} \lim_{\kappa_1 \nearrow \kappa_c} \left\{ (\kappa_1 - \kappa_2) \lim_{L_z \to \infty} L_z \cdot \Delta L_\varphi(\kappa_1, \kappa_2) \right\}$$

$$\begin{aligned} L_\varphi^{(i)}(\kappa_1,\kappa_2) &= -\frac{c_i}{\kappa_i-\kappa_c}+\gamma_i^{(0)}+\gamma_i^{(1)}(\kappa_i-\kappa_c)+\gamma_i^{(2)}(\kappa_i-\kappa_c)^2+\gamma_i^{(3)}(\kappa_i-\kappa_c)^3 \\ &\quad +\mathcal{O}\left((\Delta\kappa)^4\right)\,, \quad i=1,2 \\ a_s^2 a_t\hat{\sigma} &= L_z\,(c_1+c_2)\,, \quad \frac{1}{T_c}=a_t L_t\,, \quad \xi=\frac{a_s}{a_t}\,, \end{aligned} \tag{9.4}$$

with the difference of φ–links $\Delta L_\varphi(\kappa_1,\kappa_2) = L_\varphi^{(2)}(\kappa_1,\kappa_2) - L_\varphi^{(1)}(\kappa_1,\kappa_2)$, appropriately weighted with the coupling anisotropies according to eq. (6.24), and $\Delta\kappa = |\kappa_i - \kappa_c|$. In the spirit of the analyses on isotropic lattices in the previous chapter and refs. [136, 139], one can fit the two φ–links $L_\varphi^{(i)}$, $i=1,2$, to this ansatz individually, or their difference ΔL_φ as well. Generically, the second alternative should be preferred, and the reason is twofold: Owing to presumably large fluctuations in the positions of the interfaces, one has to account for correlations between the competing phases, which do reflect again in the autocorrelation times found above, and especially as the phase transition weakens with increasing Higgs mass, a roughening of the interfaces is to be expected. Both effects, which are not strictly distinguishable at all, are presumed to compensate to some amount, if the φ–link difference is considered.

Consequently, I carefully examined nearly all types of fits from three- to six-parametric in the Laurent ansätze of (9.4) for the two kinds of observables $L_\varphi^{(i)}$ and ΔL_φ and for every allowed fit intervals, which could be built up from the data in table 9.1 under disposal. In part, the results on σ depended on the choice of the specific fit interval and on the number of fit parameters too. Moreover, one could become aware that in most cases reasonable values of χ^2/dof were connected with those fits, which also included the narrowest κ–pair; so I will quote only the results from such fits meeting these two constraints. The three-parameter fits to the Laurent ansätze could never be trusted, since they showed the strongest dependence on the number of fitted data points and gave always incredibly large χ^2–values. The situation is much better for fits, which supplement the inverse-linear part of the general ansatz in eq. (9.4) with a fourth or a fifth fit parameter. Then the fits are acceptable throughout with tolerable χ^2/dof and can readily be extended over almost the whole range of κ–pairs. In order to control the relevance of a further degree of freedom, I also performed some fits with an additional parameter as the coefficient of a term in the ansätze, which is of higher power in $\kappa_i - \kappa_c$. This gave either doubtlessly too large (or even too small) values of χ^2/dof, or the error analysis of these fits led to very high statistical errors for the new fit parameters — and sometimes for c_i and $c' = 2(c_1+c_2)$ as well — assuring that they could not be resolved reliably.

To be more concrete now, the evaluation of the data set from the $2\times 24^2\times 192$ lattice using a four-parameter least-squares fit for $L_\varphi^{(i)}$, and a five-parameter least-squares fit for ΔL_φ yields

$$\left(\frac{\hat{\sigma}}{T_c^3}\right)_{L_\varphi} = 0.00060(8+22)\,, \quad \left(\frac{\hat{\sigma}}{T_c^3}\right)_{\Delta L_\varphi} = 0.00029(12)\,, \tag{9.5}$$

with $\chi^2_1 = 2.59, \chi^2_2 = 0.96$ for the former and $\chi^2 = 1.41$ for the latter. The quoted error on the $L^{(i)}_\varphi$–fits incorporates the statistical error from a bootstrap analysis (see section B.1.2 in appendix B) with 10000 bootstrap samples and the uncertainty of κ_c too, whereas the error on the result from the ΔL_φ–fit was obtained by repeating it with 1000 normally distributed random data around the measured mean values as input. These fits are displayed in figures 9.6 and 9.7. Since the downward (upward) variation of the coefficients c_i entering

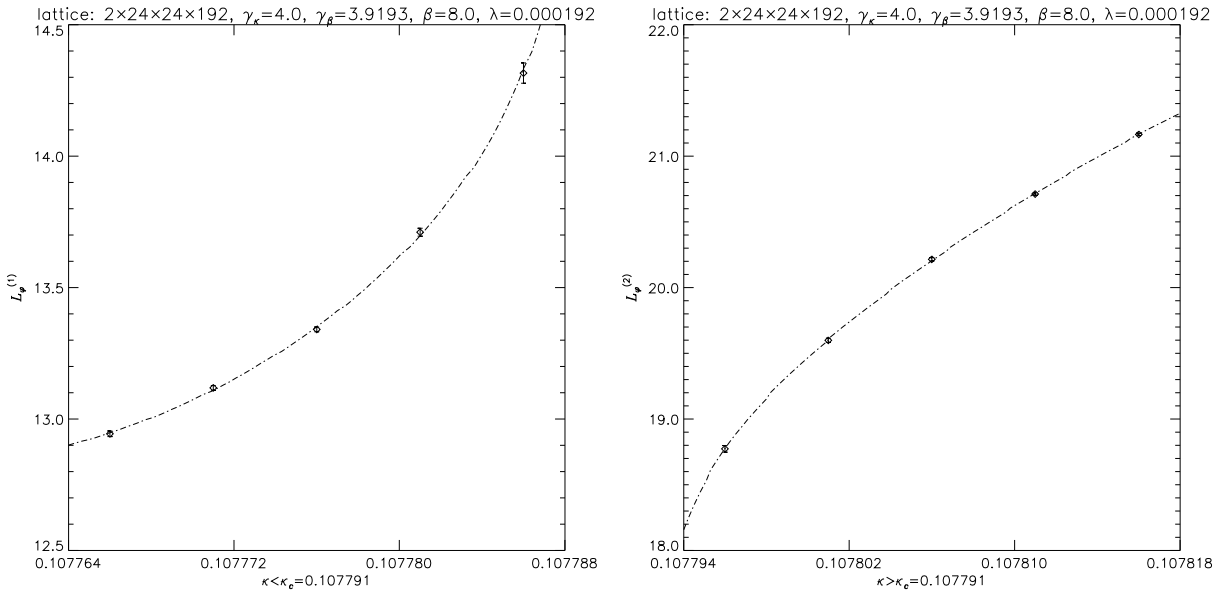

Figure 9.6: *Four-parameter least-squares fits of* $L^{(i)}_\varphi$, $i = 1, 2$, *separately in each phase. The* χ^2*–values are* $\chi^2_1 = 2.59$ *and* $\chi^2_2 = 0.96$, *respectively.*

$\hat{\sigma}/T_c^3$ in (9.4), caused by the κ_c–uncertainty in the $L^{(i)}_\varphi$–fits, is permanently dominated by the φ–link fit of that phase, which $\kappa_c \pm \Delta\kappa_c$ draws nearer (from which $\kappa_c \pm \Delta\kappa_c$ withdraws), it was combined with the c_i from the original fit of the other φ–link with respect to κ_c and vice versa. The results of those combined fits were taken to estimate the influence of the κ_c–uncertainty on the interface tension, i.e. the second entry in parentheses on the left hand side of eq. (9.5).

A four-parameter fit of the data in all six κ–pairs in the upper half of table 9.1 gives $\hat{\sigma}/T_c^3 = 0.00074$ with $\chi^2_1 = 5.84$ and $\chi^2_2 = 1.78$, which appears to be too large for the φ–link $L^{(1)}_\varphi$ in the symmetric phase. The result on $\hat{\sigma}/T_c^3$ from the $L^{(i)}_\varphi$–fits is twice as large as that from the fit of ΔL_φ, although both are just compatible inside their errors. Assuming for ΔL_φ also a four-parameter fit with the first data point of table 9.1 omitted as it has been done for the $L^{(i)}_\varphi$–fits, I find $\hat{\sigma}/T_c^3 = 0.00060$, but with a worse χ^2–value of 4.55. By the way, two separate fits of $L^{(i)}_\varphi$ with five parameters as for ΔL_φ have $\hat{\sigma}/T_c^3 = 0.00027$ and $\chi^2_1 = 0.60, \chi^2_2 = 0.36$ so that there seems to be no systematic discrepancy.

After an analogous evaluation of the data set from the $2 \times 32^2 \times 288$ lattice, one arrives

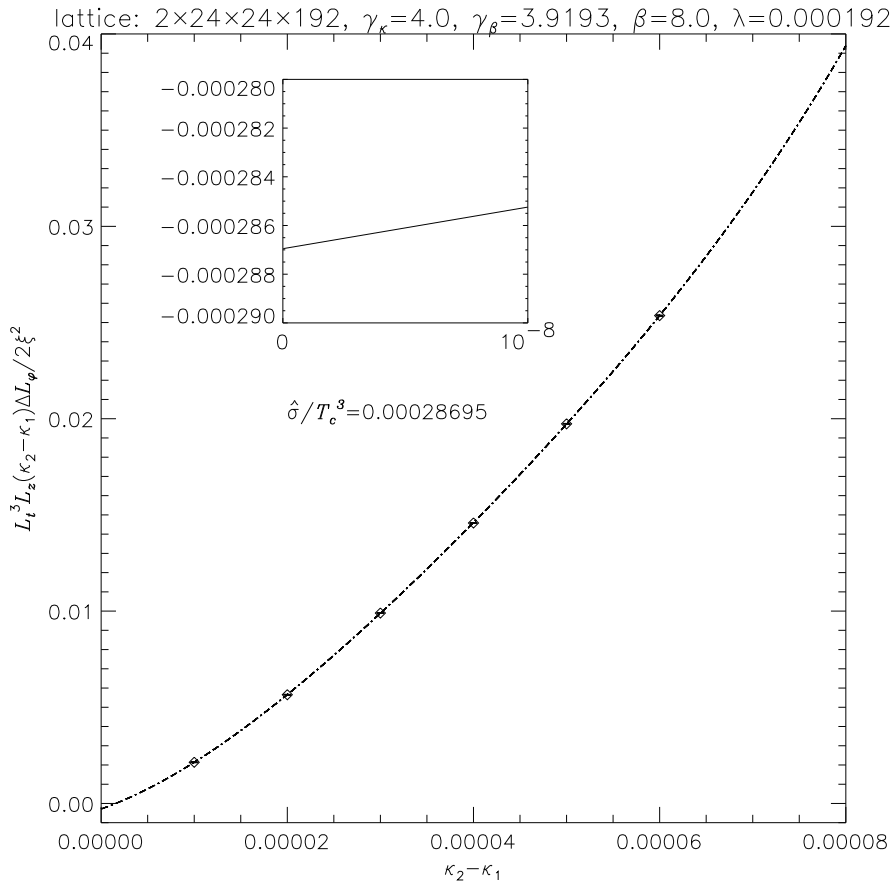

Figure 9.7: *Four-parameter least-squares fit of ΔL_φ as a function of $\kappa_2 - \kappa_1$ with $\chi^2 = 1.41$. The extrapolation to $\kappa_2 - \kappa_1 = 0$ gives the interface tension.*

at

$$\left(\frac{\hat{\sigma}}{T_c^3}\right)_{L_\varphi} = 0.00062(10+25)\,, \quad \left(\frac{\hat{\sigma}}{T_c^3}\right)_{\Delta L_\varphi} = 0.00063(8)\,, \tag{9.6}$$

which does not deviate significantly from the results for the smaller lattice. Here, I performed four-parameter fits for both observables $L_\varphi^{(i)}$ and ΔL_φ, with χ^2–values of 1.96, 2.13 and 1.06, respectively. Omitting the first data point in the lower half of table 9.1 as in the $L_\varphi^{(i)}$–fits before, one gets $\hat{\sigma}/T_c^3 = 0.00053$ with $\chi_1^2 = 1.95$ and $\chi_2^2 = 1.19$, which is in fairly good harmony with the other estimates.

Since $\hat{\sigma}/T_c^3$ obtained in these different ways covers a quite wide range, I average the numbers of eqs. (9.5) and (9.6) to a unified estimate and take their absolute spread including the errors as a measure for the sum of statistical and systematic uncertainties. The final result is

$$\left(\frac{\hat{\sigma}}{T_c^3}\right)^{\text{all}}_{2-\kappa} = 0.0006(4)\,. \tag{9.7}$$

While the size of the relative diminution of κ_c when going to larger physical volumes is consistent with the experiences made in [135] on isotropic lattices, the agreement of the

different two-coupling estimates underlines that — within the admittedly rather large errors dominated by the uncertainties in κ_c — noticeable finite-volume effects for the interface tension at $L_t = 2$ can be excluded, and eq. (9.7) represents the infinite-volume limit.

All the numbers above are about one order of magnitude smaller than the prediction of perturbation theory [105, 107],

$$\left(\frac{\sigma}{T_c^3}\right)_{\rm pert} \simeq 0.002\,, \tag{9.8}$$

and about two orders compared to $m_H \simeq 35$ GeV, see subsection 7.1.2 and eq. (9.1), however, they are in any case different from zero. This confirms that the interface tension is a steeply decreasing function of the Higgs boson mass. These estimates may also be put into perspective with results, which were reported in refs. [150, 151] for the dimensionally reduced SU(2)–Higgs model in three dimensions at a tree-level Higgs mass of $m_H^* \simeq 70$ GeV, corresponding to a physical Higgs mass of $m_H \simeq 65$ GeV after a perturbative mapping of the $3D$–lattice parameters to the variables of the $4D$–theory, from equal-weight histogram and tunneling correlation length methods:

$$\left(\frac{\sigma}{T_c^3}\right)^{D=3}_{\rm hist} \lesssim 0.00021\,, \quad \left(\frac{\sigma}{T_c^3}\right)^{D=3}_{\rm tunnel} = 0.00070(26)\,. \tag{9.9}$$

Estimates at larger m_H do not exist, because the groups employing the dimensional reduction approach claim the end of the first order phase transition line in this model already around or even below $m_H \simeq 80$ GeV [149, 145, 152].

I have to remark in this context that the present numbers (9.5) – (9.7) from the four-dimensional model at $L_t = 2$ do not perfectly follow the general trend of an approximately exponential fall off in the MC data for the interface tension in dependence on increasing Higgs mass [96, 151]. They are definitely larger than it would be expected from the σ–values at $m_H \gtrsim 50$ GeV, of which the most come from investigations in the $3D$–theory though. On the other hand, as far as no information about the interface tension at larger L_t–distances is available, the results presented here must be looked upon as preliminary.

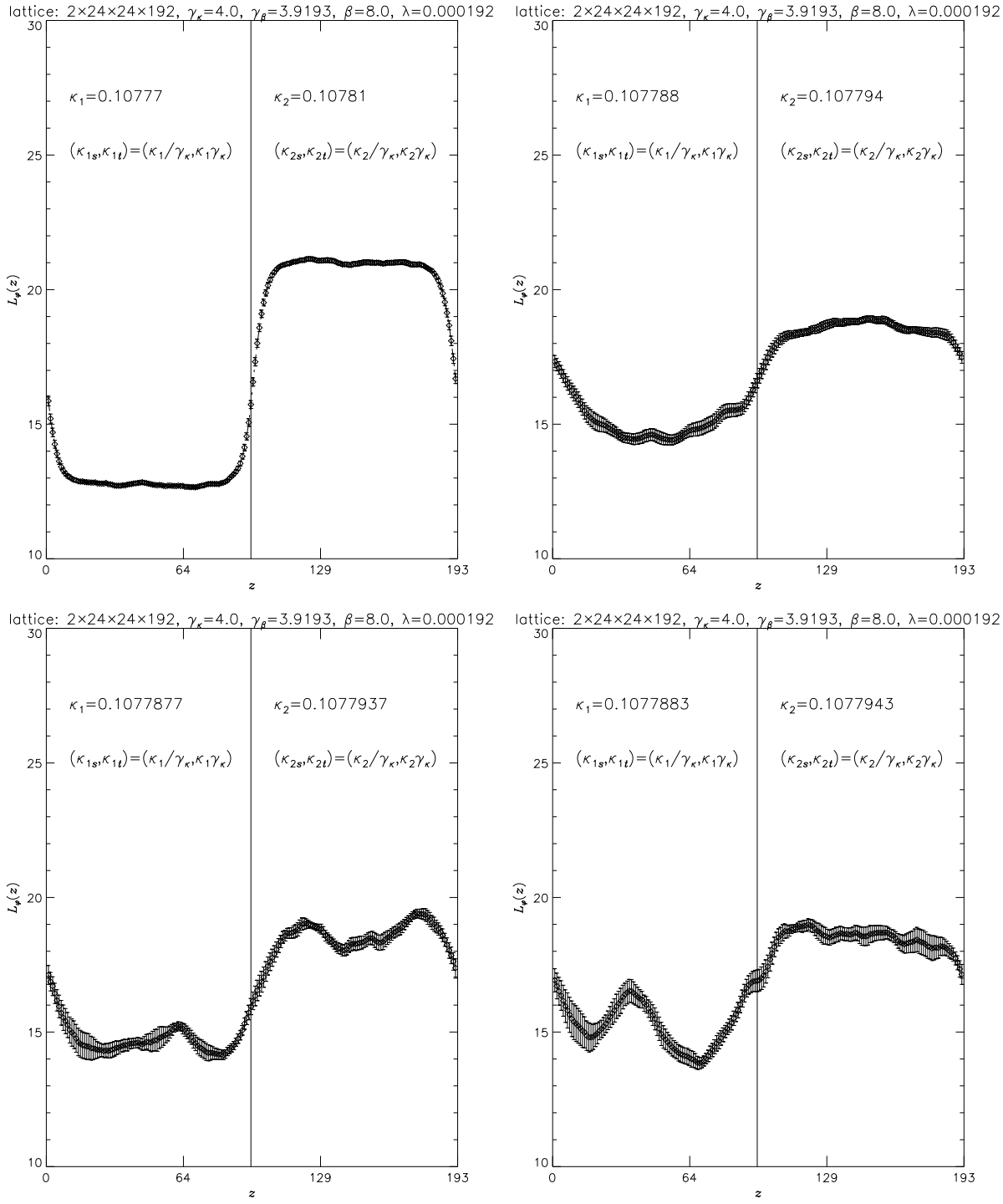

Figure 9.8: *Schematic sketch of the κ_c–determination by seeking for that κ–interval, which is minimally with respect to a stable two-phase structure in the z–slice expectation value $L_\varphi(z)$ of the φ–link operator L_φ. The κ_c–estimate (9.2) has been determined from the simulation belonging to the upper right plot, which was started on the final field configuration of the upper left simulation with a larger κ–interval. Then, after 1500 equilibration sweeps, the system was observed for 5000 measurements. In the simulations belonging to the lower plots the final κ–pair has been displaced in both directions. Now the signal is much noisier, the plateaus are manifestly disturbed, and a collapse into one single phase has to be apprehended.*

9.3 Discussion and outlook

The interface tension $\hat{\sigma}/T_c^3$, which has been determined with the two-coupling method at simulation parameters corresponding to $m_H \simeq 80$ GeV on anisotropic lattices with temporal extension $L_t = 2$, is — albeit being non-zero — considerably smaller than perturbatively. Hence, I draw the important conclusion that the phase transition is very weakly first order at this point. The extensive studies of the isotropic SU(2)–Higgs model in four dimensions have shown that for Higgs masses $m_H \lesssim 50$ GeV the scaling behaviour of most thermodynamic quantities is remarkably good, with scaling violations typically below the $\mathcal{O}(10\%)$–level [135, 137, 139]. Nevertheless, one actually has no reasonable feeling for the finite-lattice spacing effects in the case of anisotropic lattices and such large Higgs masses. Thus the attitude of only negligible scaling violations, born out of the positive experiences with investigations at lower m_H, can no longer be taken for granted, and the lattice resolution of $L_t = 2$ may be yet too coarse to resemble continuum physics. Then there is still the possibility that already at the lattice parameters chosen above, the extremely weak first order character of the phase transition and the resulting interface tension could vanish. In order to get a better control over the size of these lattice artifacts, simulations with larger L_t–values remain to be systematically tackled in future. But this goes beyond the scope of my work.

The fact that the dimensionless ratio $T_c/m_H \simeq 1.9$ at this large Higgs mass turns out to lie about 20 % below the predictions of perturbation theory and simulations of three-dimensional effective theories can hardly be accepted. This may partly emerge from the incompatibility of the renormalized gauge coupling definitions exposed in subsection 7.3.2 of chapter 7, which is still an outstanding problem when comparing the $4D$–results to the three-dimensional approach of dimensional reduction. It is not known, how the renormalized lattice gauge coupling $g_R = g_R^{(V)}$ of the $4D$–simulations, defined in terms of the static potential extracted from Wilson loops, is related to continuum physics, i.e. to the running gauge coupling $g_R = g_R^{(\overline{\rm MS})}(\mu)$ in the $\overline{\rm MS}$–scheme at a mass scale $\mu = m_W$, to which some given $4D$–simulation corresponds. For instance, if one converts the $3D$–results at $m_H^* \simeq 70$ GeV of ref. [152] to $g_R^2 > 0.5$ as inferred from the four-dimensional case[2], the authors do suggest a lowering of the critical temperature in units of the physical Higgs mass: $T_c/m_H < 2$. In addition, one may think again of some noticeable influence of the finite volume or finite lattice spacings in the actual simulations. Namely, this could affect the critical hopping parameter and thereby also the value of the on-shell Higgs mass at zero temperature in lattice units, which is rather sensitive to any variation of κ [137].

As already stated in the introduction, there are quite compelling arguments that the first order EWPT line terminates at some critical Higgs mass $m_H = m_H^{(\rm crit)}$ around [149], or even

[2] Actually, the phenomenologically established value of the electroweak fine structure constant α_W gives a renormalized gauge coupling squared, which lies below $g^2 = 4/\beta = 0.5$, as assumed in the present investigations.

below $m_H^{(\mathrm{crit})} \simeq 80$ GeV [145, 152], and turns into a smooth and regular crossover between two analytically connected Higgs and symmetry restored regions with no true local gauge invariant order parameter, which would vanish in either of them, in accordance with ref. [22]. But the exact position and the nature of the phase transition endpoint at $m_H^{(\mathrm{crit})}$ seems to be still unclear at the moment. From the theoretical point of view it might be most likely [94], and has also been conjectured by the authors of ref. [149], that at $m_H = m_H^{(\mathrm{crit})}$ the transition is of second order with a continuous change and a massless scalar excitation in the physical spectrum linked to infinite correlation length, possibly of the Ising universality class. However, any conventional methods like observing two-peak structures and a discontinuity of an order parameter as a globally averaged quantity on the lattice, driven by the temperature T at lower m_H, face the difficulty that owing to infinite or at least rapidly growing correlation lengths at $m_H \simeq m_H^{(\mathrm{crit})}$ in both regimes, this scale can not be safely disentangled from the size of the system being simulated at the alleged transition. As a consequence, a feasible infinite-volume extrapolation to reach the thermodynamic limit and to identify its asymptotic behaviour needs such increasingly large lattice volumes at the critical point that is was so far practically impossible to uniquely single out the order of the EWPT at $m_H = m_H^{(\mathrm{crit})}$. Of course, this issue also needs to be elucidated in future explorations.

In this connection I should also mention that the Higgs boson masses, to which the investigations of the four-dimensional SU(2)–Higgs model and those of the dimensionally reduced model in three dimensions refer, are not defined in the same way as well. In the former they are physical zero-temperature pole or on-shell masses (m_H, m_W) in the sense that they are determined non-perturbatively from the exponential decay of suitable correlation functions, whereas in the latter they are tree-level Higgs masses (m_H^*) of the four-dimensional finite-temperature SU(2)–Higgs theory in the continuum, from which the dimensional reduction to three dimensions and subsequent lattice discretization started, although there exist two-loop perturbative relationships in the $\overline{\mathrm{MS}}$–renormalization scheme between each set of lattice parameters of the three-dimensional model, expressed in terms of the variables of the $3D$–effective continuum theory, to a set of physical parameters of the original theory in four dimensions. So every direct comparison of results from the full $4D$– and effective $3D$–models without a proper conversion between them must be taken with some care, because in three dimensions the masses are always somewhat larger than the on-shell masses. Accounting for this difference, which has been estimated in refs. [147, 148] analytically, one can guess that the dimensional reduction implies a shift of a few (perhaps $3-6$) GeV for the endpoint of the phase transition and that its first order nature survives up to slightly larger physical Higgs masses in four dimensions. So it could be absolutely imaginable that, say, the interface tension is still finite and non-zero at $m_H \simeq 80$ GeV in the four-dimensional framework, whilst it already vanishes at $m_H^* \simeq 80$ GeV in the three-dimensional theory. Bearing these additional uncertainties in mind, there is no serious contradiction in the qualitative and quantitative line of reasoning from both approaches up to now.

Regardless of these options concerning the endpoint of the EWPT and its location under discussion, one should emphasize once more that all results from the different approaches to the finite-temperature SU(2)–Higgs sector of the minimal standard model (MSM) in four and three dimensions, also those including the U(1)–factor or the impact of fermions [147, 149, 152], especially the heaviest elementary fermion — the top quark —, can be reconciled to a common conclusion: The first order EWPT for physically realistic values of the Higgs boson mass $m_H \gtrsim 66$ GeV, if present at all, is not strong enough for an explanation of the origin of the observed baryon asymmetry in the universe. Therefore, any scenario of electroweak baryogenesis within the MSM has surely to be ruled out.

However, in spite of this — at first sight discouraging — outcome, the still viable alternative to explain the baryon asymmetry within the minimal supersymmetrically extended standard model remains, see e.g. ref. [155]. And as in principle it is possible by a suitable parameter matching to transform between both theories, the results from the SU(2)–Higgs sector of the MSM at finite temperature will not loose their importance as essential ingredients for our knowledge and understanding of cosmology and the physics in the early universe. Not least, the failure of the MSM at energy scales, which are characteristic for the electroweak epoch in the evolution of our universe ($T \simeq \mathcal{O}(100)$ GeV $\simeq \mathcal{O}(10^{16})$ K), may be interpreted as a strong indication for the prospect that some kind of, for instance minimal, extension of the MSM is realized in nature.

Summary

I examined the finite-temperature electroweak phase transition in the framework of the four-dimensional SU(2)–Higgs model non-perturbatively on the lattice. To this end, I performed high statistics and large scale numerical simulations by means of the Monte Carlo method.

In my investigations I concentrated on the determination of the phase transition point and the interface tension, the latter playing a crucial rôle in order quantify the strength of the transition in dependence on the Higgs boson mass m_H.

The numerical simulations within the SU(2)–Higgs model in the mass range between $m_H \simeq 16$ GeV and $m_H \simeq 80$ GeV always turned out to be feasible and powerful. At $m_H \simeq 16$ GeV and $m_H \simeq 35$ GeV the symmetry restoring electroweak phase transition is still relatively strongly first order, and the qualitative as well as — at least partly — quantitative agreement with two-loop resummed perturbation theory and the approach of dimensional reduction to a three-dimensional effective theory is quite good. More precisely, I found the electroweak interface tension to decrease by several orders of magnitude towards higher masses around $m_H \simeq 80$ GeV, in complete conformity with the expectation that the phase transition weakens substantially for increasing Higgs mass. However, since my estimates at $m_H \simeq 80$ GeV still hint at an extremely weak first order phase transition, the absence of its first order nature in this Higgs mass region, which is claimed by other authors using dimensionally reduced models, could not be confirmed.

Technically, the numerical simulations at such large Higgs boson masses were realized by employing an anisotropic lattice regularization with different spacings in spatial and temporal directions. In this context I non-perturbatively established the perturbative choice of suitable simulation parameters by tuning the correlation lengths in the system to recover the required rotational invariance. Then it was possible to study the thermodynamic properties of the lattice model reliably.

Nevertheless, my results on the interface tension from the SU(2)–Higgs sector of the minimal standard model support the existing theoretical belief that for $m_H \gtrsim 40$ GeV, the strength of the first order electroweak phase transition is definitely not enough to produce a sufficiently violent out of equilibrium situation in the early universe, which is fundamentally needed for the creation of the observed baryon asymmetry via physical processes at the electroweak scale.

Appendix A

Basics of simulating field theories

This appendix covers some notations and concepts, which may be helpful for the understanding of the main text with the intention to make it rather self-contained. Of course, I will be by no means complete, and unless stated otherwise, a far more detailed and extensive treatment of the material collected here can be found in standard textbooks and reviews on lattice field theory as e.g. refs. [16, 17, 18, 19, 169, 171].

A.1 Lattice notations and conventions

Let a four-dimensional hypercubic space-time lattice with sites x, extensions L_μ, and unit vectors $\hat{\mu}$ in the lattice directions $\mu = 1, \ldots, 4$ be given. Periodic boundary conditions are assumed in all directions, and for the moment I consider isotropic lattices with a lattice spacing a. The set of all lattice points is often denoted as

$$\Lambda \equiv \{x = (x_1, x_2, x_3, x_4) \in a\mathbb{Z}^4 \,|\, 0 \leq x_\mu \leq a(L_\mu - 1)\} \equiv L_1 \times L_2 \times L_3 \times L_4 \,, \tag{A.1}$$

whereas the coordinates x_μ/a also run from 1 to L_μ in some cases. Alternatively, I adopt the notations $x = (\boldsymbol{x}, t) = (\mathrm{x}, \mathrm{y}, \mathrm{z}, t)$ and $L_\mu \in \{L_\mathrm{x}, L_\mathrm{y}, L_\mathrm{z}, L_t\}$, so that $\Omega \equiv L_\mathrm{x} L_\mathrm{y} L_\mathrm{z} L_t$ is the number of lattice points and $V \equiv a^4\Omega$ its physical volume in lattice units. Modifications for subvolumes of the lattice are straightforward, e.g. for timeslices used in the calculation of correlation functions one has $\Omega_s = L_\mathrm{x} L_\mathrm{y} L_\mathrm{z}$.

Due to the identity $\mathrm{e}^{2\pi i x_\mu/a} = 1$, all Fourier transforms of lattice functions $f = f(x)$ are $2\pi/a$–periodic, and thus the lattice momenta can be restricted to the first Brillouin-Zone

$$\mathcal{B} \equiv \{p = (p_1, p_2, p_3, p_4) \,|\, -\pi/a < p_\mu \leq \pi/a\} \,, \tag{A.2}$$

which naturally regularizes the respective lattice theory through an ultraviolet momentum cutoff π/a. Explicitly, this implies for the Fourier transforms

$$\tilde{f}(p) = a^4 \sum_{x \in \Lambda} f(x)\, \mathrm{e}^{-ip\cdot x} \,, \quad f(x) = \frac{1}{a^4\Omega} \sum_{p \in \mathcal{B}} \tilde{f}(p)\, \mathrm{e}^{ip\cdot x} \,, \quad p_\mu = \frac{2\pi}{aL_\mu}\, n_\mu \tag{A.3}$$

with $n_\mu = 0, 1, \ldots, L_\mu - 1$, and in the infinite-volume limit:

$$L_\mu \to \infty \,,\, \forall \mu : \quad \frac{1}{a^4 \Omega} \sum_{p \in \mathcal{B}} \longrightarrow \int_{-\pi/a}^{\pi/a} \frac{\mathrm{d}^4 p}{(2\pi)^4} \equiv \int_p \,. \tag{A.4}$$

Finally, the lattice (forward) derivative is discretized to the finite difference

$$\triangle_\mu f(x) \equiv \frac{1}{a} \Big[\, f(x + a\hat{\mu}) - f(x) \, \Big] \,, \tag{A.5}$$

and its covariant counterpart is

$$D_\mu f(x) \equiv \frac{1}{a} \Big[\, U^{-1}(x + a\hat{\mu}, x) f(x + a\hat{\mu}) - f(x) \, \Big] \tag{A.6}$$

with $U_{x,\mu} = U(x + a\hat{\mu}, x)$ the parallel transporter (directed link, i.e. straight path from site x to site $x + a\hat{\mu}$) on the lattice as an element of the gauge group.

In the case of anisotropic lattices I consider a situation with equal lattice spacings a_s in the three spatial directions different from the lattice spacing a_t in the temporal direction. As discussed in the second part of this work, the lattice spacing anisotropy parameter

$$\xi \equiv \frac{a_s}{a_t} \tag{A.7}$$

then plays an important rôle when extracting physical quantities from an anisotropic lattice simulation. The generalization of the expressions above proceeds in the obvious manner, e.g. the physical lattice volume is $V = a_s^3 a_t \Omega$, and the functions of the momenta in the bare bosonic lattice propagators are

$$\hat{p}_\mu = \frac{2}{a_s} \sin\left(\frac{a_s p_\mu}{2}\right) \,, \quad \mu = 1, 2, 3 \,; \quad \hat{p}_4 = \frac{2}{a_t} \sin\left(\frac{a_t p_4}{2}\right) \,. \tag{A.8}$$

The two-dimensional (isotropic) lattices in the first part of this work have extensions L_1 and L_2, or equivalently L_x and L_t, sites $x = (x_1, x_2) = (\mathrm{x}, t)$, momenta $p = (p_1, p_2)$, and need no more specifications.

As it is a common practice in quantum field theory, rationalized units are chosen such that the universal physical constants $\hbar$, c, k_B, and ε_0 are equal to one. Consequently, all dimensionful quantities like masses, temperatures, inverse times, or inverse length are expressed in terms of energy units $[E] = 1$ eV. If no confusion is expected, this is sometimes supplemented by setting the lattice constant $a = 1$ (lattice units), and all dimensionless observables O, whose expectation values $\langle O \rangle$ are calculated on the lattice, are pure numbers in these units. Relaxing the condition $a = 1$, one has

$$O = O^{(\mathrm{phys})} a^{d_O} \,, \tag{A.9}$$

when $O^{(\mathrm{phys})}$ is a physical observable of mass dimension d_O, i.e. $[O^{(\mathrm{phys})}] = [m^{d_O}]$ in the formal continuum limit $a \to 0$. A prominent example would be a particle mass in lattice

units $m = m^{(\mathrm{phys})}a$, since $[m^{(\mathrm{phys})}] = [m]$ and $d_O = 1$. Provided that the a–dependence of the lattice parameters is determined in the same way, one expects scaling behaviour in the continuum limit for each $\langle O \rangle$ according to eq. (A.9), while $O^{(\mathrm{phys})}$ remains finite if so in the continuum. Then the only dimensionful parameter of the lattice theory is a itself, and physical units are recovered through reference (or better its ratio) to an external, e.g. experimentally known length scale parameter as input, typically an inverse particle mass.

A.2 Monte Carlo methods

The basic object of numerical simulations in lattice quantum field theories is the calculation of (estimators for) expectation values of functions depending on the field variables. For this purpose, the very large number of degrees of freedom to be integrated over on lattices of typical sizes compels a Monte Carlo (MC) integration by randomly generating field configurations. In order to encounter the substantial contributions to the path integral — namely those in the vicinity of the minimum of the free energy density — most efficiently, one follows the principle of importance sampling. This means to generate an, in the strict sense infinite, ensemble of field configurations weighted with the Boltzmann factor e^{-S}, for instance $S = S[U, \varphi]$ the lattice action of the gauge-Higgs system, mimicking the canonical equilibrium probability distribution. The statistical average of this ensemble equals the expectation value of some observable $O = O(\{U, \varphi\})$, here as a function of site and link variables φ_x and $U_{x,\mu}$, in its Euclidean path or functional integral representation:

$$\langle O \rangle_Z = \frac{1}{Z} \int \mathcal{D}[U, \varphi]\, \mathrm{e}^{-S[U,\varphi]}\, O(\{U, \varphi\})\,, \quad Z = \int \mathcal{D}[U, \varphi]\, \mathrm{e}^{-S[U,\varphi]}\,. \tag{A.10}$$

It has to be distinguished from the sample average in eq. (A.25) over a largest possible but finite number of configurations, which approaches $\langle O \rangle_Z$ in the limit of infinitely many evaluated configurations.

A.2.1 Standard algorithms

This setting is translated into action as a sequence of updating steps with symmetric proposal probability in the space of elementary lattice fields, which imitates the stochastic process of a Markov chain. It is ergodic by definition with the additional property of detailed balance, being a sufficient but not necessary condition for the existence of a unique fixed point of the Markov process in order to ensure that the canonical ensemble is really reached in a finite number of steps. Commonly known local algorithms in this context are:

- **Metropolis**
  Each field variable is updated by randomly proposing a new value for it and accepting with probability $P_{\mathrm{A}} = \min\{1, \mathrm{e}^{-\Delta S}\}$, if ΔS denotes the difference of lattice actions after

and before the proposal holding all other variables fixed. In a computer program, one runs through the lattice point by point, makes the updates, e.g. $f \to f' = f + \delta\,(r - \frac{1}{2})$ for a real-valued field f, and accepts only for $-\Delta S > \ln(1 - r')$ with $r, r' \in (0, 1)$ being uniform random numbers. The range of the possible proposals should be adjusted (through δ) to give acceptance rates of $50 - 60$ %.

- **Heatbath**
  As opposed to the Metropolis algorithm, the new value of a field variable is now generated with a transition probability proportional to the canonical equilibrium probability distribution of the surrounding field configuration independently from the original one. In this respect, it is usually computationally advantageous to simplify the distribution and, because of ergodicity, correct for the corresponding approximation by an Metropolis-like accept-reject step afterwards. Its acceptance rate, conveniently 90 % or even larger, decides about the quality of this implementation in practice.

- **Overrelaxation**
  The main goal of this non-ergodic algorithm is to reduce 'critical slowing down' in MC simulations — which means the worse divergence of the integrated autocorrelation time $\tau_{\rm int}$ in the continuum limit via a power law behaviour in the correlation length ξ at phase transitions, $\tau_{\rm int}[O] \sim \xi^{z(O)}$ with O some observable and $z(O)$ the dynamical critical exponent — to $z(O) \simeq 1$. It is a kind of reflection in field space, where their new values are chosen as far as possible from the old ones leaving the action, respective the energy, and the measure in the defining functional integral (approximately) invariant. Since these proposals are (nearly) always accepted, i.e. eventually in a subsequent Metropolis decision with $P_{\rm A} \simeq 1$, this algorithm is governed by the microcanonical probability distribution and thus has to be mixed with one of the former to preserve the required ergodicity in all.

In the numerical simulations of both lattice models under study a proper combination of algorithms of this type called sweep, in which each field variable is visited at least once, was periodically repeated to generate the desired field configurations.

A.2.2 Gauge and scalar field updates in the SU(2)–Higgs model

The Metropolis method I have only applied to the updates of the real-valued field variables in the U(1)–Higgs model in two dimensions. Within the framework of the four-dimensional SU(2)–Higgs model this type of algorithm was replaced by suitable heatbath algorithms [172], which often perform better and genuinely enjoy smaller autocorrelations. For the heatbath updates of the SU(2)–valued gauge field links $U_{x,\mu}$, I used the familiar algorithm originally devised in refs. [175, 176].

The reflection in the overrelaxation algorithms of the U(1)– or SU(2)–valued gauge angle variables can always be done exactly, either by explicit graphical construction as in the two-dimensional case of the former, or by adaption of a standard procedure [173, 174, 178]. For instance, the exact reflection of the gauge link (and analogously of the angular part of the Higgs field as well, if the index μ is ignored in the following notations) can be done by splitting the lattice action as $S_x(U_{x,\mu}) = \mathrm{Tr}\left(U_{x,\mu}\check{U}\right) + \text{constant}$, where the 'staple' $\check{U}$ covers all field contributions different from the variable $U_{x,\mu} \in \mathrm{SU}(2)$ under consideration. Then carry out the update $U_{x,\mu} \to U'_{x,\mu} = \check{U}_0^+ U_{x,\mu}^+ \check{U}_0^+$ with $\check{U}_0$ being normalized as $\check{U}_0 \equiv \check{U}/\sqrt{\det \check{U}}$ and thereby an element of the gauge group SU(2). The action stays unchanged and the acceptance probability of the proposal is $P_{\mathrm{A}}(U_{x,\mu} \to U'_{x,\mu}) = P_{\mathrm{A}}(U'_{x,\mu} \to U_{x,\mu}) = 1$. However, this does not work for the scalar field length, because its local potential does not possess any exact reflection symmetry as will be seen below. An elegant solution to the problem has been found in ref. [179] by dealing with the scalar field as an real-valued object in cartesian components. To restate it briefly, I restrict to the SU(2)–Higgs case and isotropic lattices; the generalization to anisotropic lattices and couplings along eqs. (5.10) – (5.34) of chapter 5 is then straightforward, and a translation to the two-dimensional U(1)–Higgs model is sketched in section 2.2 of the first part.

One starts from the observation that the complex $2 \otimes 2$ matrices φ_x can be uniquely decomposed in terms of the Pauli matrices τ_k, $k = 1, 2, 3$, as

$$\varphi_x = \phi_{x,0}\tau_0 + i\sum_{k=1}^{3} \phi_{x,k}\tau_k \,, \quad \tau_0 \equiv \mathbf{1}_{2\otimes 2} \,, \quad \tfrac{1}{2}\,\mathrm{Tr}\left(\varphi_x^+ \varphi_x\right) = \sum_{l=0}^{3} \phi_{x,l}^2 = \rho_x^2 \,, \tag{A.11}$$

and the four-component scalar field $\phi_x = \{\phi_{x,l} \in \mathbb{R} \,|\, l = 0, \ldots, 3\}$ expresses the manifest O(4)–symmetry of the pure scalar sector of the SU(2)–Higgs model. After substituting the previous identity and using the invariance of the trace operation under cyclic permutation and adjunction of its arguments in the successive manipulations, the part of the lattice action (5.14) of chapter 5 relevant for the scalar field at site $x \in \Lambda$ becomes

$$\begin{aligned} S_{\phi,x}(\varphi_x) &= -\kappa \sum_{\mu=1}^{4} \mathrm{Tr}\left(\varphi_{x+\hat{\mu}}^+ U_{x,\mu}\varphi_x + \varphi_x^+ U_{x-\hat{\mu},\mu}\varphi_{x-\hat{\mu}}\right) + \rho_x^2 + \lambda(\rho_x^2 - 1)^2 \\ &= \zeta_x \left(\phi_x - \frac{b_x}{\zeta_x}\right)^2 + \lambda\left[\rho_x^2 - \frac{1}{2\lambda}\left(2\lambda - 1 + \zeta_x\right)\right]^2 + \text{constant} \end{aligned} \tag{A.12}$$

with

$$b_{x,0} \equiv \frac{\kappa}{2}\sum_{\mu=1}^{4} \mathrm{Tr}\left(\varphi_{x+\hat{\mu}}^+ U_{x,\mu} + U_{x-\hat{\mu},\mu}\varphi_{x-\hat{\mu}}\right) \tag{A.13}$$

$$b_{x,k} \equiv \frac{i\kappa}{2}\sum_{\mu=1}^{4} \mathrm{Tr}\left(\varphi_{x+\hat{\mu}}^+ U_{x,\mu}\tau_k + \tau_k U_{x-\hat{\mu},\mu}\varphi_{x-\hat{\mu}}\right) \,. \tag{A.14}$$

Summation over the cartesian index l is understood in the first (Gaussian) term of (A.12), and ζ_x helps to shift a term proportional to ϕ_x^2 from this quadratic to the quartic part of $S_{\phi,x}$. Two algorithms are now on offer:

- Heatbath:
  Propose the new field values $\phi'_{x,l}$, $l = 0, \ldots, 3$, with a probability distribution, which only involves the Gaussian (quadratic) part of $S_{\phi,x}$:

$$\phi_{x,l} \;\to\; \phi'_{x,l} = \sqrt{-\zeta_x^{-1} \ln r}\, \sin(2\pi r') + \frac{1}{\zeta_x}\, b_{x,l}\,, \tag{A.15}$$

  with uniform random numbers $r, r' \in (0,1)$.

- Overrelaxation:
  Reflect the scalar field components as

$$\phi_{x,l} \;\to\; \phi'_{x,l} = \frac{2}{\zeta_x}\, b_{x,l} - \phi_{x,l}\,, \quad l = 0, \ldots, 3\,, \tag{A.16}$$

  which is only exact with respect to the Gaussian (quadratic) part of $S_{\phi,x}$.

Since the quartic part in eq. (A.12) has not been treated so far, both proposals are accepted in an additional accept-reject step with probability

$$\begin{aligned} P_{\mathrm{A}}(\phi_x \to \phi'_x) &= \min\{1, \mathrm{e}^{-\Delta S_{\phi,x}}\} \\ \Delta S_{\phi,x} &= \lambda \left[\left(\rho_x'^2 - \frac{2\lambda - 1 + \zeta_x}{2\lambda} \right)^2 - \left(\rho_x^2 - \frac{2\lambda - 1 + \zeta_x}{2\lambda} \right)^2 \right]. \end{aligned} \tag{A.17}$$

An optimization of the acceptance rates is achieved by coincidence of the minima of the quadratic and quartic parts in $S_{\phi,x}$, which is equivalent to the cubic equation

$$2\lambda b_x^2 = \zeta_x^2(\zeta_x + 2\lambda - 1)\,, \quad b_x^2 = |b_x|^2 = \sum_{l=0}^{3} b_{x,l}^2\,. \tag{A.18}$$

To avoid any unwanted loss of speed in both updates, it is approximately solved by writing $\zeta_x = 1 + \varepsilon_x$ (note that $\zeta_x = 1$ for $|b_x| = 1$), hence

$$\zeta_x = 1 - 2\lambda + 2\lambda b_x^2 + \mathcal{O}(\varepsilon_x^2, \lambda\varepsilon_x)\,, \tag{A.19}$$

and the acceptance condition (A.17) passes into

$$P_{\mathrm{A}}(\phi_x \to \phi'_x) = \min\{1, \mathrm{e}^{-\Delta S_{\phi,x}}\}\,, \quad \Delta S_{\phi,x} = \lambda \left[\, (\rho_x'^2 - b_x^2)^2 - (\rho_x^2 - b_x^2)^2 \,\right]. \tag{A.20}$$

Finally, I should stress that the very small values of $\lambda < \mathcal{O}(10^{-3})$ in the SU(2)–Higgs simulations of this work are crucial for the high acceptance rates larger than 98 % (or even 99 %) for the two algorithms.

At an early stage of the investigations the overrelaxation of the Higgs field length was done separately from the SU(2)–reflection of its angle by a method introduced in [178]. Here the scalar field part of the action (5.14) is arranged in the form

$$S_{\phi,x}(\rho_x) = -c_x\rho_x + \rho_x^2 + \lambda(\rho_x^2-1)^2 - 3\ln\rho_x \tag{A.21}$$

$$c_x \equiv \kappa\sum_{\mu=1}^{4}\mathrm{Tr}\left(\varphi^+_{x+\hat{\mu}}U_{x,\mu}\alpha_x + \alpha^+_x U_{x-\hat{\mu},\mu}\varphi_{x-\hat{\mu}}\right)\,, \tag{A.22}$$

in which the $\ln\rho_x$–term emerges from the transformation of the functional integral measure in polar coordinates according to $\varphi_x = \rho_x\alpha_x$. The idea is to determine a non-exact 'reflected' value $\rho'_x \neq \rho_x$ with $S_{\phi,x}(\rho'_x) = S_{\phi,x}(\rho_x)$ by polynomial approximation through a third order Taylor expansion of (A.21) and Newton iteration, and the Metropolis step with acceptance probability

$$P_{\mathrm{A}}(\rho_x \to \rho'_x) = \min\left\{1, \left|\left[\frac{\mathrm{d}S_{\phi,x}(\rho_x)}{\mathrm{d}\rho_x}\right]\left[\frac{\mathrm{d}S_{\phi,x}(\rho'_x)}{\mathrm{d}\rho'_x}\right]\right|^{-1}\right\} \tag{A.23}$$

compensates for the non-trivial functional determinant caused by the lacking symmetry of $S_{\phi,x}$ in regard of its minimum. The inclusion of this algorithm already leads to an impressive reduction of the integrated autocorrelation times compared to pure Metropolis or heatbath sweeps, typically about a factor $5-6$, but as illustrated in section 5.3 and refs. [137, 139], it can not compete with the algorithm above, which beyond that also performs faster than the overrelaxations of both Higgs degrees of freedom together.

A.3 Expectation values and autocorrelations

Suppose that the system has reached independence of the starting field configuration after a sufficient number of thermalization sweeps[1]. During the N_{meas} measurement sweeps one generically calculates the lattice averages of site and also direction dependent observables O_x and $O_{x,\mu}$, i.e. in the four-dimensional isotropic case

$$O_n \equiv \frac{1}{\Omega}\sum_{x\in\Lambda} O_x\,, \quad O_n \equiv \frac{1}{4\Omega}\sum_{x\in\Lambda}\sum_{\mu=1}^{4} O_{x,\mu}\,, \quad n \in \{1,\ldots,N_{\mathrm{meas}}\}\,. \tag{A.24}$$

The sample average over all available measurements or configurations

$$\langle O\rangle \equiv \frac{1}{N_{\mathrm{meas}}}\sum_{n=1}^{N_{\mathrm{meas}}} O_n \tag{A.25}$$

[1] A popular starting configuration is the cold one, where all fields are set to the unit element of the group they take values in.

is, under the non-realistic assumption of their statistical independence[2], related to the true expectation value by its variance Δ_O^2 as

$$\langle O \rangle_Z = \langle O \rangle \pm \Delta_O \,, \quad \Delta_O^2 \equiv \frac{\langle O^2 \rangle - \langle O \rangle^2}{N_{\rm meas} - 1} \,. \tag{A.26}$$

In order to account for the intrinsic correlations between the subsequent configurations in a simulation, quantified below by the integrated autocorrelation time $\tau_{\rm int}$, one averages first over blocks (bins) of length $l_{\rm bin}$,

$$\overline{O}_b \equiv \frac{1}{l_{\rm bin}} \sum_{n=(b-1)\cdot l_{\rm bin}+1}^{b\cdot l_{\rm bin}} O_n \,, \quad b \in \{1, \ldots, N_{\rm bin}\} \,, \tag{A.27}$$

leading to mean values over these bin averages thereafter:

$$\langle O \rangle_{\rm bin} \equiv \frac{1}{N_{\rm bin}} \sum_{b=1}^{N_{\rm bin}} \overline{O}_b = \langle O \rangle \,, \quad \langle O^2 \rangle_{\rm bin} \equiv \frac{1}{N_{\rm bin}} \sum_{b=1}^{N_{\rm bin}} \overline{O}_b^2 \,. \tag{A.28}$$

If $l_{\rm bin} \gtrsim \tau_{\rm int}$, the field configurations averaged over $N_{\rm bin} = N_{\rm meas}/l_{\rm bin}$ bins become statistically uncorrelated, and the correct statistical error estimate is

$$\langle O \rangle_Z = \langle O \rangle \pm \Delta_O \,, \quad \Delta_O^2 \equiv \frac{\langle O^2 \rangle_{\rm bin} - \langle O \rangle_{\rm bin}^2}{N_{\rm bin} - 1} \,. \tag{A.29}$$

A practical way to proceed in a computer program is then, eventually after an internal binning for data and further $\tau_{\rm int}$–reduction, to calculate the binning errors Δ_O for increasing lengths $l_{\rm bin}$ (e.g. growing like powers of 2), and to quote the true statistical error $\Delta_O^{\rm (true)}$ on the measured observable from the plateau of its so-obtained binning table, which should lie beyond the autocorrelation time but with $50 - 100$ bins at least. An immediate consequence of eqs. (A.26) and (A.29) is that $\Delta_O^{\rm (true)}$ is roughly proportional to $1/\sqrt{N_{\rm meas}}$, and allows to predict the computational costs for a gain in this error.

The $N_{\rm meas} \to \infty$ limit of the true variance of $\langle O \rangle$ now implies with $\Delta_O = \Delta_O^{\rm (naive)}$ from (A.26) the following formula for the integrated autocorrelation time:

$$\tau_{\rm int} = \tau_{\rm int}[O] \simeq \frac{1}{2} \left(\frac{\Delta_O^{\rm (true)}}{\Delta_O^{\rm (naive)}} \right)^2 \,. \tag{A.30}$$

A precise definition of $\tau_{\rm int}$ comes from the autocorrelation function [169, 170]

$$\Gamma_O(t) \equiv \lim_{N_{\rm meas} \to \infty} \frac{1}{N_{\rm meas} - t} \sum_{n=1}^{N_{\rm meas}-t} \Big(O_{n+t} - \langle O \rangle \Big) \Big(O_n - \langle O \rangle \Big) \tag{A.31}$$

[2] In the situation of uncorrelated data one also says that $\langle O \rangle$ is an unbiased estimator of the true expectation value $\langle O \rangle_Z$, i.e. $\langle \langle O \rangle \rangle_Z = \langle O \rangle_Z$.

and reads after its normalization by $\Gamma_O(0) = \frac{1}{N_{\rm meas}} \sum_{n=1}^{N_{\rm meas}} (O_n - \langle O \rangle)^2 = \Delta_O^2$, if the computer or MC time t counts the number of sweeps:

$$\tau_{\rm int}[O] \equiv \frac{1}{2} \sum_{t=-\infty}^{t=\infty} \frac{\Gamma_O(t)}{\Gamma_O(0)} = \frac{1}{2} + \sum_{t=1}^{t=\infty} \frac{\Gamma_O(t)}{\Gamma_O(0)} \,. \tag{A.32}$$

The truncation of the sum at the first zero of the autocorrelation function Γ_O, which has the largest $\tau_{\rm int}[O]$ in the system belonging to the operator O with the slowest modes, is consistent with the methods described in ref. [169]. There it is suggested too that about $20\tau_{\rm exp}$ thermalization sweeps — $\tau_{\rm exp}$ is the exponential autocorrelation time given by the large t asymptotics of the (exponentially decaying) autocorrelation and depends only on the updating process — are in most cases adequate to prepare an equilibrated field configuration. This can be controlled later on by evaluating eq. (A.31) for full measurement samples, sometimes called histories, of the observables of interest.

Appendix B

Tools of data analysis

Here I have included a sketch of some more technical tools of numerical data analysis. They are referred to without any further explanations in those passages of the main chapters, where they are used. For more details and other applications in lattice investigations the reader should consult the original literature.

B.1 Methods of error determination

Besides the statistical errors of primary quantities directly averaged in a MC run, it is also necessary to have reliable error estimates for secondary quantities, which are functions of these averages. Prominent candidates are correlation functions as defined in eq. (1.56) of section 1.2 and eq. (A.31) above, and fit parameters of primary or secondary quantities themselves. The difficulties to be faced are limited numbers of measurements, potentially wrong estimation of variances by error propagation formulas, and possible correlations between different (primary or secondary) quantities entering the same functions, whose statistical errors are desired.

B.1.1 Jackknife analysis

Given a history with $N_{\rm meas}$ measurements of some observable O_n, one calculates for $1 \leq N_{\rm jck} \leq N_{\rm meas}$ jackknife bins with length $l_{\rm jck} = N_{\rm meas}/N_{\rm jck}$ and $i, j \in \{1, \ldots, N_{\rm jck}\}$, the jackknife bin averages and jackknife sample averages by omitting a single bin:

$$O_i^{(\rm jck)} \equiv \frac{1}{l_{\rm jck}} \sum_{n=(i-1)\cdot l_{\rm jck}+1}^{i\cdot l_{\rm jck}} O_n \,, \quad \overline{O}_j \equiv \frac{1}{N_{\rm jck}-1} \sum_{i=1\,,\,i\neq j}^{N_{\rm jck}} O_i^{(\rm jck)} \,. \tag{B.1}$$

Then the jackknife average of a function $f = f(O)$ is obtained as

$$\langle f \rangle_{\rm jck} \equiv \frac{1}{N_{\rm jck}} \sum_{j=1}^{N_{\rm jck}} f(\overline{O}_j) \tag{B.2}$$

with variance

$$\langle f \rangle_Z = \langle f \rangle_{\rm jck} \pm \Delta_f \,, \quad \Delta_f^2 \equiv \frac{N_{\rm jck}-1}{N_{\rm jck}} \sum_{j=1}^{N_{\rm jck}} \Big(\langle f \rangle_{\rm jck} - f(\overline{O}_j) \Big)^2 \,. \tag{B.3}$$

For uncorrelated primary quantities (i.e. $f = {\rm id}$ and $l_{\rm jck} = 1$) the naive relation (A.26) is reproduced, and $\langle O \rangle_{\rm jck}$ is an unbiased estimator of $\langle O \rangle_Z$. The bias of secondary quantities, which here means the difference $\langle f \rangle_Z - \langle \langle f \rangle_{\rm jck} \rangle$ in dependence of $N_{\rm jck}$, is normally ignored, because it converges faster to zero than the statistical error, and the jackknife variances Δ_f of the functions $f(O)$ are superior to those from ordinary binning as it would be analogous to section A.3. This method is very popular in numerical simulations on the lattice for a long time [180, 181, 182].

The averaging in the jackknife bins is often already done during the program runs by dividing the full data sample into subsamples. Their length, which should exceed the typical autocorrelation times, determines the number of available jackknife samples, likely between 10 and 200 for the latter. By the way, it is obvious that eqs. (B.2) and (B.3) apply to functions of secondary quantities or fit parameters too, i.e. the required calculations can be done within the jackknife samples before estimating their values and errors.

B.1.2 Bootstrap analysis

The bootstrap is a method of non-parametric statistics, which has been invented in ref. [183] and used e.g. for mass calculations with correlation functions in the context of lattice field theory in ref. [185]. This method is closely related to the jackknife just described — namely, the jackknife estimators and errors are approached by the bootstrap in the limit of large samples — but it should be preferred, if the statistics is lower and large fluctuations owing to correlations between data from the same configuration are to be expected. Its characteristic feature is that is not does base on the underlying assumption of a known, in particular the normal (Gaussian), probability distribution for the data. A further textbook reference is [184], and I want to outline the bootstrap method in the following.

Consider sets $\mathcal{M}^{(i)}$ of independent measurements $O_n^{(i)}$ of primary or secondary quantities $O^{(i)}$, $1 \le i \le I$, $1 \le n \le N$, from a single MC run with $N = N_{\rm meas}$ measurements, which can be interpreted as the empirical probability distributions of these observables. Now the strategy is to draw for each $O^{(i)}$ from these original N measurements N objects independently and with repetition allowed, in order to form the so-called bootstrap samples $\mathcal{B}^{(i)}$. The total numbers of N^N such possible bootstrap samples constitutes the bootstrap distributions for

the $O^{(i)}$ specified by the original MC samples, and they are the best approximations to their true distributions, which can be made by taking a large number of completely independent sets of N configurations. Having in mind contingent correlations between the $O^{(i)}$, it is crucial that for fixed n all $O_n^{(i)}$ emerge from the same configurations for a given bootstrap sample. By the way, it is also obvious that the jackknife ensembles are carefully chosen subsets of the full bootstrap ensembles. Because of the huge number of possible bootstrap samples this procedure is realized in practice by generating many independent representative bootstrap samples $\mathcal{B}_b^{(i)} \equiv \{O_{n_b}^{(i)} \,|\, n_b = 1, \ldots, N\}$ randomly, where the same measurements may occur several times in such a set. The index $b = 1, \ldots, B$ counts the number of bootstrap iterations. In each of the so-obtained bootstrap samples one computes the averages of the primary or secondary quantities $O^{(i)}$,

$$O_b^{(i)} = \frac{1}{N} \sum_{n_b=1}^{N} O_{n_b}^{(i)}\,, \quad 1 \le i \le I\,, \tag{B.4}$$

and from these a bootstrap sample estimate f_b of a secondary quantity or some further function $f = f(\{O\})$ of it, e.g. a mass from fits of correlation functions, while for each bootstrap iteration b the once generated index set $\mathcal{I}_b \equiv \{n_b \,|\, n_b = 1, \ldots, N\}$ has to be used for all i. The bootstrap average and its variance is then

$$\langle f \rangle_{\rm bts} = \frac{1}{B} \sum_{b=1}^{B} f_b\,, \quad \Delta_f^2 \equiv \frac{1}{B-1} \sum_{b=1}^{B} \Big(\langle f \rangle_{\rm bts} - f_b \Big)^2\,, \tag{B.5}$$

however, a more meaningful estimate of the statistical error of the observable f is inferred by the dispersion of the f_b–values, more precisely by the two values left and right to the median containing 68.3 %, i.e. 34.15 % in each direction, of their (distinctly asymmetric) distribution in a histogram after B bootstrap iterations. This is motivated by the definition of a confidence interval $[F_-, F_+]$ such that one has a 15.85 % probability to find f below F_- and above F_+, respectively, which gives the statistical error through

$$\Delta_f^{(\rm bts)} = \frac{1}{2} \Big(F_+ - F_- \Big) \tag{B.6}$$

from the central $100(1-\alpha)$ % confidence interval with a confidence level $\alpha = 0.683$ corresponding to one standard deviation of the normalized Gaussian distribution in both directions.

The bootstrap procedure has been applied for the determination of the statistical error of the electroweak interface tension from the two-coupling method in the second part of this work. For this purpose it had to be slightly modified, because the relevant data were not obtained in a single MC run, but in different runs for different pairs of the scalar hopping parameter κ, labelled by $1 \le j \le J$. There the simulations provide independent histories of measurements of the φ–links $L_\varphi^{(1)}$ and $L_\varphi^{(2)}$, which are to be treated as correlated, i.e. $I = 2$ for each κ–pair under study. Hence, the separate generation of the new bootstrap samples $\mathcal{B}_b$ via

the randomly chosen index sets $\mathcal{I}_b^{(j)}$, drawn with replacement for every j as described above, is performed simultaneously for the different κ–pairs in every iteration, and for $i = 1, 2$ and fixed j-th κ-pair the $L_\varphi^{(i)}$–measurements have to be averaged within the bootstrap replicas on the same set $\mathcal{I}_b^{(j)}$. The least-squares fits of these bootstrap sample averages result in fit parameters (and thereby the interface tension, see sections 7.1, 7.2, and 9.2), which represent the desired secondary quantities in the present situation, and the distributions of their values after B bootstrap iterations determines their statistical errors in the manner of eq. B.6. In order to eliminate the influence of autocorrelations, I have combined the full samples of original measurements to bins of increasing length so that the final bootstrap error estimates can be looked up from the plateau in the error table, which develops when the bootstrap analyses are done with these bin averages considered as the raw data.

B.2 Least-squares fits

Suppose $N < N_{\mathrm{meas}}$ mean values $O_n(t)$, $n \in \{1, \ldots, N\}$, over subsamples of a primary or secondary quantity $O = O(t)$ to be statistically independent, e.g. after dividing the full history of N_{meas} data in long enough blocks, which were averaged first. For $O(t)$ one may think of a, say, timeslice correlation function with discrete arguments $t \in \{t_m \,|\, m = 1, \ldots, M\}$, but the remarks also carry over to other classes of observables. The task is now to fit these data to a theoretically given function $f = f(t; \{a\})$ and estimate the best fit parameters $\{a\} = \{a_i \,|\, i = 1, \ldots, I\}$ and their statistical errors in the resulting identification $\langle O(t) \rangle = f(t; \{a\})$. Owing to their origin from the same configuration, the data sets $O_n(t_m)$ and $O_n(t_{m'})$ usually are strongly correlated in the fitted direction. These correlations among the data reflect in the off-diagonal elements of the covariance (correlation) matrix

$$\begin{aligned} C_{mm'} &\equiv \frac{1}{N(n-1)} \sum_{n=1}^{N} \Big(O_n(t_m) - \langle O(t_m) \rangle \Big) \Big(O_n(t_{m'}) - \langle O(t_{m'}) \rangle \Big) \\ \langle O(t_m) \rangle &= \frac{1}{N} \sum_{n=1}^{N} O_n(t_m) \,, \end{aligned} \tag{B.7}$$

whose diagonal elements would equal the ordinary variances, i.e. $\langle O(t_m) \rangle_Z = \langle O(t_m) \rangle \pm \Delta_{O(t_m)}$, $\Delta_{O(t_m)} = \sqrt{C_{m,m}}$. Now the best fit is found via its maximum likelihood definition by minimizing the sum of squares

$$\chi^2 = \chi^2(\{a\}) \equiv \sum_{m,m'=1}^{M} \Big[\langle O(t_m) \rangle - f(t_m; \{a\}) \Big] C^{-1}_{mm'} \Big[\langle O(t_{m'}) \rangle - f(t_{m'}; \{a\}) \Big] \tag{B.8}$$

with respect to the fit parameters. Under the assumption of an infinitely large sample of stochastically independent measurements, the distribution of the $O_n(t_m)$ is Gaussian (central limit theorem) with probability $P(\{a\}) \propto \exp\{-\frac{1}{2}\chi^2(\{a\})\}$ to find the right answer that f

represents the data sample indeed. The same holds true for the best fit parameters, whose distribution around their ensemble averages over the subsamples is Gaussian as well [19, 186].

The χ^2–value in its minimum indicates the applicability and the quality of such a fit and serves in the following to select the most reasonable fit interval. If 'dof' denotes the number of degrees of freedom in the fit, i.e. the difference $M-I$, the occurrence of $\chi^2/\mathrm{dof} \simeq 1$ always provides a safe criterion for a good and reliable fit. The problems, which can arise in this context, are twofold. Whereas too large values of χ^2/dof doubt of a really good modelling of the distribution of the data by the fit function, one is also confronted with notoriously low χ^2/dof for many fit intervals in question so that the decision for a definite interval is made harder. On the other hand, the correlated fits, which in general could overcome these difficulties by inclusion of the correlations between the data in its off-diagonal elements, are often plagued with very small eigenvalues of the covariance matrix as a consequence of low statistics and thus large statistical errors in the inverse correlation matrix [187]. Then the inversion of $C_{mm'}$ in eq. (B.8) leads to a drastic increase of χ^2/dof and deformations of the fit function. Under these circumstances the authors of refs. [187] argue that for a suitable covariance matrix a number of at least $N \gtrsim \max\{M^2, 10(M+1)\}$ independent measurements (respective subsamples) is sufficient, and they propose the following recipe to remove any very small eigenvalues of $C_{mm'}$, if the total sample size is too small to avoid unreasonable fluctuations among the data. One calculates the normalized covariance matrix,

$$\widetilde{C}_{mm'} \equiv C_{mm}^{-1/2}\, C_{mm'}\, C_{m'm'}^{-1/2}\,, \tag{B.9}$$

its eigenvalues λ_m, which are taken to be arranged in decreasing order, and smears the $M-E$ smallest eigenvalues through substitution by their mean value

$$\lambda'_m = K \max\{\lambda_m, \lambda_{\min}\} \tag{B.10}$$

with

$$\lambda_{\min} \equiv \frac{1}{M-E} \sum_{m=E+1}^{M} \lambda_m\,, \quad K^{-1} \equiv \frac{1}{M} \sum_{m=1}^{M} \max\{\lambda_m, \lambda_{\min}\}\,, \tag{B.11}$$

while retaining the property that $\mathrm{Tr}\,\widetilde{C}_{mm'} = M$, and it is suggested to keep $E \simeq \sqrt{N}$ exact eigenvalues in practice. After choosing the largest fit interval of the available t–range, which respects the criterion $\chi^2/\mathrm{dof} \simeq 1$, the best fit parameters are obtained as results of the uncorrelated fit, i.e. neglecting the off-diagonal elements of the covariance matrix in (B.8),

$$\chi^2 = \chi^2(\{a\}) = \sum_{m=1}^{M} \left\{ \frac{\langle O(t_m)\rangle - f(t_m;\{a\})}{\Delta_{O(t_m)}} \right\}^2\,, \tag{B.12}$$

along this interval. In order to get a plain shape for the deviation between fit and data in units of its statistical errors $|\langle O(t)\rangle - f(t;\{a\})|/\Delta_{O(t)}$ against t, one typically has to discard a few data points from the beginning of the t–range examined, because these tend to contribute too much to χ^2/dof.

This Michael-McKerrel method has been employed in nearly all mass determinations from correlation functions throughout the present work; for recent applications in the SU(2)–Higgs model see refs. [137, 141]. Especially in my treatment of two-dimensional U(1)–Higgs model, an eigenvalue smearing was not necessary, because the statistics was large enough to fulfill the constraint on N. However, it readily served as a cross-check for the final estimates. I always verified that both fits fairly agreed within their errors, and other fit intervals of different lengths with similar or even lower χ^2/dof did not lead to any significant discrepancies worthy to note, signalling the stability of the method and the insensitivity of its results to the these potential uncertainties.

The statistical errors of the fit parameters can either be computed by 'simulating' the fit using normally distributed random data with mean values and variances of the original data as input or, in view of the existence of independent data subsamples, by a jackknife analysis, which is certainly more trustworthy. In this case the errors on the data in the subsamples were not used in the (correlated) Michael-McKerrel fits, whereas the errors of the data in the total data sample — to be used in the uncorrelated fits — were determined from the statistical fluctuations of the subsample data. Since the χ^2–minimization can be done analytically only for simple rational functions [192], I utilized standard library routines [191] to cope with more complicated fit functions.

B.3 Ferrenberg-Swendsen reweighting

For an arbitrary observable O in a model with action parameter β, energy density ϵ, lattice field action $S = \Omega\beta\epsilon$, and generating functional or partition function $Z = Z_\beta$, see eq. (A.10), the identity

$$\langle O \rangle_{Z_{\beta'}} = \left\langle O \, \frac{Z_\beta}{Z_{\beta'}} \, \mathrm{e}^{\,\Omega(\beta-\beta')\epsilon} \right\rangle_{Z_\beta} = \frac{\left\langle O \, \mathrm{e}^{\,\Omega(\beta-\beta')\epsilon} \right\rangle_{Z_\beta}}{\left\langle \mathrm{e}^{\,\Omega(\beta-\beta')\epsilon} \right\rangle_{Z_\beta}} \,, \tag{B.13}$$

with $Z_{\beta'}/Z_\beta = \langle \mathrm{e}^{\,\Omega(\beta-\beta')\epsilon} \rangle_{Z_\beta}$ in the second equality, relates expectation values at different β to each other. It gives rise to the histogram or reweighting method [188], which in principle is capable to obtain expectation values in form of curves in β from a single MC run. Since for too large $\Delta\beta \equiv |\beta' - \beta| \simeq \mathcal{O}(1)$ the exponential causes that only configurations with very small contributions to $\langle O \rangle_{Z_{\beta'}}$ are generated, their sample is peaked at the wrong value of ϵ, whilst those configurations with large contributions have a low proposal probability and are drastically damped. Hence, they may never occur during a simulation (importance sampling), and one has to ensure $\Omega\Delta\beta \simeq \mathcal{O}(1)$ in practice.

This technique is used within the finite-temperature SU(2)–Higgs model in the direct vicinity of the phase transition point, triggered by the scalar hopping parameter κ with all other couplings fixed. Its characteristic changes are so small in this region ($\Delta\kappa \lesssim \mathcal{O}(10^{-5})$) that the condition of a fine scale in β just mentioned is fulfilled, and eq. (B.13) is justified

to be applied. As can be read off from the lattice action (5.14) in chapter 5, the φ–link operator L_φ is conjugated in the thermodynamic sense to the coupling κ. Therefore, in order to estimate an expectation value of the considered quantity O at κ' different from that κ–value, where the simulation has been performed, the factor $\mathrm{e}^{\Omega(\beta-\beta')\epsilon}$ amounts to attach the weight

$$w_n = w_n[L_\varphi] \equiv \mathrm{e}^{8\Omega L_{\varphi,n}(\kappa'-\kappa)} \tag{B.14}$$

to the n-th entry in the history of its full measurement sample at hopping parameter κ and to calculate:

$$\langle O \rangle_{\kappa'} = \frac{1}{w_{\mathrm{tot}}} \sum_{n=1}^{N_{\mathrm{meas}}} O_n w_n \,, \quad w_{\mathrm{tot}} \equiv \sum_{n=1}^{N_{\mathrm{meas}}} w_n \,. \tag{B.15}$$

Of course, for $\kappa = \kappa'$ one gets the original average at κ, and these equations remain valid for anisotropic lattices as well, if the space- and timelike parts of the φ–link operator were combined with the coupling anisotropies according to eqs. (5.32) — (5.34) before.

Realistic statistical errors of reweighted expectation values are granted through jackknife or bootstrap methods as described in sections B.1.1 and B.1.2 of this appendix, because these account for the intrinsic correlations between numerator and denominator in eq. (B.13) in an appropriate way.

Bibliography

[1] K. Huang, *Quarks, Leptons and Gauge Fields*, World Scientific, Singapore, 1992;
S. Weinberg, *The Quantum Theory of Fields, Vols. 1 and 2*, Cambridge University Press, Cambridge, 1995 and 1996.

[2] J. F. Donoghue, E. Golowich, B. R. Holstein, *Dynamics of the Standard Model*, Cambridge University Press, Cambridge, 1992;
W. E. Burcham, M. Jobes, *Nuclear and Particle Physics*, Longman Scientific & Technical, Essex, 1995.

[3] K. Huang, *Statistical Mechanics*, John Wiley and Sons, New York, 1987.

[4] C. Itzykson, J.-M. Drouffe, *Statistical Field Theory, Vols. 1 and 2*, Cambridge University Press, Cambridge, 1989, and references therein.

[5] R. J. Rivers, *Path Integral Methods in Quantum Field Theory*, Cambridge University Press, Cambridge, 1987.

[6] J. I. Kapusta, *Finite Temperature Field Theory*, Cambridge University Press, Cambridge, 1989;
M. Le Bellac, *Thermal Field Theory*, Cambridge University Press, Cambridge, 1996.

[7] M. Nakahara, *Geometry, Topology and Physics*, Adam Hilger IOP Publishing Ltd. Bristol, 1990, and references therein.

[8] M. Daniel, C. Viallet, Rev. Mod. Phys. 52 (1980) 175;
R. Rennie, *Geometry and Topology of Chiral Anomalies in Gauge Theories*, Adv. Phys. 39 (1990) 617.

[9] R. Rajaraman, *Solitons and Instantons*, North-Holland Publishing Company, Amsterdam, 1982.

[10] T. Schäfer, E. V. Shuryak, *Instantons in QCD*, DOE-ER-40561-293 (hep-ph/9610451), 1996.

[11] E. W. Kolb, M. S. Turner, *The Early Universe*, Addison-Wesley, Redwood City, 1990.

[12] G. Altarelli, contribution to *International Symposium on Radiative Corrections (CRAD 96), Cracow, Poland*, CERN-TH/96-265 (hep-ph/9611239), 1996;
J. Ellis, contribution to *Inauguration Conference of the Asia-Pacific Center for Theoretical Physics, Seoul, Korea*, CERN-TH/96-210 (hep-ph/9611254), 1996;
J. Ellis, G. L. Fogli, E. Lisi, Phys. Lett. B389 (1996) 321.

[13] Particle Data Group (R. M. Barnett et al.), Phys. Rev. D54 (1996) 1.

[14] K. G. Wilson, Phys. Rev. D10 (1974) 2445.

[15] Div. eds. *Proceedings of the xxxth International Symposium on Lattice Field Theory*, Nucl. Phys. B (Proc. Suppl.), North-Holland Publishing Company, Amsterdam.

[16] M. Creutz, *Quarks, Gluons and Lattices*, Cambridge University Press, Cambridge, 1983.

[17] H. J. Rothe, *Lattice Gauge Theories: An Introduction*, World Scientific Lecture Notes in Physics Vol. 43, World Scientific, Singapore, 1992.

[18] F. Karsch, E. Laermann, Rept. Prog. Phys. 56 (1993) 1347.

[19] I. Montvay, G. Münster, *Quantum Fields on a Lattice*, Cambridge University Press, Cambridge, 1994, and references therein.

[20] N. Mermin, H. Wagner, Phys. Rev. Lett. 16 (1966) 1133.

[21] S. Elitzur, Phys. Rev. D12 (1975) 3978.

[22] E. Fradkin, S. H. Shenker, Phys. Rev. D19 (1979) 3682.

[23] S. Adler, Phys. Rev. 177 (1969) 2426;
J. S. Bell, R. Jackiw, Nuo. Cim. A60 (1969) 47.

[24] G. 't Hooft, Phys. Rev. Lett. 37 (1976) 8; Phys. Rev. D14 (1976) 3432; Phys. Rev. D30 (1984) 2212.

[25] K. Fujikawa, Phys. Rev. Lett. 42 (1979) 1195; Phys. Rev. D21 (1980) 2848;
M. Reuter, Phys. Rev. D31 (1984) 1374;
G. Münster, M. Reuter, Phys. Lett. B198 (1987) 73.

[26] A. A. Belavin, A. M. Polyakov, A. A. Schwartz, Y. S. Tyupkin, Phys. Lett. B59 (1975) 85.

[27] C. G. Callen, R. Dashen, D. J. Gross, Phys. Lett. B63 (1976) 334;
R. Jackiw, C. Rebbi, Phys. Rev. Lett. 37 (1976) 172;
A. M. Polyakov, Nucl. Phys. B120 (1977) 429.

[28] H. B. Nielsen, P. Olesen, Nucl. Phys. B14 (1973) 45.

[29] H. J. de Vega, F. A. Schaposnik, Phys. Rev. D14 (1976) 1100.

[30] N. S. Manton, Phys. Rev. D28 (1983) 2019;
F. R. Klinkhammer, N. S. Manton, Phys. Rev. D30 (1984) 2212.

[31] P. Arnold, L. McLerran, Phys. Rev. D36 (1987) 581;
S. Y. Khlebnikov, M. Shaposhnikov, Nucl. Phys. B308 (1988) 885.

[32] A. I. Bochkarev, M. Shaposhnikov, Mod. Phys. Lett. A2 (1987) 991.

[33] M. Shaposhnikov, Nucl. Phys. B26 (Proc. Suppl.) (1992) 78, and references therein.

[34] E. Witten, Nucl. Phys. B156 (1979) 269;
G. Veneziano, Nucl. Phys. B159 (1979) 213.

[35] B. Berg, M. Lüscher, Nucl. Phys. B190 [FS3] (1981) 412;
M. Lüscher, Nucl. Phys. B205 [FS5] (1982) 483.

[36] P. Di Vecchia, K. Fabricius, G. C. Rossi, G. Veneziano, Nucl. Phys. B192 (1981) 392.

[37] M. Lüscher, Comm. Math. Phys. 85 (1982) 39.

[38] C. Panagiotakopoulos, Nucl. Phys. B251 [FS13] (1985) 61.

[39] N. Seiberg, Phys. Lett. B148 (1984) 456;
P. Woit, Nucl. Phys. B262 (1985) 284.

[40] A. Phillips, D. Stone, Comm. Math. Phys. 103 (1986) 599; Nucl. Phys. B20 (Proc. Suppl.) (1991) 28.

[41] A. S. Kronfeld, Nucl. Phys. B4 (Proc. Suppl.) (1988) 329, and references therein.

[42] A. S. Kronfeld, M. L. Laursen, G. Schierholz, U.-J. Wiese, Nucl. Phys. B292 (1987) 330;
M. Göckeler, A. S. Kronfeld, M. L. Laursen, G. Schierholz, U.-J. Wiese, Nucl. Phys. B292 (1987) 349; Phys. Lett. B233 (1989) 192;
A. S. Kronfeld, M. L. Laursen, G. Schierholz, C. Schleiermacher, U.-J. Wiese, Comp. Phys. Comm. 54 (1989) 109.

[43] F. Karsch, M. L. Laursen, T. Neuhaus, B. Plache, Nucl. Phys. B406 [FS] (1993) 825.

[44] J. Smit, J. C. Vink, Nucl. Phys. B284 (1987) 234; Nucl. Phys. B298 (1988) 557;
M. L. Laursen, J. Smit, J. C. Vink, Nucl. Phys. B343 (1990) 522.

[45] J. Smit, J. C. Vink, Nucl. Phys. B286 (1987) 485; Nucl. Phys. B303 (1988) 36;
J. C. Vink, Phys. Lett. B212 (1988) 483; Nucl. Phys. B307 (1988) 549.

[46] J. Hoek, Phys. Lett. B166 (1986) 199;
J. Hoek, M. Teper, J. Waterhouse, Nucl. Phys. B288 (1987) 589.

[47] P. de Forcrand, M. García Pérez I. O. Stamatescu, Nucl. Phys. B47 (Proc. Suppl.) (1996) 777; Nucl. Phys. B53 (Proc. Suppl.) (1997) 557; HD-THEP-96-52 (hep-lat/9701012), 1997.

[48] B. Alles, M. D'Elia, A. Di Giacomo, Nucl. Phys. B53 (Proc. Suppl.) (1997) 541; Nucl. Phys. B494 (1997) 281; IFUP-TH 20-97 (hep-lat/9706016), 1997.

[49] T. DeGrand, A. Hasenfratz, D. Zhu, Nucl. Phys. B475 (1996) 321; Nucl. Phys. B478 (1996) 349; Nucl. Phys. B53 (Proc. Suppl.) (1997) 945;
T. DeGrand, A. Hasenfratz, T. G. Kovacs, COLO-HEP-383 (hep-lat/9705009), 1997.

[50] R. C. Johnson, Phys. Lett. B114 (1982) 147;
B. Berg, A. Billoire, Nucl. Phys. B221 (1983) 109.

[51] B. Berg, C. Panagiotakopoulos, Phys. Rev. Lett. 52 (1984) 94.

[52] P. de Forcrand, J. H. Hetrick, Nucl. Phys. B42 (Proc. Suppl.) (1995) 861.

[53] E. Seiler, contribution to *Colloquium on Random Fields, Esztergom, Hungary*, Esztergom 1979 Proc. 2 (1979), 937, and references therein;
D. Brydges, J. Fröhlich, E. Seiler, Nucl. Phys. B152 (1979) 521.

[54] D. Jones, J. Kogut, D. Sinclair, Phys. Rev. D19 (1979) 1882.

[55] M. B. Einhorn, R. Savit, Phys. Rev. D17 (1978) 2583; Phys. Rev. D19 (1979) 1198.

[56] I. Ichinose, H. Mukaida, Int. J. Mod. Phys. A9 (1994) 1043.

[57] B. Bunk, U. Wolff, Phys. Lett. B124 (1983) 383.

[58] S. Grunewald, E.-M. Ilgenfritz, M. Müller-Preussker, Z. Phys. C33 (1987) 561.

[59] P. H. Damgaard, Phys. Lett. B214 (1988) 570.

[60] I. Montvay, Int. J. Mod. Phys. C5 (1994) 339; Nucl. Phys. B34 (Proc. Suppl.) (1994) 631; Phys. Lett. B323 (1994) 378.

[61] J. Baacke, T. Daiber, Phys. Rev. D51 (1994) 795.

[62] W. H. Tang, J. Smit, Nucl. Phys. B34 (Proc. Suppl.) (1994) 616; Nucl. Phys. B42 (Proc. Suppl.) (1995) 590.

[63] E. Mendel, G. Nolte, hep-lat/9511030, 1995; Nucl. Phys. B53 (Proc. Suppl.) (1997) 567.

[64] H. Dilger, J. Heitger, Nucl. Phys. B53 (Proc. Suppl.) (1997) 587.

[65] H. Dilger, Nucl. Phys. B53 (Proc. Suppl.) (1997) 590.

[66] H. Dilger, private communication.

[67] J. M. Kosterlitz, D. J. Thouless, J. Phys. C6 (1973) L97;
J. M. Kosterlitz, J. Phys. C7 (1974) 1046.

[68] J. V. José, L. P. Kadanoff, S. Kirkpatrick, D. R. Nelson, Phys. Rev. B16 (1977) 1217.

[69] R. G. Edwards, J. Goodman, A. D. Sokal, Nucl. Phys. B354 (1991) 289.

[70] M. Hasenbusch, M. Marcu, K. Pinn, Nucl. Phys. B26 (Proc. Suppl.) (1992) 598; Physica A208 (1994) 124.

[71] F. Fucito, S. Solomon, Phys. Lett. B134 (1984) 230; Phys. Lett. B134 (1984) 235.

[72] M. L. Laursen, J. Smit, J. C. Vink, Phys. Lett. B262 (1991) 467.

[73] H. Dilger, Nucl. Phys. B434 (1995) 321; Int. J. Mod. Phys. C6 (1995) 123.

[74] A. Hasenfratz, K. Jansen, J. Jersák, C. B. Lang, T. Neuhaus, H. Yoneyama, Nucl. Phys. B317 (1989) 81.

[75] M. Lüscher, P. Weisz, Nucl. Phys. B318 (1989) 705.

[76] K. Pinn, Z. Phys. C45 (1990) 453; private communication.

[77] C. G. Callen, R. Dashen, D. J. Gross, Phys. Lett. B66 (1977) 375; Phys. Rev. D16 (1977) 2526.

[78] E. H. Monsay, T. N. Tudron, Phys. Rev. D16 (1977) 3503;
S. Raby, A. Ukawa, Phys. Rev. D18 (1978) 1154.

[79] S. Coleman, *The Uses of Instantons*, Erice Lectures 1977, in *Aspects of Symmetry*, Cambridge University Press, Cambridge, 1985.

[80] M. N. Chernodub, M. I. Polikarpov, contribution to *International Workshop on Non-perturbative Approaches to QCD, Trento, Italy*, ITEP-TH-8-95 (hep-th/9510014), 1995; M. N. Chernodub, F. V. Gubarev, M. I. Polikarpov, KANAZAWA-97-08 (hep-lat/9704021), 1997.

[81] D. Espriu, J. F. Wheater, Nucl. Phys. B258 (1985) 101.

[82] T. Kennedy, C. King, Phys. Rev. Lett. 55 (1985) 776.

[83] R. E. Shrock, Nucl. Phys. B267 (1986) 301; Nucl. Phys. B278 (1986) 380.

[84] J. Bricmont, J. Fröhlich, Phys. Lett. B122 (1983) 73.

[85] K. Fredenhagen, M. Marcu, Comm. Math. Phys. 92 (1983) 81; Phys. Rev. Lett. 56 (1986) 223.

[86] K. Jansen, J. Jersák, C. B. Lang, T. Neuhaus, G. Vones, Nucl. Phys. B265 [FS15] (1986) 129.

[87] H. G. Evertz, V. Grösch, K. Jansen, J. Jersák, H. A. Kastrup, T. Neuhaus, Nucl. Phys. B285 [FS19] (1987) 559.

[88] H. G. Evertz, K. Jansen, J. Jersák, C. B. Lang, T. Neuhaus, Nucl. Phys. B285 [FS19] (1987) 590.

[89] A. D. Linde, Rep. Prog. Phys. 42 (1979) 389.

[90] M. Dine, *Baryon Number Violation in the Standard Model*, University of Colorado Lectures 1992;
L. McLerran, Lectures contribution to *ICTP School on High Energy Physics, Trieste, Italy*, 1992.

[91] A. G. Cohen, D. B. Kaplan, A. E. Nelson, Annu. Rev. Nucl. Part. Sci. 43 (1993) 27, and references therein.

[92] P. Arnold, contribution to *Conference QUARKS 94, Vladimir, Russia*, UW-PT-94-13 (hep-ph/9410294), 1994;
L. G. Yaffe, contribution to *String Gravity and Physics at the Planck Energy Scale, Erice, Italy*, hep-ph/9512265, 1995.

[93] V. A. Rubakov, M. Shaposhnikov, *Electroweak Baryon Number Non-Conservation in the Early Universe and in High Energy Collisions*, Usp. Fiz. Nauk 166 (1996) 493, Phys. Usp. 39 (1996) 461, CERN-TH/96-13 (hep-ph/9603208), 1996.

[94] M. Shaposhnikov, *Finite Temperature Effective Theories*, Erice Lectures 1996, CERN-TH/96-280 (hep-ph/9610247), 1996.

[95] I. Montvay, contribution to *The Higgs Puzzle – What can we learn from LEP2, LHC, NLC, and FMC?, Ringberg Workshop, Germany, 1996*, DESY 97-034 (hep-lat/9703001), to be published in the Conference Proceedings, B. Kniehl (ed.), World Scientific, Singapore, 1997, and references therein.

[96] K. Kajantie, Nucl. Phys. B42 (Proc. Suppl.) (1995) 103;
K. Rummukainen, Nucl. Phys. B53 (Proc. Suppl.) (1997) 30.

[97] K. Jansen, Nucl. Phys. B47 (Proc. Suppl.) (1996) 196, and references therein.

[98] A. D. Sakharov, JETP Lett. 6 (1967) 24.

[99] D. A. Kirzhnitz, JETP Lett. 15 (1972) 529;
D. A. Kirzhnitz, A. D. Linde, Phys. Lett. B72 (1972) 471; Ann. Phys. 101 (1976) 195.

[100] V. A. Kuzmin, V. A. Rubakov, M. Shaposhnikov, Phys. Lett. B155 (1985) 36;
M. Shaposhnikov, Nucl. Phys. B287 (1987) 757.

[101] A. D. Linde, Phys. Lett. B96 (1980) 289.

[102] P. Arnold, O. Espinosa, Phys. Rev. D47 (1993) 3546.

[103] D. Bödeker, W. Buchmüller, Z. Fodor, T. Helbig, Nucl. Phys. B423 (1994) 171.

[104] W. Buchmüller, Z. Fodor, T. Helbig, D. Walliser, Ann. Phys. 234 (1994) 260.

[105] Z. Fodor, A. Hebecker, Nucl. Phys. B432 (1994) 127.

[106] M. Lüscher, unpublished notes.

[107] W. Buchmüller, Z. Fodor, A. Hebecker, Phys. Lett. B331 (1994) 131; Nucl. Phys. B447 (1995) 317.

[108] P. Arnold, L. G. Yaffe, Phys. Rev. D49 (1994) 3003;
W. Buchmüller, Z. Fodor, Phys. Lett. B331 (1994) 124.

[109] N. Tetradis, C. Wetterich, Nucl. Phys. B398 (1993) 659;
M. Reuter, C. Wetterich, Nucl. Phys. B408 (1993) 91; Nucl. Phys. B417 (1994) 181;
Nucl. Phys. B427 (1994) 291.

[110] U. Kerres, G. Mack, G. Palma, Nucl. Phys. B42 (Proc. Suppl.) (1995) 584; Nucl. Phys. B467 (1996) 510.

[111] N. Tetradis, Nucl. Phys. B488 (1997) 92; CERN-TH/96-331 (hep-ph/9611461), 1996;
CERN-TH/97-118 (hep-th/9706088), 1997;
B. Bergerhoff, C. Wetterich, Nucl. Phys. B440 (1995) 171; contribution to *International School of Astrophysics, Erice, Italy*, HD-THEP-96-51 (hep-ph/9611462), 1996.

[112] H. Kühnelt, C. B. Lang, G. Vones, Nucl. Phys. B230 [FS10] (1984) 16;
J. Jersák, C. B. Lang, T. Neuhaus, G. Vones, Phys. Rev. D32 (1985) 2761;
H. G. Evertz, J. Jersák, C. B. Lang, T. Neuhaus, Phys. Lett. B171 (1986) 271.

[113] H. G. Evertz, V. Grösch, J. Jersák, H. A. Kastrup, T. Neuhaus, D. P. Landau, J.-L. Xu Phys. Lett. B175 (1986) 335.

[114] I. Montvay, Phys. Lett. B150 (1985) 441; Nucl. Phys. B269 (1986) 170.

[115] W. Langguth, I. Montvay, P. Weisz, Nucl. Phys. B277 (1986) 11.

[116] W. Langguth, I. Montvay, Z. Phys. C36 (1987) 725.

[117] I. Montvay, Phys. Lett. B172 (1986) 71; Nucl. Phys. B293 (1987) 479;
A. Hasenfratz, P. Hasenfratz, Phys. Rev. D34 (1986) 3160.

[118] H. G. Evertz, J. Jersák, K. Kanaya, Nucl. Phys. B285 (1987) [FS19] 229.

[119] P. H. Damgaard, U. M. Heller, Nucl. Phys. B294 (1987) 253.

[120] B. Bunk, E.-M. Ilgenfritz, J. Kripfganz, A. Schiller, Phys. Lett. B284 (1992) 371; Nucl. Phys. B403 (1993) 453.

[121] E.-M. Ilgenfritz, A. Schiller, Nucl. Phys. B42 (Proc. Suppl.) (1995) 578.

[122] Y. Aoki, Nucl. Phys. B53 (Proc. Suppl.) (1997) 609; Phys. Rev. D56 (1997) 3860.

[123] S. Coleman, S. Weinberg, Phys. Rev. D7 (1973) 1888.

[124] S. Weinberg, Phys. Rev. Lett. 36 (1976) 294;
A. D. Linde, JETP Lett. 23 (1976) 73.

[125] G. Curci, G. Pafutti, R. Tripiccione, Nucl. Phys. B240 [FS12] (1984) 91.

[126] U. Heller, F. Karsch, Nucl. Phys. B251 [FS13] (1985) 254.

[127] C. Michael, Phys. Lett. B283 (1992) 103.

[128] R. Sommer, Nucl. Phys. B411 (1994) 839.

[129] A. Hasenfratz, P. Hasenfratz, Nucl. Phys. B193 (1981) 210;
F. Karsch, Nucl. Phys. B205 [FS5] (1982) 285.

[130] I. Montvay, E. Pietarinen, Phys. Lett. B110 (1982) 148;
J. Engels, F. Karsch, H. Satz, I. Montvay, Nucl. Phys. B205 [FS5] (1982) 545.

[131] G. Burgers, F. Karsch, A. Nakamura, I. O. Stamatescu, Nucl. Phys. B304 (1988) 587.

[132] F. Karsch, I. O. Stamatescu, Phys. Lett. B227 (1989) 153.

[133] I. Bender, T. Hashimoto, F. Karsch, V. Linke, A. Nakamura, M. Schiestl, I. O. Stamatescu, Nucl. Phys. B17 (Proc. Suppl.) (1990) 387; Nucl. Phys. B20 (Proc. Suppl.) (1991) 329.

[134] F. Csikor, Z. Fodor, J. Hein, K. Jansen, A. Jaster, I. Montvay, Phys. Lett. B334 (1994) 405; Nucl. Phys. B42 (Proc. Suppl.) (1995) 569.

[135] Z. Fodor, J. Hein, K. Jansen, A. Jaster, I. Montvay, Nucl. Phys. B439 (1995) 147.

[136] F. Csikor, Z. Fodor, J. Hein, J. Heitger, Phys. Lett. B357 (1995) 156.

[137] F. Csikor, Z. Fodor, J. Hein, A. Jaster, I. Montvay, Nucl. Phys. B474 (1996) 421.

[138] F. Csikor, Z. Fodor, Phys. Lett. B380 (1996) 113.

[139] J. Hein, J. Heitger, Phys. Lett. B385 (1996) 242.

[140] F. Csikor, Z. Fodor, J. Hein, J. Heitger, A. Jaster, I. Montvay, contribution to *International Conference on High Energy Physics (ICHEP 96), Warsaw, Poland*, 1996; Nucl. Phys. B53 (Proc. Suppl.) (1997) 612.

[141] F. Csikor, Z. Fodor, J. Heitger, in preparation.

[142] F. Csikor, Z. Fodor, private communication.

[143] A. Jakovác, K. Kajantie, Patkós, Phys. Rev. D49 (1994) 6810.

[144] F. Karsch, T. Neuhaus, A. Patkós, Nucl. Phys. B42 (Proc. Suppl.) (1995) 581; Nucl. Phys. B441 (1995) 629.

[145] F. Karsch, T. Neuhaus, A. Patkós, J. Rank, Nucl. Phys. B474 (1996) 217; Nucl. Phys. B53 (Proc. Suppl.) (1997) 623.

[146] K. Kajantie, R. Rummukainen, M. Shaposhnikov, Nucl. Phys. B407 (1993) 356;
K. Farakos, K. Kajantie, R. Rummukainen, M. Shaposhnikov, Nucl. Phys. B425 (1994) 67; Nucl. Phys. B442 (1995) 317;

[147] K. Kajantie, M. Laine, R. Rummukainen, M. Shaposhnikov, Nucl. Phys. B466 (1996) 189, and references therein.

[148] M. Laine, Phys. Lett. B385 (1996) 249.

[149] K. Kajantie, M. Laine, R. Rummukainen, M. Shaposhnikov, Phys. Rev. Lett. 77 (1996) 2887; Nucl. Phys. B493 (1997) 413.

[150] E.-M. Ilgenfritz, J. Kripfganz, H. Perlt, A. Schiller, Phys. Lett. B356 (1995) 561;
M. Gürtler, E.-M. Ilgenfritz, J. Kripfganz, H. Perlt, A. Schiller, hep-lat/9512022, 1995; Nucl. Phys. B483 (1997) 383; Nucl. Phys. B53 (Proc. Suppl.) (1997) 615 and 619;

[151] M. Gürtler, E.-M. Ilgenfritz, A. Schiller, UL-NTZ-08-97 (hep-lat/9702020), 1997.

[152] M. Gürtler, E.-M. Ilgenfritz, A. Schiller, Phys. Rev. D56 (1997) 3888.

[153] O. Philipsen, M. Teper, H. Wittig, Nucl. Phys. B469 (1996) 445; Nucl. Phys. B53 (Proc. Suppl.) (1997) 626.

[154] W. H. Tang, J. Smit, Nucl. Phys. B482 (1996) 265; ITFA-97-02 (hep-lat/9702017), 1997.

[155] M. Carena, M. Quiros, C. E. M. Wagner, Phys. Lett. B380 (1996) 81;
B. de Carlos, J. R. Espinosa, SUSX-TH-97-005 (hep-ph/9703212), 1997;
M. Quiros, contribution to *The Higgs Puzzle – What can we learn from LEP2, LHC, NLC, and FMC?, Ringberg Workshop, Germany, 1996*, IEM-FT-152-96 (hep-ph/9703326), to be published in the Conference Proceedings, B. Kniehl (ed.), World Scientific, Singapore, 1997, and references therein.

[156] H. J. Herrmann, W. Janke, F. Karsch (eds.), *Dynamics of First Order Phase Transitions*, World Scientific, Singapore, 1992.

[157] W. Janke, *Recent Developments in Monte Carlo Simulations of First Order Phase Transitions*, in *Computer Simulations in Condensed Matter Physics VII*, eds. D. P. Landau, K. K. Mon, H. B. Schüttler, Springer Verlag, Berlin, 1994.

[158] G. Bhanot, S. Black, P. Carter, R. Salvador, Phys. Lett. B183 (1987) 331;
G. Bhanot, K. Bitar, S. Black, P. Carter, R. Salvador, Phys. Lett. B187 (1987) 381.

[159] J. S. Langer, Ann. Phys. 54 (1969) 258; Physica 73 (1974) 61.

[160] A. D. Linde, Nucl. Phys. B216 (1983) 421.

[161] L. P. Csernai, J. I. Kapusta, Phys. Rev. D46 (1992) 1379.

[162] J. Potvin, C. Rebbi, Phys. Rev. Lett. 62 (1989) 3062;
S. Huang, J. Potvin, C. Rebbi, S. Sanielevici, Phys. Rev. D42 (1990) 2864; Phys. Rev. D43 (1991) 2056 [E].

[163] K. Binder, Z. Phys. B43 (1981) 119; Phys. Rev. A25 (1982) 1699.

[164] B. Grossmann, M. L. Laursen, Nucl. Phys. B408 [FS] (1993) 637;
Y. Iwasaki, K. Kanaya, L. Kärkkäinen, K. Rummukainen, T. Yoshie, Phys. Rev. D49 (1994) 3540.

[165] V. Privman, M. E. Fisher, J. Stat. Phys. 33 (1983) 385.

[166] K. Jansen, J. Jersák, I. Montvay, G. Münster, T. Trappenberg, U. Wolff, Phys. Lett. B213 (1988) 203;
K. Jansen, I. Montvay, G. Münster, T. Trappenberg, U. Wolff, Nucl. Phys. B322 (1989) 698.

[167] G. Münster, Nucl. Phys. B340 (1990) 559;
S. Klessinger, G. Münster, Nucl. Phys. B386 (1992) 701.

[168] B. Grossmann, M. L. Laursen, T. Trappenberg, U.-J. Wiese, Nucl. Phys. B30 (Proc. Suppl.) (1993) 865; Nucl. Phys. B396 (1993) 584.

[169] A. D. Sokal, *Monte Carlo Methods in Statistical Mechanics: Foundations and New Algorithms*, in *Cours du Troisième Cycle de la Physique en Suisse Romande*, Lausanne, 1989.

[170] H. Flyvbjerg, H. G. Petersen, J. Chem. Phys. 91 (1989) 461.

[171] A. D. Kennedy, Nucl. Phys. B30 (Proc. Suppl.) (1993) 96.

[172] M. Creutz, Phys. Rev. D21 (1980) 2308.

[173] S. L. Adler, Phys. Rev. D23 (1981) 2901; Phys. Rev. D37 (1988) 458.

[174] M. Creutz, Phys. Rev. D36 (1987) 515;
F. R. Brown, T. J. Woch, Phys. Rev. Lett. 58 (1987) 2394.

[175] K. Fabricius, O. Haan, Phys. Lett. B143 (1984) 459.

[176] A. D. Kennedy, B. J. Pendleton, Phys. Lett. B156 (1985) 393.

[177] B. A. Berg, T. Neuhaus, Phys. Lett. B267 (1991) 249; Phys. Rev. Lett. 68 (1992) 9.

[178] Z. Fodor, K. Jansen, Phys. Lett. B331 (1994) 119.

[179] B. Bunk, Nucl. Phys. B42 (Proc. Suppl.) (1995) 566.

[180] S. Gottlieb, P. B. Mackenzie, H. B. Thacker, D. Weingarten, Nucl. Phys. B263 (1986) 704.

[181] B. A. Berg, A. H. Billoire, Phys. Rev. D40 (1989) 550.

[182] B. A. Berg, Comp. Phys. Comm. 69 (1992) 7.

[183] B. Efron, Ann. Stat. 7 (1979) 1; SIAM Review 21 (1979) 460; *The Jackknife, the Bootstrap and other Resampling Plans*, SIAM, Philadelphia, PA, 1982.

[184] M. C. K. Yang, D. H. Robinson, *Understanding and Learning Statistics by Computer*, World Scientific Series in Computational Science Vol. 4, World Scientific, Singapore, 1986.

[185] R. Gupta, G. Guralnik, G. Kilcup, A. Patel, S. R. Sharpe, T. Warnock, Phys. Rev. D36 (1987) 2813;
M. C. Chu, M. Lissia, J. W. Negele, Nucl. Phys. B360 (1991) 31.

[186] D. Toussaint, *Error Analysis of Simulation Results: A Sample Problem*, in *From Actions to Answers*, eds. T. DeGrand, D. Toussaint, World Scientific, Singapore, 1990.

[187] C. Michael, Phys. Rev. D49 (1994) 2616;
C. Michael, A. McKerrel, Phys. Rev. D51 (1995) 3745.

[188] A. M. Ferrenberg, R. H. Swendsen, Phys. Rev. Lett. 61 (1988) 2635; Phys. Rev. Lett. 63 (1989) 1195.

[189] M. Abramowitz, A. Stegun, *Pocketbook of Mathematical Functions*, Verlag Harri Deutsch, Thun, 1984.

[190] N. Attig et al. *Einführung in die Benutzung der CRAY-Rechner*, KFA-ZAM-BHB-0093, Jülich, 1996.

[191] Numerical Algorithms Group Ltd. *NAG Fortran 77 Library, Mark 16*, 1996.

[192] W. H. Press, S. A. Teukolsky, W. T. Vetterling, B. P. Flannery, *Numerical Recipes in FORTRAN*, Cambridge University Press, Cambridge, 1992.

Danksagungen

An dieser Stelle möchte ich allen danken, die direkt oder indirekt zum Zustandekommen der vorliegenden Arbeit beigetragen haben:

- Herrn Prof. Dr. G. Münster für die reizvolle Themenstellung, sein stetiges Interesse am Fortgang meiner Arbeit, und nicht zuletzt auch für seine Anregung einer Teilnahme an einem gemeinsamen Projekt mit einigen Angehörigen der DESY-Theoriegruppe.
- Hermann Dilger und Dirk Talkenberger, die immer für Fragen und Gespräche zur Verfügung gestanden haben. Aus meiner Zusammenarbeit mit Hermann habe ich Vieles über Gitterfeldtheorie gelernt, und Dirk hat mich häufig unterstützt, wenn es so manches kleine oder auch grössere Rechnerproblem zu lösen galt...
- Unserer gesamten Arbeitsgruppe für die harmonische Atmosphäre im Institut, sowohl aus fachlicher als auch aus menschlicher Sicht.
- F. Csikor, Z. Fodor, J. Hein, K. Jansen, I. Montvay und R. Sommer für die gute Zusammenarbeit in der Kollaboration bzw. zahlreiche Diskussionen, von denen ich häufig für meine Arbeit profitieren konnte.
- Meinen Eltern, ohne die dieses Studium sicherlich nicht möglich gewesen wäre, und insbesondere meinem Vater Wolfgang Heitger, der in mir schon frühzeitig die Begeisterung für Physik und Mathematik geweckt hat.
- Meiner Frau Margret, die mir während der gesamten Dissertation immer verständnisvoll zur Seite gestanden hat, und meinen Kindern Tizian und Thalia; sie haben in der letzten Zeit sehr oft auf mich verzichten müssen. Für diese Geduld danke ich meiner Familie von ganzem Herzen.

Lebenslauf

Angaben zur Person

Name	Jochen Heitger
Geburt	08.06.1967 in Hamm/Westfalen
Familienstand	verheiratet mit Margret Heitger, geb. Simon, zwei Kinder
Name des Vaters	Wolfgang Heitger
Name der Mutter	Erika Heitger, geb. Graef

Schulischer Bildungsgang

Aug. 1973 – Juni 1977	Besuch der Ketteler-Grundschule in Hamm
Aug. 1977 – Mai 1986	Besuch des Gymnasiums Hammonense in Hamm
11.06.1986	Abitur am Gymnasium Hammonense in Hamm

Wehrdienst

Okt. 1986 – Dez. 1986	Grundwehrdienst in Marburg
Jan. 1987 – Dez. 1987	Wehrdienst beim Heeresmusikkorps 1, Hannover

Universitärer Bildungsgang

April 1988 – Okt. 1993	Studium der Physik und der Mathematik an der WWU Münster
18.10.1993	Diplom im Fach Physik an der WWU Münster

Tätigkeiten

Okt. 1992 – Okt. 1993	studentische Hilfskraft am Institut für Theoretische Physik I der WWU Münster
Nov. 1993 – Mai 1994	wissenschaftliche Hilfskraft am Institut für Theoretische Physik I der WWU Münster
seit Juni 1994	wissenschaftlicher Mitarbeiter am Institut für Theoretische Physik I der WWU Münster

Dissertation

November 1993	Beginn der Dissertation bei Prof. Dr. G. Münster am Institut für Theoretische Physik I der WWU Münster